1750C

VOLUME III
PART II - ANALYTICAL SOLUTION FOR THE LUNAR MISSION

Compilation Report
for
ADVANCED SPACEBORNE DETECTION, TRACKING, AND NAVIGATION SYSTEMS STUDY AND ANALYSIS

NAS 8 - 11205

July 1964

Prepared for

GEORGE C. MARSHALL SPACE FLIGHT CENTER
Huntsville, Alabama

By

WESTINGHOUSE DEFENSE AND SPACE CENTER
Aerospace Division
Baltimore, Maryland

ABSTRACT

10111

This is Volume III, the Analytical Solution, of a five-volume report compiled for the Marshall Space Flight Center by the Aerospace Division, Westinghouse Defense and Space Center, Baltimore, from industry studies conducted for the purpose of consolidating and extending studies of detection, tracking, navigation, and guidance systems for future space missions.

This volume reports the analytical solution of the problem as defined in Volume II, Problem Definition. Specifically, the problem investigated is the determination of navigation and control sensor requirements for local, or onboard guidance of manned (or unmanned) lunar missions. In Volume II the lunar mission is divided into a sequence of phases, each discussed individually. These phases are: earth launch to transfer injection; midcourse; lunar orbit; lunar landing; lunar ascent; lunar rendezvous; and atmospheric reentry. Of these, the first and the last are not given detailed consideration in this report because of the extent of prior investigation. The remaining mission phases are analyzed independently in the major sections of this volume.

Generally, the analytical solution takes the form of a determination of the degradation of navigation and control system performance caused by sensor inaccuracies. The principal measures of performance are terminal errors and fuel consumption. The information generated is examined in the light of allowable performance degradation to determine sensor accuracy requirements.

As a part of the analytical solution, control and data processing methods, as well as mathematical analysis techniques, are selected, discussed, implemented (usually by means of digital computation), and evaluated.

These studies have been organized along guidelines furnished by MIL-D-8684A, paragraphs 3.4.3.1 and 3.4.3.2.

TABLE OF CONTENTS

Paragraph	Page
1. INTRODUCTION	1-1
2. MIDCOURSE GUIDANCE	2-1
2.1 Introduction and Outline	2-1
2.2 Background From Volume II	2-4
2.2.1 Discussion of Midcourse Trajectories	2-4
2.2.2 Qualitative Problem Definition	2-6
2.3 Analysis	2-9
2.3.1 Quantitative Problem Definition	2-9
2.3.2 Statistical Analysis of Errors	2-25
2.3.3 Digital Computer Programs	2-28
2.3.4 Analysis of Optical Measurement Errors	2-30
2.4 Results	2-35
2.4.1 General Discussion of Guidance Scheduling	2-35
2.4.2 Development of Standard Guidance Schedule for Analysis	2-41
2.4.3 Variation of Onboard Guidance System Parameters	2-47
2.4.4 Effect of Nominal Trajectory	2-54
2.4.5 Other Error Sources	2-57
2.4.6 Other System Configurations	2-60
2.5 Conclusions	2-70
2.5.1 Onboard System Requirements	2-70
2.5.2 Navigation Schedules	2-72
2.5.3 Trajectory Variations	2-72
2.5.4 Ranging for Midcourse Guidance	2-72
2.5.5 Comparison of Onboard and Ground-Tracking Systems	2-72
2.5.6 Unresolved Problem Areas	2-73
3. LUNAR PARKING AND DESCENT ORBIT PHASE	3-1
3.1 Introduction	3-1
3.2 Background	3-3

	Page
3.3 Analysis	3-6
3.3.1 Background Analysis	3-9
3.3.2 Error Analysis	3-19
3.4 Results	3-28
3.4.1 Discussion of Digital Simulation	3-29
3.4.2 Numerical Results	3-30
3.4.3 Discussion	3-42
3.5 Discussion of Onboard Computation Requirements	3-44
3.6 Conclusions	3-47
4. LUNAR LANDING PHASE	4-1
4.1 Introduction	4-1
4.2 General Background	4-3
4.2.1 Mission Profile	4-4
4.2.2 Trajectory Considerations	4-4
4.2.3 Functional Description of the Landing Guidance System	4-5
4.2.4 Analytical Assumptions	4-6
4.2.5 Definition of Sensor Error Model	4-7
4.3 Analysis	4-8
4.3.1 Lunar Landing Using Linear Predictive Guidance	4-8
4.3.2 Lunar Landing Using Modified Proportional Navigation	4-53
4.4 Comparative Discussion of Guidance Concepts	4-80
4.4.1 Nominal Fuel Consumption	4-80
4.4.2 Comparison of Terminal Errors	4-85
4.4.3 Onboard Computation	4-85
4.4.4 Sensor Dynamic Range	4-87
5. LUNAR ASCENT PHASE	5-1
5.1 Introduction	5-1
5.2 Background	5-2
5.2.1 Description of Problem	5-3
5.2.2 Definition and Comparison of Parking and Direct Ascents	5-3
5.2.3 Assumptions	5-7

	Page
5.3 Analysis	5-8
5.3.1 Background Analysis	5-8
5.3.2 Error Analysis	5-19
5.4 Results	5-31
5.4.1 Sensor Requirements for Lunar Ascent	5-31
5.4.2 Error Comparison at Terminal Rendezvous	5-31
5.4.3 Mission Contraints and Tradeoff Considerations	5-38
5.5 Conclusions	5-40
6. LUNAR RENDEZVOUS	6-1
6.1 Introduction	6-1
6.2 Background	6-2
6.2.1 Mission Profile	6-2
6.2.2 Guidance and Control	6-3
6.2.3 Observables	6-5
6.2.4 Error Characterization	6-5
6.2.5 Error Criterion	6-6
6.3 Analysis	6-7
6.3.1 Model	6-7
6.3.2 Error Analysis - Digital Program	6-20
6.4 Results	6-23
6.4.1 Results of Injection Analysis	6-23
6.4.2 Results of Active Rendezvous Analysis	6-23
6.5 Conclusions	6-29
6.5.1 Injection Sensor Requirements	6-30
6.5.2 Rendezvous Sensor Requirements	6-30
6.6 Additional Analysis	6-30
7. REFERENCES	7-1

LIST OF ILLUSTRATIONS

Figure		Page
2-1	Geometry of Midcourse Guidance	2-5
2-2	Angle Measurements for Onboard System Model	2-8
2-3	Earth-Centered Coordinate System	2-11
2-4	Functional Block Diagram of Space Guidance System	2-13
2-5	Input-Output Diagram of Statistical Analysis Program	2-29
2-6	Types of Optical Measurements	2-31
2-7	Optical Measurements Results	2-32
2-8	Angle Difference Between Horizon and Earth-Center Measurements	2-34
2-9	Geometry of Reference Point Errors	2-35
2-10	Effects on Reducing Uncertainties of Taking Different Types of Measurements	2-37
2-11	Guidance Schedule Used on Standard Case	2-39
2-12	Step Reduction in Position Uncertainty vs Time	2-47
2-13	Rotation of Sight Line to Moon During Terminal Phase of Midcourse	2-48
2-14	Effect of Instrument Accuracy on Guidance Parameters for 63.9- and 72.2-Hour Trajectories	2-49
2-15	Effect of Variation of Correction Accuracy at Periselenum	2-52
2-16	Reduction in Miss Distance Obtained by Addition of Five Ranging Measurements to Optical Angle System	2-64
2-17	Optical Ranging	2-66
2-18	Power Requirements for Ranging Off Lunar Surface for Various Antenna Sizes	2-67
3-1	Plan View of Lunar Flightpath	3-5
3-2	Celestial Sphere	3-10
3-3	Angle Between Star and Local Vertical	3-18
3-4	Schematic of Lunar Navigation Simulation	3-20
3-5	Total Position Uncertainty vs Time, Cases 1, 2, and 3	3-32

Figure		Page
3-6	Total Position Uncertainty vs Time, Case 4	3-34
3-7	Total Position Uncertainty vs Time, Cases 5 and 6	3-35
3-8	Total Position Uncertainty vs Time, Case 7	3-36
3-9	Total Position Uncertainty vs Time, Case 8	3-37
3-10	Total Position Uncertainty vs Time, Case 9	3-38
3-11	Final Miss Distance as a Function of Instrument Error and Measurement Frequency	3-39
4-1	Overall Navigation, Guidance, and Control System; Block Diagram	4-5
4-2	Landing Phase Geometry	4-10
4-3	Velocity-Acceleration Diagram of Landing Maneuver	4-12
4-4	Linearized Equations of Motion Used in Error Analysis; Block Diagram.	4-15
4-5	Linearized Navigation Equations: Block Diagram	4-18
4-6	Doppler Navigator Geometry	4-21
4-7	Linearized Guidance Equations; Block Diagram	4-24
4-8	Analytical Control Subsystem Model; Block Diagram	4-29
4-9	Linearized Navigation, Guidance, and Control System Model.	4-30
4-10	Equivalent Linearized System Model Actually Used for Error Analysis	4-31
4-11	Error Sensitivity Coefficients Relating Terminal Altitude Errors to Navigation Sensor Errors (Beacon Tracker Observables)	4-39
4-12	Error Sensitivity Coefficients Relating Terminal Central Angle Errors to Navigation Sensor Errors (Beacon Tracker Observables)	4-40
4-13	Error Sensitivity Coefficients Relating Terminal Velocity Errors to Navigation Sensor Errors (Beacon Tracker Observables)	4-41
4-14	Error Sensitivity Coefficients Relating Terminal Altitude Errors to Navigation Sensor Errors (Doppler Navigation Observables)	4-42
4-15	Error Sensitivity Coefficients Relating Terminal Central Angle Errors to Navigation Sensor Errors (Doppler Navigation Observables)	4-43

Figure		Page
4-16	Error Sensitivity Coefficients Relating Terminal Velocity Errors to Navigation Sensor Errors (Doppler Navigation Observables)	4-44
4-17	Error Sensitivity Coefficients Relating Terminal State Errors to Control Sensor Errors	4-45
4-18	Guidance Geometry	4-54
4-19	Acceleration Diagram	4-56
4-20	Geometry Pertinent to the MPN/VT-B Guidance Concept	4-60
4-21	Effect of Specific Impulse on Touchdown Mass	4-63
4-22	Comparative ΔV Requirements	4-81
4-23	Comparative ΔV Requirements (After Normalization)	4-82
5-1	Direct Ascent to Rendezvous	5-5
5-2	Parking Ascent to Rendezvous	5-6
5-3	Optimum Boost Geometry	5-11
5-4	Geometry of Boost Trajectory	5-12
5-5	Constant Thrust Optimized Lunar Ascent	5-13
5-6	Direct Ascent Nominal Boost Acceleration Profiles	5-15
5-7	Parking Ascent Nominal Boost Acceleration Profiles	5-16
5-8	Ascent Trajectory	5-20
5-9	Orientation of Inertial Sensors and Navigation Reference Frame	5-23
5-10	Position Errors at a 30-Kilometer Altitude Caused by Launch Site Location Uncertainties	5-29
5-11	Velocity Errors at a 30-Kilometer Altitude Caused by Launch Site Location Uncertainties	5-30
6-1	Phase Plane Representation of Longitudinal Control	6-4
6-2	Lunar Orbital Rendezvous	6-8
6-3	Rendezvous Guidance (Lunar Orbital Rendezvous)	6-10
6-4	Variation of Range With Transit Time	6-11
6-5	Variation of Elevation Angle With Transit Time	6-12
6-6	Longitudinal Control - Coarse	6-14
6-7	Longitudinal Control - Vernier	6-16

Figure		Page
6-8	Digital Data Smoother	6-18
6-9	Effect of Rendezvous Sensor Errors on Propellant Consumption	6-24
6-10	Effect of Initial Altitude Error on Propellant Consumption.	6-25
6-11	Effect of Initial Velocity Error on Propellant Consumption.	6-25
6-12	Effect of Initial Attitude Error on Propellant Consumption.	6-26
6-13	Effect of Initial Phasing Error on Propellant Consumption.	6-26
6-14	Rendezvous Phase Plane Illustrating Effect of Injection Errors	6-27
6-15	Variation in Elevation Angle With Range.	6-28

LIST OF TABLES

Table		Page
2-1	General Characteristics of Model Trajectories	2-6
2-2	Model for Analysis of Onboard Guidance Requirements	2-7
2-3	Ground Tracking Model for Analysis	2-7
2-4	Physical Constants	2-12
2-5	Computer Run Comparison	2-41
2-6	Standard Case Parameters	2-42
2-7	Initial Guidance Schedules	2-42
2-8	Results of Scheduling Runs	2-44
2-9	Improved Guidance Schedules	2-46
2-10	Effect of Correction Errors at Periselenum	2-51
2-11	Effect of Initial Errors at Periselenum	2-52
2-12	Effect of Landmark and Horizon Uncertainties at Periselenum	2-53
2-13	Effect of Flight Time on Guidance Performance	2-55
2-14	71.5-Hour Trajectory With ΔV_3 at 69.0 Hours	2-56
2-15	Astrodynamic Constant Uncertainties	2-58
2-16	Results Without Errors Compared to Compensated Errors (Ref. 2-7)	2-59
2-17	Results on 225-Measurement Schedule (Ref. 2-7)	2-59
2-18	Comparison of Single- and Double-Angle Measurements at Periselenum	2-61
2-19	Reduction in Miss Distance at Periselenum with Ranging Measurements	2-63
2-20	Effect at Periselenum of Ranging Measurements Near Periselenum	2-65
3-1	Navigation Stars	3-11
3-2	Standard Run Conditions	3-31
3-3	RMS Miss Distance Components at Periselenum (Meters) - Series B	3-40

Table		Page
3-4	RMS Miss Distance Components at Periselenum (Meters) - Series C	3-41
4-1	Mean Squared Terminal Errors Caused by Control Sensor Errors (Sample Computation, h_o = 20 km, τ_o = 1 sec)	4-46
4-2	Mean Squared Terminal Errors Caused by Navigation Sensor Errors (Sample Computation; Observables $R\ \dot{R}\phi\ \dot{\phi}$; h_o = 20 km; τ_o = 1 sec)	4-47
4-3	Mean Squared Terminal Errors Caused by Navigation Sensor Errors (Sample Computation; Observables $h\ \dot{R}_1\ \phi\ \dot{R}_2$; h_o = 20 km; τ_o = 1 sec)	4-48
4-4	Comparison of Mean Squared Terminal Errors Resulting From Beacon Tracking and Doppler Navigation Sensor Errors (Based on State of the Art Sensor Capability)	4-51
4-5	Typical Sensor Error Levels (Used for Sample Computation)	4-70
4-6	Results of Sample Computation for Showing Terminal Effects of Random Sensor Errors	4-72
4-7	Breakdown of Touchdown Errors Caused by Sensor Bias Errors	4-75
4-8	Touchdown Errors Caused by Engine Lag	4-77
4-9	Effect of Sensor Bias Errors and Engine Lags on Fuel Consumption. (As Measured by the Parameter ΔV.)	4-77
4-10	Maximum Touchdown Velocity (99 Percent Confidence Level)	4-78
4-11	Sensor Dynamic Range Requirements	4-79
4-12	Comparison of Terminal Errors	4-86
5-1	Optimized Boost Trajectory Parameters	5-14
5-2	Accelerometer Position and Velocity Errors for Direct Ascent	5-32
5-3	Gyro Position and Velocity Errors for Direct Ascent	5-33
5-4	Platform Position and Velocity Errors for Direct Ascent	5-34
5-5	Accelerometer Position and Velocity Errors for Parking Ascent	5-35
5-6	Gyro and Platform Position and Velocity Errors for Parking Ascent	5-36
5-7	3-σ Errors at Thrust Termination (30 Kilometers)	5-37

Table		Page
5-8	Sensors Specifications for Lunar Ascent Type-All Inertial, Space Stabilized Platform-All Sensors Orthogonally Oriented	5-37
5-9	Terminal Rendezvous Errors	5-39
6-1	Miss Distance Sensitivity Coefficients (30/200-km) Lunar Orbit Transfer	6-21
6-2	Injection Sensor Errors	6-27
6-3	Rendezvous Sensor Requirements	6-29
6-4	Injection Sensor Requirements	6-30

TABLE OF CONTENTS

Page

APPENDIX A
SYNOPSIS OF MATHEMATICAL TECHNIQUES

1. Introduction A-1
2. Characterization of Trajectories A-3
3. Preparation for Usage of System Equations A-6
4. Characterization of Random Variables A-10
5. Application of Analytical Model to Orbital Flight A-17
5.1 Navigation Data Processing by Least Squares A-18
5.2 Navigation Data Processing by Minimum Variances A-20
5.3 End Point Guidance With a Fixed Arrival Time A-26
6. Application of Linearized Analysis to Powered Flight A-29
6.1 Application of Adjoint Analysis to Guidance Law Determination. . A-29
6.2 Application of Adjoint Analysis to Sensor Error Evaluation A-34

APPENDIX B
MIDCOURSE PHASE

1. Computation of Transition Matrices B-5
2. Application of Kalman's Results B-7
3. Derivation of Relations Between State Variables and Observables. B-11
3.1 Angle Between Planet Center and Star Direction. B-11
3.2 Direct Range Measurements B-14
3.3 Range Rate Measurements B-15
3.4 Optical Ranging by Measurement of Planet Disc B-15
3.5 Star-Horizon Measurements B-16
4. Effect of Velocity Corrections on Estimation and Deviation Statistics B-17
5. Equations Used in Computer Programs B-22
5.1 Nominal Trajectory Program B-22

TABLE OF CONTENTS (Continued)

APPENDIX B (Continued)

		Page
5.2	Transition Matrix Program	B-24
5.3	Statistical Program	B-25
6.	Effect of Measurement Timing Errors	B-31
7.	Bias and Astrodynamic	B-33
8.	Change of Coordinate System	B-41
9.	Power and Antenna Size Requirements for Two-Way Microwave Ranging Off Lunar Surface	B-45
10.	Coordinate Rotation	B-50

APPENDIX C
LUNAR PARKING AND DESCENT ORBITS

1.	Determination of Nominal Flightpath	
2.	Typical Input Error Magnitudes	C-9
2.1	Thrust Tolerances	C-9
2.2	Initial Conditions	C-11
2.3	Measurement Errors	C-12
3.	Triaxial Lunar Oblateness (Ref. 5)	C-12
4.	State Transition Matrix	C-13

APPENDIX D
LUNAR LANDING ANALYSES

1.	Optimum Trajectory Program	D-3
1.1	Equations of Motion	D-3
1.2	Optimization of Pitch Program	D-6
1.3	Typical Optimum Trajectory Characteristics	D-9
2.	Line or Predictive Guidance	D-9
2.1	Navigation Equations	D-9
2.1.1	Beacon Tracking Navigation Equations	D-9
2.1.2	Doppler Navigation Equations	D-21
2.2	Gravity Turn Nominal Trajectory	D-26

TABLE OF CONTENTS (Continued)

APPENDIX D (Continued)

		Page
2.2.1	Trajectory Determination Program	D-26
2.2.2	Nominal Trajectory Characteristics	D-28
3.	Modified Proportional Navigation Guidance Law	D-41
3.1	Modified Proportional Navigation Guidance Digital Simulation	D-41
3.1.1	Coordinate Systems and Equations of Motion	D-41
3.1.2	Guidance Equations	D-44
3.2	A Modified Proportional Navigation Guidance System with a Vertical Landing Velocity Constraint	D-50
3.2.1	Derivation of Guidance Equations	D-51
3.2.2	Evaluation of Guidance Technique	D-57
3.3	Lunar Landing Tradeoffs and System Design	D-57
3.3.1	Assumptions	D-63
3.3.2	Determination of I_{sp}	D-63
3.3.3	Determination of Periselenum Altitude and Thrust Level	D-64
3.3.4	Selection of Guidance Technique	D-71
3.4	Lunar Landing Sensor Error Digital Program	D-80
3.4.1	Linearization of Kinematics and Control Equations	D-81
3.4.2	Adjoint Model	D-84
3.4.3	Nominal Solution	D-85
3.4.4	Method of Application	D-87

APPENDIX E
LUNAR ASCENT

1.	Error Equations for Guidance System	E-1
2.	Transfer Matrix	E-8
3.	Parking Orbit Initial Error Propagation	E-13
4.	Velocity Requirements Between Two Circular Co-Planar Orbits	E-14
5.	Parking Orbit Transfer Considerations	E-23

TABLE OF CONTENTS (Continued)

Page

APPENDIX F
LUNAR RENDEZVOUS

1.	Computer Simulation of Lunar Rendezvous Techniques	F-2
1.1	Initial Positioning of Target and Chaser	F-3
1.2	General Flow of the Program	F-4
1.3	Firing Laws	F-5
1.4	Corrections to Chaser Orbit for Firing.	F-8
1.5	Noise Generation and Smoothing	F-9
1.6	Corrections to Smoother Input for Firing.	F-10
1.7	Transformations between Selenocentric Coordinates and Orbital Elements	F-11
1.7.1	Selenocentric Rectangular Coordinates from Orbital Elements	F-12
1.7.2	Orbital Elements from Selenocentric Rectangular Coordinates	F-16
1.7.3	Solution of Kepler's Equation	F-18
2.	Inputs for Analysis of Lunar Ascent to Rendezvous	F-18

LIST OF ILLUSTRATIONS

Figure		Page
	APPENDIX B	
1	Geometry of Earth-Star Measurement	B-12
2	Planar Geometry of Star Horizon Angle Measurement	B-16
3	Geometry of Timing Errors	B-32
4	Illustration of Effect of Uncertainty in Moon's Position	B-43
5	Ranging Error Due to Curvature	B-46
6	Range Spreading Error as a Function of Range From Moon for 0.5 and 1 Degree Beams	B-48
7	Geometry of Coordinate Conversion From XYZ System to Altitude - Downrange-Crossrange System	B-51
8	Difference Between Real Error Distribution	B-54
	APPENDIX D	
1	Lunar Landing Geometry	D-4
2	Typical Optimum Pitch Programs	D-10
3	Typical Landing Trajectory Profile	D-11
4	Typical Landing Trajectory Profile	D-12
5	Typical Plots of Line-of-Sight Angular Rate, $\dot{\Omega}$ vs Time	D-13
6	Characteristic Velocity (ΔV) Required for Optimum Descent	D-14
7	Landing Phase Geometry	D-15
8	Vector Diagram of Landing Maneuver	D-17
9	Geometry of a Three-Beam Doppler System for Velocity Determination	D-22
10	Nominal Trajectory Characteristics, T_o and T_o/m_o vs h_o	D-31
11	Nominal Trajectory Characteristics, θ_o vs h_o	D-32

LIST OF ILLUSTRATIONS (Continued)

APPENDIX D (Continued)

Figure		Page
12	Nominal Trajectory Characteristics, t_f vs h_o	D-33
13	Nominal Trajectory Characteristics, h vs t	D-34
14	Nominal Trajectory Characteristics, θ vs t	D-35
15	Nominal Trajectory Characteristics, γ vs t	D-36
16	Nominal Trajectory Characteristics, V vs t	D-37
17	Nominal Trajectory Characteristics, $\dot{h}$ vs h	D-37
18	Nominal Trajectory Characteristics, h vs θ	D-39
19	Nominal Trajectory ΔV Requirements	D-42
20	Nominal Trajectory Fuel Consumption	D-43
21	Lunar Landing Geometry	D-45
22	Reference Coordinate System	D-51
23	Admissible Values for Guidance Parameters	D-56
24	Comparison of Analytical and Computer Results	D-58
25	Comparison of Analytical and Computer Results	D-59
26	Comparison of Analytical and Computer Results	D-60
27	Comparison of Analytical and Computer Results	D-61
28	Characteristic Velocity Required for Landing vs Periselenum Altitude	D-62
29	Touchdown Mass vs Fuel Specific Impulse	D-64
30	Spacecraft Altitude vs Distance to Horizon	D-66
31	Altitude at Which Landing Site in Located on the Horizon at Thrust Initiation vs Initial Thrust-to-Mass Ratio	D-67
32	Characteristic Velocity vs Initial Thrust-to-Mass Ratio	D-68
33	Touchdown Mass vs Initial Thrust-to-Mass Ratio	D-69
34	Touchdown Mass vs Initial Thrust-to-Mass Ratio	D-70
35	Comparison of Modified Proportional Navigation Trajectories With a Minimum Fuel Trajectory	D-75
36	Comparison of Thrust-Limited Modified Proportional Navigation Trajectory With an Optimum Trajectory	D-76

LIST OF ILLUSTRATIONS (Continued)

Figure		Page
	APPENDIX D (Continued)	
37	Comparison of Trajectories During Final Portion of the Landing Manuever	D-78
38	Adjoint System Block Diagram	D-86
	APPENDIX E	
1	Misalignment Angles of Accelerometer Input Axes	E-6
2	Gyroscope Orientation	E-7
3	Effect of Initial State Errors on Final State Position Errors for Near Circular Orbits	E-15
4	Effect of Initial State Errors on Final State Velocity Errors for Near-Circular Orbits	E-16
5	Tangential Capture for Transfer Between Circular Orbits	E-17
6	Total Required Velocity Increment for Minimum Energy Circle-to-Circle Transfer	E-20
7	Total Velocity Requirements vs Parking Altitude for Various Central Transfer Angles (200-km Target Orbit)	E-24
8	Percentage of Fuel Required for Transfer vs Parking Altitude for Various Central Transfer Angles (200-km Target Orbit)	E-26
9	Percentage of Fuel Required for Transfer vs Central Transfer Angle for Various Parking Altitudes (200-km Target Orbit)	E-27
10	Total Required Transfer Velocity Increment vs Parking Altitude for Various Central Transfer Angles (200-km Target Orbit)	E-28
	APPENDIX F	
1	Orbit Diagram - Lunar Orbit Rendezvous	F-4
2	Orientation of the Orbital Plane	F-14
3	Eccentric Anomaly and Focal Polar Coordinates	F-15

LIST OF TABLES

Table		Page
	APPENDIX D	
1	Trajectory Determination Input Conditions	D-29
2	Values of Computed Nominal Trajectory Parameters	D-30
3	Thrust to Mass Ratio	D-63
4	Comparison of Guidance System Performance	D-73
5	Comparison of Terminal Phase	D-79
	APPENDIX E	
1	Velocity and Position Integrals for Direct Ascent	E-3
2	Velocity and Position Integrals for Parking Ascent	E-4
	APPENDIX F	
1	Injection Sensor Requirements	F-19

SUMMARY

The following sections examine in turn the Midcourse, Lunar Parking and Descent Orbit, Lunar Landing, Lunar Ascent, and Lunar Orbit Rendezvous Phases of a typical manned (or unmanned) lunar mission. These mission phases are defined in the Part I, Problem Definition (Volume II). Detailed summaries of the analytical studies are presented in Volume I.

These phases are treated in detail, with a section for each phase, with each section divided into five subsections as follows:

- Introduction
- General Background: This section links the Part I and Part II reports.
- Analysis: This section describes the analytical effort and is, in turn, divided into two parts:
  - Background Analysis: Analytical sections that begin with the system concept generated in Volume II and result in a specific system model that can be used in the analysis of sensor errors.
  - Error Analysis: The techniques used, and their application to the problem of determining sensor error effects are discussed.
- Results: This section includes the presentations of numerical results obtained from the error analysis, as well as discussion and interpretation of these results with regard to sensor accuracy requirements. Where applicable, sample computations are included.
- Conclusions

The only major section that deviates appreciably from this format is Section 4 which deals with lunar landing. Here, two separate systems are analyzed independently; there are separate analysis, results, and conclusions subsections for each concept. The two concepts are then compared to the extent made possible by material developed in this report.

The successive mission phases are summarized, in order, in the subsequent paragraphs.

Section 2 examines the manned lunar Midcourse Phase beginning after injection into the earth-moon transfer orbit, and ending just prior to injection into a circular lunar parking orbit. Control during midcourse consists of a total of three corrective impulses at scheduled intervals during flight. A minimum variance data processing scheme operating on optically measured planet-star angles is used for navigation. The principal areas investigated are: observation scheduling; the effect of angle measurement accuracy on navigation and guidance system performance; the effect of velocity correction accuracy on guidance system performance; and the effect of trajectory variations on guidance system performance.

The following conclusions are drawn from the Midcourse Phase Analysis:

a. In general, observations should be made to a star in the trajectory plane, the primary factors determining final star selection being visibility and ease of recognition. The same star can be used for all in-plane measurements to a particular planet throughout most of the flight. The range of near-optimum measurement and correction schedules is found to be very broad.

b. Generally, terminal miss distance and fuel consumption increase sharply with increasing sensor error, while knowledge of the terminal error is degraded only slightly. Angle measurement accuracy on the order of 10 to 20 arc-sec 1σ is shown to be required for acceptable midcourse guidance and navigation.

c. Guidance system performance is shown to be relatively insensitive to velocity correction errors as compared to the sensitivity of performance to navigation sensor errors.

d. Increasing the magnitude of initial errors is found to increase correction fuel requirements, but have very little effect on terminal error statistics.

e. It is shown that variations in trajectory parameters, such as mission time, trajectory plane orientation, and periselenum altitude have some effect on guidance system performance, but these effects are minor compared to the performance sensitivity to navigation sensor errors.

f. The usefulness of range measurement capability for midcourse guidance is established. Preliminary investigation of basic sensor requirements indicates that they are severe.

Discussion concerning the Lunar Parking and Descent Orbit Phase is presented in Section 3. Immediately following the Midcourse Phase, the vehicle is injected into a circular lunar parking orbit. At some later time, all or part of the orbiting vehicle is injected into a synchronous, elliptical descent orbit with the periselenum at the desired point of Lunar Landing Phase initiation. Control during orbit consists of a thrust impulse at injection into the circular parking orbit, and a second impulsive maneuver to inject into the descent orbit. Navigation is performed by minimum variance data processing of observed data. A fixed time of arrival (FTOA) guidance is used for determining the descent orbit injection impulse. The observables considered are star angle measurements, referenced to local vertical, and attitude above the lunar surface. The problem is analyzed by linearized techniques, as well as by direct simulation of the nonlinear system, thereby establishing a basis for the evaluation of linearization error. The principal areas of investigation are: evaluation of the effects of navigation sensor errors on guidance system performance; evaluation of the minimum variance navigation technique; and determination of the required number and position of navigation stars.

The following conclusions are drawn from the Lunar Parking and Descent Orbit Phase Analysis:

a. Provided that the parking orbit has a duration of a half revolution or greater, it is permissible to limit the navigation observables to two or three known stars and the local vertical. A properly chosen set of three stars (two in the orbital plane and one near the pole of the orbit) provides navigation accuracy comparable to that obtainable with 57 navigation stars. Acceptable performance is also obtainable with two stars, both about 30 degrees out of the orbital plane.

b. Overhead stars (i.e., stars near the local vertical line) are not acceptable navigation stars.

c. The advantages of the star-vertical measurements are continuous accessibility (including the flight over the dark and unknown sides of the moon); low requirements for accompanying astrophysical data, power consumption, and field of view; insensitivity to lunar rotation; and ease of both manual and automatic implementation.

d. With direct radial position information (i.e., altitude measurements), the navigation errors can in some cases be reduced faster. Because of the prominence of tangential errors, however, no appreciable permanent improvement is achieved.

e. The measurement sensitivities and the state transition matrices used in the minimum variance equations must be computed from the updated trajectory estimate, rather than from a given nominal orbit.

f. With repeatedly updated Keplerian equations used for navigation, the observed trajectory takes the form of a time-varying conic. Because this is a valid representation of a perturbed orbit, and because actual navigation measurements include the effects of orbital perturbations, it is permissible to use two-body equations for navigation, even in the presence of perturbing forces.

g. Complete knowledge of the initial uncertainty covariance matrix is not necessary; a pessimistic, diagonal initial matrix leads to a conservative result. Since final navigation errors are insensitive to initial navigation errors, the result is only slightly pessimistic.

h. Measurement timing uncertainties on the order of tenths of a second have little effect upon navigation accuracy, in the cases under consideration here.

i. Additional sources of error, not treated in this analysis, have been covered in other related studies. Lack of precise knowledge of sensor error statistics is apparently not critical, and the effects of unknown measurement bias and astrodynamical uncertainties can be counteracted.

j. The simulation conducted here supports the principle that terminal navigation errors (i.e., state vector uncertainties) are insensitive to initial errors. The guidance errors (i.e., final miss vector components), however, are somewhat sensitive to initial conditions. The reason is traceable to trajectory modifications, necessitated by large displacements from reference position with fixed time guidance.

k. The total rms final miss distance is directly proportional to the rms measurement error, and to the square root of the time interval between successive measurements. The slope of this line, however, is somewhat sensitive to initial errors, as explained in the preceding statement.

Section 4 contains analysis of the Lunar Landing Phase. This is a powered phase beginning at periselenum of the synchronous descent orbit and terminating with the vehicle in a hover state at some arbitrary distance above the lunar surface. This arbitrary terminal altitude can be taken to be

zero; however, when it is not zero, the hover-to-touchdown maneuver is assumed to be under manual control. Navigation, guidance, and control are essentially continuous processes during the landing maneuver. Two navigation schemes are treated during the discussion, and are denoted as beacon tracking and doppler navigation respectively. The former is dependent on the presence of a beacon on the lunar surface, while the latter is not. Two guidance concepts are investigated in independent analyses. These concepts, termed linear predictive guidance and modified proportional navigation, are representative of two approaches to the guidance of powered flight as discussed in Volume II. The principal area of investigation with regard to each guidance concept is the evaluation of the effect of navigation and control sensor errors on overall guidance system performance. Both linearized and simulation analysis techniques are employed. The principal numerical results of both analyses are sensitivity coefficients which allow the determination of terminal error components caused by navigation and control sensor inaccuracies that exist during flight. (For a comparative discussion of the two approaches see subsection 4.4.)

Conclusions pertinent to the analysis of lunar landing using linear predictive guidance are:

a. Characteristics of terminal error distributions for any given group of sensors are highly dependent on which sensor is the dominant error source.

b. Generally, decreasing the bandwidth of the engine control subsystem results is increased terminal error statistics.

c. When state of the art sensor capabilities are assumed for both beacon tracking and doppler navigation schemes, doppler navigation results in smaller terminal errors.

d. Terminal position errors caused by navigation and control sensor inaccuracies are not serious, being on the order of a few meters (based on sample computations). The situation with regard to velocity errors is not so clear-cut. The landing mission profile as envisioned for this study is composed of two subphases: descent-to-hover and hover-to-touchdown. Linear predictive guidance is assumed to be used down to the hover point with some undefined guidance system controlling the hover-to-touchdown maneuver. For manned flights, this touchdown maneuver is considered to be under manual control. For this case, velocity errors of the magnitude indicated in tables 4-4 and 4-5 based on typical state of the art sensor accuracies are felt to be satisfactory. For the unmanned case, relaxed touchdown velocity requirements can be expected, so that the terminal (hover point) velocity errors resulting from state

of the art sensor capability are expected to be satisfactory even if the hover-to-touchdown guidance system offers no reduction of the velocity errors.

Conclusions pertinent to the analysis of lunar landing using modified proportional navigation guidance are:

a. A combination of two proportional navigation guidance laws provides a guidance concept which approaches an optimum fuel trajectory over most of the flight and then makes a vertical approach to touchdown.

b. Terminal vertical velocity errors are significant for all three assumed levels of sensor capability. Terminal altitudes, horizontal position, and horizontal velocity errors are not critical even at the highest level of sensor error assumed.

c. The most significant random error contributors to the terminal velocity error come from the range and line-of-sight angle observation sensors. (Beacon tracking navigation is used.)

d. Sensor bias errors contribute significantly to the terminal velocity error at all assumed error levels. Bias errors in the observation of range and range rate are the most critical.

e. The increase in fuel consumption caused by engine lag and sensor bias errors is not particularly significant. If high level bias errors in all observations are assumed to exist simultaneously, the increase in fuel consumption is approximately 1 percent of the nominal value.

Section 5 examines the Lunar Ascent Phase of the manned lunar mission. This is a powered phase wherein inertial guidance is employed. Because of choice of a self-contained inertial guidance package is obviously best if it is adequate to perform the task, an alternate choice is not considered. The principal area of investigation is the evaluation of the effects of navigation, guidance, and control sensor inaccuracies, as well as selenophysical uncertainties on the performance of the ascent guidance system. The principal results are tables of sensitivity coefficients which allow determination of terminal errors caused by sensor inaccuracies as well as several other error sources; namely: thrust termination errors, transfer errors, selenophysical uncertainties. Sensor errors are construed to mean error sources contained within the guidance system. For the inertial guidance scheme analyzed, the following error sources are evaluated: accelerometer errors; gyro errors; alignment errors; and computer errors. These sensitivity coefficients are

used to distribute the maximum allowable terminal errors (based on fuel considerations) among the error sources, thereby creating specific requirements (table 5-8).

The following conclusions are drawn from the Lunar Ascent Phase Analysis:

a. Sensor requirements for the Lunar Ascent Phase are within the present state of the art.

b. The difference between sensor requirements for direct ascent to rendezvous as opposed to an ascent involving an intermediate parking orbit are not sufficient to dictate the selection of one approach over the other.

c. The major portion of the velocity error at thrust termination is contributed by guidance system errors.

d. The major portion of the position error at thrust termination is contributed by uncertainty in the knowledge of launch site position.

e. Launch site uncertainties representing the maximum expected error in position coordinates do not present a major obstacle to lunar ascent guidance.

Finally, the Lunar Orbit Rendezvous Phase is examined in Section 6. At initiation of this phase, the chaser and target vehicles are assumed to be in approximately circular parking orbits. For analytical purposes, rendezvous is considered to terminate when the chaser target range is reduced to some preselected standoff value. The subsequent docking maneuver is assumed to be under manual control. All navigation, guidance, and control functions are performed on board the chaser vehicle. An on-off guidance logic based on switching boundaries established in the range versus range rate phase plane is used for terminal rendezvous maneuvering. The navigation observables used during active rendezvous are line-of-sight range, range rate, and angle rate to the target. The principal area of investigation is the evaluation of navigation and control errors on the performance of the rendezvous guidance system. The error analysis technique used is Monte Carlo simulation.

The following conclusions are drawn from the Lunar Orbit Rendezvous Phase Analysis:

a. Sensor requirements for rendezvous are within the present state of the art.

b. The injection and active rendezvous phases can be performed with sufficient accuracy to eliminate the need for a midcourse correction.

c. There is a direct relationship between sensor inaccuracies and fuel consumption.

In general, the analysis technique used for this study has been to select as basic, as simple, and as representative a system as possible to study with regard to sensor requirements. As a result, the sensor accuracies derived may, in general, be considered to be fundamental to the mission phase considered, rather than dependent upon the idiosyncrasies of a particular detailed mechanization assumed. It is believed that the work presented in this Part II document proves the feasibility and usefulness of this approach.

Sensor accuracy requirements are presented in sections of this report for a variety of initial and terminal conditions. In the lunar descent trajectory analysis, results are presented in the form of error coefficients, relating sensor accuracy to terminal errors. For this phase a particular set of sensor accuracies may be assumed, and an approximation to the terminal errors can be obtained by multiplying the assumed sensor errors by the appropriate coefficients and adding, in rms fashion, the results for each component of terminal error.

1. INTRODUCTION

This document presents the Analytical Solution to the specific problem defined in Volume II; i.e., to determine navigation and control sensor requirements for local, or onboard guidance of manned or unmanned lunar missions. The material presented herein is a compilation of the Analytical Solutions generated under independent, but parallel investigations performed by the Westinghouse Electric Corporation and the Raytheon Company.

In the era of interest (post-Apollo), a wide variety of space missions are considered to be feasible. To ensure that the study effort is expended most profitably, an order of mission priority is established in Volume II with the aid of NASA. Manned lunar missions are given the highest priority, followed by earth space station, unmanned lunar, and interplanetary missions in descending order. The analysis pertaining to earth orbital rendezvous, which presents the principal navigation and control problem associated with an earth orbiting space station, is presented separately in Volume IV. Thus, the material presented in this volume deals almost exclusively with navigation and control aspects of lunar missions, with the emphasis on manned lunar missions.

The Apollo mission profile is used as an example of a typical manned lunar mission. The total Apollo missions can be visualized as a sequence of mission phases: earth launch and midcourse injection; earth-moon transfer (midcourse); lunar orbit; lunar landing; lunar ascent; lunar orbit rendezvous; a second midcourse phase; and atmospheric reentry. The analyses reported in this volume examine the problem of sensor inaccuracies in each of these mission phases except the first (earth launch) and the last (atmospheric reentry), which are omitted from this study because of the extent of prior investigations in these areas. Much of the material presented is also directly applicable to unmanned lunar missions. This is most true of mission phases which take place in the vicinity of the moon; e.g., lunar orbit and lunar landing.

All of the navigation and control techniques investigated are considered to be onboard systems; i.e., they do not make use of earth-based communication or computer facilities. It is considered that investigation of earth-based navigation and control techniques as typified by DSIF would represent an unwarranted duplication of effort.

The intent of this study is to investigate navigation and control sensor accuracy requirements in as objective a manner as possible. Thus, the navigation and control systems used are defined only in as much detail as is required to allow determination of the effects of sensor inaccuracies. Consideration of system mechanization is kept to a minimum.

The general analytical approach is to ascertain the navigation and control system performance degradation that occurs when sensor inaccuracies are introduced. The measures of system performance used most often are terminal position and velocity error, and fuel consumption. Then, sensor accuracy requirements are generated on the basis of allowable performance degradation.

2. MIDCOURSE GUIDANCE

2.1 INTRODUCTION AND OUTLINE

In this section, system requirements are developed for onboard guidance of a manned space vehicle on a lunar mission. In addition, the general principles of space navigation on ballistic trajectories are discussed to clarify some simple concepts which have been obscured by advanced mathematics in other papers on midcourse guidance.

Subsection 2.2 gives a general description of the midcourse guidance mission and also includes the qualitative problem definition from Volume II. Subsection 2.3 contains the analysis, and in paragraph 2.3.1 a quantitative definition of the problem is given. This paragraph also includes derivation of equations representing guidance systems and four typical midcourse trajectories. In paragraph 2.3.2, the equations which are used for statistical analysis of the guidance system are developed. Paragraph 2.3.3 describes the digital computer program used for this statistical analysis and paragraph 2.3.4 includes a discussion of various types of measurements and measurement errors.

Subsection 2.4 presents the results of the midcourse analysis. These results include a general discussion of the scheduling problem for low data-rate navigation systems. General principles of space navigation are presented in paragraph 2.4.1. In paragraph 2.4.2, a standard midcourse guidance schedule is developed as a base for comparison and in paragraph 2.4.3, the results of using the computer program to vary parameters of the onboard system model are given. In paragraph 2.4.4, the effects of varying nominal trajectory parameters such as flight time and target altitude are investigated. In paragraph 2.4.5, pertinent error sources not included in the computer program are discussed, and results from other studies are extrapolated to the onboard system analyzed here. In paragraph 2.4.6, the results of trying systems other than the basic onboard optical system are given. Included in this paragraph is a brief comparison of onboard and ground-tracking systems. Statistical quantities are 1σ unless otherwise stated.

The conclusions drawn from the analysis are given in subsection 2.5.

The following list of symbols defines the notation used in this section:

SUMMARY OF NOTATION

R	Range from planet center
μ_e, μ_m, μ_s	Gravitation constants of earth, moon, sun
X, Y, Z	Spacecraft position components
X_m, Y_m, Z_m	Moon position components (in earth-centered nonrotating cartesian coordinate system)
t	Time
t_o	Time of launch into lunar trajectory
ψ_o	Longitude of moon at t_o measured in lunar orbit plan positive from the ascending line of nodes
ϕ	Inclination of lunar orbit with respect to earth's equator
r_e, r_m	Earth and moon radii
T	Orbital period of moon
$\Delta X, \Delta Y, \ldots$ etc	Deviations of spacecraft trajectory from nominal trajectory
$\underline{x}(t)$	Six component state vector whose components are ΔX, ΔY $\ldots \Delta \dot{Z}$
$F(t)$	Time-varying matrix composed of partial derivatives from nominal trajectory
$\Phi(t, t_o)$	Transition matrix which relates state deviations to t to state deviation at t_o
$E(\ )$	Expected value
$\underline{y}(t)$	Measurement (may be vector or scaler)
$H(t)$	Matrix relating observables to state variables
$\underline{n}(t)$	Measurement noise
$\underline{u}_n(t)$	Gaussian noise which is forcing function in measurement noise process
$B(t)$	A matrix related to measurement noise process
$\Phi_n(t)$	Transition matrix of noise process
$M(t)$	Augmented H-matrix
$\Phi^*(t_2, t_1)$	Superscript (*) used to denote that augmented state vector $\underline{x}^*$ is being considered. Also $\hat{\underline{x}}^*$, P^*, K^*, Q^*
$P(t)$	Covariance matrix of estimation errors

$K(t)$	Weighting matrix, used to weight each new observation
$\underline{\tilde{x}}$	Error in the estimate of $\underline{x}$
$\underline{\hat{x}}$	Estimate of $\underline{x}$
Q	Variance of measurement errors
ζ	Measured angle between star and earth or moon reference point
$A_i(t_k)$	3 x 3 submatrix of $\Phi(t_A, T_k)$ where t_A is the nominal time of arrival at periselenum
O_{ij}	i x j null matrix
I_{ii}	i x i unit matrix
$\underline{\Delta}v$	Commanded velocity vector
$\underline{\epsilon}$	Error in applying velocity correction
C	Convariance matrix of errors in measuring the velocity correction
G'	Matrix relating estimated state to commanded correction velocity
N	Covariance matrix of expected trajectory deviations
V	Covariance matrix of velocity corrections
S'	Covariance matrix of errors in applying the velocity corrections
σ_k^2	Variance of errors in percentage magnitude of applied velocity
σ_ϵ^2	Variance of errors in magnitude of applied velocity correction due to pulse timing errors
σ_γ^2	Variance of errors in pointing direction of velocity correction vector
u (or Δv)	RMS velocity correction magnitude
$\sigma_x^2, \sigma_y^2, \ldots \sigma_z^2$	RMS values of trajectory deviations in each component
$\sigma_{\tilde{x}}^2, \sigma_{\tilde{y}}^2, \ldots \sigma_{\tilde{z}}^2$	RMS values of estimation errors in each component
$Tr(\ )$	Trace of a matrix (sum of its diagonal terms)
σ^2	Variance of optical instrument error
k_i^2	Variance of error in defining reference point on earth (i=1) or moon (i=2)

$\underline{S}$	Unit vector in direction of star used for angle measurement
θ	Half-subtended angle formed by planet disc
ζ_h	Measurement of star elevation from near horizon
ζ_f	Measurement of star elevation from far horizon
a, b, c	Direction cosines of measurement star; i.e., components of $\underline{S}$
s	Range from spacecraft to horizon
$\sum \Delta v$	Sum of rms correction velocities required during flight
r	RMS position deviation from nominal at t_A (nominal time of periselenum)
v	RMS velocity deriation from nominal at t_A
$\tilde{r}$	RMS error in position estimate at t_A
$\tilde{v}$	RMS error in velocity estimate at t_A
E, M	Earth, moon (in schedule tables)
a, d	Azimuth, declination measurements (in schedule tables)
J_1	First harmonic in earth's gravitational potential field

2.2 BACKGROUND FROM VOLUME II

2.2.1 Discussion of Midcourse Trajectories

The Midcourse Phase is here defined as that portion of a lunar mission between ejection from earth orbit into a lunar trajectory and retrothrust into a lunar orbit or direct descent. A typical earth-moon trajectory is shown in figure 2-1.

The space vehicle is accelerated by rocket engines until it achieves near-escape velocity at a point about 175 degrees from the predicted earth-moon line at arrival. The vehicle is then allowed to coast on a long earth-centered elliptical trajectory whose major axis is about twice the earth-moon distance. As the vehicle approaches the lunar gravitational sphere of influence, the trajectory is gradually perturbed and the vehicle goes into a moon-centered hyperbolic trajectory. If a large retrothrust is initiated as the vehicle passes close by the moon, a lunar orbit can be achieved.

The trajectory shown in figure 2-1 is typical of the type of trajectory which can be used to achieve a lunar orbit. This trajectory is circumlunar; i.e., if no retrothrust at the moon is made, the vehicle will return to the vicintiy of the earth.

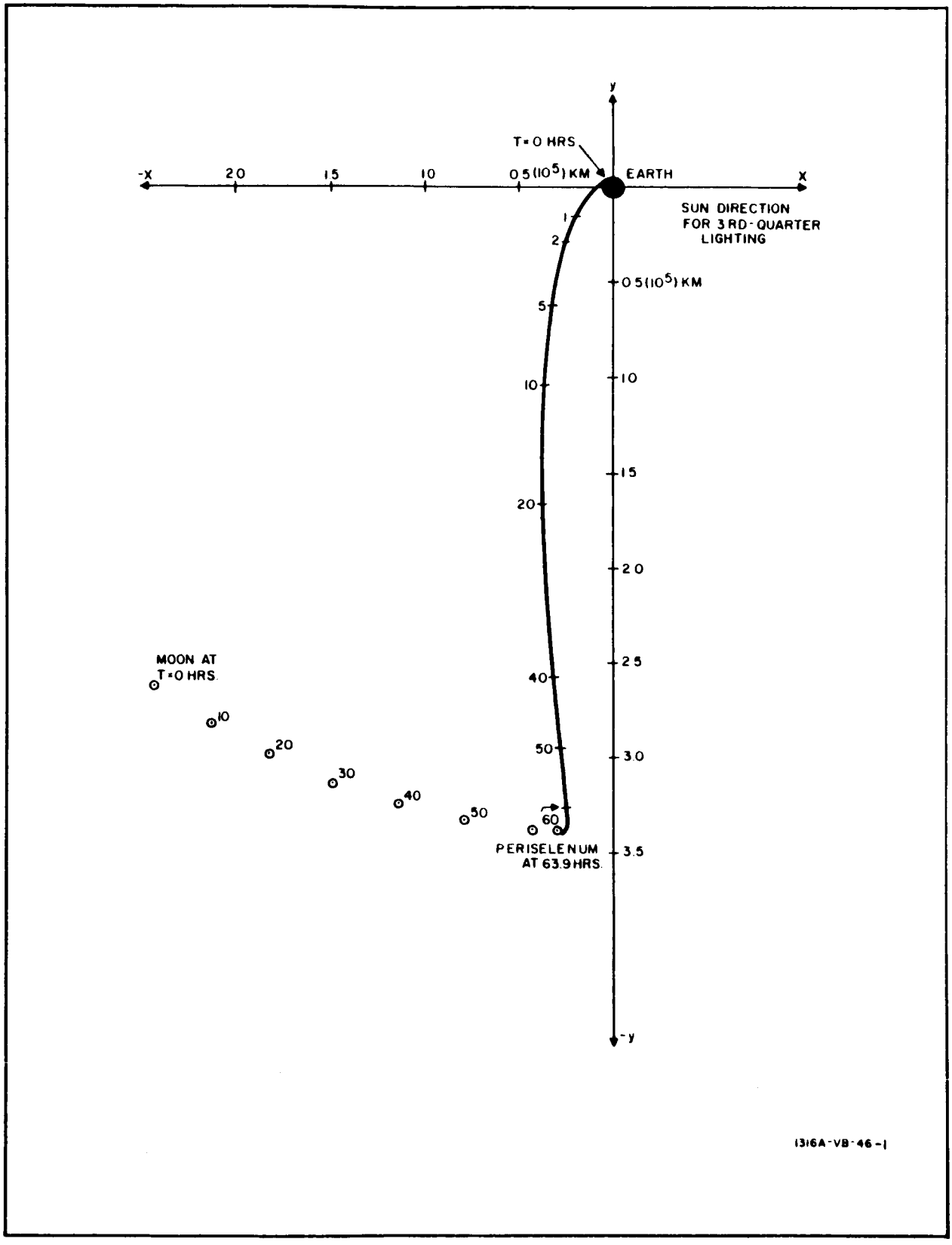

Figure 2-1. Geometry of Midcourse Guidance

2.2.2 Qualitative Problem Definition

In Volume II, Section 4, the guidance problem for the Midcourse Phase is stated as follows:

"Determine the guidance system requirements and techniques necessary to achieve the guidance of a manned space vehicle to a preselected point above the lunar surface with a velocity such that appropriate landing techniques may be used. The following constraints are imposed on this guidance system: Near-minimum fuel expenditure, reliability consistent with manned operation, and compatibility with predicted post-Apollo launch and spacecraft equipment."

To determine system requirements for midcourse guidance, models for analysis are generated in a qualitative way in Volume II. These models consist of a nominal trajectory and a hypothetical guidance system. The general characteristics of the models chosen are listed in tables 2-1 (trajectory models), 2-2, and 2-3 (system models) and are discussed in the following paragraphs.

In table 2-1, four earth-moon trajectories are listed. These trajectories were chosen so that their features would illustrate the effects of different nominal trajectories on guidance system requirements.

Trajectory I is representative of a typical trajectory for a manned lunar mission and has parameters similar to those proposed for the first Apollo mission. This trajectory is the one on which most of the analytical results in this study are based, and other trajectories are used for comparison.

TABLE 2-1

GENERAL CHARACTERISTICS OF MODEL TRAJECTORIES

Trajectory No.	Characteristics
I	In-lunar-plane launch from 185-km earth parking orbit to 200-km periselenum in 72 hr. Arrival near maximum declination of moon.
II	Same as trajectory I, except that flight time is 63.9 hours to a 133-km periselenum.
III	Same as trajectory I, except that trajectory plane is tilted 27.5 degrees to lunar orbit plane and vehicle arrival occurs at 0-degree declination (descending)of moon.
IV	Same as trajectory I, except that periselenum altitude is 100 km.

TABLE 2-2

MODEL FOR ANALYSIS OF ONBOARD GUIDANCE REQUIREMENTS

Item	Description
Observables	Single angle between star direction and landmark or horizon on earth or moon.
Sensor device	Onboard optical instrument.
Navigation method	Use of minimum variance technique to statistically weight data. Use of linearized deviations about reference trajectory.
Guidance logic	Fixed time of arrival.
Control mechanization	High-thrust rocket motor.
Control command monitoring	Onboard accelerometers (3-axis).

TABLE 2-3

GROUND TRACKING MODEL FOR ANALYSIS

Item	Description
Stations	(3) Johannesburg, Rosman, Carnarvon, (6) Johannesburg, Rosman, Carnarvon, Hawaii, Houston, and Madrid
Observables	Transponder range and range rate
Accuracies	10 meters - 24 meters (1 σ range accuracy)
Data rates	0.077-0.237 m/sec (1 σ range rate accuracy) (1 pt/min and 1 pt/10 min)

Trajectory II is used to determine the effects of quicker flight times and the attendant higher velocities. Trajectory III is used to determine the effect of an out-of-plane (of the lunar orbit) flight. Trajectory IV is used to determine the effect of changes in the periselenum (point of lunar close approch) altitude.

In Volume II, Section 4, it is shown that all reasonable midcourse navigation schemes can be classed under the three general headings of ground tracking, onboard passive methods, and onboard active methods and that onboard active methods are not considered because of their large power requirements. Therefore, this analysis is concerned with ground tracking and onboard passive methods with emphasis on the latter since the capabilities of ground tracking systems have been thoroughly investigated and reported by the Jet Propulsion Laboratory.

Tables 2-2 and 2-3 describe the characteristics of the onboard optical angle-measuring system and the ground tracking system assumed as navigation system models in this study. The ground tracking system model was taken from Ref. 2-1, which was used as a reference for comparison of onboard and ground-tracking results. Figure 2-2 illustrates the type of angle measurements made in the onboard system model. In the figure, it can be seen that each observation consists of the measurement of the angle between some star direction and some reference point on the earth or moon, either a landmark (at close ranges) or the horizon (at long ranges or when surface features are not visible).

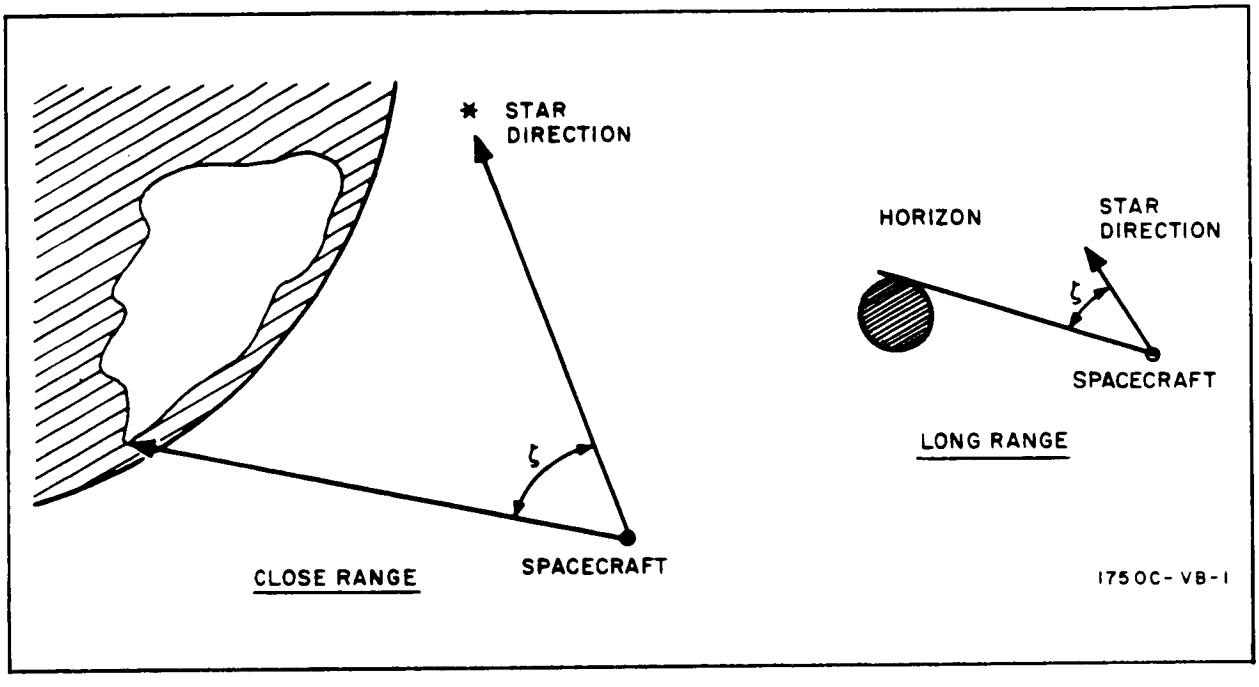

Figure 2-2. Angle Measurements for Onboard System Model

A summary of the characteristics chosen for the onboard system model is given in table 2-2. The feasibility of using single-angle measurements (i.e., sextant-type measurements) was shown by Battin (Ref. 2-2). Although single-angle measurements are considered the principal type of observable in this study, double-angle (theodolite) results are also studied for comparison. It is assumed that each measurement is taken by a human operator, but this is not necessary.

The navigation computation method used consists of the minimum variance method. This method uses partial orbital data, such as the angular measurements, to update the trajectory estimate by means of a linearized recursive procedure wherein each observation is statistically weighted according to

the a priori estimate of measurement error and trajectory estimation uncertainty. The advantages of this process are:

a. It gives a minimum variance estimate of the trajectory, utilizing all information available.

b. It is a recursive procedure, so that previous measurements need not be stored.

Fixed time of arrival (FTOA) guidance logic is used to compute commands for the high-thrust velocity correction motor, the performance of which is monitored by a 3-axis accelerometer system. FTOA, though not necessarily most economical, is a reasonable guidance method for lunar missions because of the relatively small corrections required during midcourse (~25 m/sec for three corrections).

In table 2-3, characteristics of the ground tracking model used in this study are given. Everything about this system (navigation computations, guidance laws, and mechanization) is identical to the onboard case except for the observables. For ground tracking, the observables consist of the range, range rate, and angle measurements obtained at the tracking stations listed in table 2-3.

2.3 ANALYSIS

2.3.1 Quantitative Problem Definition

The qualitative problem definition in paragraph 2.2.2 consists of trajectory models and guidance system models. To define the guidance problem quantitatively, specific trajectories must be generated, and equations describing the operation of the guidance system models must be written. In paragraph 2.3.1.1, the equations used for trajectory generation are derived and numerical values for the astronomical constants used in this study are given. In paragraph 2.3.1.2, the fundamental guidance problem is discussed; in paragraphs 2.3.1.3 and 2.3.1.4, equations describing the spacecraft navigation and guidance systems are developed.

2.3.1.1 Trajectory Computation

The astronomical model assumed in this (midcourse) study consists of a spherical homogeneous earth and moon and their gravitational potential fields. Although on an actual mission at least the sun's gravitational field and the first term in the earth's oblateness must be considered, these are not necessary for a parametric analysis of guidance requirements. In other words, the astronomical model assumed here results in a gravitational field

which is similar to that which actually occurs, as far as its effect on spacecraft position and velocity is concerned. In addition to this approximation to the actual potential field, the moon's motion about the earth is assumed to be circular rather than slightly elliptical as in the real case. Again, this is not expected to have much effect as the moon travels only 30 to 40 degrees around the earth during a lunar flight; over this short arc, the circular approximation is reasonable.

Since velocity corrections during the Midcourse Phase of a lunar mission are brief, it can be assumed that the spacecraft is in free-flight, throughout most of the flight; i. e., it is acted upon only by gravitational forces. The restricted equation of motion for a particle in space acted upon by n gravitational bodies is (Ref. 2-3):

$$\ddot{R}_{vr} = -\frac{\mu_r \underline{R}_{vr}}{\left|\underline{R}_{vr}\right|^3} - \sum_{\substack{i=1 \\ i \neq r}}^{n} \mu_i \left[\frac{\underline{R}_{vi}}{\left|\underline{R}_{vi}\right|^3} - \frac{\underline{R}_{ri}}{\left|\underline{R}_{ri}\right|^3}\right] \tag{2-1}$$

where $\underline{R}$ is the position vector, μ_i is the gravitational constant of the ith planet and the subscripts v and r refer to the vehicle and the planet at which the reference coordinate system is located.

Assume an earth-centered nonrotating coordinate system as shown in figure 2-3 where the Z-axis is along the earth's north pole. The position of the space vehicle and the moon are (X, Y, Z) and (X_m, Y_m, Z_m) respectively. With this coordinate system and the assumptions of only earth and moon gravity and the moon moving in a circular path about the earth, equation 2-1 can be written in three components as follows:

$$\ddot{X} = -\frac{\mu_e X}{R_e^3} - \frac{\mu_m}{R_{vm}^3}(X - X_m) - \frac{\mu_m X_m}{R_m^3} \tag{2-2}$$

$$\ddot{Y} = -\frac{\mu_e Y}{R_e^3} - \frac{\mu_m}{R_{vm}^3}(Y - Y_m) - \frac{\mu_m Y_m}{R_m^3}$$

$$\ddot{Z} = -\frac{\mu_e Z}{R_e^3} - \frac{\mu_m}{R_{vm}^3}(Z - Z_m) - \frac{\mu_m Z_m}{R_m^3}$$

where

$$R_e = \sqrt{X^2 + Y^2 + Z^2}$$

$$R_m = \sqrt{X_m^2 + Y_m^2 + Z_m^2}$$

$$R_{vm} = \sqrt{(X - X_m)^2 + (Y - Y_m)^2 + (Z - Z_m)^2}$$

and μ_e and μ_m are the gravitational constants of the earth and moon, respectively.

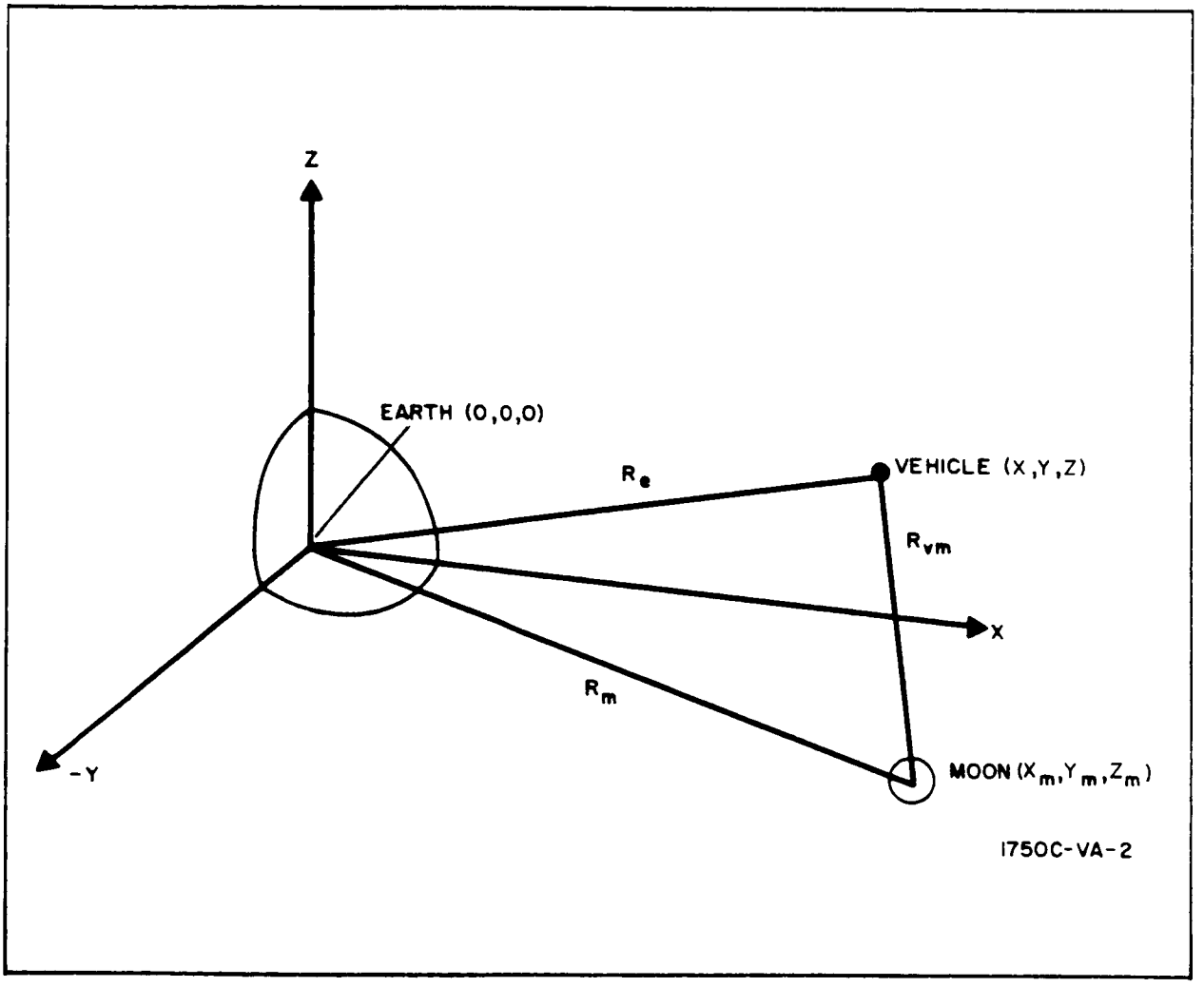

Figure 2-3. Earth-Centered Coordinate System

The moon's rotation about the earth is described by:

$$X_m = R_m \cos\left[\frac{2\pi\,(t - t_o)}{T} + \psi_o\right] \tag{2-3}$$

$$Y_m = R_m \sin\left[\frac{2\pi (t - t_o)}{T} + \psi_o\right] \cos \phi$$

$$Z_m = R_m \sin\left[\frac{2\pi (t - t_o)}{T} + \psi_o\right] \sin \phi$$

where R_m is the earth-moon distance, ϕ is the inclination of the lunar orbit plane to the earth's equator, T is the lunar orbital period, and ψ_o is the angle between moon's ascending line of nodes (0 degree declination) and the earth-moon line at $t = t_o$ (time of injection into the lunar midcourse trajectory).

Thus, the motions of the spacecraft and the moon in the earth-centered coordinate system are completely specified by equations 2-2 and 2-3. Equations 2-2 are nonlinear differential equations to which there is no known general solution. However, solutions to these equations may be obtained for any time point by specifying six initial conditions and integrating the equations by numerical techniques. In this way, the time history of the vehicle's position and velocity can be generated.

Thus, for the model chosen, the vehicle trajectory can be completely determined by specifying the initial conditions X_o, Y_o, Z_o, $\dot{X}_o$, $\dot{Y}_o$, $\dot{Z}_o$, and ψ_o at time $t = t_o$ and the constants μ_e, μ_m, T, ϕ, and R_m. The values used in this study for these constants and the radii of the earth and moon are listed in table 2-4.

TABLE 2-4

PHYSICAL CONSTANTS

Quantity	Symbol	Value
Earth-moon distance	R_m	382,830 km
Inclination of moon's orbit	ϕ	27.55 degrees
Lunar period	T	2.3587 (10^6) sec (27.3 days)
Earth gravitational constant	μ_e	3.986135 (10^{14}) m^3/sec^2
Lunar gravitational constant	μ_m	4.8982 (10^{12}) m^3/sec^2
Earth radius	r_e	6378 km
Moon radius	r_m	1738 km

A digital computer program was written to solve equations 2-2 for various trajectories. This computer program is described in paragraph 2.3.3.

2.3.1.2 Midcourse Guidance Problem

Present-day launch and injection equipment is not sufficiently accurate to deliver a space vehicle to the vicinity of the moon with the precision required on a manned mission. Thus, some trajectory corrections will be required

during the flight to reduce the miss distance from thousands of kilometers (with no corrections) to several kilometers. The first correction, normally made 10 to 15 hours after injection, removes most of the launch errors and succeeding velocity changes are vernier corrections on the previous maneuver. Information for making each of the velocity corrections is obtained by revising the trajectory estimate according to the data measured during the flight.

Figure 2-4 is a functional block diagram of a generalized space guidance system. Observations of the vehicle's translational state (position and velocity) are used to revise the original trajectory estimate and produce an improved estimate of the vehicle's trajectory. This improved estimate is then used to generate velocity correction commands which will reduce the predicted miss distance. The velocity corrections can be monitored by additional sensors (accelerometers) to evaluate the accuracy of each velocity change and thereby make a more precise trajectory estimate.

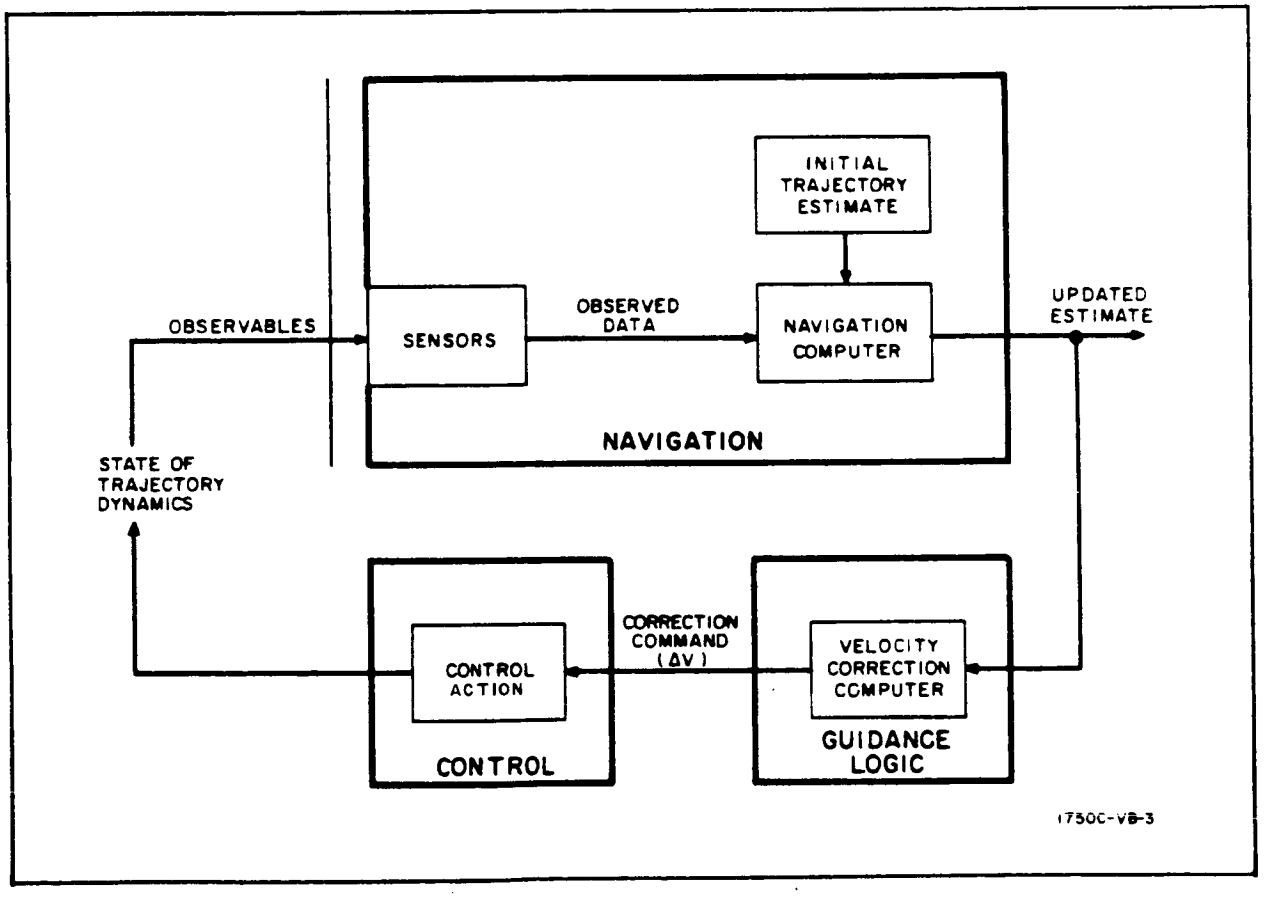

Figure 2-4. Functional Block Diagram of Space Guidance System

Figure 2-4 shows that the guidance system is actually a feedback control system. However, during the Midcourse Phase, the control action is so brief that the system is actually operating open-loop most of the time.

Since this is the case, the navigation (estimation) and guidance-logic and control aspects of the problem can be analyzed independently. This was the procedure actually adopted during this study.

2.3.1.3 Navigation Equations

The navigation problem for the Midcourse Phase can be stated as follows: Given some initial estimate of the vehicle's translational state (position and velocity) at $t = t_o$ and some noisy observations of the vehicle's state in the time interval $t = [t_o \text{ to } t_k]$, what is the best estimate of the vehicle's state at $t = t_k$ and its future state $(t > t_k)$? This problem has been solved for space trajectories by the Weighted Least Squares data processing technique, in which the a posteriori distribution of injection conditions is maximized for the data points received. A difficulty involved in using this technique is that it is required to invert a matrix whose rows are equal to the number of measurements taken; i.e., the total set of observed data is used on each estimate.

The minimum variance technique, applied to space navigation in 1961 to 1962 by G.S. Smith, S. Schmidt, et. al. at Ames Research Center avoids this problem through use of a recursive technique for generating the minimum variance weighting coefficient at each observation. Thus, only the latest trajectory estimate and the most recent observation are required to generate the new estimate. In addition, the minimum variance technique incorporates the a priori estimate of the observation error, as does the Weighted Least Squares process. In fact, the two processes give the same results, under certain conditions, but the computational simplicity of the minimum variance equations has led to their use in this study.

The following analysis is devoted to deriving the minimum variance equations for orbit determination. All this work was originally reported in Ref. 2-4, but since the treatment in that paper divides the derivation between the appendix and text and since several steps are omitted, it is repeated here.

To apply the minimum variance technique, it is necessary to linearize the equations describing the vehicle motion (equation 2-2) since the technique was developed for application to linear systems. Writing equations 2-2 in symbolic form:

$$\begin{aligned} \ddot{X} &= f_1 (X, Y, Z, t) \\ \ddot{Y} &= f_2 (X, Y, Z, t) \\ \ddot{Z} &= f_3 (X, Y, Z, t) \end{aligned} \qquad (2\text{-}4)$$

The usual technique is to utilize linear difference equations in terms of the deviations from some reference trajectory, rather than the actual coordinates. Letting X_R, Y_R, Z_R represent the coordinates on the reference trajectory and performing a Taylor series expansion on equation 2-4 at some time t there is:

$$(\ddot{X} + \Delta\ddot{X}) = f_1 + \left(\frac{\partial f_1}{\partial X}\right) \Delta X + \left(\frac{\partial f_1}{\partial Y}\right) \Delta Y + \left(\frac{\partial f_1}{\partial Z}\right) \Delta Z + \text{H.O.T.} \tag{2-5}$$

$$(\ddot{Y} + \Delta\ddot{Y}) = f_2 + \left(\frac{\partial f_2}{\partial X}\right) \Delta X + \left(\frac{\partial f_2}{\partial Y}\right) \Delta Y + \left(\frac{\partial f_2}{\partial Z}\right) \Delta Z + \text{H.O.T.}$$

$$(\ddot{Z} + \Delta\ddot{Z}) = f_3 + \left(\frac{\partial f_3}{\partial X}\right) \Delta X + \left(\frac{\partial f_3}{\partial Y}\right) \Delta Y + \left(\frac{\partial f_3}{\partial Y}\right) \Delta Z + \text{H. O. T}$$

where $\Delta X = (X - X_R)$, $\Delta Y = (Y - Y_R)$, etc, the partials are evaluated on the reference trajectory at time = t and H.O.T. = higher order terms. Subtracting equation 2-4 form 2-5 and ignoring the higher-order terms:

$$\Delta\ddot{X} = \left(\frac{\partial f_1}{\partial X}\right) \Delta X + \left(\frac{\partial f_1}{\partial Y}\right) \Delta Y + \left(\frac{\partial f_1}{\partial Z}\right) \Delta Z \tag{2-6}$$

$$\Delta\ddot{Y} = \left(\frac{\partial f_2}{\partial X}\right) \Delta X + \left(\frac{\partial f_2}{\partial Y}\right) \Delta Y + \left(\frac{\partial f_2}{\partial Z}\right) \Delta Z$$

$$\Delta\ddot{Z} = \left(\frac{\partial f_3}{\partial X}\right) \Delta X + \left(\frac{\partial f_3}{\partial Y}\right) \Delta Y + \left(\frac{\partial f_3}{\partial Z}\right) \Delta Z$$

where equations 2-6 are now linear in the difference quantities ΔX, ΔY, and ΔZ. To write equation 2-6 in standard matrix form, define the deviation state vector $\underline{x}$ as the 6-vector whose elements are ΔX, ΔY, ΔZ, $\Delta\dot{X}$, $\Delta\dot{Y}$, $\Delta\dot{Z}$. Then:

$$\dot{\underline{x}} = \begin{bmatrix} \Delta\dot{X} \\ \Delta\dot{Y} \\ \Delta\dot{Z} \\ \Delta\ddot{X} \\ \Delta\ddot{Y} \\ \Delta\ddot{Z} \end{bmatrix} = \begin{bmatrix} 0 & 0 & 0 & 1 & 0 & 0 \\ 0 & 0 & 0 & 0 & 1 & 0 \\ 0 & 0 & 0 & 0 & 0 & 1 \\ \frac{\partial f_1}{\partial X} & \frac{\partial f_1}{\partial Y} & \frac{\partial f_1}{\partial Z} & 0 & 0 & 0 \\ \frac{\partial f_2}{\partial X} & \frac{\partial f_2}{\partial Y} & \frac{\partial f_2}{\partial Z} & 0 & 0 & 0 \\ \frac{\partial f_3}{\partial X} & \frac{\partial f_3}{\partial Y} & \frac{\partial f_3}{\partial Z} & 0 & 0 & 0 \end{bmatrix} \begin{bmatrix} \Delta X \\ \Delta Y \\ \Delta Z \\ \Delta\dot{X} \\ \Delta\dot{Y} \\ \Delta\dot{Z} \end{bmatrix} \tag{2-7}$$

Writing this as a matrix equation:

$$\dot{\underline{x}}(t) = F(t)\,\underline{x}(t) \tag{2-8}$$

where $F(t)$ and $\underline{x}(t)$ are defined in equation 2-7. Equation 2-8 is the matrix differential equation representing the linearized equations of motion of the spacecraft.

It is known (e.g., Ref. 2-5) that an equation of the following form:

$$\dot{\underline{x}}(t) = F(t)\,\underline{x}(t) + G(t)\,\omega(t) \tag{2-9}$$

has as its general solution:

$$\underline{x}(t + \Delta t) = \Phi(t + \Delta t,\ t)\,\underline{x}(t) + \int_t^{t+\Delta t} \Phi(t, \tau)\, G(\tau)\, \omega(\tau)\, d\tau \tag{2-10}$$

where $\Phi(t, t_o)$ is defined by $\dot{\Phi} = F(t)\,\Phi$ and $\Phi(t_o, t_o) = I$.

Therefore, the general solution to equation 2-8 is:

$$\underline{x}(t + \Delta t) = \Phi(t + \Delta t,\ t)\,\underline{x}(t) \tag{2-11}$$

since the forcing function, $\omega(t) = 0$.

Equation 2-11 shows how, in the absence of any input, the state deviation vector $\underline{x}(t + \Delta t)$ is determined entirely by its initial value $\underline{x}(t)$ and the "transition" matrix $\Phi(t + \Delta t,\ t)$. This transition matrix has the properties that $\Phi(t, t) = I$ and $\Phi(t_o, t) = \Phi(t, t_o)$. The transition matrix can be thought of as a time-translation matrix which determines the way in which the components of the state vector (in this case the deviation quantities ΔX, ΔY ... $\Delta \dot{Z}$) vary as a function of time. In this study, the Φ matrices were computed numerically for each of the trajectories, using a 6-minute Δt. See Volume V, Appendix B, Section 1 for detailed description of this computation.

Knowing the Φ matrices and initial state $\underline{x}(t_o)$ (which corresponds to the injection conditions) the state $\underline{x}(t)$ at any later time can be determined directly by equation 2-11, assuming that the linear relationships hold. However, the injection conditions, $\underline{x}(t_o)$, are never known exactly, and statistical methods must be used.

The use of statistical methods on vector quantities such as $\underline{x}$ requires the introduction of covariance matrices for second-order statistical analysis. Defining $\underline{x}$ as a 6-vector whose components are random variables representing the deviations from some reference trajectory, then the covariance matrix of $\underline{x}$ is given by

$$\operatorname{cov} \underline{x} = E(\underline{x}\,\underline{x}^T) = E \begin{bmatrix} (\Delta X)^2 & \Delta X \Delta Y & \Delta X \Delta Z & \Delta X \Delta \dot{X} & \Delta X \Delta \dot{Y} & \Delta X \Delta \dot{Z} \\ \Delta Y \Delta X & (\Delta Y)^2 & \Delta Y \Delta Z & \Delta Y \Delta \dot{X} & \Delta Y \Delta \dot{Y} & \Delta Y \Delta \dot{Z} \\ \Delta Z \Delta X & \Delta Z \Delta Y & (\Delta Z)^2 & \Delta Z \Delta \dot{X} & \Delta Z \Delta \dot{Y} & \Delta Z \Delta \dot{Z} \\ \Delta \dot{X} \Delta X & \Delta \dot{X} \Delta Y & \Delta \dot{X} \Delta Z & (\Delta \dot{X})^2 & \Delta \dot{X} \Delta \dot{Y} & \Delta \dot{X} \Delta \dot{Z} \\ \Delta \dot{Y} \Delta X & \Delta \dot{Y} \Delta Y & \Delta \dot{Y} \Delta Z & \Delta \dot{Y} \Delta \dot{X} & (\Delta \dot{Y})^2 & \Delta \dot{Y} \Delta \dot{Z} \\ \Delta \dot{Z} \Delta X & \Delta \dot{Z} \Delta Y & \Delta \dot{Z} \Delta Z & \Delta \dot{Z} \Delta \dot{X} & \Delta \dot{Z} \Delta \dot{Y} & (\Delta \dot{Z})^2 \end{bmatrix}$$

If the random variables ΔX, etc have zero mean, then it can be seen that the terms along the major diagonal represent the variances of the individual components while the cross terms are the product of the standard deviations of each of the variables and the correlation coefficient.

Equation 2-11 is a linearized model of the dynamic process by which the initial uncertainties propagate along the trajectory. Now assume that during the course of the flight, some observations, $\underline{y}(t)$ are made, where the observations are related to the trajectory deviations by the relation:

$$\underline{y}(t) = H(t)\ \underline{x}(t) + \underline{n}(t) \tag{2-12}$$

where $\underline{n}(t)$ is the additive noise on each observation and $H(t)$ is the matrix relating the observables to the state variables. Assuming that the noise $\underline{n}(t)$ can be represented as the output of a linear dynamic system excited by white noise, then:

$$\dot{\underline{n}}(t) = B(t)\ \underline{n}(t) + \underline{u}_n(t) \tag{2-13}$$

where $\underline{u}_n(t)$ is the Gaussian noise input. Just as equation 2-8 represents the dynamic process governing the trajectory uncertainties, equation 2-13 represents the dynamic process governing the observation noise $\underline{n}(t)$, the difference being that $\underline{u}_n(t)$ is an input in equation 2-13, whereas equation 2-8 has no forcing function. The solution of equation 2-13 is:

$$\underline{n}(t + \Delta t) = \Phi_n\ (t + \Delta t,\ t)\ \underline{n}(t) + \int_t^{t + \Delta t} \Phi_n(t + \Delta t,\ \tau)\ \underline{u}_n\ (\tau)\ d\tau \tag{2-14}$$

where Φ_n is defined by $\Phi_n(t) = B(t)\ \Phi_n$ and $\Phi_n(t,\ t) = I$. Equation 2-14 is the solution of the equations representing the time-varying error process and is analogous to equation 2-11 for the trajectory deviations. Defining:

$$u' = \int_t^{t + \Delta t} \Phi_n(t + \Delta t,\ \tau)\ \underline{u}_n(\tau)\ d\tau \tag{2-15}$$

then equation 2-14 and 2-11 can be written:

$$\underline{x}\,(t + \Delta t) = \Phi\,(t + \Delta t,\ t)\ \underline{x}(t) \tag{2-16}$$

$$\underline{n}\,(t + \Delta t) = \Phi_n(t + \Delta t,\ t)\ \underline{n}(t) + u'$$

Equations 2-16 describe the dynamics of both the trajectory deviations and the observation noise. Adjoining the two equations, there is:

$$\begin{bmatrix} \underline{x} \\ \underline{n} \end{bmatrix}_{t+\Delta t} = \begin{bmatrix} \Phi & 0 \\ 0 & \Phi_n \end{bmatrix} \begin{bmatrix} \underline{x} \\ \underline{n} \end{bmatrix}_t + \begin{bmatrix} 0 \\ u' \end{bmatrix} \tag{2-17}$$

Now, defining the "augmented" state vector, $\underline{x}^*$ as the vector consisting of both the trajectory deviations and the observation noise, equation 2-17 can be written:

$$\underline{x}^*(t + \Delta t) = \Phi^*\,(t + \Delta t,\ t)\ \underline{x}^*(t) + U \tag{2-18}$$

where

$$\Phi^* = \begin{bmatrix} \Phi & 0 \\ 0 & \Phi_n \end{bmatrix} \text{and } U = \begin{bmatrix} 0 \\ u' \end{bmatrix}$$

The observation process, equation 2-12, can now be written:

$$\underline{y}(t) = M(t)\ \underline{x}^*(t) \tag{2-19}$$

where:

$$M(t) = \begin{bmatrix} H & 0 \\ 0 & I \end{bmatrix}$$

Equations 2-18 and 2-19 represent the state of the system and observations of the state, respectively. The estimation problem can now be re-stated: Given a dynamic process described by the state equation 2-18 and some observations of the process, $\underline{y}(t)$, $\underline{y}(t_{k1})$, $\underline{y}(t_{k2})$, what is the best estimate of the state of the system $\underline{x}^*(t_k)$ at some time t_k? Constraining this "best estimate" to some linear function of the observations $\underline{y}(t_{k1})$, Kalman derived a recursive solution to the above problem (Ref. 2-6). The solution is given by:

$$\hat{\underline{x}}^*(t_k) = \Phi^*\,(t_k,\ t_{k-1})\ \hat{\underline{x}}^*(t_{k-1}) + K^*(t_k)\left\{\underline{y}(t_k) - M(t_k)\ \Phi\,(t_k,\ t_{k-1})\ \hat{\underline{x}}^*(t_{k-1})\right\} \tag{2-20}$$

$$K^*(t_k) = P^*(t_k)\, M^T(t_k) \left\{ M(t_k)\, P^*(t_k)\, M^T(t_k) \right\}^{-1} \tag{2-21}$$

$$P^*(t_{k+1}) = \Phi^*(t_{k+1}, t_k) \left\{ P^*(t_k) - K^*(t_k)\, M(t_k)\, P^*(t_k) \right\} \Phi^{*T}(t_{k+1}, t_k) + Q^*(t_{k+1}, t_k) \tag{2-22}$$

where

$$Q^*(t_{k+1}, t_k) = \begin{bmatrix} 0 & 0 \\ 0 & Q' \end{bmatrix}$$

and

$$Q' = \int_{t_k}^{t_{k+1}} \Phi_n(t_{k+1}, t_k)\, E\left\{ \underline{u}_n(\tau)\, \underline{u}_n^T(\tau) \right\} \Phi_n^T(t_{k+1}, t_k)\, d\tau$$

Also $P^*(t_k)$ is the covariance matrix of the error in the estimate $\hat{\underline{x}}^*(t_k)$; i.e.:

$$P^*(t_k) = E(\tilde{\underline{x}}^*(t_k)\, \tilde{\underline{x}}^{*T}(t_k)$$

where $\tilde{\underline{x}}^* = \underline{x}^* - \hat{\underline{x}}^*$. Thus, the formulation of the estimate includes the generation of estimated error in the estimate.

The notation is different in Ref. 2-6, as explaned in Volume V, Appendix B, Section 2.

The recursion relations in equations 2-20, 2-21, and 2-22 solve for the minimum variance estimate of $\underline{x}^*(t)$ or both $\underline{x}(t)$, the state deviation vector and $\underline{n}(t)$, the measurement noise. Now, assume that the noise on the measurements is uncorrelated from one measurement to the next. This is a likely situation in the case of a low data-rate optical observation system (but not likely in the case of a high data-rate radar ground tracking system). In any case, if the measurements errors are uncorrelated, then the portion of $\underline{x}^*(t)$ relating to the noise $\underline{n}(t)$ need not be computed and equations 2-20, 2-21, and 2-22 can be simplified to the following forms (as shown in Ref. 2-4, Appendix D).

$$\hat{\underline{x}}(t_k) = \Phi(t_k, t_{k-1})\, \hat{\underline{x}}(t_{k-1}) + K(t_k) \left\{ \underline{y}(t_k) - H(t_k)\, \Phi(t_k, t_{k-1})\, \hat{\underline{x}}(t_{k-1}) \right\} \tag{2-23}$$

$$K(t_k) = P(t_k)\, H^T(t_k) \left\{ H(t_k)\, P(t_k)\, H^T(t_k) + Q(t_k) \right\}^{-1} \tag{2-24}$$

$$P(t_{k+1}) = \Phi\,(t_{k+1}, t_k) \left\{ P(t_k) - K(t_k)\, H(t_k)\, P(t_k) \right\} \Phi^T(t_{k+1}, t_k) \qquad (2\text{-}25)$$

where $Q(t_k)$ is the covariance matrix of the measurement noise, and $H(t_k)$ the matrix relating the observations $\underline{y}(t_k)$ to the state $\underline{x}(t_k)$, as shown by equation 2-12.

The derivation given is not the simplest; since using the assumptions of uncorrelated measurement noise and an estimate which is a <u>linear</u> function of the measurements, a very simple derivation can be achieved as shown by Battin in Ref. 2-2 (see also Volume V, Appendix A, Section 5). The derivation shown in this paragraph is used to supply some of the missing steps in the derivations of Ref. 2-4 and also to show the analytical foundation for use of the augmented state vector formulation which can be used to estimate systematic errors, (see Volume V, Appendix B, Section 7).

In this study, it was assumed that equations 2-23 through 2-25 represent the navigation equations used in the guidance computer. For simplicity in discussion, the equations are rewritten here with all time arguments assumed to be t_k except where subscripted:

$$\hat{\underline{x}} = \Phi\, \hat{\underline{x}}_{k-1} + K\left[\underline{y} - H\Phi\, \hat{\underline{x}}_{k-1}\right] \qquad (2\text{-}26)$$

$$K = PH^T \left\{ HPH^T + Q \right\}^{-1} \qquad (2\text{-}27)$$

$$P_{k+1} = \Phi_{k+1} \left[P - KHP \right] \Phi^T_{k+1} \qquad (2\text{-}28)$$

Equation 2-26 shows how the state deviation estimate $\hat{\underline{x}}$, is updated each time a measurement $\underline{y}$ is made. $\Phi\, \hat{\underline{x}}_{k-1}$ is the estimate of $\underline{x}$ at t_k <u>without</u> any measurement. Thus the predicted measurement is $H\Phi\hat{\underline{x}}_{k-1}$ since H relates the observables to the state deviations. The difference between the <u>actual</u> measurement $\underline{y}$ and the <u>predicted</u> measurement is weighted by the matrix K and this result adds to the quantity $\Phi\, \hat{\underline{x}}_{k-1}$ which is the estimate of $\underline{x}$ at t_k if no measurement is made.

It is clear that the key to this process is the weighting matrix K, since K determines how heavily the new data will be weighted compared to the best previous estimate. In equation 2-27, K is seen to vary inversely with Q, the covariance of measurement errors. Thus, the greater the assumed measurement errors, the less heavily will new data be weighted compared to the previous estimate.

Equation 2-28 shows how P, the covariance matrix of estimation errors, is reduced after each measurement. This reduction is given by $[P - KHP]$. The operation $\Phi_{k+1}(\quad)\Phi^T_{k+1}$ shows the time-transition of P between measurements.

Equations 2-26 through 2-28 represent a general data-processing system which can be used to solve any estimation or prediction problem, given the assumption of uncorrelated errors. Next, the application of these equations to the space navigation problem is discussed.

First, consider the onboard, optical angle-measuring system described in paragraph 2.2.2. The quantities required for the recursion process are as follows:

$\hat{\underline{x}}_o$	The initial estimate of trajectory deviations
P_o	The initial covariance matrix of trajectory estimation errors
Φ_1, Φ_2, etc	The transition matrices between measurement time t_o and t_1, t_1 and t_2, etc
$H(t_1)$, $H(t_2)$, etc	The matrices showing the relationships between the measurements $\underline{y}$ and the state $\underline{x}$
Q	The covariance matrix of measurement errors.

The starting points for the recursion equations are $\hat{\underline{x}}_o$, P_o and $\Phi(t_1, t_o)$, the transition matrix between $t = t_o$ and the first measurement at $t = t_1$. After this measurement is made the updated estimate of trajectory deviations is given by:

$$\hat{\underline{x}}_1 = \Phi(t_1, t_o)\,\hat{\underline{x}}_o + K_1\left[y_1 - H_1\,\Phi(t_1, t_o)\,\hat{\underline{x}}_o\right] \tag{2-29}$$

$$K_1 = P_1 H_1^T\left[H_1 P_1 H_1^T + Q\right]^{-1} \tag{2-30}$$

$$P_1 = \Phi(t_1, t_o)\left[P_o\right]\Phi^T(t_1, t_o) \tag{2-31}$$

where $K_o H_o P_o = 0$ in equation 2-31 since no measurement was taken at t_o. The procedure thus described is repeated throughout the estimation process each time a new measurement is made.

The fact that, in the system being described here, each observation consists of only one angle results in some simplification of the computations. For one thing the measurement y is now a scalar, and Q is just a scalar (the measurement variance) as is the quantity HPH^T, so that matrix inversion in equation

2-27 is not required. Then H is a row matrix consisting of the partials of the angle with respect to each coordinate. Thus

$$H = \left[\frac{\partial \zeta}{\partial X} \quad \frac{\partial \zeta}{\partial Y} \quad \frac{\partial \zeta}{\partial Z} \quad 0 \quad 0 \quad 0 \right] \tag{2-32a}$$

The partials in H are time-varying, of course, and are derived for each of the various measurement types in Volume V, Appendix B, Section 3. Although the primary concern is with onboard optical systems, it is to be noted that as far as the analysis is concerned, the only difference between the computations required for onboard and ground-tracking systems is in the H-matrix. For a ground tracking system using range as the observable, then:

$$H = \left[\frac{\partial R}{\partial X} \quad \frac{\partial R}{\partial Y} \quad \frac{\partial R}{\partial Z} \quad 0 \quad 0 \quad 0 \right] \tag{2-32b}$$

The equations 2-32 complete the derivation of the equations used in the navigation system model being investigated. Equations 2-26 through 2-28 are the navigation equations and other required quantities are $\hat{\underline{x}}_o$, the initial estimate, P_o, the assumed covariance of initial errors; the transition (Φ) matrices; the H-matrices and Q, the assumed measurement variance.

It should be pointed out here that two significant error sources will probably be present on an actual mission that are not considered here. These are:

a. Bias or other time-correlated measurement errors
b. Uncertainties in the astrodynamic constants.

These errors are discussed in paragraph 2.4.3. It has been shown (Ref. 2-7) that the mathematical formulation of equations 2-26 through 2-28 can be used in an actual system even in the presence of bias errors and astrodynamic uncertainties, by using a larger value for Q, the measurement variance, than would ordinarily be assumed.

Another problem not considered here is the errors due to nonlinearities. In the formulation of equations 2-26 through 2-28, it is assumed that the equations of motion governing $\underline{x}$ and the relationship between $\underline{x}$ and the measured angle y are linear. Since neither of these assumptions is true, there is some inaccuracy because of the linear approximations. However, this error will be small as long as the deviations from the reference trajectory are not large. This will be the case if the estimated trajectory is used for reference rather than the preplanned nominal trajectory. In this study, it is assumed that the estimated trajectory is used as the reference trajectory.

2.3.1.4 Guidance Equations

The previous paragraphs are concerned with developing equations for the navigation phase of the midcourse guidance problem. This is only half the computational problem. Having determined the spacecraft deviations from the reference trajectory, it remains to predict target deviations and compute and apply the thrust required to null out or reduce the predicted miss distance.

From a computational and analytical standpoint, the simplest type of space guidance is the use of an impulsive velocity change to null out the predicted miss distance at nominal time of arrival. Although this type of guidance logic is not a minimum-fuel correction scheme, the correction velocities required in midcourse are small, and the simplicity of this fixed time of arrival (FTOA) guidance weighs in its favor. Therefore, in this study, it is assumed that all trajectory corrections are high-thrust impulsive velocity changes designed to null out the predicted miss distance at nominal time of periselenum.

The onboard computations required for this guidance are now derived. Equation 2-11 shows how the transition matrices are used to determine the trajectory deviations at some future time $(t + \Delta t)$ from knowledge of these deviations at time t. Thus, letting t_C equal the time at which it is desired to make a correction and t_A equal the nominal time of arrival at periselenum, deviations at t_A are given by:

$$\underline{x}(t_A) = \Phi(t_A, t_C)\,\underline{x}(t_C) \tag{2-33}$$

where the $\underline{x}$'s are six vectors (three position components and three velocity components) and $\Phi(t_A, t_C)$ is a 6x6 matrix.

Letting $\Phi(t_A, t_C) = A$ and rewriting equation 2-33 in partitioned form:

$$\begin{bmatrix} \underline{r}_A \\ \underline{v}'_A \end{bmatrix} = \begin{bmatrix} A_1 & A_2 \\ A_3 & A_4 \end{bmatrix} \begin{bmatrix} \underline{r}_C \\ \underline{v}_C \end{bmatrix} \tag{2-34}$$

where A_1, A_2, etc are 3 x 3 submatrices of A, and $\underline{r}$ and $\underline{v}$ are 3 x 1 vectors of position and velocity deviations from the reference trajectory.

Since a single impulsive thrust can correct only three components of the predicted deviations at t_A, it is assumed that the velocity correction vector $(\Delta\,\underline{v})$ is applied in such a way as to null out the predicted position errors at t_A. This is reasonable, since mission safety depends most strongly on position errors and the velocity deviations from the nominal at t_A are eliminated by the large retrothrust required to inject the vehicle into a lunar orbit.

If the correction ($\Delta \underline{v}$) is applied to reduce the predicted position error ($\underline{r}_A$) to zero, then equation 2-34 becomes:

$$\begin{bmatrix} O_{31} \\ \underline{v}'_A \end{bmatrix} = \begin{bmatrix} A_1 & A_2 \\ A_3 & A_4 \end{bmatrix} \begin{bmatrix} \underline{r}_C \\ \underline{v}_C + \Delta\underline{v} \end{bmatrix} \tag{2-35}$$

where $\underline{v}'_A$ is the new predicted velocity deviation at periselenum. Expanding the first line of the matrix equation 2-35, and solving for $\Delta\underline{v}$:

$$O_{31} = A_1 \underline{r}_C + A_2 (\underline{v}_C + \Delta\underline{v}) \tag{2-36}$$

$$\Delta\underline{v} = - A_2^{-1} A_1 \underline{r}_C - \underline{v}_C \tag{2-37}$$

$$\Delta\underline{v} = - \begin{bmatrix} A_2^{-1} A_1 & I_{33} \end{bmatrix} \begin{bmatrix} \underline{r}_C \\ \underline{v}_C \end{bmatrix} \tag{2-38}$$

$$\Delta\underline{v} = G_C' \, \underline{x}(t_C) \tag{2-39}$$

where $G_C' = - \begin{bmatrix} A_2^{-1} A_1 & I_{33} \end{bmatrix}$. Thus, the indicated velocity correction at any t_C is computed as a function of the deviation at that time.

The estimate of the state deviations $\underline{x}'(t_C)$ after a velocity correction is:

$$\underline{x}'(t_C) = \underline{x}(t_C) + \begin{bmatrix} O_{31} \\ \Delta\underline{v} + \Delta\tilde{\underline{v}} \end{bmatrix} \tag{2-40}$$

where $\Delta\tilde{v}$ is the error in making the correction.

After a correction is made, not only must the three velocity components of $\underline{x}(t_C)$ be revised, but also the covariance of estimation errors must be increased because of the uncertainties involved in measuring the velocity change.

Partitioning the covariance matrix P, such that:

$$P = \begin{bmatrix} P_1 & P_2 \\ P_3 & P_4 \end{bmatrix} \tag{2-41}$$

Then, after a correction:

$$P_C = \begin{bmatrix} P_1 & P_2 \\ P_3 & (P_4 + C) \end{bmatrix} \tag{2-42}$$

where C is the assumed covariance matrix of errors in measuring the velocity correction. The derivation of equation 2-42 is simple enough; the steps are shown in Volume V, Appendix B, Section 4.

2.3.2 Statistical Analysis of Errors

In the previous paragraph, the equations describing the operation of a guidance system model have been derived. To analyze the performance of such a system using different system parameters and different trajectories, one might attempt a Monte Carlo analysis, employing equations 2-26 through 2-28 and the actual equations of motion. Such an approach would be impractical, however, for two reasons:

a. The necessity for integrating the equations of motion on each trial
b. The necessity for making many runs on each set of initial conditions in order to get statistically valid results.

These difficulties make the use of ensemble statistical analysis attractive. Ensemble statistical analysis consists in using average statistical quantities to determine the guidance system performance over the ensemble of trajectory-system models which have certain parameters in common. Ensemble methods were used to generate the numerical data for this study.

Three statistical quantities are sufficient to specify guidance system performance on an average basis:

P, the covariance matrix of estimation errors
N, the covariance matrix of deviations from the nominal trajectory
V, the covariance matrix of velocities required for each correction

These quantities are defined as follows:

$$P = E(\underline{\tilde{x}}\,\underline{\tilde{x}}^T) \tag{2-43}$$

where $\underline{\tilde{x}} = \underline{\hat{x}} - \underline{x}$

$$N = E(\underline{x}\,\underline{x}^T) \tag{2-44}$$

$$V_i = E(\Delta\underline{v}_i\,\Delta\underline{v}_i^T) \tag{2-45}$$

Equations 2-27 and 2-28 show that P, the covariance of estimation errors, can be generated using only P_o, Q, H(t) and $\Phi(t)$; i.e., the estimate $\underline{\hat{x}}$ is not required. Thus, statistical information about the ensemble of flights having certain things in common can be developed. This procedure implicitly assumes that the $\Phi(t)$ matrices and H(t) matrices on any flight are always reasonably similar to the $\Phi(t)$ and H(t) matrices computed from the nominal trajectory. This will be true as long as the actual trajectory never deviates far from the nominal trajectory. Thus, it can be seen that although the navigation equations 2-26 through 2-28 can be utilized even in case of an abort, the statistical analysis detailed in this paragraph is applicable only in nonabort situations.

Equations 2-27 and 2-28 show how P is computed during periods when no thrust is being made; when a correction is made, equation 2-42 is utilized.

N is the covariance matrix of deviations from the nominal trajectory, and its calculation is required to determine the target miss.

Since $\underline{x}_k = \Phi(t_k, t_o)\,\underline{x}_o$, then:

$$N_k = E\left[\underline{x}_k \underline{x}_k^T\right] = E\left[\Phi(t_k, t_o)\,\underline{x}_o \underline{x}_o^T \Phi^T(t_k, t_o)\right]$$

$$N_k = \Phi(t_k, t_o)\; N_o\, \Phi^T(t_k, t_o) \tag{2-45a}$$

Thus, given N_o, the covariance of initial deviations, and the Φ matrices, then the covariance of deviations at any later time can be developed, so long as no velocity corrections are made.

The change in N when a velocity correction is made is rather complicated, so is not given here, but is shown in Appendix B, Volume V, Section 4. Calling N the trajectory deviations before the correction and N_c, the deviations after the correction, N_c is given as:

$$N_c = \left[I_{66} + G\right]\left(N - P\right)\left[I_{66} + G\right]^T + P + S \tag{2-46}$$

where

$$G = -\begin{bmatrix} O_{33} & O_{33} \\ A_2^{-1} A_1 & I_{33} \end{bmatrix} = \begin{bmatrix} O_{36} \\ G' \end{bmatrix} \tag{2-47}$$

and S is the covariance matrix of the errors made in applying the velocity correction:

$$S = \begin{bmatrix} O_{33} & O_{33} \\ O_{33} & S' \end{bmatrix} \tag{2-48}$$

$$S' = \left(\sigma_k^2 + \frac{\sigma_\epsilon^2}{u^2}\right) V + \frac{\sigma_\gamma^2}{2}\left(u^2 I_{33} - V\right) \tag{2-49}$$

where σ_k^2 and σ_ϵ^2 are the variances in the thrust percentage accuracy and cutoff magnitude error, respectively, σ_γ^2 is the variance in the assumed pointing error and u^2 is the trace of V. Thus, equation 2-44 and equations 2-46 through 2-49 specify N over all periods of the trajectory.

The covariance of commanded velocity corrections at each maneuver is given by:

$$V = E\left(\Delta\underline{v}\,\Delta\underline{v}^T\right) = G'\,E\left(\underline{x}\,\underline{x}^T\right) G'^T = G' N G'^T \tag{2-50}$$

where G' is defined by equation 2-39.

Having developed the covariance matrices P, N and V, one can then obtain the pertinent rms quantities for guidance system evaluation. Since $P = E(\underline{\tilde{x}}\,\underline{\tilde{x}}^T)$, then:

$$P = E\begin{bmatrix} \tilde{x}^2 & \tilde{x}\tilde{y} & - & - & - & - \\ \tilde{y}\tilde{x} & \tilde{y}^2 & - & - & - & - \\ - & - & \tilde{z}^2 & - & - & - \\ - & - & - & \dot{\tilde{x}}^2 & - & - \\ - & - & - & - & \dot{\tilde{y}}^2 & - \\ - & - & - & - & - & \dot{\tilde{z}}^2 \end{bmatrix} = \begin{bmatrix} \sigma_{\tilde{x}}^2 & \rho_{xy}\sigma_{\tilde{x}}\sigma_{\tilde{y}} & - & - & - & - \\ - & \sigma_{\tilde{y}}^2 & - & - & - & - \\ - & - & \sigma_{\tilde{z}}^2 & - & - & - \\ - & - & - & \sigma_{\dot{\tilde{x}}}^2 & - & - \\ - & - & - & - & \sigma_{\dot{\tilde{y}}}^2 & - \\ - & - & - & - & - & \sigma_{\dot{\tilde{z}}}^2 \end{bmatrix} \tag{2-51}$$

when $\tilde{X}$, $\tilde{Y}$, etc are assumed to have zero mean.

Thus, it can be seen that the P matrix is composed of the variances of each component along the major diagonal, and the correlation coefficients between the variables (times the product of the standard deviations) as the off-diagonal members. Then, since $\tilde{r}$, the rms position estimation error, is given by

$$\tilde{r} = \sqrt{\sigma_{\tilde{x}}^2 + \sigma_{\tilde{y}}^2 + \sigma_{\tilde{z}}^2} \tag{2-52}$$

$$\tilde{r} = \sqrt{Tr\,(P_1)} \tag{2-53}$$

where Tr indicates the trace and P_1 is the upper left-hand 3 x 3 submatrix of P. Thus, by similar analyses, the rms quantities for position and velocity deviations, position and velocity estimation errors and velocity corrections can be developed. These are:

$$\left.\begin{array}{lll} \text{Position deviations} & r & = \sqrt{Tr\,(N_1)} \\ \text{Velocity deviations} & v & = \sqrt{Tr\,(N_4)} \\ \text{Position estimation errors} & \tilde{r} & = \sqrt{Tr\,(P_1)} \\ \text{Velocity estimation errors} & \tilde{v} & = \sqrt{Tr\,(P_4)} \\ \text{Correction velocity} & \Delta v & = \sqrt{Tr\,(V)} \end{array}\right\} \tag{2-54}$$

2.3.3 Digital Computer Programs

The previous paragraph describes the equations necessary to perform a second-order[1/] statistical analysis of the guidance system described in paragraph 2.3.1. In this paragraph, the digital computer program which was utilized for parametric analyses of various systems is described.

Actually, three separate programs were used: one to generate nominal trajectories, one to compute the Φ matrices for each trajectory, and one to determine the statistical quantities described in the previous section.

Generation of trajectories for the assumed astronomical model entails integration of the equations of motion (equations 2-2 and 2-3) and printing out results at various time points. This process is carried out by a digital program using a fourth-order Runge-Kutta numerical integration routine. This routine, written in double-precision for the IBM 7094, selects the size of the integration step automatically to reduce the truncation error to less than some preset amount. If the step-size is too small, roundoff error can become a problem, but successive runs of the program with the same initial conditions but employing different values of truncation error resulted in nearly identical numerical results, indicating that roundoff error problems had been eliminated by use of a double-precision routine.

There is no direct method of achieving desired end conditions by exact choice of initial conditions in equation 2-2. However, since the requirements on trajectory characteristics are not exact, an approximate method of linear interpolation was used to obtain the desired trajectories. It was found that, given an initial altitude, flight time can be controlled by choice of the initial velocity magnitude, and that the inclination of the trajectory is determined by the orientation of the initial velocity. Having chosen these parameters, it remains only to specify the initial longitude of the vehicle in the lunar plane, ψ_o. It was found that the altitude of lunar close approach varies nearly linearly with this initial angle, ψ_o. In summary, the procedure used to obtain trajectories having desired characteristics was to choose initial position and velocity components of the vehicle in order to achieve the desired trip time and plane relationships approximately and then vary the initial position of the moon in its orbit to adjust the altitude of periselenum passage to the desired value. This method is not discussed in greater detail as more sophisticated and exact methods are available and this study is not concerned with the trajectory design problem, per se.

1/ Second-order means that only second moments; i.e., variances are employed.

When the correct initial conditions are determined using the program just described, it is required to generate a printout of trajectory parameters (position and velocity in both earth and moon coordinate systems) and also generate the transition (Φ) matrices described in paragraph 2.3.1.3. It was decided, somewhat arbitrarily, to compute the trajectory parameters and the Φ matrices at 6-minute intervals over each trajectory. Thus, the Φ matrices generated are Φ (6-minutes, 0), Φ (12-minutes, 6 minutes) and so on. In Section 1 of Appendix B (Volume V), the equations for generation of the Φ matrices are developed. In the computer program, the Φ matrices are generated by simultaneous solution of equations 2-7 and 2-2.

The two programs described above serve to provide inputs for the statistical analysis program which was the primary analytical tool used in this study. The statistical analysis program is described schematically in figure 2-5.

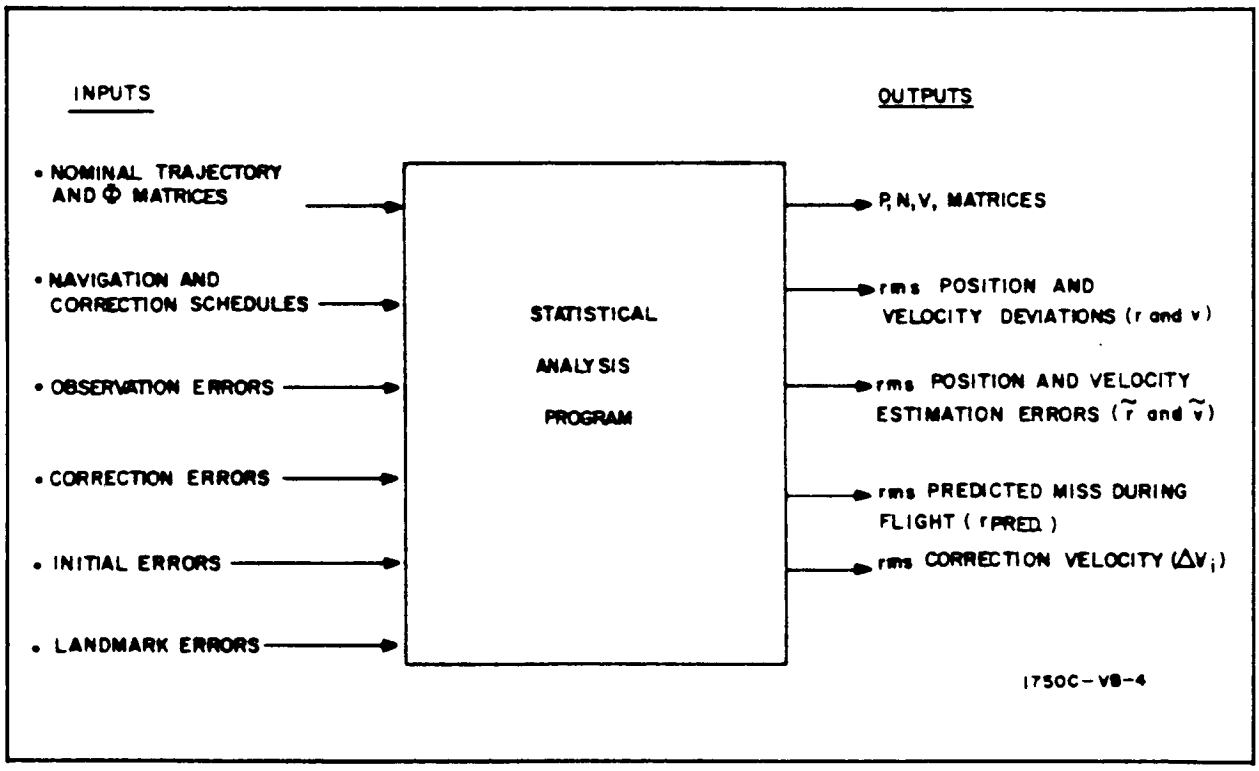

Figure 2-5. Input-Output Diagram of Statistical Analysis Program

The inputs listed on the left side of the figure are the quantities which are varied throughout the course of the study.

a. Nominal Trajectory (and Φ Matrices) - These include the four trajectories described in paragraph 2.3.1.1.

b. Navigation and Correction Schedules - These include the list of times at which observations and corrections are made, together with the type of observation (star-planet combination).

c. Observation Errors - It is assumed that the observation errors are uncorrelated from one measurement to the next and that the variance Q of the observation errors is given by:

$$Q = \sqrt{\sigma^2 + \left(k_i/R_i\right)^2} \tag{2-55}$$

where σ is the error due to the optical instrument and k_i/R_i is the error due to the uncertainty of the reference point on the planet, (earth or moon). Thus σ, the sensor error, and k_i, the landmark uncertainty, are program inputs.

d. Correction Errors - These errors are described by equations 2-46 through 2-49. The program inputs are σ_k^2, the variance in the thrust percentage accuracy, σ_ϵ^2, the variance of magnitude errors due to cutoff inaccuracy and σ_γ^2, the variance of pointing uncertainties. In this study, it is assumed that no correction monitoring is done.

e. Initial Errors - The initial uncertainty and deviation matrices are assumed equal ($P_o = N_o$), thus implying that no trajectory data is available between translunar injection and the start of the midcourse navigation measurements.

Program outputs are shown in figure 2-5. The most important criteria for evaluation of the guidance system performance are the estimation errors $\tilde{r}$ and $\tilde{v}$ at periselenum, the deviation (miss) quantities r and v at periselenum and the total correction velocity required, $\Sigma\, \Delta v$. In addition to this end-point (periselenum) data, these quantities are also computed throughout the trajectory to determine the usefulness of various guidance operations.

The equations used to determine these quantities are derived in paragraphs 2.3.1 and 2.3.2. A complete summary of the equations used in the computer programs is given in Section 5 of Appendix B, (Volume V).

2.3.4 Analysis of Optical Measurement Errors

In paragraph 2.3.2, equations are developed for the analysis of a guidance system whose navigation measurement errors have a variance of Q and are uncorrelated from one measurement to the next. In this paragraph, optical angle measurement errors are examined in somewhat greater detail to determine the fundamental limitations on optical measurements.

The various types of optical measurements which can be made are shown in figure 2-6. In Section 3, Appendix B (Volume V), the angle ζ is derived for the three types of measurements in figure 2-6. In addition, the H-matrix (which is the matrix of partial derivatures with respect to the state variables) is generated for optical angle measurements, direct range measurements and direct range-rate measurements. The results pertaining to the optical measurements are summarized here. Assume a star direction defined by $\underline{S} = a\underline{i} + b\underline{j} + c\underline{k}$ and a vehicle position $\underline{R} = X\underline{i} + Y\underline{j} + Z\underline{k}$ as shown in figure 2-7.

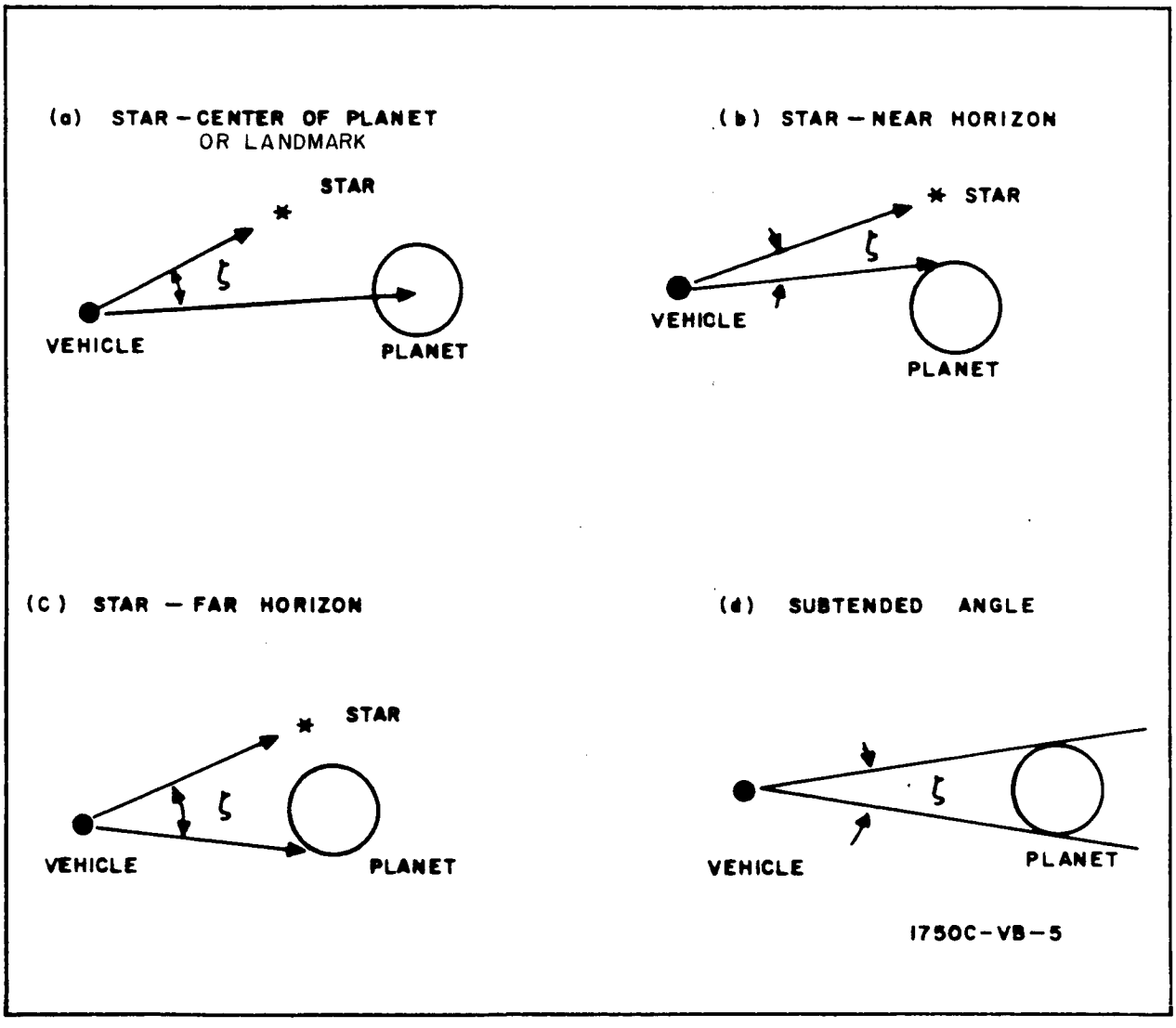

Figure 2-6. Types of Optical Measurements

In figure 2-7, it can be seen that measurement of the star angle to the near horizon is given by:

$$\zeta_h = \zeta - \theta \tag{2-56}$$

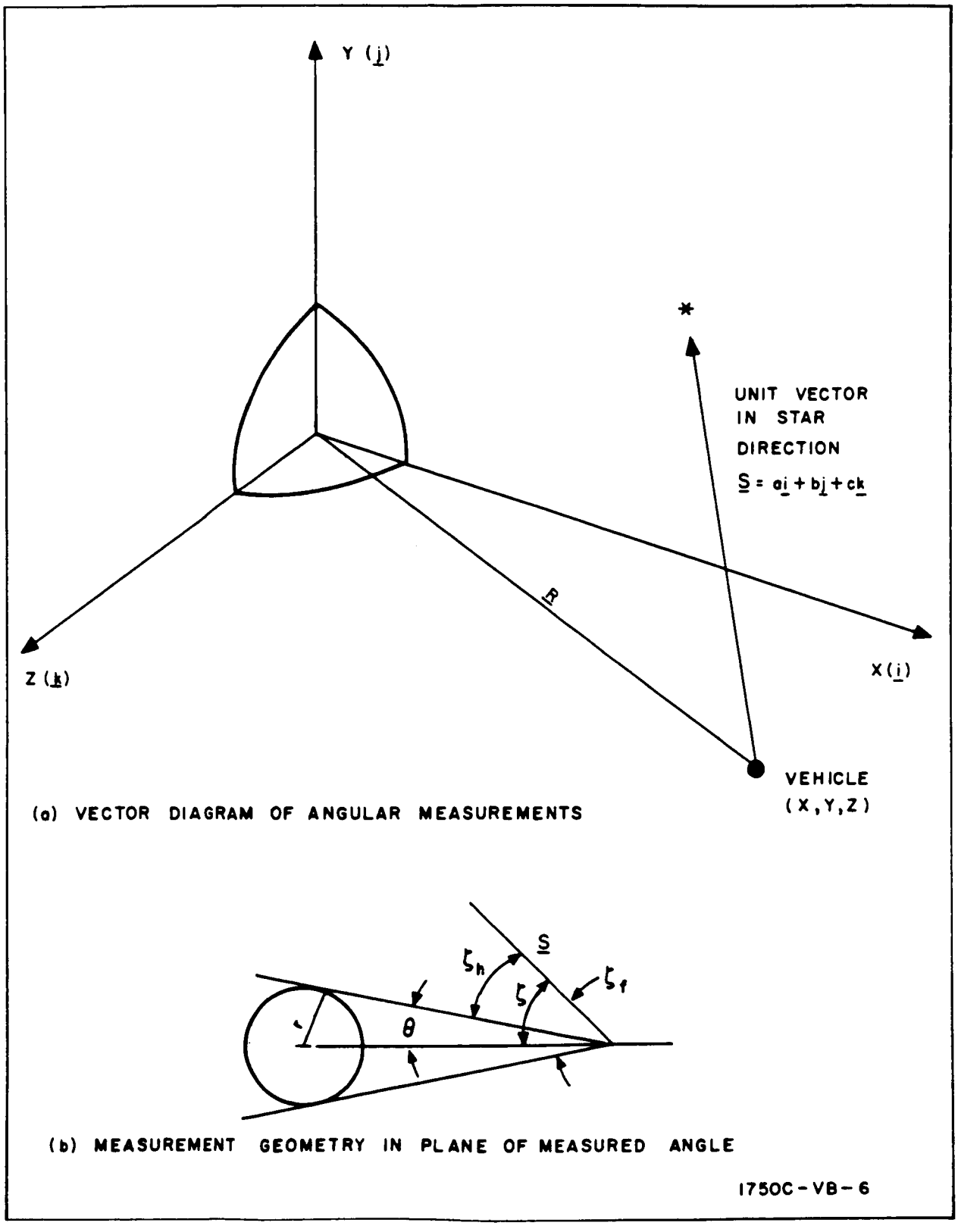

Figure 2-7. Optical Measurements Results

and the angle to the far horizon is:

$$\zeta_f = \zeta + \theta \tag{2-57}$$

where ζ is the angle from the center of the planet to the star direction and θ is the half-subtense angle. In Appendix B of Volume V it is shown that these angles are:

$$\zeta = \cos^{-1}(d) \tag{2-58}$$

where $d = \left(-\frac{aX + bY + cZ}{R}\right)$ and $R = \sqrt{X^2 + Y^2 + Z^2}$

and $$\theta = \sin^{-1}\left(\frac{r}{R}\right) \tag{2-59}$$

where r is the planet radius. For each type of angle measurement, the H-matrix (which is the linearized relationship between angle measurement deviations and trajectory deviations) is given by

$$H = \left[\frac{\partial \zeta_o}{\partial X} \quad \frac{\partial \zeta_o}{\partial Y} \quad \frac{\partial \zeta_o}{\partial Z} \quad 0 \quad 0 \quad 0\right] \tag{2-60}$$

where ζ_o represents one of the four angle measurements described.

The partials which make up the H-matrix for each measurement type are listed in Section 3, Appendix B of Volume V.

In the computer program used in this study, it was assumed that all measurements were made between some star direction and the planet center. This was done to avoid having to analyze the differences between measurements a and b in figure 2-7. These differences are expected to have only a slight effect on system performance for two reasons:

a. The magnitude of the angular difference between a star/planet-center measurement (ζ), and a star/near-horizon measurement (ζ_h) is small once the vehicle is an appreciable distance from the planet. A plot of this angular difference as a function of time from launch on the 72.2-hour trajectory is given in figure 2-8.

b. The plane of the measured angle is identical for a particular star, regardless of which of the three measurements is being used. Thus, there will be little difference between measurements in reduction of uncertanties in this plane.

For these reasons, it was expected that choice of planet center, horizon or landmarks as a reference point for measurements will have little effect on the results of the present study, which are intended to be applicable to all these

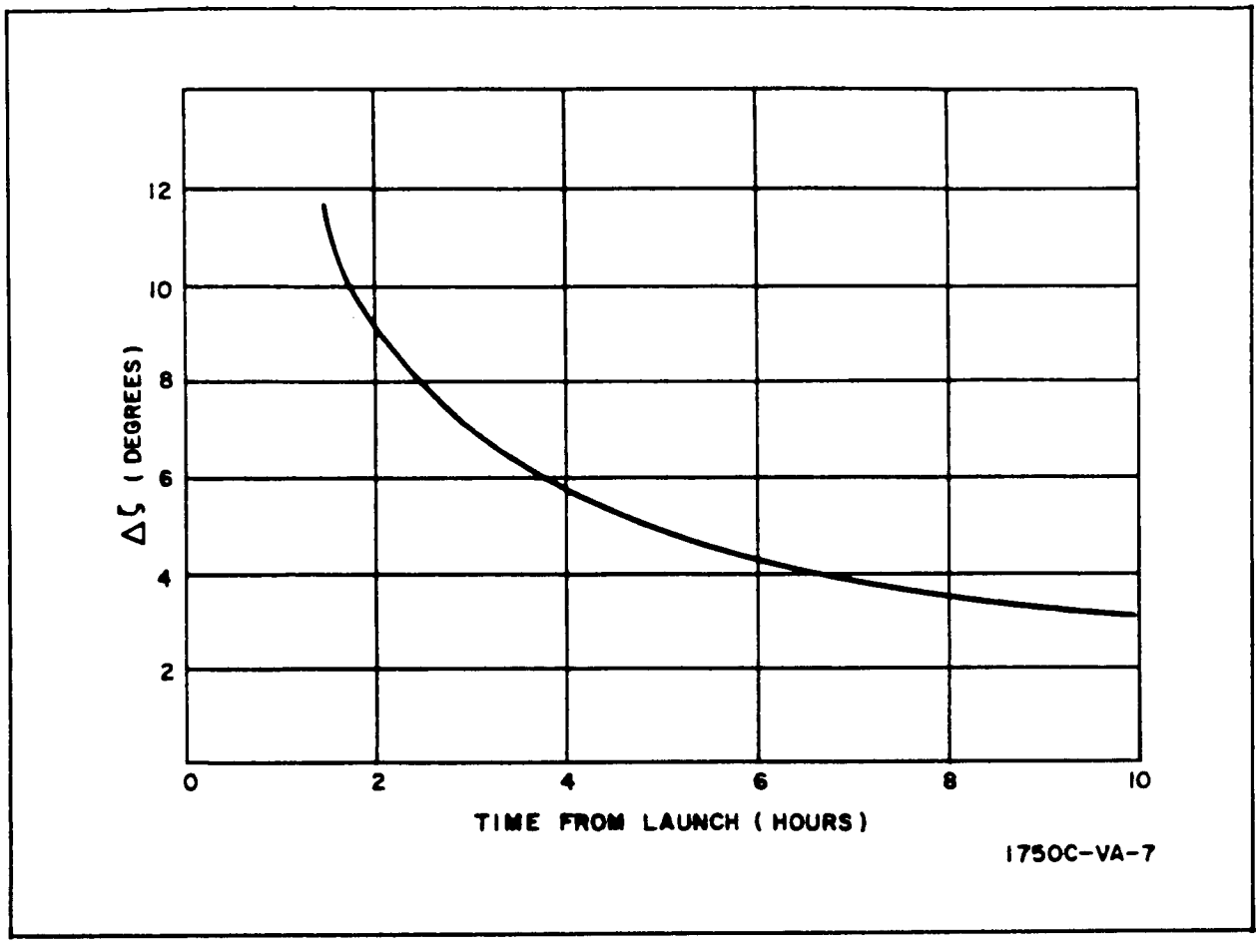

Figure 2-8. Angle Difference Between Horizon and Earth-Center Measurements

measurements. The primary difference between the measurements is evidently one of mechanization and the range at which the measurement is taken; i.e., landmark-star measurements might be used at close ranges and horizon/star measurements at long ranges.

In the computer program, the variance, Q, of the measurement errors is given by:

$$Q = \sqrt{\sigma^2 + (k/R)^2} \qquad (2\text{-}61)$$

where σ^2 is the variance of instrument errors and $(k/R)^2$ is the variance of range-dependent errors caused by uncertainties in defining the planet reference point. This latter term is primarily to account for the random errors which may occur in attempting to define the earth or moon horizon. In the present program there is no provision for systematic errors such as might exist in determining the location of a landmark on the moon. However, the assumed $(k/R)^2$ error is large enough to account for the effects of such a systematic error even through the mathematical model employed is not exact.

Figure 2-9 shows the geometry used in deriving the $(k/R)^2$ term. The angular error $\Delta\zeta$ caused by an error k in the planet radius is given as:

$$\Delta\zeta \cong \frac{k}{s} \cong \frac{k}{R} \tag{2-62}$$

If k is the rms value of the radius error, the variance of the angle measurements is $(k/R)^2$.

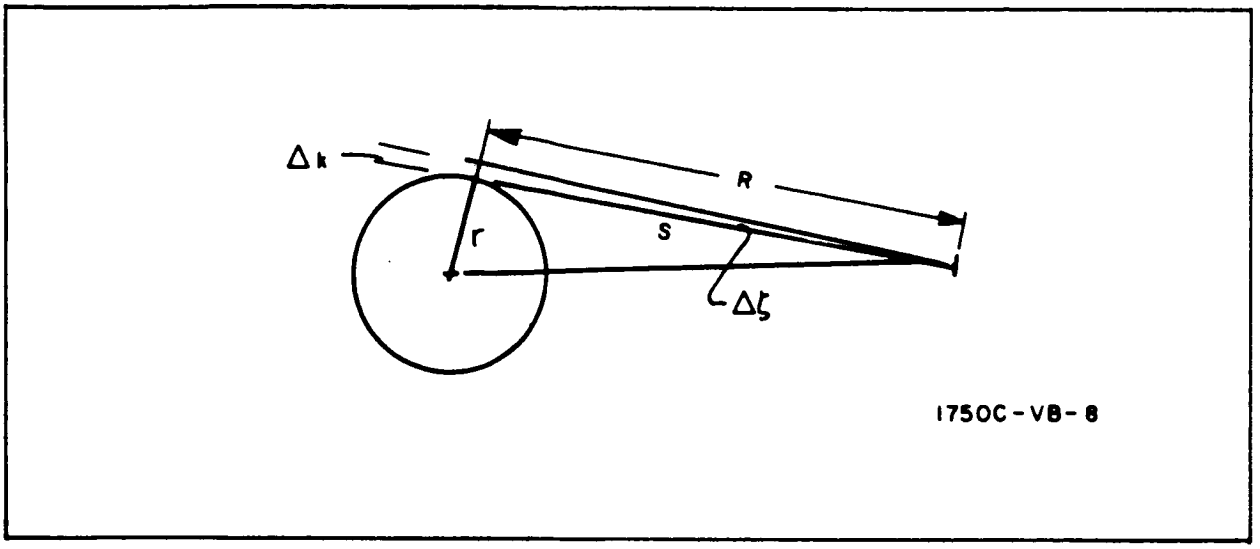

Figure 2-9. Geometry of Reference Point Errors

2.4 RESULTS

This subsection describes the outputs of the midcourse guidance study, including both general conclusions and specific numerical results.

2.4.1 General Discussion of Guidance Scheduling

Before going into specific numerical results from the computer program, some of the pertinent factors affecting the choice and scheduling of midcourse operations will be discussed. These principles, although simple enough in themselves have evidently not appeared in the literature before and have often been ignored in past investigations.

To specify guidance requirements, a schedule of guidance operations (observations and velocity corrections) must be assumed since it is obvious that the more measurements which can be made, the more precisely the trajectory can be determined. However, it is clear that there must be some "cost" attached to each optical measurement, since this measurement may involve vehicle orientation, operator participation, computer operation, and reliability factors. Also, it is obvious that the miss distance can be reduced by postponing velocity corrections but that this delay will in turn require

larger corrections. Thus, it can be seen that guidance system requirements for midcourse must consist not only of specification of hardware functions and accuracies, but also of the guidance schedule (at least approximately) which must be used with a given system. In other words, lack of appreciation of the guidance scheduling problem could result in overspecifying or underspecifying system requirements.

Several papers (Ref. 2-2 and 2-8) have been concerned with the scheduling problem. When this study began the only reference work was that of Battin (Ref. 2-2), and it will be shown that his methods do not yield optimum results. Denham (Ref. 2-8) has recently derived a more fundamental (and considerably more complicated) approach to this problem, but the results are not considered here. Good results were achieved in this study by choosing guidance schedules on a cut-and-try procedure; the numerical results of Ref. 2-2 were improved upon significantly.

2.4.1.1 Effect of Individual Measurements

First, consider the reduction in the trajectory uncertainties which result from taking optical measurements. From equation 2-28, it can be seen that the reduction in estimation uncertainty which results from each measurement is given by P-KHP where P is the uncertainty before the measurement, K is the weighting vector defined by equation 2-27, and H is the geometry matrix defined by:

$$H = \left[\frac{\partial \zeta}{\partial X} \; \frac{\partial \zeta}{\partial Y} \; \frac{\partial \zeta}{\partial Z} \; 0 \; 0 \; 0 \right] \tag{2-62}$$

where ζ is the angle measured. Since the quantity KHP increases monotonically with increasing H; i.e., the amount of reduction in estimation uncertainty depends directly upon H and, therefore, directly upon the partial derivatives $\partial\zeta/\partial X$, $\partial\zeta/\partial Y$, $\partial\zeta/\partial Z$. Thus, the magnitude of the partial derivative $\partial\zeta/\partial X$ indicates the relative geometric efficiency of the angle measurement in reducing the uncertainties in the X-direction - which is rather obvious when one considers the geometry of the situation.

Figure 2-10 illustrates the effects on reducing uncertainties of taking different types of measurements. The angles are measured in the XY-plane.

Figure 2-10(a) illustrates the fact that the value of angular measurement is inversely proportional to range to the planet from which the angle is being measured. If $\Delta X_1 = \Delta X_2$:

$$\Delta\zeta_2 > \Delta\zeta_1 \text{ and } \left.\frac{\partial\zeta}{\partial X}\right|_{X_2} > \left.\frac{\partial\zeta}{\partial X}\right|_{X_1} .$$

Figure 2-10(b) shows that the uncertainties are reduced most strongly in a plane perpendicular to the line of sight. Consider the coordinates X and X'.

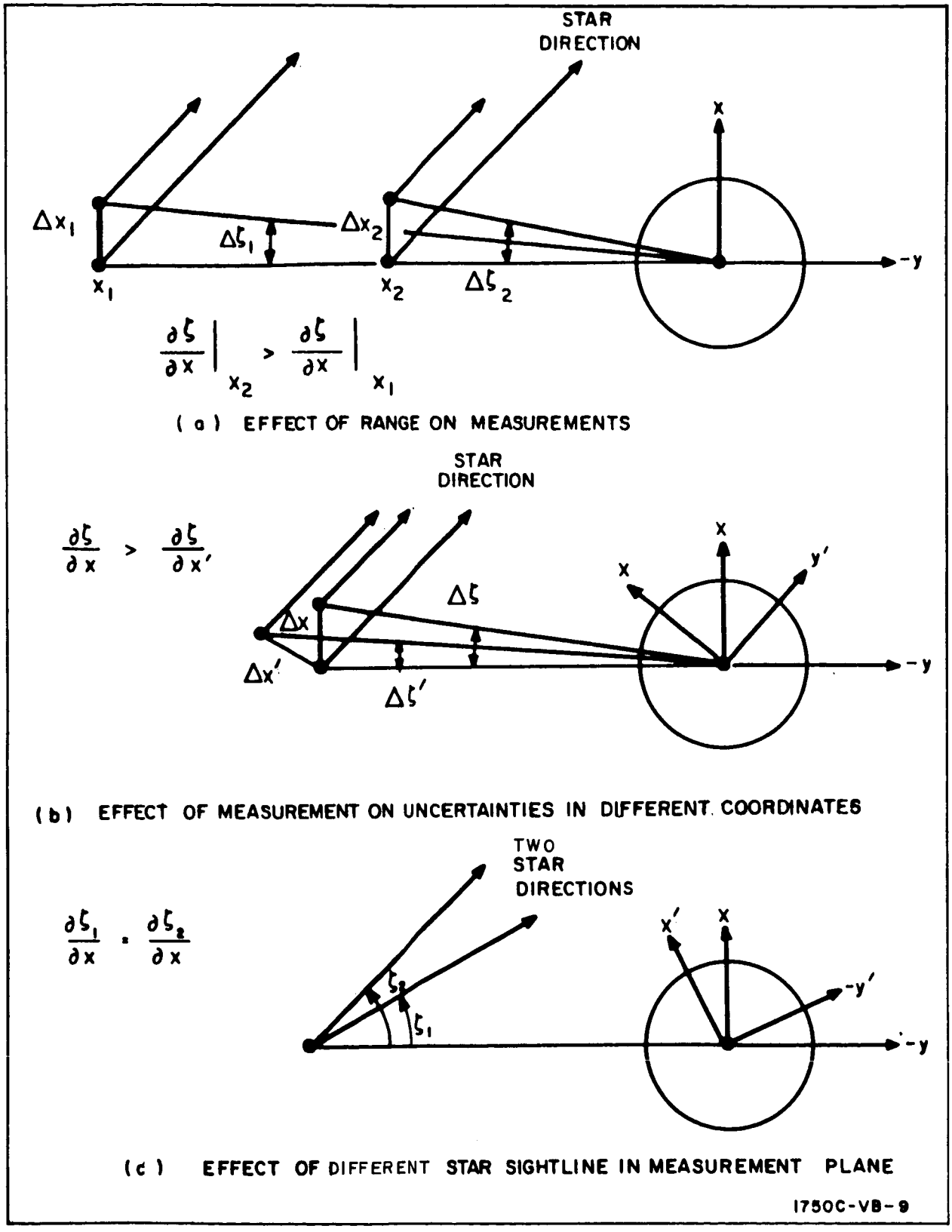

Figure 2-10. Effects on Reducing Uncertainties of Taking Different Types of Measurements

For $\Delta X = \Delta X'$:

$$\frac{\partial \zeta}{\partial X} > \frac{\partial \zeta}{\partial X'}$$

showing that the indicated measurement is more effective in reducing the uncertainities in the X-direction than the X'-direction. In fact, since $\partial \zeta / \partial Y = 0$, no information about uncertainties in the Y-direction can be obtained with measurements in which the sightline to the planet is along the Y-axis.

The above two effects strongly influence observation scheduling for lunar trajectories. Figure 2-11, which is a typical schedule, shows that during the time period of 34-59 hours, no measurements are taken. If measurements were taken during this period, they would be relatively ineffective since: the range to the earth is large, and the sightline to the moon rotates very little during this period. As a result, the uncertainty along the sightline to the moon becomes large but cannot be efficiently reduced.

Figure 2-10(c) illustrates the fact that reduction of the uncertainties in a given plane is independent of the direction of the star sightline, so long as the star sightline is in the plane of interest. In the figure it is obvious that $\partial \zeta_1 / \partial X = \partial \zeta_2 / \partial X$ and $\partial \zeta_1 / \partial X' = \partial \zeta_2 / \partial X'$. This is another significant point in observation scheduling. If the trajectory plane and the plane of the moon's orbit are coplanar (and this is a desirable situation for achieving an orbit about the moon's equator), then the largest trajectory uncertainties will be in this common plane. Since this is the case, most of the angle measurements should be made to lie in the plane of the trajectory and it is relatively unimportant, for trajectory estimation, exactly where in the plane the star sightline is. It is this fact which makes trial-and-error guidance scheduling simple, since choice of stars in some precise "optimum" direction is not required. Thus, the important constraints on the choice of stars for measurements on an actual flight would be field of view required and visibility.

In the "optimized" trajectory described later, 39 observations to stars in the trajectory plane were taken, and 6 observations were taken of star-planet angles whose plane was perpendicular to the trajectory plane. Taking fewer or more "perpendicular" measurements degraded the results somewhat.

Since trajectory uncertainties are reduced most sharply in a plane perpendicular to the sightline to the planet, it is advantageous to have this sightline in as many different directions as possible. This is one reason why, as the vehicle nears the moon and the sightline direction begins rotating rapidly, the efficiency of optical measurements is greatly enhanced, as shown by the sharp difference between r, the miss distance, and $\tilde{r}$, the estimation error, in all these results. This implies that measurement accuracy requirements for navigation in a lunar orbit are much less severe than for the Midcourse

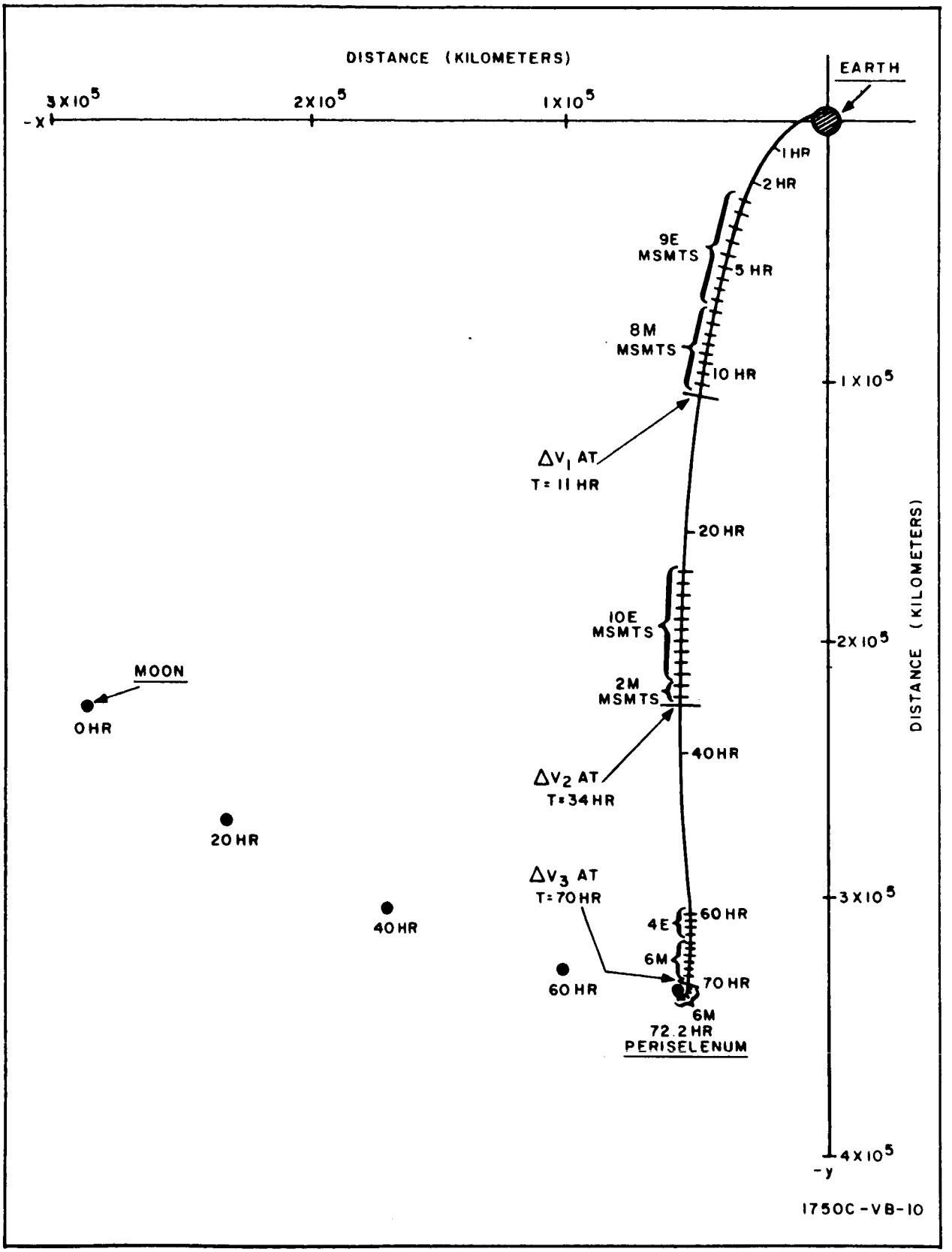

Figure 2-11. Guidance Schedule Used on Standard Case

Phase; in a lunar orbit, landmark and timing uncertainties have a much greater effect than in midcourse and are the limiting factors.

2.4.1.2 Sequential Optimization of Operations

The navigation scheduling problem can be stated as follows: Given some requirements on the target miss and estimation accuracy, determine the guidance schedule which will achieve these end conditions with the minimum number of observations and the minimum amount of correction fuel.

An attempt at solution of this problem is outlined in Ref. 2-2. In that paper, a sequential optimization is used, wherein at various time points throughout the trajectory, a decision logic is employed to (1) decide whether to make a correction, an observation, or do nothing at all and (2) in the case of an observation, take that measurement which will reduce the predicted target uncertainties by the greatest amount. Although this process is useful for preliminary analysis, a truly optimum schedule cannot result from this process because of the sequential nature of the optimization process.

The difficulties involved in sequential scheduling can be appreciated by considering the following examples:

a. Assume that at some time t_k, the decision criterion described above shows that it is advantageous to make a correction. Although a correction at t_k may be useful, it is not known whether or not it would be even better to postpone the correction until some later time t_{k+1}, with a possible improvement in expected system performance.

b. Assuming it has been decided that a measurement should be taken, which measurement shall it be? A sequential optimization technique based on reducing the predicted target errors by the maximum amount on each measurement will reduce the largest error component at the time of measurement. However, as in (a) above it may be better to defer this measurement until some later, more advantageous time.

To illustrate (b) above, consider the group of observations before the first correction is made on the standard trajectory described in paragraph 2.4.2. Application of the sequential decision method would result in the choice of a "perpendicular" measurement (see paragraph 2.4.1.1) at the second observation since the first observation will have reduced in-plane uncertainties to less than out-of-plane uncertainties. However, several computer runs indicated that overall system performance could be improved slightly by postponing this measurement and making a temporarily less efficient in-plane measurement at observation two.

Although the above mentioned effect was slight, the timing and number of velocity corrections derived in Ref. 2-2 by use of this decision logic produced results which could be improved upon. Table 2-5 compares the results of computer runs done for this study with similar work done in Ref. 2-2.

TABLE 2-5

COMPUTER RUN COMPARISON

Study	r(km)	v(m/s)	$\tilde{r}$(km)	$\tilde{v}$(m/s)	$\Sigma\Delta v$(m/s)
62.56-hour trajectory (Ref. 2-2)	18.0	27.0	1.93	1.75	34.6
63.9-hour trajectory (this study)	17.6	11.8	2.65	1.61	38.2

The trajectories used were similar (63.9 hours to 133-km periselenum compared with 62.56 hours to 97.5-km periselenum) and the errors in making observations and corrections were identical, so that the differences between the results were almost entirely due to different scheduling and injection conditions. The somewhat higher injection errors assumed on the 63.9-hour trajectory resulted in a higher total correction velocity ($\Sigma\Delta v$). But the most striking difference between the results is the much larger velocity deviation (v) at periselenum on the 62.56-hour trajectory. This was due to the fact that the 62.56-hour schedule employed four corrections compared to three on the 63.9-hour flight and the fourth correction was made only 45 minutes before periselenum. The low position estimation error ($\tilde{r}$) on the 62.56-hour trajectory was due to making the final observation only 9 minutes from periselenum compared to 24 minutes on the other trajectory. In summary, the results obtained using three corrections were equivalent to those obtained using four, except for the final velocity deviation which was much worse on the four-correction schedule.

2.4.2 Development of Standard Guidance Schedule for Analysis

To analyze the effect of system parameter variations, it was decided to generate one standard case and then vary the different parameters one at a time. This standard case consists of a trajectory, a guidance schedule, and system parameters.

The standard case used in this analysis is not recommended for any particular mission but rather is intended to be a representative group of numbers to serve as a starting point for the analysis. The trajectory used is trajectory I (paragraph 2.3.1), a 72.2-hour in-plane flight to a 200-km periselenum. The guidance schedule is one selected after several cut-and-try attempts at improving the schedule. Typical system parameters were assumed after study of two references which analyzed similar systems (Ref. 2-2 and 2-9).

The system parameters assumed for the standard case are as shown in table 2-6.

Most of these assumed parameters come from similar studies of the mid-course guidance problem in which only one value of each parameter was used. The initial condition errors were supplied by the Marshall Space Flight Center.

The standard guidance schedule was based on several scheduling runs on the digital computer program described in paragraph 2.3.3. To develop a useful standard guidance schedule, an initial schedule was assumed, and variations in the schedule were tried to optimize the performance. Table 2-7 shows the initial guidance schedules used on the 72.2-hour trajectory and also on a trajectory which arrives at a 133-km periselenum after 63.9 hours.

TABLE 2-6

STANDARD CASE PARAMETERS

Description		Standard Value	
RMS optical instrument error		σ = 10 arc-seconds	(Ref. 2-2)
RMS errors:	earth	k_1 = 1.6 km	(Ref. 2-2)
	moon	k_2 = 0.8 km	(Ref. 2-2)
RMS correction errors:	percentage thrust	σ_k = 1 percent	(Ref. 2-10)
	cutoff magnitude	σ_ϵ = 0.1 m/s	(Ref. 2-10)
	thrust direction	σ_γ = 0.5 degrees	(Ref. 2-10)
RMS initial errors:	position	r_o = 2.76 km	(Ref. 2-11)
	velocity	v_o = 4.24 m/s	(Ref. 2-11)

TABLE 2-7

INITIAL GUIDANCE SCHEDULES

Basic 72.2-hour trajectory (run 3):

(2.5 hr - 10.5 hr) 0.5 hr spacing	a a a a a a a a d | a a a a a a a a d 9E 8M	Δv_1 at 11.0 hours
(22 hr - 33 hr) 1-hr spacing	a a a a a d a a a a | a d 10E 2M	Δv_2 at 34.0 hours
(60 hr - 65 hr) 1-hr spacing	a a a a | a d 4E 2M	Δv_3 at 66.0 hours
(67 hr - 70 hr) 1-hr spacing (70.3 hr - 71.8 hr) 0.3-hr spacing	a a a a a d a a a a 10M	periselenum at 72.2 hours

(See key on next page)

TABLE 2-7 (Continued)

Basic 63.9-hour trajectory (run 10):

(1.5 hr - 9.5 hr) 0.5-hr spacing	a a a a a a a a d | a a a a a a a a 9E 8M	Δv_1 = 10 hr
(23 hr - 34 hr) 1-hr spacing	a a a a a d | a a a a a a d 6E 6M	Δv_2 = 35.0 hr
(53 hrs. - 60 hrs.) 1-hr spacing (60.5 hrs - 61.5 hrs.) 0.5 - hr spacing	a a a a | a a d a a a a d 4E 8M	Δv_3 = 62.0 hr
(62.6 hrs - 63.5 hrs.) 0.3 hr spacing	a a a a 4M	periselenum at 63.9 hours

Key:

a - observation of angle in trajectory plane
d - observation of angle perpendicular to trajectory plane
E - observation of angle between earth and star
M - observation of angle between moon and star
Δv - trajectory thrust correction

In each of these schedules, 45 measurements are made in groups bounded by three velocity corrections.

Table 2-8 shows the results of computer runs in which some improvement on these initial schedules is attempted without additional measurements or corrections. In discussing results from the computer program, the quantities r, v, $\tilde{r}$, $\tilde{v}$, and $\Sigma \Delta v$ are shown for comparison. These quantities are again defined for convenience:

r = rms position deviation at t_A, nominal time of periselenum

v = rms velocity deviation at t_A

$\tilde{r}$ = rms position estimation error at t_A

$\tilde{v}$ = rms velocity estimation error at t_A

$\Sigma \Delta v$ = sum of rms correction velocities during flight

It should also be mentioned here that although r is the rms position deviation at t_A, most of this miss is in the downrange direction and is actually an error in time of arrival. Thus, the geometric miss is considerably smaller than r. Typically the periselenum altitude miss is approximately 0.2r and the cross-range miss is 0.1r.

TABLE 2-8

RESULTS OF SCHEDULING RUNS

No.	Description	r	v	$\tilde{r}$	$\tilde{v}$	$\Sigma\Delta v$
3	Basic 72.2-hr (table 2-7)	21.38	11.71	2.51	1.57	20.4
4	2nd Δv at 37.0 instead of 35.0	20.66	11.32	2.51	1.57	20.3
5	Observations at 1.5, 2.0 instead of 22, 23	21.46	11.71	2.51	1.57	19.7
6	3rd Δv at 70 instead of 66	16.81	12.24	2.38	1.50	24.4
7	10 elevation measurements instead of 6	23.29	12.71	2.58	1.60	20.4
8	2nd leg = 8E, 4M instead of 10E, 2M	23.87	12.87	2.43	1.52	20.1
9	1st leg = 12E, 5M instead of 9E, 8M	21.17	11.58	2.51	1.57	19.9
10	Basic 63.9 hr (table 2-7)	16.58	11.34	2.53	1.53	25.0
11	2nd Δv at 37 instead of 35	16.42	10.98	2.54	1.54	24.8
13	2nd leg = 8E, 4M instead of 6E, 6M	16.23	11.01	2.53	1.54	24.5
14	3rd Δv at 63 (43 measurements)	8.11	15.42	8.11	4.50	33.5
15	4 Δv's (at 10, 35, 60, 63)	6.19	6.73	4.18	2.43	26.9
16	9 elevation measurements instead of 5	17.18	11.60	2.56	1.55	25.1
17	1st leg = 6E, 11M instead of 9E, 8M	16.98	11.75	2.57	1.56	26.6
18	1st leg = 12E, 5M; 2d leg = 8E, 4M	15.98	10.78	2.51	1.53	23.3

Key:

r = rms position deviation from nominal at periselenum (in km)

v = rms velocity deviation from nominal at periselenum (in m/sec)

$\tilde{r}$ = rms position estimation error at periselenum (in km)

$\tilde{v}$ = rms velocity estimation error at periselenum (in m/sec)

$\Sigma\Delta v$ = sum of rms velocity corrections (in m/sec)

Runs 3 through 9 in table 2-8 were made using the 72.2-hour schedule, while runs 10 through 18 used the 63.9-hour trajectory. A summary of results follows.

Run 3 used the initial guidance schedule shown in table 2-7 and served as a starting point for the cut-and-try procedure used to generate the standard schedule for the 72.2-hour trajectory.

On run 4, the second correction was made at 37 hours instead of 34 hours, as on the initial schedule. This resulted in a slight improvement in system performance over run 3.

On run 5, measurements were made at 1.5 and 2.0 hours instead of 22 and 23 hours. Although the guidance accuracy, r, was slightly degraded, note that $\Sigma\Delta v$, the total corrective velocity, was decreased. This is because 19 measurements were made before the first correction, rather than 17, and less error was made in the first correction, thus requiring a smaller second correction.

On run 6, the third velocity correction was moved from 66 to 70 hours. As expected, miss distance was decreased at the cost of a higher fuel requirement.

On run 7, ten angle measurements were made perpendicular to the trajectory plane rather than six. These less efficient measurements resulted in some degradation from the results obtained in run 3.

Run 8 had less earth measurements in the second group of observations, producing a degradation in system performance, while run 9 had more earth measurements in the first group, producing an improvement.

In summary, the runs on the 72.2-hour trajectory showed slight changes as a result of scheduling changes. Run 6, in which the final correction was made at 70.0 hours, was selected as the standard trajectory for this study, although runs 4 and 9 indicated that the schedule could still be improved slightly by making the second correction later and taking more earth measurements in the first group of observations.

Runs 10 through 18 were made on the 63.9-hour trajectory. The effects of various schedule changes were similar to results obtained on the 72.2-hour trajectory, and the improved schedule selected as the standard 63.9-hour schedule was run 18. The improved schedules for both trajectories are shown in table 2-9.

TABLE 2-9

IMPROVED GUIDANCE SCHEDULES

Improved 72.2-hour trajectory:

(2.5 - 10.5 hr) 0.5-hr spacing	a a a a a a a a d 9E	a a a a a a a d 8M	Δv_1 at 11.0 hr
(22 - 33 hr) 1-hr spacing	a a a a a d a a a a 10E	a d 2M	Δv_2 at 34.0 hr
(60 - 69 hr) 1-hr spacing	a a a a 4E	a d a a a a 6M	Δv_3 at 70.0 hr.
(70.3 - 71.8 hr) 0.3-hr spacing	a d a a a a 6M	Periselenum at 72.2 hr	

Improved 63.9-hour trajectory:

(1.5 - 9.5 hr) 0.5-hr spacing	a a a a a a a a d a a a 12E	a a a a a 5M	Δv_1 at 10.0 hr
(23 - 34 hr) 1-hr spacing	a a a a a d a a 8E	a a a d 4M	Δv_2 at 35.0 hr
(53 - 60 hr) 1-hr spacing	a a a a 4E	a a d a a a a d 8M	Δv_3 at 62.0 hr
(60.5-61.5 hr) 0.5-hr spacing (62.6 - 63.5 hr) 0.3-hr spacing	a a a a 4M	Periselenum at 63.9 hr	

Key:

- a - observation of angle in trajectory plane
- d - observation of angle perpendicular to trajectory plane
- E - observation of angle between earth and star
- M - observation of angle between moon and star
- Δv_i - i^{th} velocity correction.

The standard navigation schedule for the 72.2-hour trajectory is illustrated in figure 2-11. Note that the observations have been grouped toward the end of the subtrajectories bounded by velocity corrections. In this way, trajectory information is utilized as soon as possible (by making a velocity correction), and long periods of time when no observations are made are available to the crew.

In figure 2-12, the step reduction in position uncertainty as a function of time is shown. Note that over periods when no observations are made, the

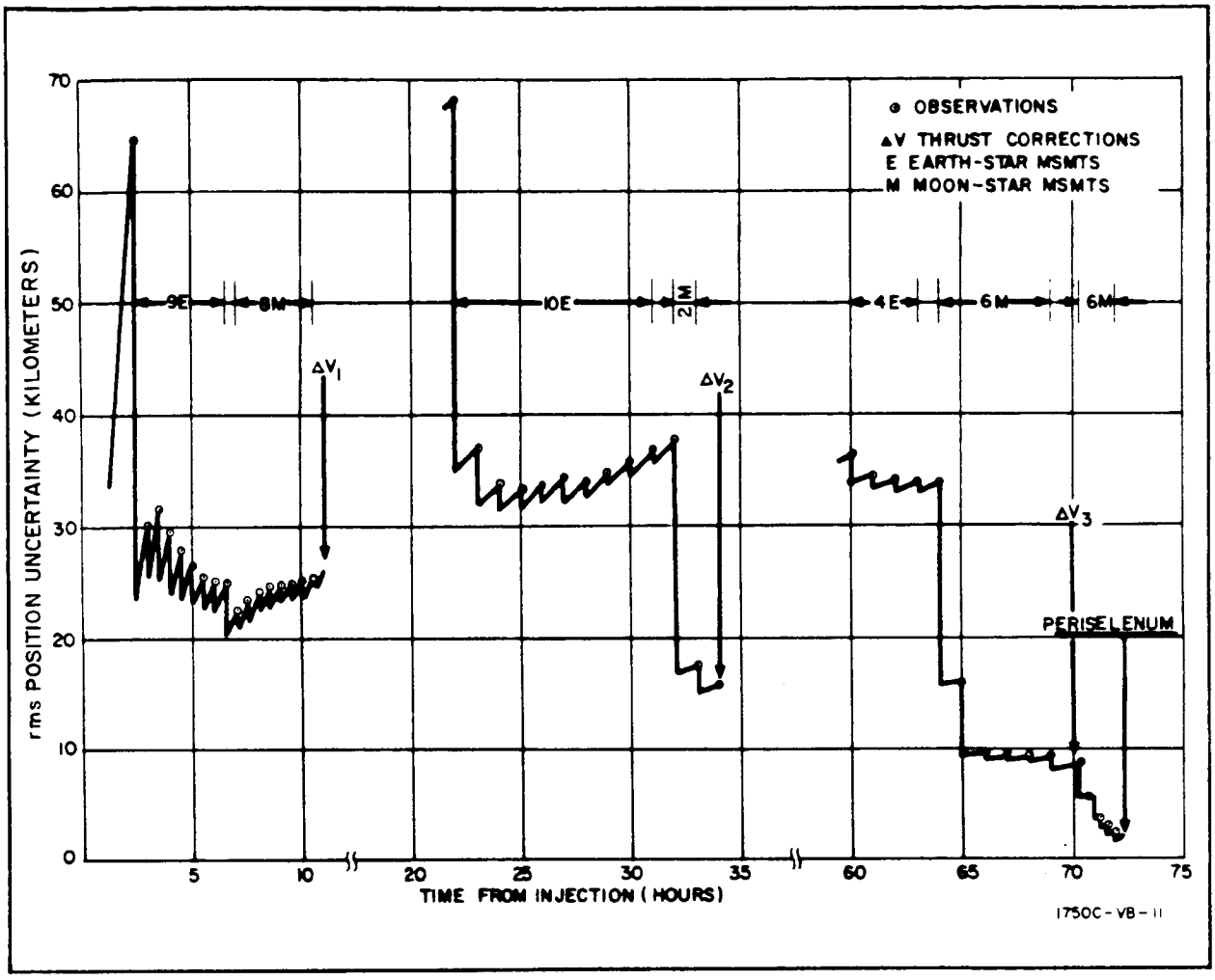

Figure 2-12. Step Reduction in Position Uncertainty vs Time

estimation error builds up (e.g., from 26.2 km at 11 hours to 68.4 km at 23 hours) but is quickly reduced by the first several measurements in the next group of observations. Note also that the estimation errors are reduced very strongly as the vehicle nears the moon. This is because of the decreased range and rotating sightline (to the moon) which occur as the vehicle nears periselenum. Figure 2-13 shows the rotation of the sightline to the moon in the last few hours before periselenum on the 72.2-hour trajectory.

2.4.3 Variation of Onboard Guidance System Parameters

In this paragraph, the parameters of the onboard optical guidance system model are varied about those standard values given in table 2-6 to determine performance sensitivity to each of the parameters. The standard 45-measurement, 3-correction guidance schedules developed in the previous paragraph were used on all the computer runs.

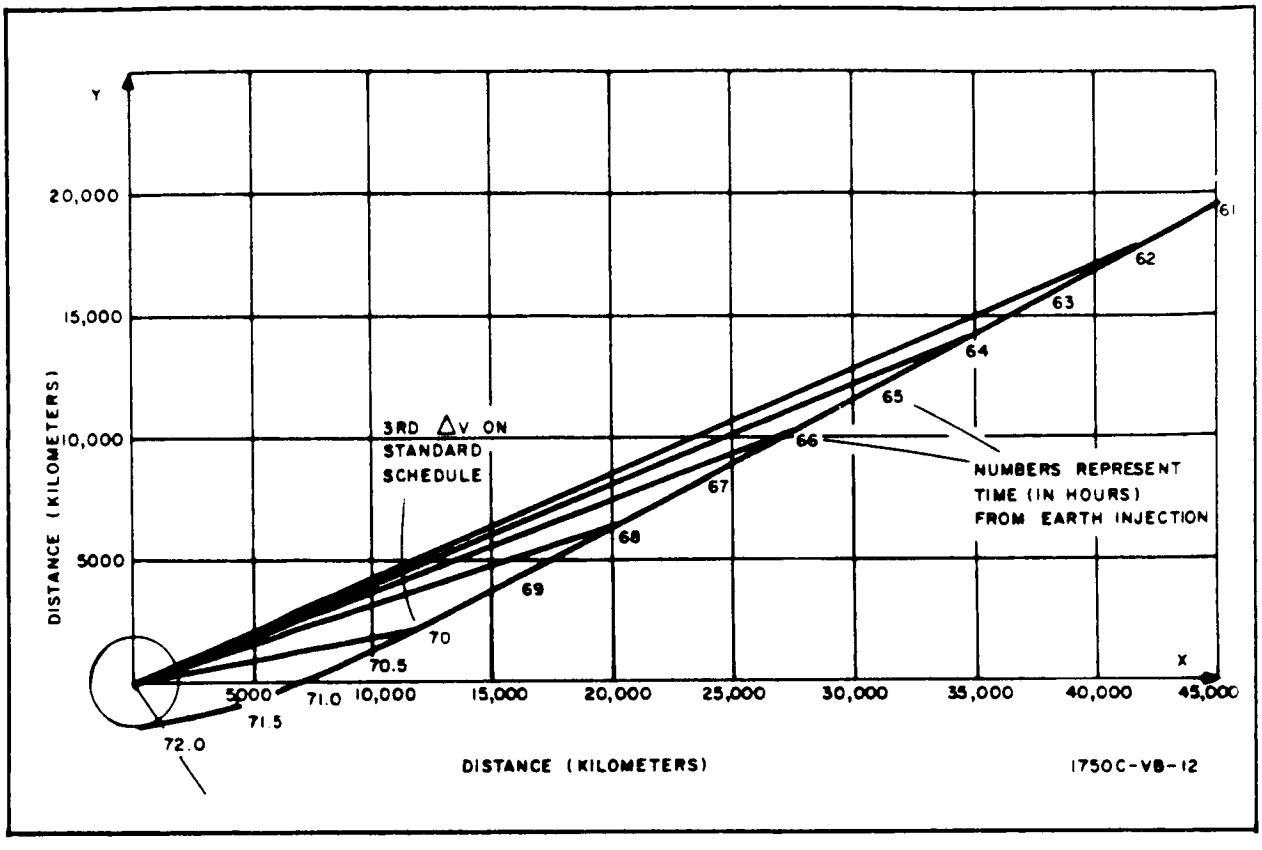

Figure 2-13. Rotation of Sight Line to Moon During Terminal Phase of Midcourse

2.4.3.1 Optical Instrument Accuracy

Computer runs were made in which all the standard parameters of table 2-6 were used, except for σ, the rms value of the optical instrument accuracy, which was varied from 5 arc-seconds to 30 arc-seconds. The results are shown in figure 2-14.

From figure 2-14, it is apparent that r and v, the periselenum deviations in position and velocity and $\Sigma\Delta v$, the total correction velocity required, all increase sharply with increasing instrument errors. However $\tilde{r}$ and $\tilde{v}$, the periselenum estimation errors are relatively insensitive. This difference is due to the fact that the miss quantities, r and v, and the total correction velocity, $\Sigma\Delta v$, are completely determined by the operations prior to and including the third and (final) velocity correction. However, the periselenum estimation errors, $\tilde{r}$ and $\tilde{v}$, are primarily determined by the measurements taken after the final correction. As can be seen in figure 2-13, these measurements are taken at much shorter ranges and are made with reference to a rotating sightline. Thus, the measurement accuracies requirements may be greatly relaxed, and accuracies up to 1 minute of arc are quite sufficient for accurate

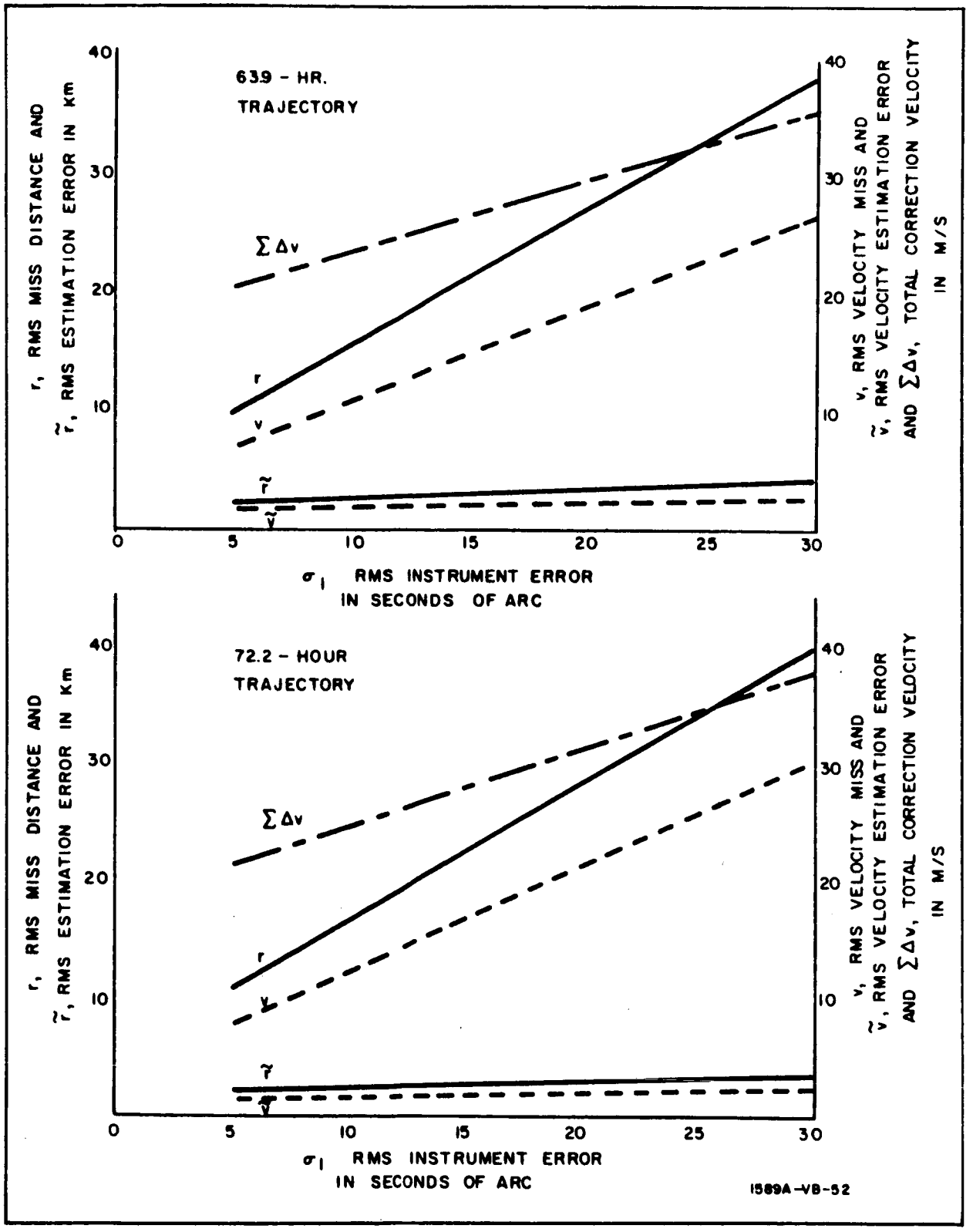

Figure 2-14. Effect of Instrument Accuracy on Guidance Parameters for 63.9- and 72.2-Hour Trajectories

trajectory estimation. Another reason the estimation errors are less sensitive to instrument errors is that during the terminal phase of the mission, the instrument errors of 5 to 30 arc-seconds are small compared to the landmark (or lunar reference) errors.

In addition to pointing up the sharp difference in optical accuracy requirements for the Midcourse and Orbiting Phases, the results of figure 2-14 indicate that a propellant-vs-accuracy tradeoff is possible if instrument accuracies on the order of 10 arc-seconds cannot be achieved. By postponing the third correction until a half-hour or so before periselenum, the trajectory can be determined with reasonable accuracy by an optical instrument whose accuracy is on the order of 30 arc-seconds. Another way of accomplishing the same result would be to use four corrections, with one shortly before periselenum (this is the Apollo schedule). In either case, requirements on the optical sensor accuracy can be relaxed at the expense of extra fuel. This tradeoff was not examined extensively, but some indication of the possibilities can be obtained by comparing run 10 and run 15 in table 2-8. Note the sharp reduction in miss distance for a relatively small fuel increase when a fourth correction is added to the initial guidance schedule. Note also, that run 14 indicates that merely postponing the third Δv is not nearly as effective as adding a fourth Δv.

In summary, it can be concluded that the optical instrument accuracy is a critical system parameter and should be kept to about 10 arc-seconds to achieve acceptable guidance with near-minimum fuel requirements.

2.4.3.2 Velocity Correction Accuracy

Table 2-10 lists the results of computer runs in which the quantities σ_K, σ_ϵ, and σ_γ are varied to determine the effect of velocity correction accuracy on guidance system performance. It can be seen from these results that accuracy in implementing the velocity corrections is not critical to performance of the type of system considered here. Figure 2-15 shows that even tripling the standard errors assumed in table 2-6 does not greatly degrade the periselenum results. Conversely, reducing the errors to zero does not greatly improve performance. This is because, for the type of system considered here, the greatest source of error in each velocity correction is the uncertainty in the trajectory estimate rather than the error in making the corrections.

This would not always be the case depending upon the guidance system being considered. In a ground tracking system, for instance, where the high data rate and more accurate measurements yield a more precise orbit determination, the correction errors can be the fundamental limitation on the accuracy of the guidance scheme.

In runs 131 through 133 (table 2-10), one of the standard correction errors is doubled, while the other two remain constant. Evidently, variations in σ_γ, the pointing error, have the greatest effect.

TABLE 2-10

EFFECT OF CORRECTION ERRORS AT PERISELENUM

No.	Description	r(km)	v(m/sec)	$\tilde{r}$(km)	$\tilde{v}$(m/sec)	$\Sigma \Delta v$(m/sec)
23	63.9 hr - zero correction errors	13.46	9.32	2.20	1.30	22.57
18	63.9 hr - standard correction errors	15.98	10.78	2.51	1.53	23.33
128	72.2 hr - zero correction errors	13.85	10.56	1.95	1.17	23.67
6	72.2 hr - standard correction errors	16.81	12.20	2.38	1.50	24.37
129	72.2 hr - doubled correction errors	18.55	14.03	3.20	2.11	26.03
130	72.2 hr - tripled correction errors	20.01	16.12	4.17	2.82	28.10
131	72.2 hr - σ_k doubled, $\sigma_\epsilon = \sigma_\gamma = 0$	16.18	11.78	2.17	1.36	24.40
132	72.2 hr - σ_ϵ doubled, $\sigma_k = \sigma_\gamma = 0$	15.30	12.27	2.63	1.72	23.27
133	72.2 hr - σ_γ doubled, $\sigma_\epsilon = \sigma_k = 0$	17.69	12.35	2.30	1.41	23.92

Standard Correction Errors

σ_k = standard deviation of percentage error in magnitude of thrust = 1 percent

σ_γ = standard deviation of pointing error = 0.5 degree

σ_ϵ = standard deviation of error due to cutoff inaccuracy = 0.1 m/sec

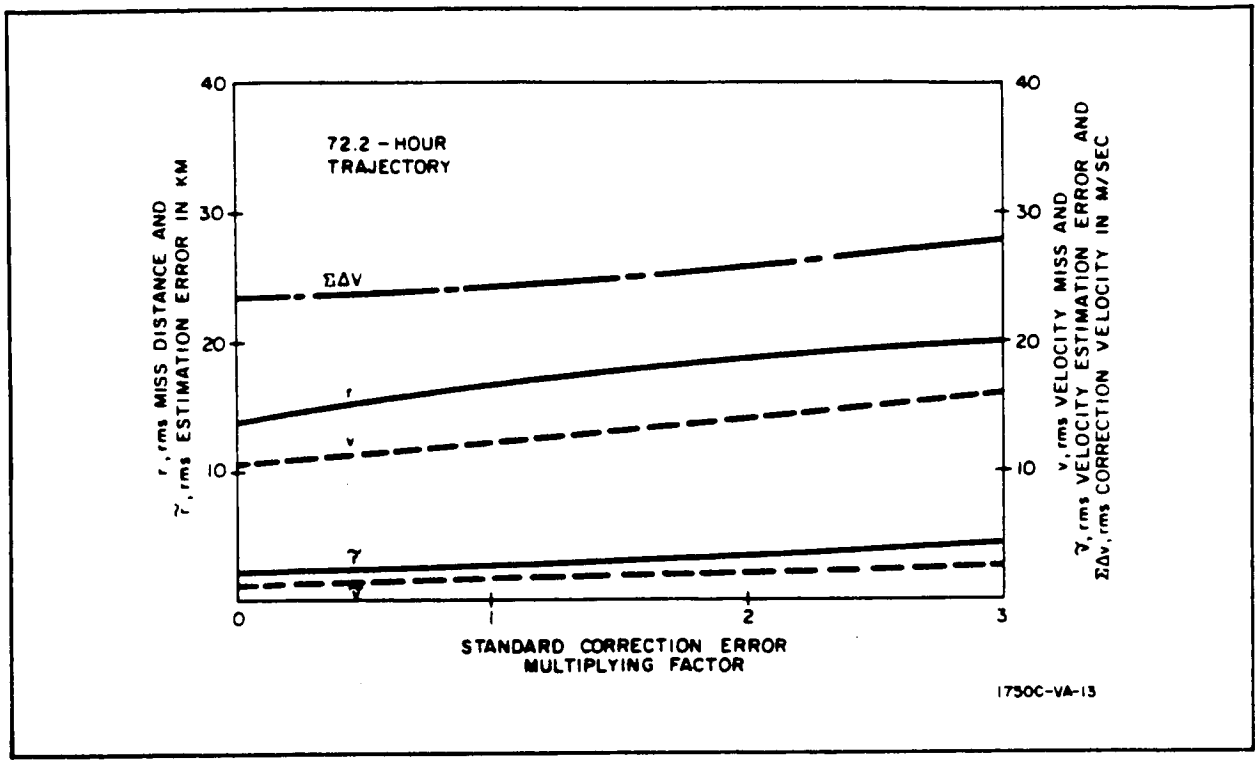

Figure 2-15. Effect of Variation of Correction Accuracy at Periselenum

2.4.3.3 Initial Condition Accuracy

In Ref. 2-9, it was shown that initial errors strongly affect the amount of correction velocity required but do not greatly influence the miss or estimation errors at periselenum. This conclusion is supported by results of this study, in which the initial errors of table 2-6 are doubled to determine their effect. The results are shown in table 2-11:

TABLE 2-11

EFFECT OF INITIAL ERRORS AT PERISELENUM

Item	r(km)	v(m/sec)	$\tilde{r}$(km)	$\tilde{v}$(m/sec)	$\Sigma\Delta v$(m/sec)
Standard Errors*	16.8	12.1	2.38	1.50	24.3
2 x Standard Errors	18.0	13.2	2.42	1.52	40.9

* r_o = 2.76 km, v_o = 4.24 m/sec

Despite doubling the injection errors, the position and velocity deviations, r and v, are only slightly degraded and the estimation errors are virtually

identical. The only quantity which is sharply affected is $\Sigma\Delta v$, the total correction velocity. This is primarily because of the much larger first correction which is required because of larger initial errors.

The errors assumed as standard are representative of the predicted performance of the Saturn V launch guidance system after a short parking orbit (Ref. 2-11). It is also assumed that no trajectory information will be available between injection and the first optical measurement (i.e., $N_o = P_o$).

2.4.3.4 Landmark Uncertainty

As shown in subsection 2.3, the variance of the measurement error can be represented by:

$$Q = \sqrt{\sigma^2 + (k_i/R_i)^2}$$

where σ is the rms instrument error and k_i is the uncertainty of the reference point on the planet to which the angle is being measured.

The values of k_1 = 1.6 km (earth) and k_2 = 0.8 km (moon) were used by Battin (Ref. 2-2) and presumably are the result of Apollo studies (although this has not been verified). The larger figure for k_1 is evidently due to the earth's atmosphere.

These errors have little effect at long ranges but, in the terminal phase, can be significant. Computer runs were made in which k_1 and k_2 were doubled. The results are shown in table 2-12.

TABLE 2-12

EFFECT OF LANDMARK AND HORIZON UNCERTAINTIES AT PERISELENUM

Item	r(km)	v(m/sec)	$\hat{r}$(km)	$\hat{v}$(m/sec)	$\Sigma\Delta v$(m/sec)
Standard (k_1 = 1.6 km, k_2 = 0.8 km)	16.8	12.2	2.38	1.50	24.4
Doubled (k_1 = 3.2 km, k_2 = 1.6 km)	18.8	13.0	3.68	2.23	24.7

Table 2-12 shows that doubling the landmark and horizon uncertainties only slightly affects the position and velocity miss and the correction fuel. This is because these quantities are only affected by operations performed before the third velocity correction at 70 hours which is at a range of 12,261 km from the moon. At such long ranges, landmark or horizon uncertainties are relatively insignificant when compared to the assumed instrument uncertainty of 10 seconds of arc.

After the third correction, as the vehicle approaches the moon, landmark uncertainties become a more important factor as can be seen by examination of $\tilde{r}$ and $\tilde{v}$ for the two cases. However, the results are still reasonable, even with the doubled errors.

2.4.3.5 Effect of Measurement Timing Errors

Measurement timing errors were not mechanized in the computer program used in this study. This is because equations developed in Section 6 of Appendix B (Volume V), indicated that measurement timing is not a critical error source. It is shown that on measurements before the third correction, timing errors of 1 second have negligible effect on results. For the last few measurements before periselenum 0.1-second timing accuracy is required.

If only 1-second timing precision is available during this terminal period, the result is to increase $\tilde{r}$ and $\tilde{v}$ in a manner similar to the doubled landmark errors in table 2-12.

2.4.4 Effect of Nominal Trajectory

Most of the preceding results were generated using a 72.2-hour in-plane trajectory to a 200-km periselenum. To determine what effect, if any, different nominal trajectories would have on guidance system requirements, three other trajectories were generated. These trajectories include a 63.9-hour in-plane flight to a 133-km periselenum, a 71.5-hour in-plane flight to a 200-km periselenum, and a 72.1-hour in-plane flight to a 200-km periselenum.

Computer results obtained using these other trajectories are presented and compared to the 72.2-hour trajectory (trajectory I). However, the only conclusion which is drawn is that the effects of nominal trajectory variations are slight, although the out-of-plane case is evidently slightly more difficult. The reason more definite conclusions are not drawn is that it is not always possible to be sure that the differences noted when comparing one trajectory to another are not due to some other factor (such as scheduling) since the differences are slight.

2.4.4.1 63.9-Hour Trajectory (Trajectory II)

Comparison of the standard cases on the 72.2-hour trajectory (to 200-km periselenum) and 63.9-hour trajectory to 133-km periselenum reveals that guidance performance is better on the faster trajectory. However, this result is not general and, in fact, was due to the more restrictive assumptions made on the 72.2-hour schedule. Comparison of the standard schedules for the two trajectories in table 2-9 shows that the 63.9-hour schedule has several advantages. These are:

	63.9-hour	72.2-hour
Final correction (ΔV_3)	1.9 hours before end-point	2.2 hours before end-point
Measurements before ΔV_3	41	39
Time between measurement and ΔV_3	0.5 hour	1 hour
Second correction (ΔV_2)	t = 35 hours	t = 34 hours

All the factors listed above tend to make the miss quantities r and v greater on the 63.9-hour trajectory. In order to make a valid comparison of results on trajectories having different flight times, an improved schedule was generated for the 72.2-hour trajectory. This schedule, and the results obtained with the schedule compared to the standard cases, are shown in table 2-13.

TABLE 2-13

EFFECT OF FLIGHT TIME ON GUIDANCE PERFORMANCE

	r(km)	v(m/sec)	$\tilde{r}$(km)	$\tilde{v}$(m/sec)	$\Sigma\Delta v$(m/sec)
Optimized schedule (72.2 hours)	14.0	10.4	2.36	1.48	23.5
Standard case (72.2 hours)	16.8	12.2	2.38	1.50	24.4
Standard case (63.9 hours)	16.0	10.8	2.51	1.53	23.3

Optimized 72.2- hours Trajectory:

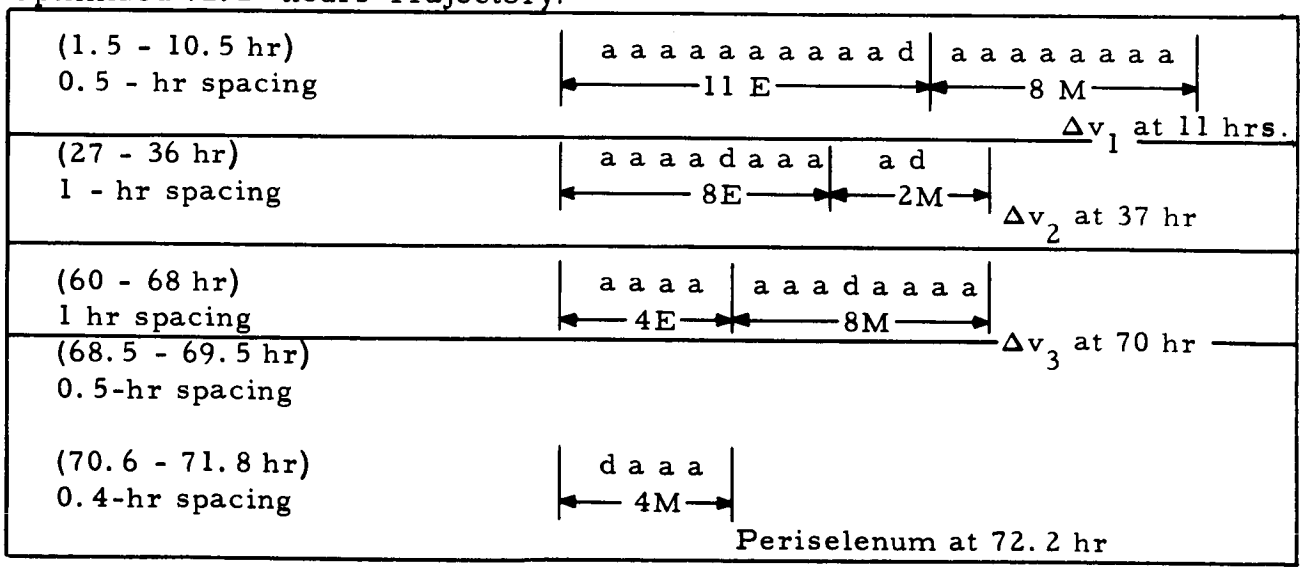

A comparison of the results for the "optimized" 72.2-hour schedule and the 63.9-hour schedule shows that the guidance performance is not quite as good on the faster flight. This is what would be expected theoretically because: (1) the moon sweeps out less arc (in an earth-centered system) on the 63.9-hour flight, thus providing less sightline rotation during the flight for optical

measurements; (2) velocities are higher, causing errors (in a fixed time of arrival system) to propagate more quickly; and (3) the 133-km periselenum on the 63.9-hour flight compared to the 200-km periselenum on the 72.2-hour flight is expected to make guidance slightly more difficult on the shorter flight. The importance of this last effect is not known exactly, but is probably small.

The conclusion which is drawn from all this is that mission flight time has only a slight effect on guidance system performance. In other words, mission flight time might have some small effect on expected errors but not a large enough effect to justify specifying different sensor requirements for different mission times.

2.4.4.2 71.5-hour Out-of-Plane Trajectory (Trajectory III)

The 71.5-hour out-of-plane (of the lunar orbit) trajectory was generated not only for comparison with the standard trajectory I but also to determine whether or not more angle measurements sould be taken perpendicular to the trajectory plane for a trajectory which makes an angle (23 degrees in this case) with the lunar orbit plane. The results of computer runs are shown in table 2-14.

Table 2-14 shows that addition of extra elevation measurements (i.e., perpendicular to trajectory plane), degrades results somewhat on this trajectory as well as the standard trajectory. Comparison of runs 60 and 6 indicates that the out-of-plane case requires somewhat better guidance. This is not a firm conclusion, however. For one thing, the final correction on the 71.5-hour trajectory is made 2.5 hours before periselenum compared to 2.2 hours before periselenum on the 72.2-hour trajectory.

TABLE 2-14

71.5-HOUR TRAJECTORY WITH ΔV_3 AT 69.0 HOURS**

Run	Description	r	v	$\sum\Delta v$
6	Standard 72.2 hour	16.8	12.2	24.4
60	71.5 hour (6 el msmts*)	19.9	12.6	23.5
61	71.5 hour (12 el msmts)	22.2	13.5	23.4
62	71.5 hour (9 el msmts)	20.6	12.8	23.4
63	71.5 hour (8 el msmts)	20.0	12.6	23.5

* el msmts are measurements of angles perpendicular to the trajectory plane.

** Useful data on $\tilde{r}$ and $\tilde{v}$ not obtained.

2.4.4.3 72.1-Hour Trajectory (Trajectory IV)

A 72.1-hour trajectory to 100-km periselenum was generated for comparison with the 200-km periselenum of the standard case. Actually, however, the difference between the two cases is not great, since actually periselenum radii of 1938 and 1838 km are being compared. The results of computer runs showed little difference between the two cases.

2.4.5 Other Error Sources

In the computer program used in this study, the only observation errors considered are those from random instrument errors and landmark uncertainties. These errors are assumed unbiased from one observation to another. On a real mission, however, at least two other errors sources may be significant and must at least be accounted for in an analysis, if not on a mission. these are:

a. Instrument bias errors or other time-correlated measurement errors
b. Uncertainties in the astrodynamic constants

These error sources have been the subject of investigation by G. L. Smith of Ames Research Center in his recent paper (Ref. 2-7). Although Smith's work is not perfectly suited to the problem at hand and contains some questionable points which are discussed in Section 7 of Appendix G, (Volume V), the theoretical treatment of the topic is excellent and Smith's results are utilized directly in this study as much as possible.

If it is suspected that some systematic error, such as an uncertainty in a physical constant, is present, then it may be accounted for in the navigation equations by use of "augmented" state equations such as equations 2-20 through 2-22, which are the optimal estimation equations for a system described by equations 2-18 and 2-19. But recall that in simplifying equations 2-20 through 2-22 to obtain equations 2-23 through 2-25, it is stated that since no time-correlated errors are present, the equations relating to the error process can be dropped. However, for systematic errors, these terms are not dropped and equations 2-20 through 2-22 are used. The state vector $\underline{x}^*$ now consists of all the trajectory deviation quantities ΔX, ΔY --- $\Delta \dot{Z}$ plus a_1, a_2 --- a_n, where the a's are systematic errors. This process is derived in detail in Section 7 of Appendix B (Volume V).

Since these systematic errors can be accounted for, the problem is to determine just how many of these errors are significant enough to be included in an onboard computer system and what happens if they are not accounted for. This last problem is discussed by Smith in Ref. 2-7 and the results of his study, where applicable, are presented here.

Table 2-15, from Ref. 2-7, lists the estimated uncertainties in each of the astrodynamic constants according to Ref. 2-12. Also listed is the maximum acceleration which can result from an error of the size listed. It can be seen that the errors caused by the assumed uncertainties in R_{es}, J_1, and μ_s are negligible and are given no further consideration.

TABLE 2-15

ASTRODYNAMIC CONSTANT UNCERTAINTIES

Constant	Symbol	Error Magnitude	Percentage	Max $\Delta\ddot{X}$ (g's)
Earth gravitation	μ_e	$\pm 9\ (10^9)\ m^3/sec^2$	0.002	$2\ (10^{-5})$
Lunar gravitation	μ_m	$\pm 3\ (10^9)\ m^3/sec^2$	0.06	10^{-4}
Sun gravitation	μ_s	$\pm 4\ (10^{16})\ m^3/sec^2$	0.03	$9\ (10^{-10})$
Earth-moon distance	R_{em}	±2 km	0.0005	$3.7\ (10^{-4})$
Earth-sun distance	R_{es}	$\pm 4\ (10^4)$ km	0.03	$1.9\ (10^{-9})$
First harmonic in Earth's potential	J_1	$\pm 5\ (10^{-8})$	0.003	$4.5\ (10^{-8}$

Table 2-15 indicates that the three constants of interest are μ_e, μ_m, and R_{em}. It should be pointed out that this error model assumes that all significant uncertainty in the position of the moon with respect to the earth is along the earth-moon line. If this is not true, then errors in all three dimensions must be considered.

Smith makes the conservative assumption that the errors listed in table 2-15 are 1-σ values, then compares computer runs in which

a. No astrodynamic errors are present,
b. Astrodynamic errors are present and the augmented state equations are used to compute them.

Unfortunately, no runs are made in which astrodynamic errors are present but ignored in the navigation equations.

A direct application of the numerical results of Ref. 2-7 would be unwise here because of the assumptions made in that study. For one, the trajectory used in Ref. 2-7 is circumlunar, with a 4766-km periselenum at 79.9 hours, evidently resulting in less severe guidance requirements than the trajectories used in this study. Also the injection errors are assumed to be only 1 km in position and 1 m/sec in velocity compared to 2.76 km and 4.24 m/sec assumed standard in this study. In addition, each observation consisted of the simultaneous measurement of azimuth, elevation and subtended angle of the earth or moon. Finally, the work done in Ref. 2-7 evidently assumes that an earth-centered coordinate system is used throughout the flight. This assumption makes the error in earth-moon distance (ΔR_{em}) have a greater effect on periselenum performance than would be the case if a moon-centered

coordinate system were used near the moon. In Section 8 Appendix B (Volume 5) it is shown that switching to a moon-centered coordinate system will tend to reduce the effects of initial uncertainties in the moon's distance from the earth.

Despite these difficulties, some results from Ref. 2-7 are shown in table 2-16 for discussion. These results were generated using a 45-measurement, 3-correction schedule.

TABLE 2-16

RESULTS WITHOUT ERRORS COMPARED TO COMPENSATED ERRORS (REF. 2-7)

Item	r_p(km)	r(km)	v(m/s)	$\tilde{r}$(km)	$\tilde{v}$(m/s)	$\sum\Delta v$(m/s)
No. Astro. Errors	2.39	10.6	1.73	1.79	0.170	10.86
Compensated Astro. Errors	3.92	13.1	1.96	2.96	0.354	10.96

(r_p is periselenum altitude miss. All other quantities are identical to those used in this study).

It can be seen that results achieved when ignoring the astrodynamic constants are somewhat optimistic. The question of just how optimistic is not firmly resolved here, since the conditions assumed by Smith yield periselenum results (without errors) which are much better than those achieved in this study, primarily because of the lower injection errors and higher periselenum passage. Thus, the percentage increase in periselenum errors does not apply to situations in which the trajectory estimation is less accurate. This is shown in table 2-17 by the results generated on a 225-measurement schedule.

TABLE 2-17

RESULTS ON 225-MEASUREMENT SCHEDULE (REF. 2-7)

Errors	r_p(km)	r(km)	v(m/sec)	$\tilde{r}$(km)	$\tilde{v}$(m/sec)	$\sum\Delta$(m/sec)
No. Astro. Errors	1.67	4.76	1.17	0.79	0.077	9.76
$\Delta\mu_e$	1.71	4.79	1.18	0.82	0.082	9.81
$\Delta\mu_m$	2.40	8.96	1.46	0.91	0.185	9.78
ΔR_{em}	2.72	5.23	1.19	1.98	0.083	9.78
$\Delta\mu_e$, $\Delta\mu_m$, ΔR_{em}	3.29	9.29	1.49	2.11	0.187	9.78

In table 2-17, it is seen that although the magnitude of the increase in uncertainties due to astrodynamic uncertainties is about the same as in table 2-16, the percentage is greater because of the fine trajectory estimation achieved on this 225-measurement schedule.

Another point brought out in table 2-17 is that the uncertainty in μ_m, the lunar gravitational constant, is the chief source of error. ΔR_{em} has some effect on $\tilde{r}$ and $\tilde{v}$ in table 2-17, but as previously mentioned, this can be avoided by switching from an earth-centered to a moon-centered coordinate system.

Another result from Ref. 2-7 is that the estimates in the astrodynamic constants can be improved somewhat by employing the augmented navigation equations. This improvement is relatively small, however, and is evidently proportional to the effect of the uncertainty on the trajectory. Thus, the estimate of μ_m can be significantly improved by a circumlunar flight while R_{em} and μ_e would only be changed slightly. Even μ_m can not be greatly refined on an outbound flight, so that any real improvement in the astrodynamic constants must be the result of a previous flight.

In summary, it can be concluded that uncertainties in the knowledge of μ_e, μ_m, and R_{em} cause measurable errors, with the most significant being $\Delta\mu_m$, and that uncertainty in R_{em} can be partially offset by using lunar coordinates near the moon. It is further concluded that error analyses in which astrodynamic constant errors are ignored are somewhat optimistic. Thus, on the curve on figure 2-14, showing guidance performance as a function of instrument accuracy, an rms instrument error of 10 arc-seconds would actually achieve results corresponding to 12-13 arc-seconds on the curve, after the effects of other error sources are taken into account.

In Ref. 2-7, the effects of a bias error are also considered, and equations are worked out for statistical analysis of the effect of ignoring bias errors in the onboard computations. Because of the assumptions made in the analysis, the results are even less applicable to this study than the work pertaining to astrodynamic constants. Several points are of interest, however. For one thing, it turns out that a bias error is approximately equivalent to a random error of the same magnitude in its effect on guidance system performance. Also, it appears that one can allow for a bias error in an onboard computer (or in an analysis) by increasing the estimate of Q, the measurement variance, in the navigation equations.

2.4.6 Other System Configurations

So far, all the results generated have been for the case of an onboard navigation system in which each observation consists of the measurement of the

space angle between some star direction and a reference point on the earth or moon. Four other possibilities are considered in this paragraph:

a. Double-angle measurements
b. Passive ranging by disc-measurement,
c. Active ranging by a microwave system
d. Ground tracking systems

2.4.6.1 Double-Angle Measurements

At Ames Research Center, a theodolite device which simultaneously measures the azimuth and elevation of a planet in an inertial coordinate system and also the subtended angle of the planet has been investigated. It was found in Ref. 2-4 that measurement of the subtense angle contributes little information and that double-angle measurements (azimuth and elevation) are nearly as good as triple-angle measurements.

Several computer runs on a double-angle system were made in this present study to compare the results with those obtained with single-angle (sextant) measurements. The results are shown in table 2-18.

TABLE 2-18

COMPARISON OF SINGLE- AND DOUBLE-ANGLE MEASUREMENTS AT PERISELENUM

No.	Description	r(km)	v(km)	$\tilde{r}$(km)	$\tilde{v}$(m/sec)	$\sum\Delta v$(m/sec)
6	Single angle- 45 msmts σ = 10 sec	16.81	12.2	2.38	1.50	24.37
53	Double angle- 45 msmts σ = 10 sec	15.38	10.34	2.05	1.26	22.81
54	Double angle- 30 msmts σ = 10 sec	19.68	12.69	*	*	24.00
55	Double angle- 20 msmts σ = 10 sec	21.81	14.13	*	*	25.24
140	Double angle- 45 msmts σ = 20 sec	26.20	17.82	2.51	1.55	28.14

* No estimation data on these runs.

Four computer runs on the 72.2-hour trajectory were made in which each observation consists of an elevation angle measurement and an azimuth angle measurement. Run 6 was made using the standard conditions (single-angle measurements). Run 53 in table 2-18 shows that although for an equal number of observations, the double-angle scheme gives somewhat better results, the overall system performance is improved only 10 to 20 percent. The reason for this small improvement, despite the doubled data rate, (90 angles measured instead of 45) is that most of the extra angles measured (39) are taken perpendicular to the trajectory plane and so are of little value as pointed out in paragraph 2.4.2.

Runs 54 and 55 were made to see if using the double-angle measurements would appreciably lessen the total number of observations required. Run 140 was made to see if use of double-angle measurements can lessen the instrument accuracy requirements. The results are negative in both cases, since the results of all three runs are appreciably poorer than run 6.

Since the double-angle measurements give so little improvement over the single-angle results, their use can not be recommended unless a double-angle measurement device is as easy to mechanize as a sextant-type device.

2.4.6.2 Onboard Ranging Measurements

Investigation of the estimation error volume for both the 63.9- and 72.2-hour trajectories reveals that just before the third correction, the error along the sightline to the moon is large. This is because angular measurements give no information along the sightline to the observed planet, and the sightlines to the earth and moon rotate very slowly just prior to the third correction. Therefore, an onboard ranging device, which measures range along the sightline to the center of the planet involved would improve the position estimate greatly at the time of the third correction and thereby reduce the miss distance.

Another time at which a ranging device might be valuable is in the final hour before periselenum, as the space vehicle nears the moon. Here, the advantage is not because of greater efficiency, since optical measurements in this period are quite valuable in reducing estimation errors. The principal advantage is one of mechanization, since as pointed out previously, timing and landmark errors begin to become important in this stage. In addition, the crew of a manned vehicle is likely to be busy during this period, and there may also be recognition difficulties in using landmarks very close to the moon.

To determine the guidance system improvement available by taking range measurements before the final midcourse correction, seven computer runs were made on the 72.2-hour trajectory. The results of these runs, together with Runs 6 and 3 which are used as references for comparison, are given in table 2-19.

Both groups of runs (with the final correction at 66.0 hours and 70.0 hours) show striking reductions in the miss distance when five ranging measurements are added to the angle-measuring schedules. This is true even when the ranging accuracy is only 20 km. A plot of miss distance versus ranging accuracy is given in figure 2-16 for Δv_3 at 70.0 hours.

TABLE 2-19

REDUCTION IN MISS DISTANCE AT PERISELENUM WITH RANGING MEASUREMENTS

No.	Description	r(km)	v(m/sec)	$\tilde{r}$(km)	$\tilde{v}$(m/sec)	$\sum\Delta v$(m/sec)
3	Δv_3 at 66.0 hr	21.38	11.7	2.51	1.57	20.41
40	Δv_3 at 66.0 hr plus 5 R msmts (t=65.1-65.5) ΔR=10 km	10.29	6.47	2.41	1.51	20.47
41	Δv_3 at 66.0 hr plus 5 R msmts(t=65.1-65.5) ΔR=20 km	15.4	8.80	2.49	1.59	20.45
42	Δv_3 at 66.0 hr plus 5R msmts (t=65.1-65.5) ΔR= 5 km	6.64	5.02	2.24	1.39	20.48
6	Δv_3 at 70.0 hr (standard case)	16.81	12.2	2.38	1.50	24.37
134	Δv_3 at 70.0 hr plus 5 R msmts (t=69.1-69.5) ΔR=10 km	8.40	9.44	2.33	1.47	24.51
135	Δv_3 at 70.0 hrs plus 5 R msmts (t=69.1-69.5) ΔR=20 km	12.64	10.68	2.36	1.49	24.45
136	Δv_3 at 70.0 hr plus 5 R msmts (t=69.1-69.5) ΔR=5 km	4.85	8.72	2.22	1.39	24.54
46	Δv_3 at 70.0 hr 1 R msmts at (t=69) ΔR = 10 km	14.64	11.34	2.43	1.53	24.4

Key: R = range measurement
ΔR = standard deviation of error in range measurement
t = time

Five additional measurements are made on each run since it is assumed that a ranging device requires less preparation time (sighting, etc) than an optical angle-measuring device. However, the difference in information content between the two types of measurements is shown by comparison of runs 6 and 46. These runs are identical except that on run 46 the angle measurement at t = 69 hours has been replaced by a ranging measurement of 10-km accuracy. The result is a reduction in miss distance of 2.2 km.

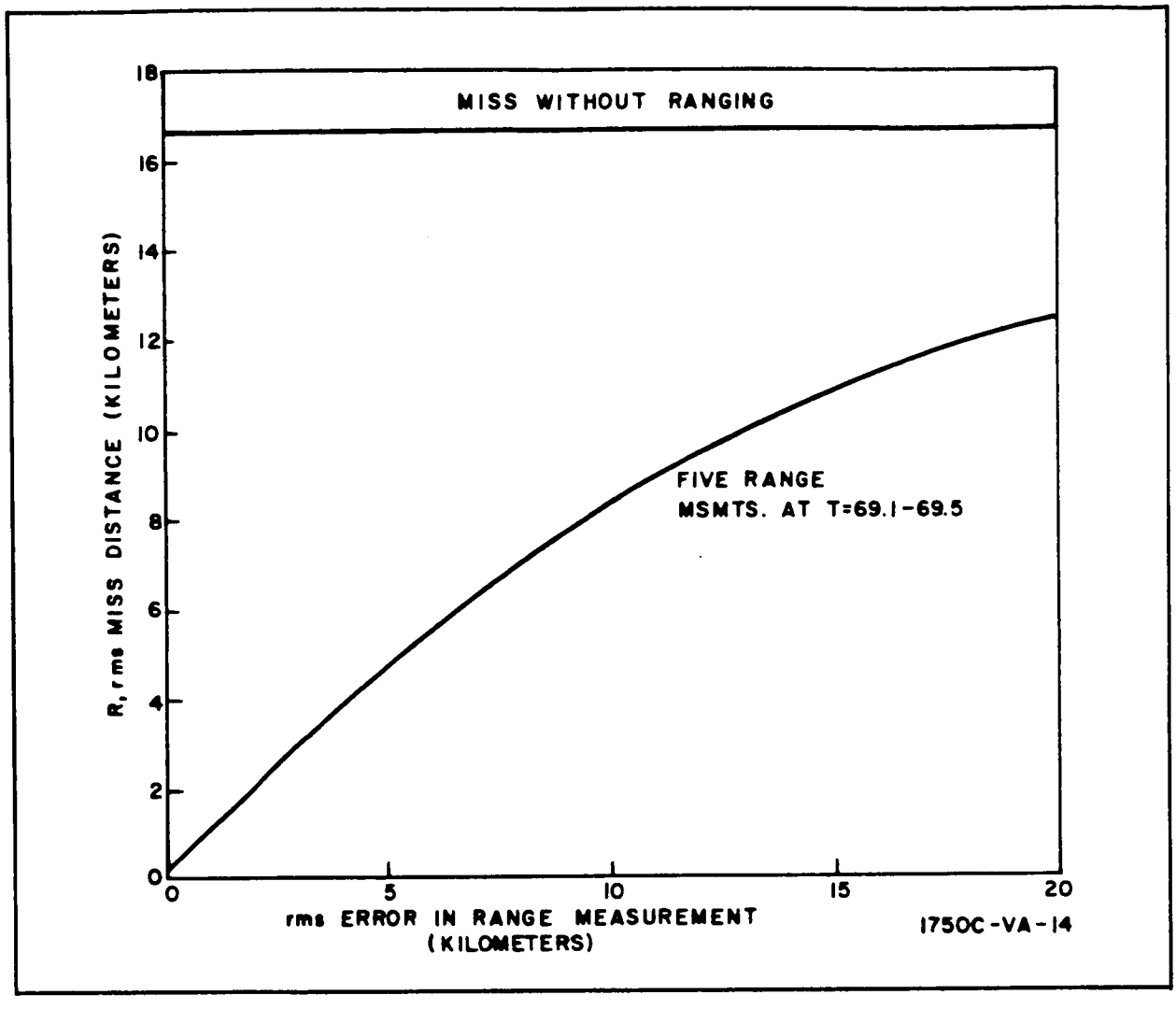

Figure 2-16. Reduction in Miss Distance Obtained by Addition of Five Ranging Measurements to Optical Angle System

To analyze the effect of adding range measurements after the final velocity, two additional computer runs were made on the 72.2-hour trajectory. The results of these runs together with run 3 are shown in table 2-20.

Comparison of these runs shows that ranging with an accuracy of 5 km produces a small increase in estimation accuracy while 10-km accuracy helps very little. These results are not too conclusive, however, since a ranging device such as a radar has a high data-rate and only three measurements were added in these runs.

TABLE 2-20

EFFECT AT PERISELENUM OF RANGING MEASUREMENTS*
NEAR PERISELENUM

No.	Description	r(km)	v(m/sec)	$\tilde{r}$(km)	$\tilde{v}$(m/sec)	$\sum\Delta v$(m/sec)
3	Standard trajectory (Δv_3 at 66 hour)	21.38	11.71	2.51	1.57	20.41
137	3 range measurements near end of trajectory, ΔR = 5 km	21.38	11.71	2.28	1.43	20.41
48	3 range measurements near end of trajectory, ΔR = 10 km	21.38	11.71	1.53	1.53	20.41

* (Ranges at which measurements are made are 1068 km, 645 km and 334 km).

2.4.6.3 Onboard Ranging Requirements

There are two obvious methods of determining range to a planet from a spacecraft with an independent sensor system. One is by measuring the angle subtended by the planet by optical means. The other is to use an active microwave or laser system to bounce signals off the planet and time their return. The problems involved in mechanizing either of these two methods are considered briefly here.

Measuring the subtended angle of a planet is attractive from the standpoint of power required, since it is a passive method. However, some of the problems involved are:

a. At long ranges, the subtended angle changes very slowly with increasing range, so that accuracy is poor.

b. At least half (and probably more) of the disc must be illuminated if optical methods are to be used.

c. At very short ranges, the field of view requirements will be severe. The geometry of the optical ranging method is illustrated simply in figure 2-17.

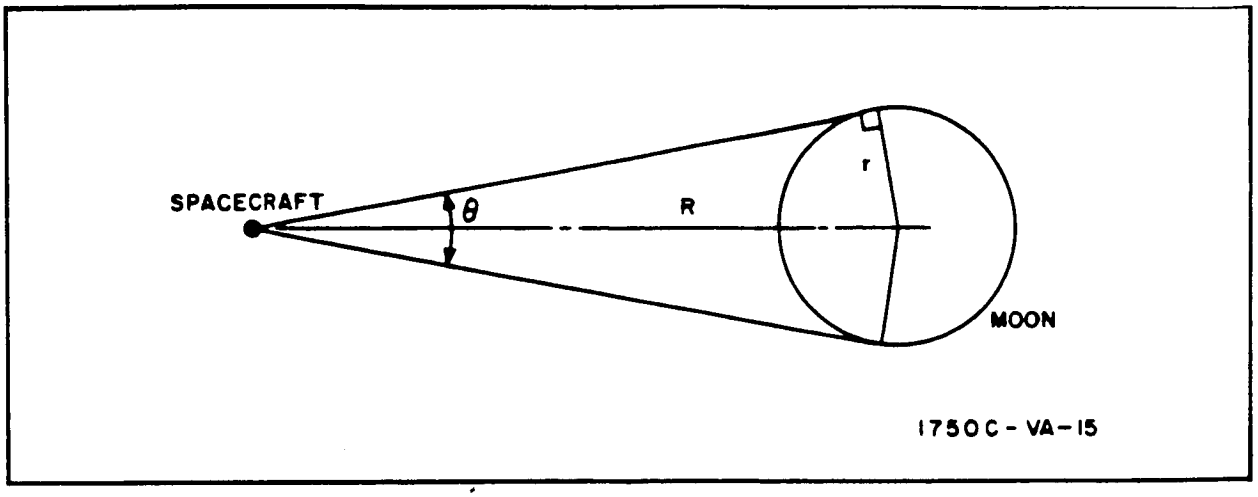

Figure 2-17. Optical Ranging

By taking the total differential of the range R in equation 2-59 the error in ranging by use of the half subtense angle θ is determined as:

$$\Delta R = \left(-\frac{r\cos\theta}{\sin^2\theta}\right)\Delta\theta + \left(\frac{1}{\sin\theta}\right)\Delta r$$

$$\Delta R \cong \left(-\frac{r}{\theta^2}\right)\Delta\theta + \left(\frac{1}{\theta}\right)\Delta r$$

for small θ, where $\Delta\theta$ is the uncertainty in the angular measurement and Δr is the uncertainty due to horizon irregularities.

Since the two error sources are independent, they may be treated separately and the root sum square taken to find the average deviation. For a distance (R) of 16,403 km (the range at 69.1 hours just prior to the third correction on the 72.2-hour trajectory), $\theta \cong 0.106$ radian. Assuming $\Delta\theta = 10$ seconds of arc and r = 0.8 km, the standard deviation of the error in optical ranging at this distance is:

$$\sigma_R = \sqrt{\left[\left(-\frac{r}{\theta^2}\right)\Delta\theta\right]^2 + \left[\left(\frac{1}{\theta}\right)\Delta r\right]^2} = \sqrt{\left[-\frac{1738}{0.106^2}(4.85)(10^{-5})\right]^2 + \left[\frac{0.8}{0.106}\right]^2}$$

$$\sigma_R = \sqrt{7.93^2 + 7.53^2} \cong 10.6 \text{ km}$$

Thus, it can be seen that optical ranging at this distance requires a measurement accuracy ($2\Delta\theta$) on the order of 20 seconds of arc accuracy.

Since useful optical ranging may be difficult to achieve because of illumiation conditions, a brief analysis was made of the power and dish-size requirements for active microwave ranging from the spacecraft. This analysis is presented in Section 9 of Appendix B, (Volume V). The results obtained, using a simple pulse-timing system with a 1σ accuracy of 10 km, are shown in figure 2-18 which is a plot of the following equation:

$$\text{Power (peak)} = \left[20 \log_{10}\left(\frac{\text{Range}}{\text{Dish Diameter}}\right) - 118.75\right] \text{dbw}$$

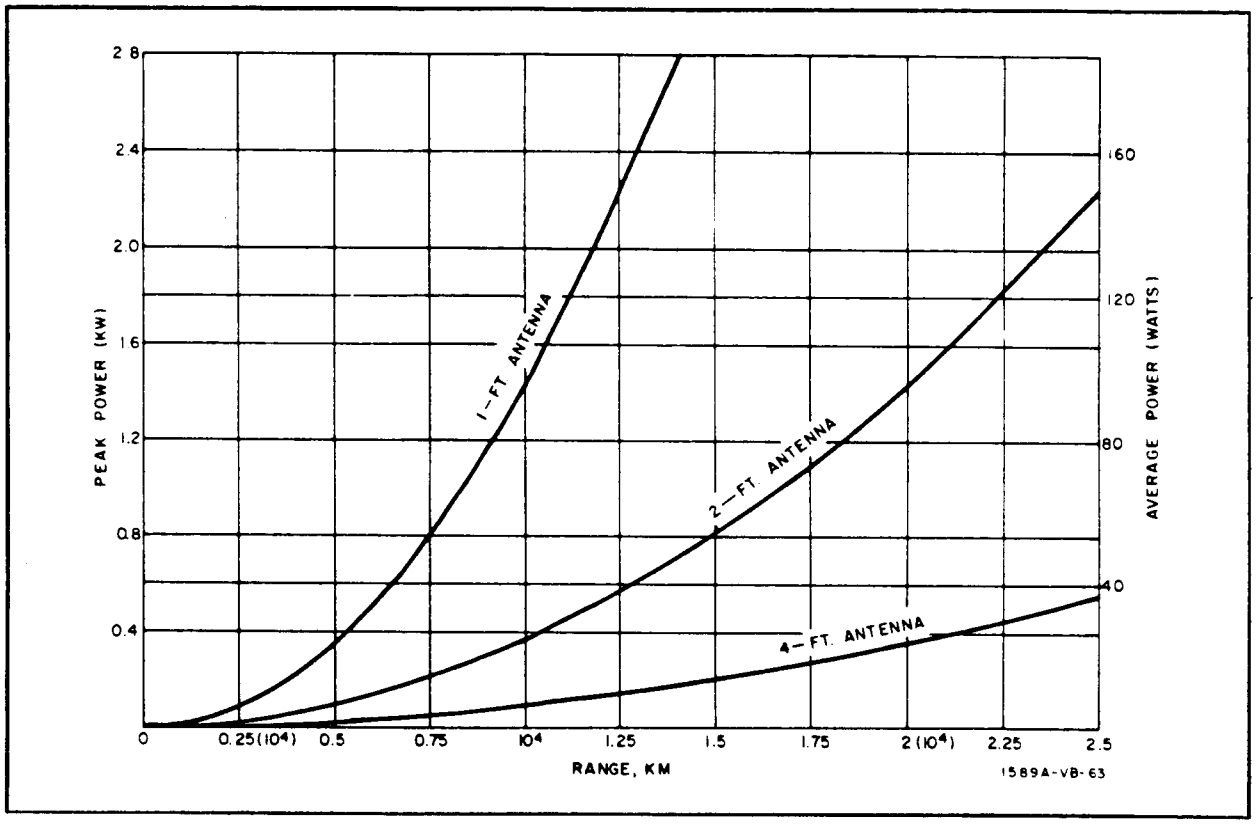

Figure 2-18. Power Requirements for Ranging Off Lunar Surface for Various Antenna Sizes

Clearly, the requirements shown in figure 2-18 are not easy to achieve. Even with a 2-foot antenna, the power requirements for ranging at 16,000 km are 1 kw peak and 70 watts average.

Even these requirements are based on assumptions which may be optimistic. For one thing, the lunar reflection coefficient is frequency dependent, and the value used (-12 db) is not at all certain, as this coefficient is the subject of considerable study at present by Evans and Pettengill at MIT.

Secondly, the results obtained assume that all the transmitted main beam energy is returned from a target area none of which is more than 10 km further from the spacecraft than the near point of the moon. This required a beamwidth of 1 degree or less. Wider beamwidths can be used, but then the power must be increased since some of the energy is returned from regions greater than 10 km (the required error) away.

2.4.6.4 Comparison of Onboard and Ground-Tracking Systems

The emphasis in this study was on onboard optical systems. An extensive analysis of ground-tracking systems was not attempted, due to the complexity of making such a study and the existence of several fine papers on the topic. One of these (Ref. 2-1) is used in this paragraph as a numerical comparison of onboard and tracking methods.

In Ref. 2-1, a comparison was made between a midcourse guidance system using ground tracking measurements for navigation and a system using both ground tracking and onboard optical data. The results indicate that in both systems, the trajectory uncertainties are reduced to levels which are insignificant compared to the errors in mechanizing velocity corrections. This is directly opposite to the results of this present study, in which the guidance system performance is sharply dependent upon measurement accuracy, while correction accuracy was found to have a less important effect. The reason for this difference is that in the ground-tracking situation, a large number of accurate measurements are taken; and since this resulting trajectory estimation is very fine, the whole guidance system is limited only by correction accuracy. Using onboard navigation, the estimate is not nearly so precise, so that guidance performance varies directly with measurement accuracy.

In Ref. 2-1, results are given which show the comparison in performance between a system using ground tracking and one using onboard methods. The results at periselenum are shown below:

	Ground-Tracking	Onboard
Observables:	Range and range rate to 3 stations	Elevation and azimuth of moon or earth
Measurements:	531	45
Accuracy:	$\sigma_R \cong 10 - 24$ meters $\sigma_{\dot{R}} \cong 0.077 - 0.237$ m/sec	$\sigma \cong 10$ arc sec plus range factor
Injection errors:	$r_o = 6$ km $v_o = 5$ m/sec	$r_o = 6$ km $v_o = 5$ m/sec

	Ground-Tracking	Onboard
Correction accuracies:	σ_k = 1 percent	σ_k = 1 percent
	σ = 1 degree	σ = 1 degree
	σ_ϵ^γ = 0.2 m/sec	σ_ϵ^γ = 0.2 m/sec
Periselenum results:	r = 13.5 km	r = 25.9 km
	v = 9.8 m/sec	v = 17.2 m/sec
	$\tilde{r}$ = 0.6 km	$\tilde{r}$ = 4.6 km
	$\tilde{v}$ = 0.5 m/sec	$\tilde{v}$ = 2.7 m/sec
	$\sum\Delta v$ = 22.6 m/sec	$\sum\Delta v$ = 24.8 m/sec

A comparison of results for the onboard and radar tracking cases shows that the latter system achieves a much more accurate estimate of uncertainties, a significantly lower miss distance, but only a slight savings in fuel for the conditions assumed. These results indicate that the estimation accuracy obtainable by tracking is much better than that achieved by onboard measurements but overall system performance is not much greater due to the limitations imposed by the errors in making velocity corrections.

It should be pointed out that the results shown for the onboard system are poorer than those shown in this study, for several reasons:

a. Initial errors are larger in Ref. 2-1, making $\sum\Delta v$ requirements higher

b. Correction errors are larger, making the deviations (r and v) larger

c. In Ref. 2-1, the third velocity correction was made earlier, also making r and v larger.

This last effect is quite important, as it has been found in this present study that postponement of the third velocity correction to t = 70 hours results in a significant decrease in miss distance at a small cost in fuel.

More dramatic evidence of the superiority of tracking methods over onboard methods is given in Ref. 2-1 by a plot of the position estimation error for each system as a function of time from injection into the lunar trajectory. This plot shows that $\tilde{r}$, the rms position estimation error varies from 10 to 50 km with onboard measurements and is reduced to less than 10 km only near the moon. However, the radar tracking system keeps $\tilde{r}$ to 1-2 km throughout the flight.

In appraising the applicability of the results of Ref. 2-1, the conclusion is that the investigation has been very thorough (including errors in station location, velocity of light, etc) except in one respect: errors in knowledge of

the position of the moon with respect to the earth are evidently not considered. These errors are expected to be of some significance in the comparison of onboard and tracking methods. As far as the radar error model assumed in Ref. 2-1 is concerned, no statement is given as to the source of the error model, but the magnitude of the errors considered is in line with other references and the error model assumed is rather conplex. (bias, randon, and slowly varying errors) indicating that some care has been taken in defining the model.

The natural conclusion to be drawn from the results in Ref. 2-1 is that while use of radar tracking allows a much more precise trajectory estimate to be made, with respect to the earth, the midcourse guidance system accuracy is then limited by the accuracy with which the lunar position is shown and velocity correction accuracy of the vehicle, so that the improvement over an onboard system is significant but is considerably less than an order of magnitude.

The superiority of radar tracking compared to onboard systems for trajectory estimation is due to two factors. These are:

a. Greater accuracy of each individual measurement
b. Higher data rate

The higher data rate possible with radar tracking is the result of requiring only onboard transponder operation compared to onboard optical methods which require more precise vehicle orientation and stabilization. A more significant advantage of radar tracking is the greater accuracy obtainable with state-of-the-art equipment. As an example, it is expected that radar ranging over cislunar distance can be done to accuracies on the order of 10 to 100 meters. Consider the accuracy required in an optical sensor to make this fine a measurement. At a distance of 100,000 km, an error of 100 meters implies an angular accuracy of 0.2 arc-second, which would be difficult to achieve.

2.5 CONCLUSIONS

2.5.1 Onboard System Requirements

Primary emphasis in this study is on the use of onboard optical methods for navigation measurements during the Midcourse Phase. Although an exact list of guidance system requirements cannot be drawn up, since tradeoffs are available in several areas, the following specifications have been shown to give reasonable results:

Instrument accuracy	=	12.5 arc-seconds, (rms + bias)
Field of view	=	65 degrees
Correction accuracy	=	1 percent rms error in percentage thrust magnitude
	=	0.1 m/sec rms error in magnitude due to cutoff errors
	=	0.5 degree rms error in pointing
Timing accuracy	=	1 second, rms, except for 0.1 second rms near periselenum.

The above parameters, when applied to 45-measurement, 3-correction schedule on a 72.2-hour trajectory with initial injection uncertainties of 2.76 km in position and 4.24 m/sec in velocity, yield the following results at periselenum:

RMS position miss	r	= 20 km (altitude component: 4 km)
RMS velocity miss	v	= 12.3 m/sec
RMS position estimation error	$\tilde{r}$	= 2.4 km
RMS velocity estimation error	$\tilde{v}$	= 1.4 m/sec
Total correction velocity	$\sum\Delta v$	= 26.1 m/sec

For the above figures, an uncertainty of 0.8 km in defining lunar landmarks and 1.6 km in defining earth landmarks (or horizon) is assumed.

The results listed above can be degraded by 10 to 20 percent by the present-day uncertainty in μ_m, the lunar gravitational constant. Uncertainties in the earth's gravitational constant μ_e and the earth-moon distance R_{em} will have lesser effects and other uncertainties are insignificant. Even the error in μ_m will be insignificant if it is first reduced by tracking lunar flights.

Of the sensor requirements listed, the instrument accuracy of 12.5 arc-seconds is most critical to system performance, especially the miss (r and v) and fuel requirements ($\Sigma\Delta v$). Trajectory estimation in the vicinity of the moon is possible with a less accurate sensor. But the 12.5 arc-second accuracy requirement can only be relaxed by significantly increasing correction fuel or taking many more measurements.

The 65-degree field of view is primarily to ensure capability of measuring to some star in a nearly polar direction. This requirement can be made less stringent, by taking a few extra elevation measurements.

As pointed out previously, variations in the correction errors or injection conditions listed do not greatly affect guidance system performance, except that higher injection errors increase the correction fuel requirement.

Timing accuracy is important only near the planets when angles are changing rapidly. One-second timing accuracy is sufficient to achieve the miss distance and correction fuel listed. If 0.1-second timing accuracy of the last few measurements cannot be achieved, the result is a slight degradation of estimation errors at periselenum.

2.5.2 Navigation Schedules

In general, most of the measurements should be made to some star in the trajectory plane and the primary requirements on the choice of star are visibility and recognizability. In fact, the same star could be used for all in-plane measurements to a particular planet throughout most of the trajectory. This fact might be utilized in mechanizing an automatic (unmanned) system.

The schedule of measurements and corrections depends primarily on the correction velocity fuel allotment for the particular mission since miss distance can be reduced at the cost of fuel if correction are made later or an additional correction is added.

2.5.3 Trajectory Variations

Variations in the nominal trajectories considered have only slight effects on the sensor requirements.

2.5.4 Ranging for Midcourse Guidance

The usefulness of some ranging device capable of operating at 20,000 km from the moon is established. General requirements for achieving this capability indicate that optical ranging is more promising since power and antenna-size requirements for microwave ranging are severe.

2.5.5 Comparison of Onboard and Ground-Tracking Systems

Results from Ref. 2-1 indicate that, at least for lunar midcourse guidance, ground tracking is quite superior to onboard navigation. This is because of the much larger data rate and the greater accuracy per measurement. However, even ground-tracking methods are limited, primarily by the accuracy with which velocity corrections can be implemented.

2.5.6 Unresolved Problem Areas

- Assuming that in a manned flight, an onboard navigation system should be available for redundancy and operation on the far side of the moon, one problem is just how complex should the navigation computer be. It is shown that many error sources can be taken into account, but in an onboard computer this is done at the expense of increasing complexity and deceasing reliability.

- Another problem is that of determing midcourse guidance criteria, so that tradeoffs and system optimization can be achieved.

- Further work is also needed in determing whether to use fixed time of arrival or variable time of arrival guidance logic during midcourse.

- Another problem is to determine the usefulness of a lunar beacon in conjunction with a vehicle navigating by onboard or ground-traking methods.

- Finally, additional work on the effect of the nominal trajectory on guidance requirements should be done.

3. LUNAR PARKING AND DESCENT ORBIT PHASE

3.1 INTRODUCTION

This section describes the simulation of a self-contained onboard navigation system which utilizes Kalman's (Ref. 3-1) minimum variance estimation scheme in a vehicle orbiting the moon. By accounting for a number of practical navigation problems, this simulation has made it possible to draw important conclusions about the system requirements and performance.

The application of recursive minimum variance filter theory to celestial navigation was pioneered by Dr. Stanley F. Schmidt and his associates (Ref. 3-2 and 3-3) and by Dr. R.H. Battin (Ref. 3-4). Following these and other related theoretical studies, some of the underlying simplifications common to early investigations were examined in more detail by Smith and McGee (Ref. 3-5) and by Gunckel (Ref. 3-6). This section continues the investigation of the idealizations present in earlier publications in a study which is directed toward the determination of sensor requirements in the orbiting phase of a lunar mission.

The following summary of notation is applicable to the lunar parking and descent orbit phase.

SUMMARY OF NOTATION

English Alphabet

B Astronomical length vector
E Eccentric anomaly beyond periselenum
F Velocity increment vector
G Guidance law matrix
H Row vector of partial derivatives of observables with respect to state variables
$\mathcal{H}$ Submatrix of H
I Identity matrix
K Six-dimensional weighting vector
M Total number of observations on parking orbit
N Covariance matrix of deviations from nominal state
P Covariance matrix of errors in estimated state
Q Variance of measurement errors
R Selenocentric instantaneous vehicle position vector
S Selenocentric unit vector in the direction of a known star

T Period of parking orbit
U Unit eigenvector corresponding to maximum position uncertainty
V Selenocentric instantaneous vehicle velocity vector
W Direction cosine matrix for final tangential, vertical, and transverse error
X Six-dimensional state vector
Y Magnitude of an observable
a Parking orbit radius, semimajor axis (general)
a_d Descent orbit semimajor axis
b Length or component of $\underline{B}$
c Random error
d Dot product of $\underline{R}$ and $\underline{V}$
e_d Descent orbit eccentricity
f Deviation from nominal velocity increment vector
i Inclination angle between the earth's equator and the earth-moon plane
q Mean lunar radius
r Magnitude of $\underline{R}$
s Component of $\underline{S}$-vector
t Time
u Component of U-vector
v Magnitude of $\underline{V}$
x Deviation from nominal state vector
y Deviation of observable from reference value

Greek Alphabet

β Unit vector normal to $\underline{R}$ in star-vertical measurement plane
Γ Covariance matrix of input errors
δ Variation
Θ_M Displacement of moon beyond vernal equinox
Θ_S Displacement of sun beyond vernal equinox
Λ Eigenvalue of position uncertainty covariance matrix
λ Selenocentric latitude
μ Lunar gravitational constant
μ_E Gravitational constant of the earth
μ_S Gravitational constant of the sun
ν Incremental eccentric anomaly
σ Standard deviation
τ Time interval between observations on parking orbit
Φ State transition matrix
ψ Selenocentric longitude (counterclockwise with respect to earth sightline in figure 3-1)

Superscripts

$[\,]^T$ Matrix transpose
$[\,]^{-1}$ Matrix inverse

Subscripts

A	Pertaining to termination of midcourse
E	Pertaining to termination of parking orbit
F	Pertaining to beginning of descent orbit
i, j	Vector or matrix components[1/]
L	Pertaining to termination of descent orbit
m	Pertaining to the mth observation
M	Pertaining to the last observation
n	Star index number
O	Pertaining to the beginning of parking orbit
P	Pertaining to the first pass over desired periselenum
1, 2, 3	x, y, and z cartesian position components respectively
4, 5, 6	x, y, and z cartesian velocity components respectively

Symbols Above Letters

$\overline{(\ )}$	Predicted value
$(\ )'$	Actual value
$(\tilde{\ })$	Uncertainty; error in estimated value
$(\hat{\ })$	Indicated or observed value
$\underline{(\ )}$	Vector

3.2 BACKGROUND

Given the task of establishing sensor requirements for space missions, the study is split into two parts:

- Part I - Problem Definition

- Part II - Analytical Solution

The approach taken in defining the problem is as follows:

- Establishment of Mission Priority from the standpoint of political and economical considerations, value of mission output, and era of feasibility

- Accumulation of information (physical data, orbital laws, constraints, analytical techniques, state of the art in all pertinent fields) from available technical literature and from discussions during visits to NASA centers

- Determination from the results of above two investigations of the conditions under which each mission can be regarded as successful. (This is facilitated by separating each mission into phases and finding boundaries for allowable guidance errors in each phase.)

1/ For time-varying vectors and matrices, the first subscript (m) denotes the time.

- Determination of nominal trajectories for each mission phase from considerations of safety, the nature of the mission itself, anticipated guidance capability, and fuel economy

- Selection of all guidance and navigation aids (observables, which suggest corresponding sensors) for possible use in tracking and/or guiding the space vehicle in flight

- Selection of a method of processing the information obtained from the navigation aids

- Listing of the various factors (errors, environmental conditions, parameter variations) which may affect navigation accuracy and,consequently, mission success

- Selection of a suitable analytical model of the navigation scheme, whereby a substantial amount of numerical data can be obtained.

After completion of this procedure, the sensor requirement study for each mission phase is expressible as a concrete, well-defined numerical problem.

As applied to the Orbiting Phase of the lunar mission, the outcome of the above approach is the following set of conditions:

- The nominal lunar trajectory consists of a circular parking orbit and, for the landing vehicle, an elliptical descent arc of 90 degrees eccentric anomaly (figure 3-1). The landing vehicle begins its descent during the second revolution in the circular orbit.

- Requirements for guidance accuracy during this phase are defined by the allowable 3 σ errors at initiation of the landing phase; i.e., 5 kilometers and 2.5 kilometers tangential and vertical error respectively (Ref. 3-7).

- Deviations of the actual trajectory from the nominal are to be compensated by correcting the thrust to be applied at initiation of the parking orbit and the descent arc. A fixed-time-of-arrival (FTOA) end-point guidance scheme is selected.

- Thrust vector corrections are to be computed from optimally selected navigation data accumulated by an onboard monitoring system. Kalman's recursive minimum variance technique (Ref. 3-1) has been selected for optimum data smoothing.

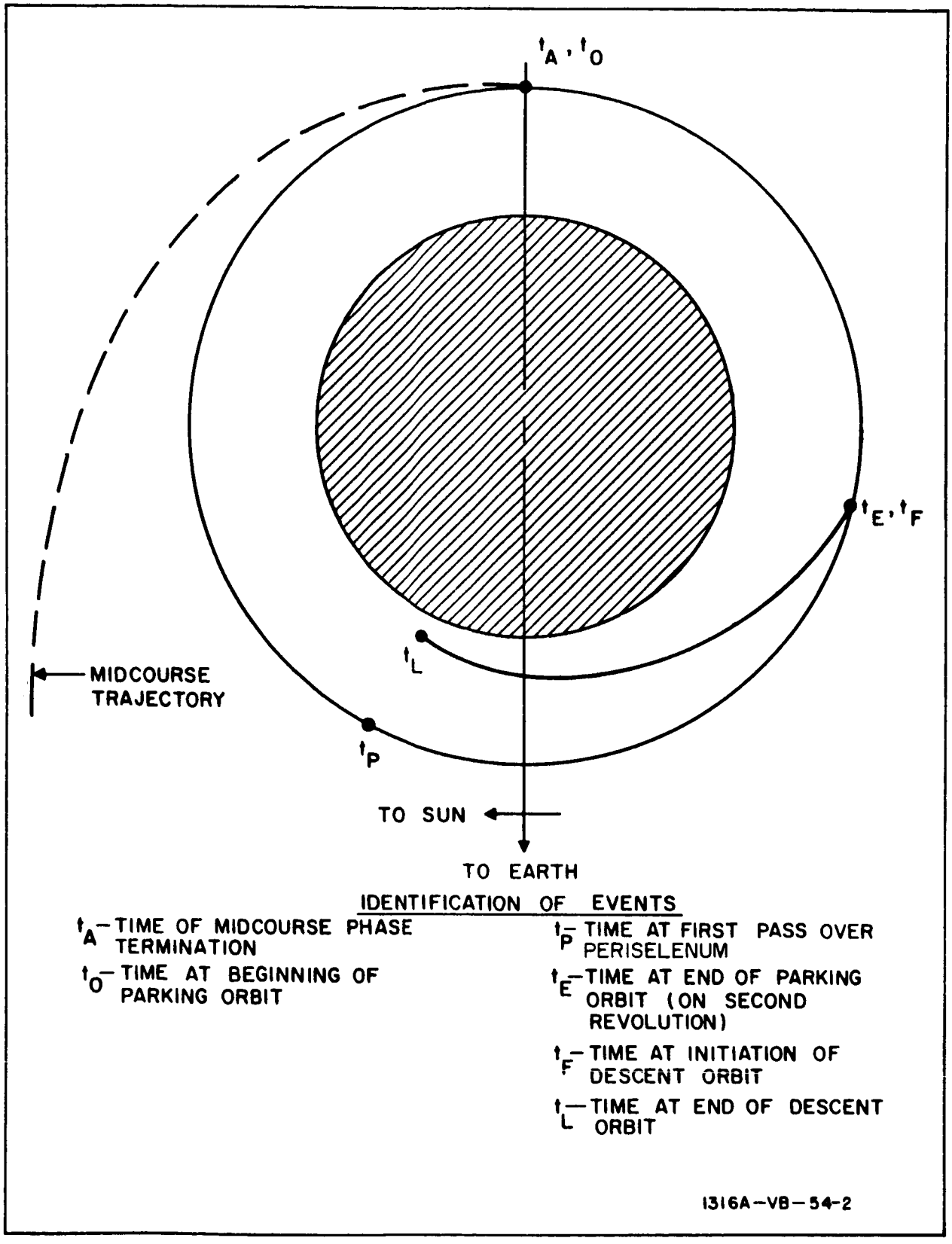

Figure 3-1. Plan View of Lunar Flightpath

The observables are chosen in accordance with considerations of accessibility, field of view, power, versatility, and minimum auxiliary data requirements for processing the measured readings. The angle between a known star and the instantaneous local vertical is suitable for parking orbits of 1/2 period or greater in duration. The errors affecting this type of measurement are:

- Local vertical pointing error
- Star tracker error (including uncertainties in selenocentric star coordinates)
- Measurement timing error.

The variances of the first two errors are obviously additive; the measurement timing error effects are shown in the text to be additive also. Overall measurement error is dominated by the local vertical pointing error, and can be assumed Gaussian.

In the analysis which follows, factors which can complicate the simulation are sidestepped whenever it is apparent that the outcome would not depend upon the analytical model. Applied thrust is treated as a velocity impluse, and the cartesian components of thrust error are assumed to be independent normally distributed random variables with zero mean and equal variance. Components of all simulation input error vectors are assumed to be independent and Gaussian with zero mean. Space geometry is idealized wherever permissible.

Finally, no consideration is given here to measurement bias or astrodynamical uncertainties, since these items are covered in previously mentioned references, and the possibility of instrument failure or gross measurement error is beyond the scope of this analysis.

3.3 ANALYSIS

The mathematical problem to be solved is derived from the guidelines established in the preceding sections. A vehicle, using FTOA end-point guidance, is injected into a parking orbit nominally defined as in figure 3-1. At regular intervals along the parking orbit, prescribed navigation measurements are taken and incoporated into recursive equations to obtain an updated trajectory estimate. This operation continues until, after the last measurement, the estimated orbit and the desired future position are used to compute a guidance command. At the proper time, the vehicle is injected into an

elliptical descent arc which is aimed toward a preselected periselenum for landing initiation. A comparison of the final miss vector and the allowable error volume is used as a criterion of success.[2/]

In a physical system there are errors in every step of the guidance and navigation procedure. The most obvious error sources which must be accounted for are:

- Deviations from the nominal initial position and velocity
- Uncertainties in the initial position and velocity
- Errors in the applied thrust vector at both injection and descent
- Thrust measurement errors at both injection and descent
- Navigation measurement errors.

There are, however, additional sources of error which are more subtle, and which depend upon the methods used in processing the navigation data. Specification of the recursive minimum variance method does not completely define the data processor to be used for orbital navigation. There are two further decisions which will influence the complexity of the entire process to a significant extent:

- It must be determined whether all sensitivity coefficients can be computed from the same nominal trajectory. If not, the partial derivatives used to calculate the state vector corrections will be computed from the updated trajectory estimate.

- If sensitivity coefficients are computed from successive updated orbits, and updated Keplerian equations are used as a basis for all onboard computations, the estimated trajectory can be described as a time-varying conic. Because a patched conic is a valid approximation to a perturbed orbit, and because the actual observables will contain the effects of orbital perturbations, it is of interest to investigate the use of two-body orbit equations in the actual onboard system. This, of course, is extremely desirable from the standpoint of onboard computer simplicity.

The errors arising from these approximations in the onboard data processor can be adequately characterized only through simulation of the actual nonlinearities and perturbations which are inherently present. At this point the

2/ The maximum allowable error of 5 km at periselenum, specified in subsection 3.2, applied to both the observed and the actual miss distance. The requirement for observed miss distance can be ignored; however, the rms observed miss distance is always less than the rms actual miss distance (equation D18 of Ref. 3).

intended analytical approach departs from most of the literature referenced earlier. In addition to the conventional linearized analysis of the type performed in earlier celestial navigation studies, the parking orbit analysis is to include a simulation of dynamic and geometric nonlinearities. This extension of the error analysis is made without sacrificing any information obtainable from the conventional approach; the complete calculation of error statistics is readily carried through the simulation.[3/]

In addition to the errors considered up to this point, the lack of complete information on board must be covered, either by analysis or by reference to the literature. Items of interest in this category are listed below.

- The initial uncertainty covariance matrix can only be approximated.
- Measurement timing is subject to small errors.
- There are uncertainties in astronomical constants.
- Measurement error statistics may not be accurately known.

Some of these have been covered in recent publications and need not be analyzed in this study. Lack of precise knowledge of sensor error statistics is apparently not critical (Ref. 3-6) and the effects of unknown measurement bias and astrodynamical uncertainties can be counteracted (Ref. 3-5). This latter reference also contains an investigation of computer truncation errors. The remainder of the above-mentioned items, however, are included in the analytical study. In addition, the implications of practical restrictions upon the available field of observables are included in the analysis to give practical significance to the final results.

The details of the various steps in the simulation are explained in this section. Throughout the analysis the concept of a six-dimensional state vector is used, which can be partitioned into the cartesian position and velocity vectors

$$\underline{X}_m = \underline{X}(t_m) = \begin{bmatrix} \underline{R}_m \\ \underline{V}_m \end{bmatrix} \tag{3-1}$$

The deviation of this vector from its instantaneous nominal value can be approximated by the linear equation

$$\underline{x}_m = \Phi(t_m, t_{m-1})\, \underline{x}_{m-1} \tag{3-2}$$

3/ Ref. 3-6 also includes a verification of linearized analysis through actual simulation. However, a more complete investigation is envisioned here, through simulation of a navigation scheme which uses Keplerian equations while the space vehicle is in a perturbed orbit.

where Φ is a 6 x 6 state transition matrix with a general term defined by

$$\Phi_{mij} \triangleq \frac{\partial X_{mi}}{\partial X_{m-1,\ j}} \tag{3-3}$$

It is to be emphasized that in computing these elements and the measurement sensitivities, only the observed past state (denoted by a circumflex above the symbol) and the predicted future state (denoted by a bar over the symbol) are available to the simulated onboard computer. These notations for state variables and related quantities are used in the development which follows wherever they enhance the description of the simulation.

3.3.1 Background Analysis

3.3.1.1 Cartesian Coordinates

In figure 3-2, i is the inclination angle between the earth's equator and the ecliptic, and the time of the month is denoted by the angle (Θ_M) in the earth-moon plane, referenced to the vernal equinox.[4/] A similar angle, (Θ_S) (not shown in the figure), completes the definition of the sun's position. In earth coordinates, them the position vector of the moon is:

$$\underline{B}_{EM} = b_{EM} \begin{bmatrix} \cos \Theta_M \\ \cos i \sin \Theta_M \\ \sin i \sin \Theta_M \end{bmatrix} \tag{3-4}$$

And the position vector of the sun is:

$$\underline{B}_{ES} = b_{ES} \begin{bmatrix} \cos \Theta_S \\ \cos i \sin \Theta_S \\ \sin i \sin \Theta_S \end{bmatrix} \tag{3-5}$$

where b_{EM} and b_{ES} are the corresponding scalar total distances. It is now convenient to define a right-handed selenocentric coordinate system in which the x-axis points to the center of the earth and the z-axis is normal to the earth-moon plane. From the figure it is seen that the transformation from earth to selenocentric coordinates is given by:

4/ For an actual space flight, the transformations employed here would have to be corrected to account for displacement of the earth-moon plane from the ecliptic.

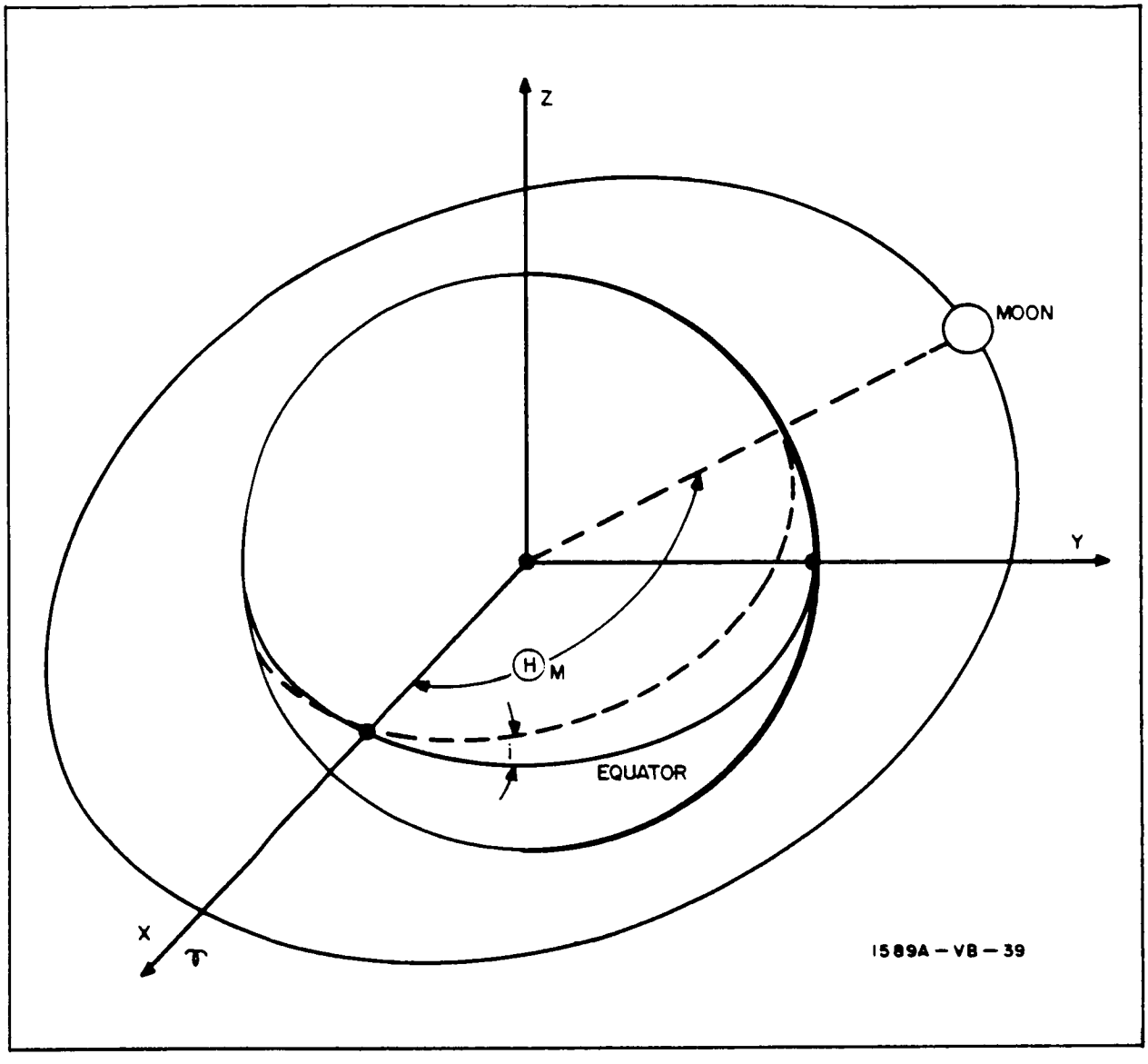

Figure 3-2. Celestial Sphere

$$\left[\pi + \theta_M\right]_z \left[i\right]_x = \begin{bmatrix} -\cos \Theta_M & -\sin \Theta_M & 0 \\ \sin \Theta_M & -\cos \Theta_M & 0 \\ 0 & 0 & 1 \end{bmatrix} \begin{bmatrix} 1 & 0 & 0 \\ 0 & \cos i & \sin i \\ 0 & -\sin i & \cos i \end{bmatrix} \tag{3-6}$$

In selenocentric coordinates, the position vector of the earth is:

$$\begin{bmatrix} b_{E1} \\ b_{E2} \\ b_{E3} \end{bmatrix} = \left[\pi + \Theta_M\right]_z \left[i\right]_x \left[- \frac{B}{EM}\right] = \begin{bmatrix} +b_{EM} \\ 0 \\ 0 \end{bmatrix} \tag{3-7}$$

as expected from the definition of the coordinate system; the position vector of the sun in selenocentric coordinates is denoted as:

$$\begin{bmatrix} b_{S1} \\ b_{S2} \\ b_{S3} \end{bmatrix} = \begin{bmatrix} \pi + \theta_M \end{bmatrix}_z \begin{bmatrix} i \end{bmatrix}_x \begin{bmatrix} \underline{B}_{ES} - \underline{B}_{EM} \end{bmatrix} \tag{3-8}$$

Table 3-1 gives the declination (dec) and sidereal hour angle (SHA) for the navigation stars taken from Ref. 3-8. In selenocentric coordinates, then, a unit vector in the direction of a given star is:

TABLE 3-1

NAVIGATION STARS

No.	Mag	SHA	Dec	No.	Mag	SHA	Dec	No.	Mag	SHA	Dec
1	2.2	358	N 29	20	0.5	246	N 5	39	2.9	138	S 16
2	2.4	354	S 43	21	1.2	244	N 28	40	2.2	137	N 74
3	2.5	350	N 56	22	1.7	235	S 59	41	2.3	127	N 27
4	2.2	350	S 18	23	2.2	223	S 43	42	1.2	113	S 26
5	0.6	336	S 57	24	1.8	222	S 70	43	1.9	109	S 69
6	2.2	329	N 23	25	2.2	219	S 8	44	2.6	103	S 16
7	3.1	316	S 40	26	1.3	208	N 12	45	1.7	97	S 37
8	2.8	315	N 4	27	2.0	195	N 62	46	2.1	97	N 13
9	1.9	310	N 50	28	2.2	183	N 15	47	2.4	91	N 51
10	1.1	292	N 16	29	2.8	177	S 17	48	2.0	85	S 34
11	0.3	282	S 8	30	1.1	174	S 63	49	0.1	81	N 39
12	0.2	282	N 46	31	1.6	173	S 57	50	2.1	77	S 26
13	1.7	279	N 6	32	1.7	167	N 56	51	0.9	63	N 9
14	1.8	279	N 29	33	1.2	159	S 11	52	2.1	54	S 57
15	1.8	276	S 1	34	1.9	154	N 50	53	1.3	50	N 45
16	0.1-1.2	272	N 7	35	0.9	150	S 60	54	2.5	34	N 10
17	-0.9	264	S 53	36	2.3	149	S 36	55	2.2	29	S 47
18	-1.6	259	S 17	37	0.2	147	N 19	56	1.3	16	S 30
19	1.6	256	S 29	38	0.1	141	S 61	57	2.6	14	N 15

$$\begin{bmatrix} s_{n1} \\ s_{n2} \\ s_{n3} \end{bmatrix} = \begin{bmatrix} \pi + \Theta_M \end{bmatrix}_z \begin{bmatrix} i \end{bmatrix}_x \begin{bmatrix} \cos(\text{dec}) \cos(\text{SHA}) \\ -\cos(\text{dec}) \sin(\text{SHA}) \\ \sin(\text{dec}) \end{bmatrix} \tag{3-9}$$

In this analysis, the instantaneous selenocentric position vector of the space vehicle consists of the first three components of the state vector:

$$\underline{R}(t) = \begin{bmatrix} X_1 \\ X_2 \\ X_3 \end{bmatrix} \tag{3-10}$$

The instantaneous distances from the vehicle to the earth and to the sun are then:

$$b_{VE} = \sqrt{(b_{E1} - X_1)^2 + (b_{E2} - X_2)^2 + (b_{E3} - X_3)^2} \tag{3-11}$$

and

$$b_{VS} = \sqrt{(b_{S1} - X_1)^2 + (b_{S2} - X_2)^2 + (b_{S3} - X_3)^2} \tag{3-12}$$

respectively; the distance from the center of the moon to the earth is:

$$b_{OE} = b_{EM} \tag{3-13}$$

and the distance from the center of the moon to the sun is:

$$b_{OS} = \sqrt{(b_{S1})^2 + (b_{S2})^2 + (b_{S3})^2} \tag{3-14}$$

For spherical selenocentric coordinates (radius r; latitude λ; longitude ψ) the zero latitude locus is defined as the lunar equator and zero longitude is defined as the intersection of the earth-moon line with the lunar equator.

3.3.1.2 Flightpath Geometry

The flightpath sequence is indicated in figure 3-1. The nominal circular orbit begins with an impulsive tangential injection (at time $t_A = t_o$) from the periselenum point of a midcourse trajectory with the proper final inclination angle at zero latitude and 180 degrees longitude as shown. To set aside at least one full revolution for orbit determination, the descent initiation is assumed to take place on the second passage through point E. The arc (EL) is an elliptical segment with periselenum at point (L).

It is seen that the true anomaly ($< ECL = < FCL$) is greater than 90 degrees. The term "90-degree descent" refers to the eccentric anamoly (E_F) of the descent arc. When this is 90 degrees, the periods of the ellipse and the circular orbit are equal, providing an "automatic rendezvous" feature in the event that a decision is made not to initiate a landing.

The following parameters, determined from the Problem Definition study, are sufficient to define the parking and descent orbits completely:

$r_o = r_p = q + 2 \times 10^5$ meters

$\psi_o = 180$ degrees; $\lambda_o = 0$ degree

$\psi_p = -45$ degrees; $\lambda_p = 30$ degrees

$E_F = -90$ degrees; $r_L = q + 2 \times 10^4$ meters

A complete geometric analysis appears in Volume V, Appendix C.

3.3.1.3 Guidance Law

As explained in Volume V, Appendix C, the nominal injection impulse is parallel to both the terminal midcourse velocity vector and to the orbital plane. The nominal impulse magnitude is the difference between the nominal midcourse periselenum speed (v_A) and the circular velocity of the parking orbit.

At the time of midcourse termination, the observed deviation from the nominal state is to be corrected by the FTOA guidance scheme, derived in Ref. 3-3 and discussed in Volume V, Appendix A. This compensation is obtained by superposition of a corrective thrust vector upon the nominal injection impulse. The basic approach is as follows.

The observed deviation from the nominal state vector at the time of injection into the circular orbit is denoted by $\hat{\underline{x}}_A$. The indicated state vector correction is then the product $G\,\hat{\underline{x}}_A$, where G is a fixed time of arrival (FTOA) guidance law matrix (Ref. 3-3):

$$G = -\begin{bmatrix} O_{33} & O_{33} \\ A_2^{-1} A_1 & I_{33} \end{bmatrix} \tag{3-15}$$

in which O_{33} and I_{33} represent the 3 x 3 null and identity matrices respectively, and the A matrices are taken from the partitioned transition matrix:

$$\Phi(t_E, t_o) = \begin{bmatrix} A_1 & A_2 \\ A_3 & A_4 \end{bmatrix} \tag{3-16}$$

The initial postinjection state vector deviation (and therefore the actual orbit) can now be defined as the resultant of the actual preinjection deviation $\underline{x}_A$ from nominal, the indicated correction $G\,\hat{\underline{x}}_A$, and a mechanization error:

$$\underline{x}_O = \underline{x}_A + G\,\hat{\underline{x}}_A + \begin{bmatrix} \underline{O}_{31} \\ \underline{E}_1 \end{bmatrix} \tag{3-17}$$

where $\underline{O}_{ij}$ is an i x j null matrix and $\underline{E}_1$ is an 3 x 1 velocity impulse error vector, representing the applied thrust error.

The observed postinjection state vector deviation, which is used to start the onboard navigation computations, is simply:

$$\hat{\underline{x}}_O = \hat{\underline{x}}_A + G\,\hat{\underline{x}}_A + \begin{bmatrix} \underline{O}_{31} \\ \underline{E}_1 \end{bmatrix} + \begin{bmatrix} \underline{O}_{31} \\ \underline{E}_2 \end{bmatrix} \tag{3-18}$$

where $\underline{E}_2$ represents the error in measuring the applied thrust.

The FTOA end-point guidance technique is also used to compensate for deviations off nominal at descent initiation with one important modification; with the initial state deviations and uncertainties and the injection errors considered in this study, the space vehicle can easily be well over a hundred kilometers off nominal at time t_E, the end of the parking orbit. (This is discussed in greater detail in paragraph 3.4.3.) At this distance the linearized guidance law, used for computation of a correction to the nominal thrust vector, is not sufficiently accurate to guide the vehicle within 5 kilometers (3 σ) of nominal periselenum. It is therefore necessary to simulate the onboard fixed time guidance law by

- Computing the desired descent orbit, which is defined by two position vectors (i.e., the observed position vector at t_E and the nominal periselenum vector at t_L) and the time ($t_L - t_F$) between them

- Computing the velocity vector at t_F which corresponds to this new orbit

- Subtracting the observed velocity vector at time t_E from the desired velocity vector at t_F.

The only complicating factor in this procedure is the computation of an orbit from two position vectors and the elapsed time. The method used here involves a solution of five simultaneous equations in which the unknowns cannot in general be expressed explicity.

Given the observed position vector $\hat{\underline{R}}_E$, the desired position vector $\underline{R}_L$, and the elapsed time $t_L - t_E = t_L - t_F$, two equations with three unknowns (a_d, ν_L, d_F) can be written 5/:

5/ A derivation of these equations appears in Ref. 3-9.

$$r_L = a_d (1 - \cos \nu_L) + \hat{r}_E \cos \nu_L + d_F \sqrt{\frac{a_d}{\mu}} \sin \nu_L \tag{3-19}$$

$$\sqrt{\frac{\mu}{a_d}} (t_L - t_F) = a_d (\nu_L - \sin \nu_L) + \hat{r}_E \sin \nu_L + d_F \sqrt{\frac{a_d}{\mu}} (1 - \cos \nu_L) \tag{3-20}$$

With d_F tentatively set at its value on the nominal orbit, these two equations can be solved iteratively for a_d and ν_L. The velocity vector $\underline{V}_F$ corresponding to this orbit is then computed and the dot product:

$$d_F = \hat{\underline{R}}_F \cdot \underline{V}_F = \hat{\underline{R}}_E \cdot \underline{V}_F \tag{3-21}$$

is formed, and equations 3-19 and 3-20 are again solved for a_d and ν_L. The procedure is repeated until the computed velocity vector $\underline{V}_F$ converges to a fixed value.

From the standpoint of guidance accuracy alone, this computation is entirely adequate 6/ and the number of iterations required for solution is not prohibitive. The fixed time constraint, however, can be expected to exact an unnecessary increase in fuel expenditure. Thus the guidance technique used here, while adequate for a navigation error analysis, is not suitable for use in the actual onboard system.

3.3.1.4 Equations of Motion

For a lunar orbit perturbed by earth and solar gravitation and lunar oblateness, the equations of motion in selenocentric coordinates can be written as 7/

6/ In a test run with deviation of 200 kilometers off nominal at time t_E, the vehicle was guided to within 25 meters of nominal periselenum position at t_L, as observed by actual simulation. Furthermore, most of this small error was attributed to uncertainties at time t_E of about 15 meters and 0.01 meter/sec.

7/ Although these equations are approximate, they are sufficiently accurate for the purpose of this report. Clearly, discrepancies in perturbative forces are second order errors.

$$\frac{d^2 X_1}{dt^2} = -\frac{\mu X_1}{r^3}\left\{1 + \frac{0.5955\, q^2}{r^2}\left[0.000245466\left(1 - \frac{5 X_2^2}{r^2}\right) + 0.0006294\left(1 - \frac{5 X_3^2}{r^2}\right)\right]\right\} - \frac{\mu_E}{b_{VE}^3}\left(X_1 - b_{E1}\right) - \frac{\mu_E\, b_{E1}}{b_{OE}^3} - \frac{\mu_S}{b_{VS}^3}\left(X_1 - b_{S1}\right) - \frac{\mu_S\, b_{S1}}{b_{OS}^3} \tag{3-22}$$

$$\frac{d^2 X_2}{dt^2} = -\frac{\mu X_2}{r^3}\left\{1 + \frac{0.5955\, q^2}{r^2}\left[0.000245466\left(3 - \frac{5 X_2^2}{r^2}\right) + 0.0006294\left(1 - \frac{5 X_3^2}{r^2}\right)\right]\right\} - \frac{\mu_E}{b_{VE}^3}\left(X_2 - b_{E2}\right) - \frac{\mu_E\, b_{E2}}{b_{OE}^3} - \frac{\mu_S}{b_{VS}^3}\left(X_2 - b_{S2}\right) - \frac{\mu_S\, b_{S2}}{b_{OE}^3} \tag{3-23}$$

$$\frac{d^2 X_3}{dt^2} = -\frac{\mu X_3}{r^3}\left\{1 + \frac{0.5955\, q^2}{r^2}\left[0.000245466\left(1 - \frac{5 X_2^2}{r^2}\right) + 0.0006294\left(3 - \frac{5 X_3^2}{r^2}\right)\right]\right\} - \frac{\mu_E}{b_{VE}^3}\left(X_3 - b_{E3}\right) - \frac{\mu_E\, b_{E3}}{b_{OE}^3} - \frac{\mu_S}{b_{VS}^3}\left(X_3 - b_{S3}\right) - \frac{\mu_S\, b_{S3}}{b_{OS}^3} \tag{3-24}$$

where μ, μ_S, and μ_E are the gravitational constants of the moon, sun, and earth respectively and q is the mean lunar radius.

The actual orbit is computed from these expressions, using the initial conditions:

$$\begin{bmatrix} X_1(0) \\ X_2(0) \\ X_3(0) \end{bmatrix} = \underline{R}_o + \begin{bmatrix} x_{01} \\ x_{02} \\ x_{03} \end{bmatrix} \tag{3-25}$$

$$\begin{bmatrix} \dot{X}_1(0) \\ \dot{X}_2(0) \\ \dot{X}_3(0) \end{bmatrix} = \underline{V}_o + \begin{bmatrix} x_{04} \\ x_{05} \\ x_{06} \end{bmatrix} \tag{3-26}$$

where $\underline{R}_o$ and $\underline{V}_o$ are the nominal position and velocity vectors respectively immediately after injection, and the error components are taken from equation 3-17.

3.3.1.5 Observables

The angle between a known star and the instantaneous local vertical is illustrated in figure 3-3.

$$Y_m = \text{arc cos}\left(-\frac{1}{r_m}\underline{S}_m \cdot \underline{R}_m\right) \tag{3-27}$$

where $\underline{S}_m$ is a unit vector in the direction of the star chosen for observation on the mth measurement. The above expression is rewritten as

$$r_m \cos Y_m = -\underline{S}_m^T \underline{R}_m \tag{3-28}$$

and, taking variations in $\underline{R}_m$,

$$\delta r_m \cos Y_m - r_m \sin Y_m \, \delta Y_m = -S_m^T \, \delta R_m \tag{3-29}$$

Since

$$\delta r_m = \frac{1}{r_m} \underline{R}_m^T \, \delta \underline{R}_m \tag{3-30}$$

the preceding expression is equivalent to:

$$\delta Y_m = \frac{1}{r_m} \left[\frac{\left(\frac{\cos Y_m}{r_m}\right)\underline{R}_m + \underline{S}_m}{\sin Y_m}\right]^T \delta \underline{R}_m \tag{3-31}$$

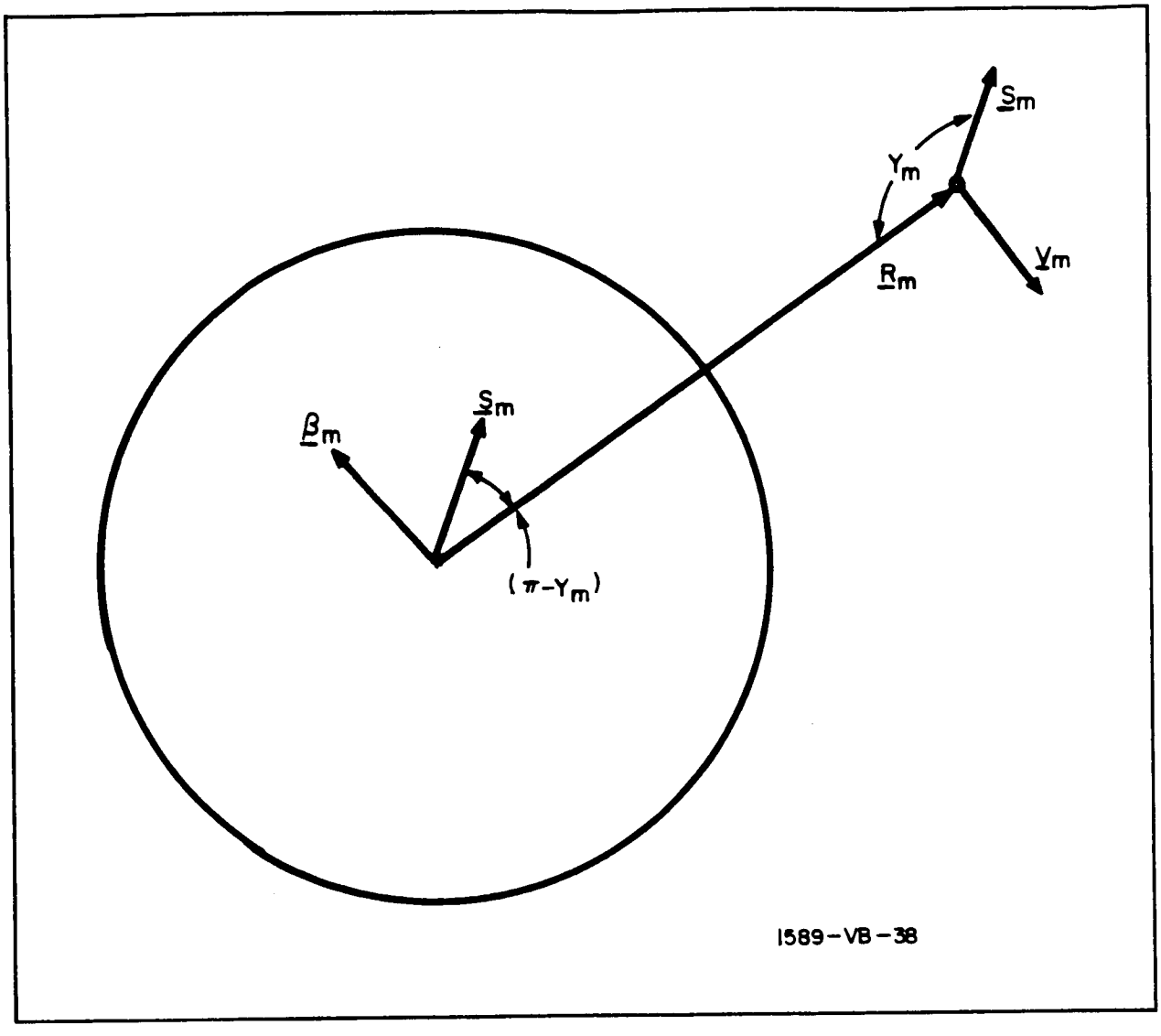

Figure 3-3. Angle Between Star and Local Vertical

In figure 3-3, $\underline{\beta}_m$ is a unit vector normal to $\underline{R}_m$ in the plane of the measurement (Ref. 3-10). It can be seen that:

$$\underline{S}_m = \frac{1}{r_m} \underline{R}_m \cos\left(\pi - Y_m\right) + \underline{\beta}_m \sin\left(\pi - Y_m\right) \tag{3-32}$$

Solving this for $\underline{\beta}_m$ and combining the result with the preceding equation,

$$\delta Y_m = \frac{1}{r_m} \underline{\beta}_m^T \delta \underline{R}_m \tag{3-33}$$

The partial derivatives of the observed angle with respect to the state vector components are written as:

$$h_{mj} \triangleq \frac{\partial Y_m}{\partial X_{mj}} = \csc Y_m \left[\frac{r_m^2 \, s_{mj} - (\underline{S}_m \cdot \underline{R}_m) X_{mj}}{r_m^3} \right]$$

$$1 \leq j \leq 3$$

$$h_{mj} = 0, \qquad 4 \leq j \leq 6 \tag{3-34}$$

3.3.2 Error Analysis

An overall picture of the entire simulation program is given in figure 3-4. The development which follows, augmented by the preceding background analysis, is intended to pinpoint the approach taken in deriving the numerical results.

3.3.2.1 Simulated Equations of Motion

The expressions used to simulate the onboard navigation computations are the vector solutions to the two-body problem[8/] (Ref. 3-9). At time t_m the predicted position vector components are

$$\bar{X}_{mj} = \left[1 - \frac{a_{m-1}}{\hat{r}_{m-1}} \left(1 - \cos \nu_m \right) \right] \hat{X}_{m-1,\, j} + \left[t_m - t_{m-1} - \frac{a_{m-1}^{3/2}}{\sqrt{\mu}} \left(\nu_m - \sin \nu_m \right) \right] \hat{X}_{m-1,\, j+3} \tag{3-35}$$

where

$j = 1, 2, 3$

8/ If sensitivity coefficients are computed from successive updated orbits and updated Keplerian equations are used as a basis for all onboard computations, the estimated trajectory can be described as a time-varying conic. Because a patched conic is a valid approximation to a perturbed orbit, and because the actual observables will contain the effects of orbital perturbations, it is of interest to investigate the use of two-body orbit equations in the actual onboard system. This, of course, is extremely desirable from the standpoint of onboard computer simplicity.

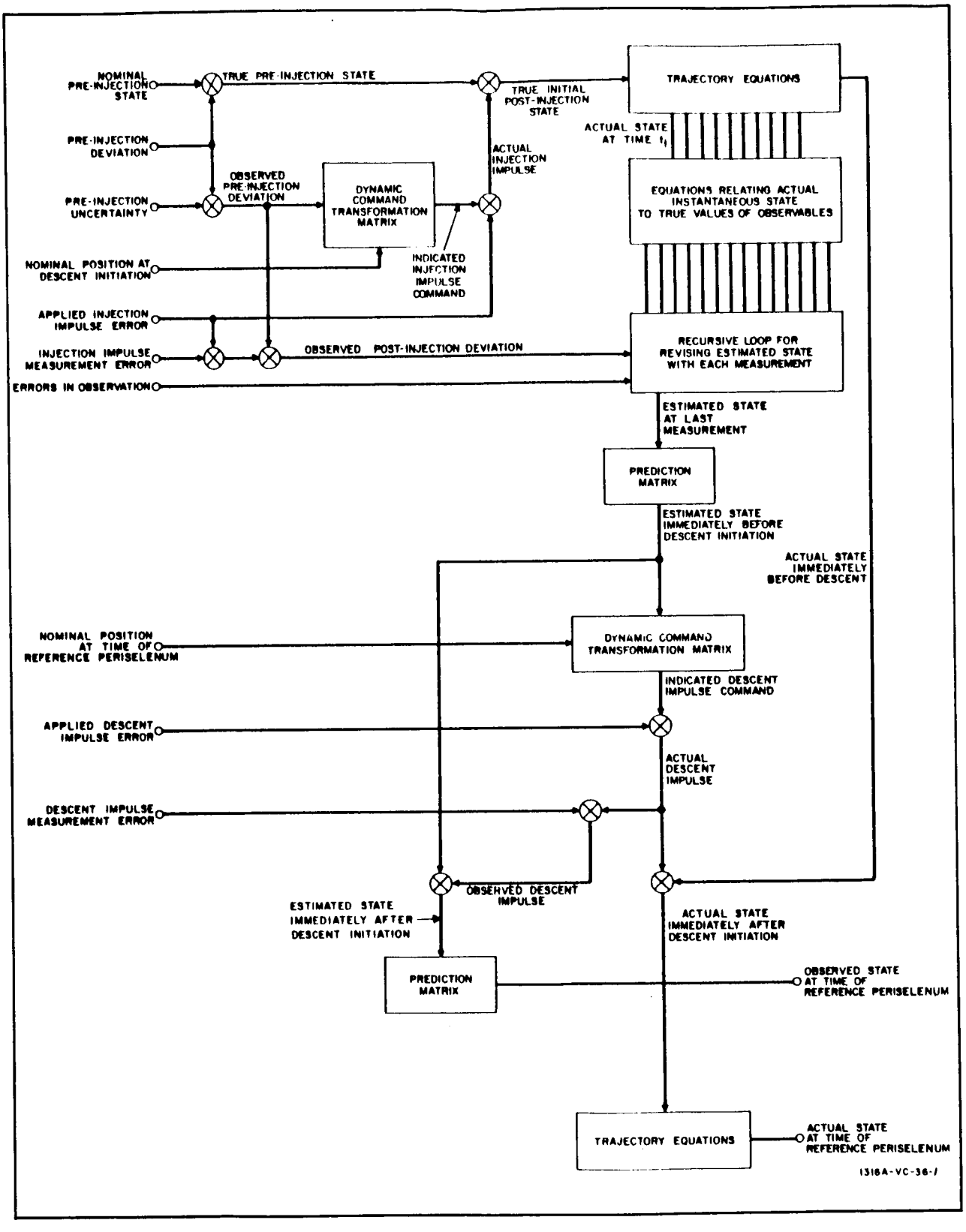

Figure 3-4. Schematic of Lunar Navigation Simulation

and the predicted velocity vector components are:

$$\bar{X}_{mj} = \left[- \frac{\sqrt{\mu\, a_{m-1}}}{\bar{r}_m\, \hat{r}_{m-1}} \sin \nu_m \right] \hat{X}_{m-1,\ j-3}$$

$$+ \left[1 - \frac{a_{m-1}}{\bar{r}_m} \left(1 - \cos \nu_m \right) \right] \hat{X}_{m-1,\ j} \qquad (3\text{-}36)$$

where

$j = 4,\ 5,\ 6$

and the incremental eccentric anomaly, ν_m, is the solution to the transcendental equation:

$$\frac{\sqrt{\mu}}{a_{m-1}^{3/2}} \left(t_m - t_{m-1} \right) = \nu_m - \sin \nu_m + \frac{\hat{r}_{m-1}}{a_{m-1}} \sin \nu_m$$

$$+ \frac{d_{m-1}}{\sqrt{\mu\, a_{m-1}}} \left(1 - \cos \nu_m \right) \qquad (3\text{-}37)$$

and the quantities:

$$\hat{r}_m = \sqrt{\hat{X}_{m1}^2 + \hat{X}_{m2}^2 + \hat{X}_{m3}^2} \qquad (3\text{-}38)$$

$$\hat{v}_m = \sqrt{\hat{X}_{m4}^2 + \hat{X}_{m5}^2 + \hat{X}_{m6}^2} \qquad (3\text{-}39)$$

$$a_m = \frac{\mu\, \hat{r}_m}{2\mu - \hat{r}_m\, \hat{v}_m^2} \qquad (3\text{-}40)$$

$$d_m = \hat{X}_{m1}\, \hat{X}_{m4} + \hat{X}_{m2}\, \hat{X}_{m5} + \hat{X}_{m3}\, \hat{X}_{m6} \qquad (3\text{-}41)$$

are computed from each set of updated state variables. The initial conditions used to start these computations are:

$$\begin{bmatrix} \hat{X}_{01} \\ \hat{X}_{02} \\ \hat{X}_{03} \end{bmatrix} = \underline{R}_o + \begin{bmatrix} \hat{x}_{01} \\ \hat{x}_{02} \\ \hat{x}_{03} \end{bmatrix} \qquad (3\text{-}42)$$

$$\begin{bmatrix} \hat{X}_{04} \\ \hat{X}_{05} \\ \hat{X}_{06} \end{bmatrix} = \underline{V}_o + \begin{bmatrix} \hat{x}_{04} \\ \hat{x}_{05} \\ \hat{x}_{06} \end{bmatrix} \tag{3-43}$$

where the error vector components are taken from equation 3-18.

3.3.2.2 State Transition Matrix

All elements of Φ follow from partial differentiation of equations 3-35 and 3-36. Complete expressions appear in Volume V, Appendix C.

3.3.2.3 Measurement Sensitivity

In the simulation the predicted position vector $\overline{R}_m$ is used in equation 3-27 to compute the predicted observable $\overline{Y}_m$, and both of these quantities are used in equation 3-34 to compute the measurement sensitivities used on-board. It is convenient to arrange these derivatives as the partitioned row vector:

$$\underline{H} = \left[\underline{\mathcal{H}} \quad \underline{O}_{13}\right] \tag{3-44}$$

where

$$\underline{\mathcal{H}} = \frac{1}{r_m} \underline{\beta}_m^T \tag{3-45}$$

so that the error introduced into a measurement by a timing uncertainty can be written as:

$$y_t = \underline{H} \left[\underline{X}(t_m + \delta t) - \underline{X}(t_m)\right] = \underline{\mathcal{H}} \left[\underline{R}(t_m + \delta t) - \underline{R}(t_m)\right] \tag{3-46}$$

For a reasonably small uncertainty in timing:

$$y_t \doteq \frac{1}{r_m} \delta t \left(\underline{\beta}_m^T \underline{V}_m\right) \tag{3-47}$$

When the chosen observable is a straight-ahead star (as is often desirable), the error reaches a maximum value of:

$$y_t = \frac{v_m}{r_m} \delta t \tag{3-48}$$

which, in a lunar circular orbit, is roughly 0.8 milliradian per second of timing error. 9/

3.3.2.4 Data Processing

The minimum variance recursion equations, contained in the aforementioned references, are stated here without proof:

$$P_m = \Phi(t_m, t_{m-1})(I_{66} - \underline{K}_{m-1}\underline{H}_{m-1})P_{m-1}\Phi^T(t_m, t_{m-1}) \tag{3-49}$$

$$\underline{K}_m = P_m \underline{H}_m^T (\underline{H}_m P_m \underline{H}_m^T + Q_m)^{-1} \tag{3-50}$$

In these equations, I_{66} is the 6 x 6 identity matrix, P_m is the uncertainty covariance matrix of the state vector, and Q_m is the variance of the measurement error (including the effects of timing uncertainty).

Since in the present simulation, the latest state vector estimate is substituted directly into the nonlinear orbit equations, the updating equation is:

$$\hat{\underline{X}}_m = \bar{\underline{X}}_m + \underline{K}_m(\hat{Y}_m - \bar{Y}_m) \tag{3-51}$$

where $\hat{Y}_m$ is the observed angle, computed by adding a random error of variance (Q_m) to the true value:

$$Y'_m = \arccos\left(-\frac{1}{r'_m}\underline{S}_m \cdot \underline{R}'_m\right) \tag{3-52}$$

with $\underline{R}'_m$ as the solution to the actual equations of motion 3-22 to 3-24, and where $\underline{S}_m$, again, is defined in figure 3-3.

The initial conditions corresponding to equations 3-49 and 3-50 are:

$$\underline{K}_o = \underline{O}_{61};\ \underline{H}_o = \underline{O}_{16} \tag{3-53}$$

(because no measurement is taken during the injection thrust impulse), and P_o is the combined result of midcourse navigation errors and injection thrust uncertainties. While the onboard data processing scheme is devised on the basis of a known (P_o) matrix, the requirement for known initial error statistics is easily circumvented. Consider a series of navigation computations in which the initial error covariance matrix is assumed to be diagonal (Ref. 3-11) and the variance elements are set at the largest values conceivable. The assumed error statistics are clearly conservative, and, since final uncertainties are substantially independent of initial uncertainties (Ref. 3-3), the results are only slightly pessimistic.

9/ It is of interest to note that this peak error sensitivity is equal to the angular velocity of the vehicle. The instantaneous time derivative of the true anomaly would be the peak timing error sensitivity in the most general case.

3.3.2.5 Data Conditioning

The definition of the vector $\underline{\beta}_m$ (figure 3-3) shows that, given the plane of a measurement, the measurement sensitivities are independent of the orientation of the star sightline in that plane. The plane itself, however, can be optimally selected. Battin (Ref. 3-4) has shown that, to minimize the rms position error after an observation, the direction of $\underline{\beta}_m$ should coincide with the principal eigenvector ($\underline{U}_m$) of the position uncertainty covariance matrix. Applied rigorously to a finite star field, this indicates a selection, to be made before each measurement, of the star which yields the largest absolute value of the scalar triple product:

$$\frac{\left[\underline{R}_m \times (\underline{S} \times \underline{R}_m)\right]}{\left|\underline{R}_m \times (\underline{S} \times \underline{R}_m)\right|} \cdot \underline{U}_m \equiv \frac{(\underline{U}_m \times \underline{R}_m) \cdot (\underline{S} \times \underline{R}_m)}{r_m \left|\underline{S} \times \underline{R}_m\right|} \tag{3-54}$$

It immediately follows that the star sightline should be chosen in the plane of ($\underline{U}_m$) and ($\underline{R}_m$) and, as expected, radial uncertainties cannot be eliminated by these angle measurements.[10]

In this system when Battin's minimum position error condition is satisfied, the mean squared position uncertainty is reduced, as a result of measurement, by an amount approaching the maximum eigenvalue of the position uncertainty covariance matrix. To show this, equation 3-50 is written in partitioned form as

$$\begin{bmatrix} \underline{K}^{(1)} \\ \underline{K}^{(2)} \end{bmatrix} = \frac{1}{g} \begin{bmatrix} P^{(1)} & P^{(2)} \\ P^{(3)} & P^{(4)} \end{bmatrix} \begin{bmatrix} \underline{\mathcal{H}}^T \\ \underline{O}_{31} \end{bmatrix} = \frac{1}{g} \begin{bmatrix} P^{(1)} & \underline{\mathcal{H}}^T \\ P^{(3)} & \underline{\mathcal{H}}^T \end{bmatrix} \tag{3-55}$$

where the scalar (g) is defined as:

$$g = \underline{H}P\underline{H}^T + Q = \underline{\mathcal{H}}\, P^{(1)} \underline{\mathcal{H}}^T + Q \tag{3-56}$$

and all subscripts have been tentatively omitted for simplicity.

From equation 3-45 it is recognized that when $\underline{\beta}$ is the eigenvector corresponding to the largest eigenvalue (Λ) of $P^{(1)}$

$$g = \frac{\Lambda}{r^2} + Q \tag{3-57}$$

10/ This problem is not serious in a parking orbit of sufficient duration, where the nonmeasurable (radial) direction rotates through a wide angle. It should be noted, however, that an earth-moon transfer trajectory contains a comparatively straight segment of considerable length, so that additional observables for that phase would be extremely desirable.

The step reduction in P due to the measurement is:

$$KHP = \frac{1}{g} \begin{bmatrix} P^{(1)} \underline{\mathcal{H}}^T & \underline{\mathcal{H}} & O \\ P^{(3)} \underline{\mathcal{H}}^T & \underline{\mathcal{H}} & O \end{bmatrix} \begin{bmatrix} P^{(1)} & P^{(2)} \\ P^{(3)} & P^{(4)} \end{bmatrix} \tag{3-58}$$

From the upper left submatrix of the above product, the step reduction in the total mean squared position uncertainty is the trace (see Volume V, Appendix A):

$$\mathrm{tr} \left\{ \frac{1}{g} P^{(1)} \underline{\mathcal{H}}^T \underline{\mathcal{H}} P^{(1)} \right\} = \frac{1}{g r^2} \mathrm{tr} \left\{ P^{(1)} \underline{\beta} \underline{\beta}^T P^{(1)} \right\} \tag{3-59}$$

Since $P^{(1)}$ is symmetric, the above expression reduces to:

$$\frac{1}{\Lambda + Q r^2} (P^{(1)} \underline{\beta})^T (P^{(1)} \underline{\beta}) = \frac{\Lambda}{1 + \frac{Q r^2}{\Lambda}} \tag{3-60}$$

This expression represents the largest step reduction obtainable in mean squared position uncertainty. In addition to the insight it provides, it is potentially valuable in predetermining the usefulness of a measurement before it is actually taken. The utility of this development apparently stops here, however, for two practical reasons:

- It has already been decided that the system must function without complete knowledge of the uncertainty covariance matrix. This precludes the computation of a true set of eigenvectors.

- The number of stars to be tracked must be held to a minimum.

In view of these requirements, the field of observables was limited to three stars for most computer runs described here. Selection of stars was governed by the following considerations:

- Between measurements the uncertainty can be expected to grow most rapidly in the direction of motion. It follows that stars near the orbital plane should be chosen often.

- When a continuously monitored star lies in the orbital plane, the situation will eventually arise in which the angle to be measured approaches 180 degrees, so that the plane of the measurement and the algebraic sign of the observed angle deviation are ill-defined.

- No out-of-plane information is available from coplanar star measurements.

From these conditions it follows that two stars should be chosen as nearly as possible in the orbital plane and a third should lie near the normal to the plane. The star near the pole of the orbit should be observed when, and only when, the acute angle between the local vertical line and the visible in-plane star becomes less than a prescribed minimum (Y_{min}) and, since each in-plane star will be eclipsed for roughly half of the orbit, it is desirable that these two stars have equal and opposite declination angles and a sidereal hour angle separation of 180 degrees. Accordingly, stars number 2 and number 32 (roughly 6-1/2 degrees and 15 degrees out of the nominal orbital plane, respectively) and number 18 (about 78-1/2 degrees out of the plane) are chosen from table 3-1 as the available stars in the standard case.

Although the practical feasibility of a complete navigation star field can be questioned, it is of interest to determine the performance obtainable when several or all of the stars in table 3-1 are made available. In conjunction with this investigation, a modified data conditioning procedure is postulated, whereby the scalar in equation 3-54 is replaced by:

$$\left|(\underline{U}_m \times \underline{R}_m) \cdot (\underline{S} \times \underline{R}_m)\right|$$

Selection of the star sightline, $\underline{S}$, which maximizes this quantity will provide a preconditioned measurement, subject to the constraint that stars near the local vertical are to be avoided. 11/

One final addition to the navigation procedure is considered. It is of interest to determine the improvement provided by an altimeter, which is made available whenever the eigenvector, $\underline{U}_m$, is within 45 degrees of the local vertical. The observable in this instance is:

$$Y_m = \sqrt{X_{m1}^2 + X_{m2}^2 + X_{m3}^2} - q \tag{3-61}$$

and its sensitivities to position and velocity are respectively:

$$h_{mj} = \frac{X_{mj}}{r_m}, \; j = 1, 2, 3$$
$$h_{mj} = 0, \; j = 4, 5, 6 \tag{3-62}$$

An investigation of this point has been included in the simulation.

11/ In practice it is found that this procedure tends to select stars within 30 degrees of the horizontal. This fulfills the original intention of ignoring overhead stars and also ensures that the chosen star will not be eclipsed by the moon at the orbital altitude considered here.

3.3.2.6 Linearized Computation of Error Statistics

In accordance with the previously stated assumptions (subsection 3.2) equivariant and independent Cartesian components of all input error vectors, it is clear that the initial covariance matrices can be written in partitioned form as

$$N_A = \begin{bmatrix} \Gamma_1 & O_{33} \\ O_{33} & \Gamma_2 \end{bmatrix} \tag{3-63}$$

for initial state vector deviations from nominal, and

$$P_A = \begin{bmatrix} \Gamma_3 & O_{33} \\ O_{33} & \Gamma_4 \end{bmatrix} \tag{3-64}$$

for initial state vector uncertainties, where:

$$\Gamma_i = \sigma_i^2 I_{33} \tag{3-65}$$

and (σ_1), (σ_2), (σ_3), (σ_4) represent rms initial position deviation, velocity deviation, position uncertainty, and velocity uncertainty per axis respectively.

Convariance matrices for both deviations and uncertainties undergo linear transformations with time and step transformations with the application of a velocity impulse, and the uncertainty covariance matrix experiences a step reduction with each measurement. This step reduction and the extrapolation of uncertainty with time are both illustrated in equation 3-49. Extrapolation of the state vector deviation convariance matrix is treated in the same manner; i.e., premultiplication by the state transition matrix and postmultiplication by its transpose. The step increase in the uncertainty covariance matrix with a velocity impulse is expressed as:

$$P_o = P_A + \begin{bmatrix} O_{33} & O_{33} \\ O_{33} & \Gamma_6 \end{bmatrix} \tag{3-66}$$

$$P_F = P_E + \begin{bmatrix} O_{33} & O_{33} \\ O_{33} & \Gamma_8 \end{bmatrix} \tag{3-67}$$

where (σ_6) and (σ_8) represent the rms integrated thrust measurement errors per axis for injection and descent respectively (i.e., in each of three mutually perpendicular directions). Volume V shows that the step change in the state vector deviation covariance matrix resulting from a velocity impulse is expressed by:

$$N_o = (G_A + I_{66})(N_A - P_A)(G_A + I_{66})^T + P_A + \begin{bmatrix} O_{33} & O_{33} \\ O_{33} & \Gamma_5 \end{bmatrix} \tag{3-68}$$

and

$$N_F = (G_E + I_{66})(N_E - P_E)(G_E + I_{66})^T + P_E + \begin{bmatrix} O_{33} & O_{33} \\ O_{33} & \Gamma_7 \end{bmatrix} \tag{3-69}$$

where G_A is computed from $\Phi(t_E, t_o)$ as explained in paragraph 3.3.1.3, G_E is computed in a similar manner from $\Phi(t_L, t_F)$, and (σ_5) and (σ_7) are the rms applied velocity impulse errors per axis at injection and descent respectively.

Coordinate rotations of final error statistics are performed by means of the rotation matrix:

$$W = \begin{bmatrix} \frac{1}{v_L} X_{L4} & \frac{1}{v_L} X_{L5} & \frac{1}{v_L} X_{L6} \\ \frac{1}{r_L} X_{L1} & \frac{1}{r_L} X_{L2} & \frac{1}{r_L} X_{L3} \\ \frac{1}{r_L v_L} (\underline{I}\, \underline{V}_L\, \underline{R}_L) & \frac{1}{r_L v_L} (\underline{J}\, \underline{V}_L\, \underline{R}_L) & \frac{1}{r_L v_L} (\underline{K}\, \underline{V}_L\, \underline{R}_L) \end{bmatrix} \tag{3-70}$$

where the $\underline{I}$, $\underline{J}$, and $\underline{K}$ in the scalar triple product expressions represent unit vectors in the x, y, and z directions respectively. Any 3 x 3 deviation or uncertainty covariance submatrix can be transformed into tangential, vertical, and transverse errors through premultiplication by W and postmultiplication by its transpose.

3.4 RESULTS

The flight path shown in figure 3-1 was simulated under various combinations of navigation computation procedures, available observables, input errors, and measurement schedules, in order to determine the navigation system requirements for the allowable periselenum miss distance specified in subsection 3.2. This subsection contains a detailed description of the simulated conditions and a presentation of quantitative results, with subsequent interpretative discussion.

3.4.1 Discussion of Digital Simulation

The combined orbital flight simulation and linearized analysis described in figure 3-4 has been implemented through double-precision digital computation. The program is arranged so that one member of the ensemble is carried through the simulation concurrently with the linearized statistical computations.

The primary outcome of this program consists of the deviations and the uncertainties at all labeled points of figure 3-1 at all measurement times as computed by both simulation and by linearized analysis. Also, to provide further insight into the minimum variance scheme, the following information was read out at each measurement time:

- All six components of the instantaneous state vector in the nominal, actual, predicted, and observed simulated orbits
- All six components of state vector deviations, uncertainties before and after measurement, and magnitudes of position and velocity uncertainties, as computed by actual flight simulation
- The square root of each diagonal term in the uncertainty error covariance matrix, immediately before and immediately after measurement, and the total rms position and velocity uncertainty, as determined by linearized analysis
- The three eigenvalues and direction cosines for the three eigenvectors of the premeasurement position uncertainty covariance matrix, used to select the next observation
- The selected observable (star number), the nominal, actual, and observed measurement value, and the random measurement error
- All six components of the weighting vector used to update the estimated state
- Partial derivatives of the observable with respect to each state vector component, as computed from the nominal, actual, and observed orbits

The ultimate criteria of navigation system performance are:

- The final errors, as determined from the associated covariance matrices
- The extent to which the simulation agrees with the linearized computations

Throughout this subsection, the results of the covariance matrix analysis are stated as rms errors. It is understood that the rms component of error in a given direction is the square root of the corresponding diagonal element of the covariance matrix, and the rms total error is the square root of the trace of the associated error covariance matrix. Agreement between the simulation results and the linearized analysis will be understood to mean that the error as observed by simulation was within the rms level in the majority of cases.

3.4.2 Numerical Results

To achieve the study objectives with a reasonable number of computer runs, an ordered sequence had to be planned whereby specific conclusions could be drawn quickly. This was possible because a number of the decisions which had to be made are not greatly influenced by exact position of earth, moon, and sun, the selenocentric longitude of the landing site, etc. A standard set of conditions was therefore adopted as a basis of comparison for the first series of runs (Series A). This standard consists of a single Monte Carlo trial, simulated concurrently with the linearized covariance matrix computation, for a vehicle making three revolutions in a lunar parking orbit.[12] The conditions which characterize the standard run are summarized in table 3-2. Standard units are meters and seconds.

12/ For the purpose of the first set of runs it was not necessary to include the descent guidance of the landing vehicle. Of greater interest here is the accuracy of the celestial navigation scheme over extended periods of time.

TABLE 3-2

STANDARD RUN CONDITIONS

$\mu = 4.8982 \times 10^6$	$i = 30$ deg	$q = 1,738,070$
$\Theta_M = 30$ deg	$\Theta_S = 60$ deg	
$\lambda_o = 0$ deg $\quad \psi_o = 180$ deg	$\lambda_p = 30$ deg	$\psi_P = -45$ deg
$r_o = r_p = q + 200,000$	$r_L = q + 20,000$	$\tau = 300 \quad Y_{min} = 25$ deg
$E_F = -90$ deg	$v_A = 2400$ (See Volume V, Appendix C)	

- All sensitivity coefficients are computed from the latest updated trajectory estimate.
- No orbital perturbations are assumed present.
- Available observables are limited to stars number 2, 32, and 18, from table 3-1.

RMS measurement error (σ_m) = 1 milliradian (no bias). See Volume V, Appendix C.

RMS error in each component of initial state vector. (See Volume V, Appendix C):

Position deviation	10,000
Position uncertainty	1000
Velocity deviation	10
Velocity uncertainty	1
Applied injection thrust	5
Measured injection thrust	0.05

NOTE: Standard units are meters and seconds.

The earliest efforts in evaluating the navigation scheme were directed toward the specification of onboard computation procedures. With the above-mentioned inputs the standard run (Case 1) was made, and the total position uncertainty (including both the square roots of the traces of the position uncertainty covariance matrices before and after each measurement and the error as determined from the Monte Carlo simulation trail) were plotted at each measurement time. For the second run (Case 2) the program was modified so that the sensitivity coefficients used in processing the measurements were computed from the nominal orbit; the inputs, and even the random number starters for Monte Carlo simulation, were matched to the first run. A third run (Case 3) was made, in which the actual trajectory (but not the nominal or observed trajectory) was computed from the perturbed orbit equations (3-22 through 3-24), but all conditions were otherwise identical to those of the first run.

Since the covariance matrix analysis contains the inherent assumption that no errors are introduced by idealization of onboard computations, the above three runs do not exhibit any appreciable difference in linearized ensemble statistics. That is, the linearized statistical results appear satisfactory in all three cases. As shown by the simulation results, plotted in figure 3-5,

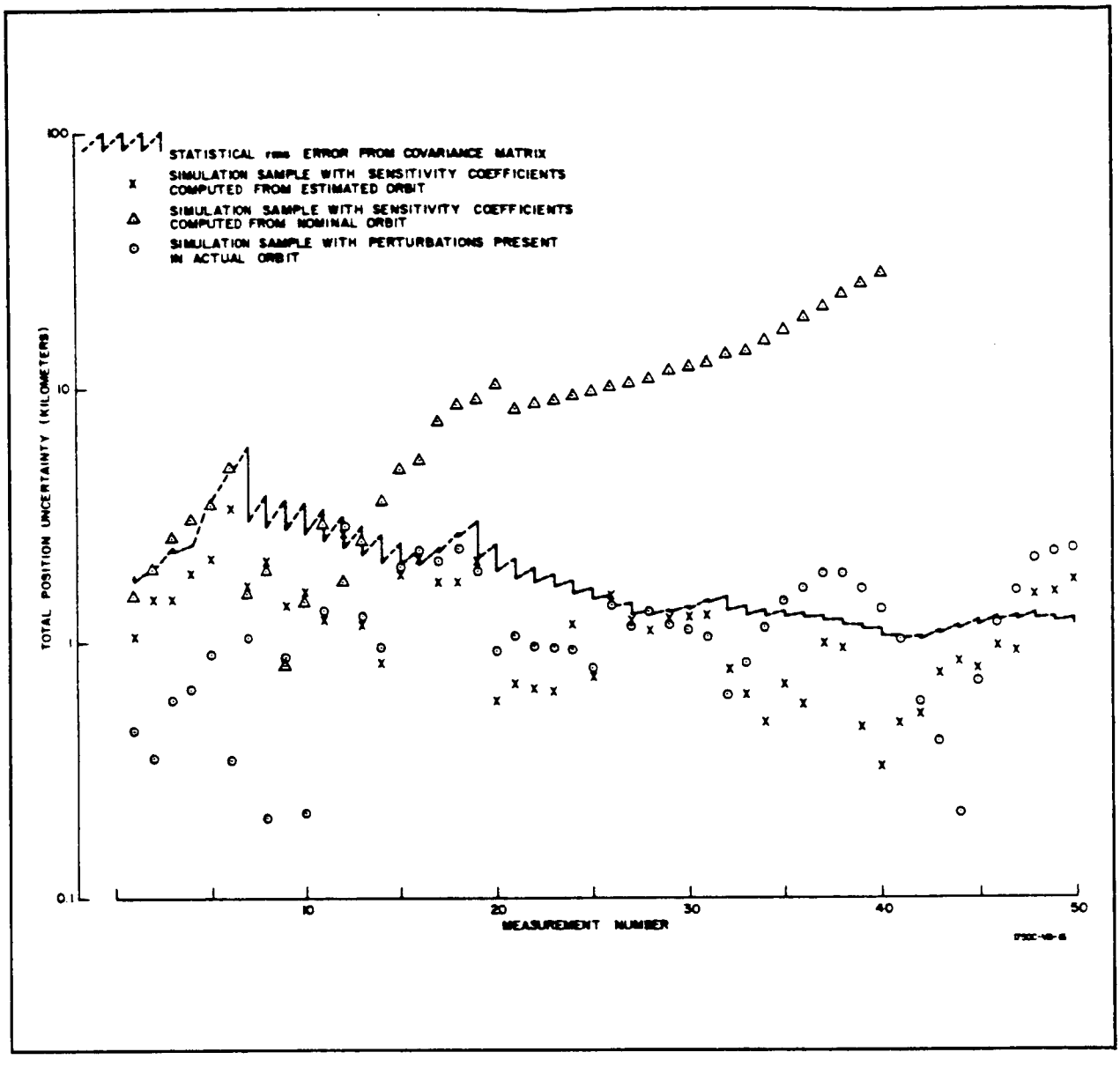

Figure 3-5. Total Position Uncertainty vs Time, Cases 1, 2, and 3

however, the three conditions are not equivalent.[13/] In particular, the use of a preselected nominal trajectory suffers from the persistent increase in the departure from that nominal, due to period variations. Whenever the vehicle reaches about 100 kilometers off nominal, the measurement partial derivatives as computed from the nominal orbit were not in agreement with those of the actual and observed orbits. This causes a divergence between

13/ The simulation results, of course, do not form a smooth curve, since they do not represent the average of a large number of trials.

simulated and linearized results, as shown in figure 3-5. The use of two-body equations in the onboard computer, however, shows considerable promise, in spite of the presence of orbital perturbations.

The first run of this series was then repeated with various modifications for comparison of performance provided by different sets of observables. Four basic variations in the field of observables were investigated:

Stars number 2 and 32 of table 3-1 were replaced by the pair (numbers 10 and 42), which are 33 and 25-1/2 degrees out of the nominal orbital plane respectively. Star number 18, near the pole of the orbit, was retained. (Case 4)

The 20 first-magnitude stars, shown circled in table 3-1, were all made available, and the modified star selection technique described in paragraph 3.3.2.5 was used. (Case 5)

All 57 navigation stars were used with the above-mentioned selection technique. (Case 6)

An altimeter with an rms error (including terrain uncertainties) of 1 kilometer was added to the run with 57 stars, and the corresponding data-conditioning technique described in paragraph 3.3.2.5 was used. (Case 7)

The results of Case 4 are shown in figure 3-6. It is seen that with only three stars available the ultimate effect of selecting stars which are farther removed from the orbital plane is a degradation in performance.[14]

14/ Case 4 does show a temporary advantage over Case 1 because, with the farther-removed stars, the star sightline is never within 25 degrees of the local vertical line. This allows more in-plane information to be accumulated at the beginning of Case 4, while Case 1 is observing the less informative pole star. It must also be acknowledged that the two stars (numbers 10 and 42) alone are sufficient to provide adequate performance.

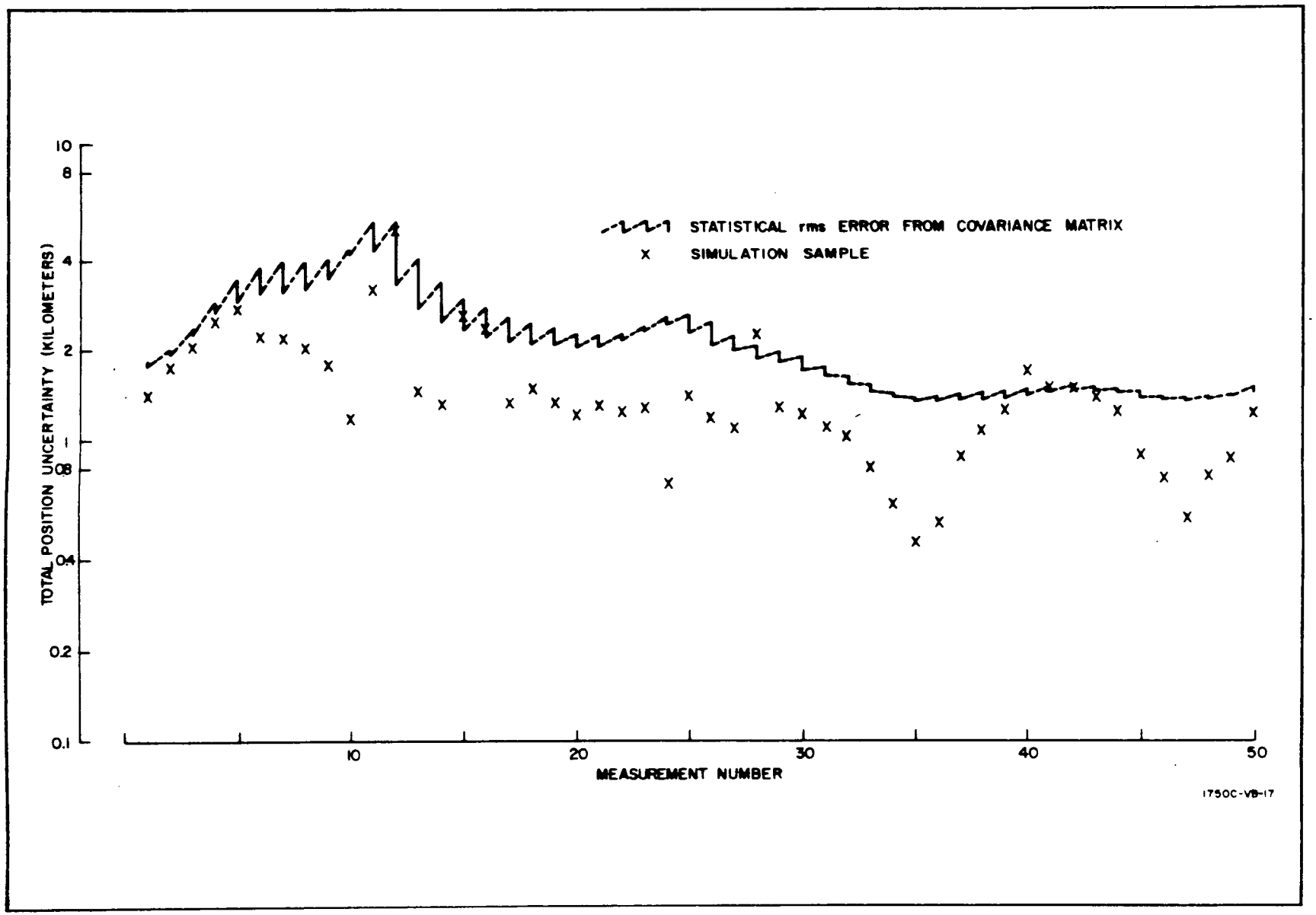

Figure 3-6. Total Position Uncertainty vs Time, Case 4

From figure 3-7 it is concluded that a selection of 20 stars offers little more than a properly chosen set of 3. A similar statement can be made in regard to the complete selection of 57 navigation stars; the statistical results of Cases 5 and 6 were essentially the same. The addition of an altimeter, as shown in figure 3-8, provides a temporary advantage which would be significant for translunar missions with short coasting segments.[15/]

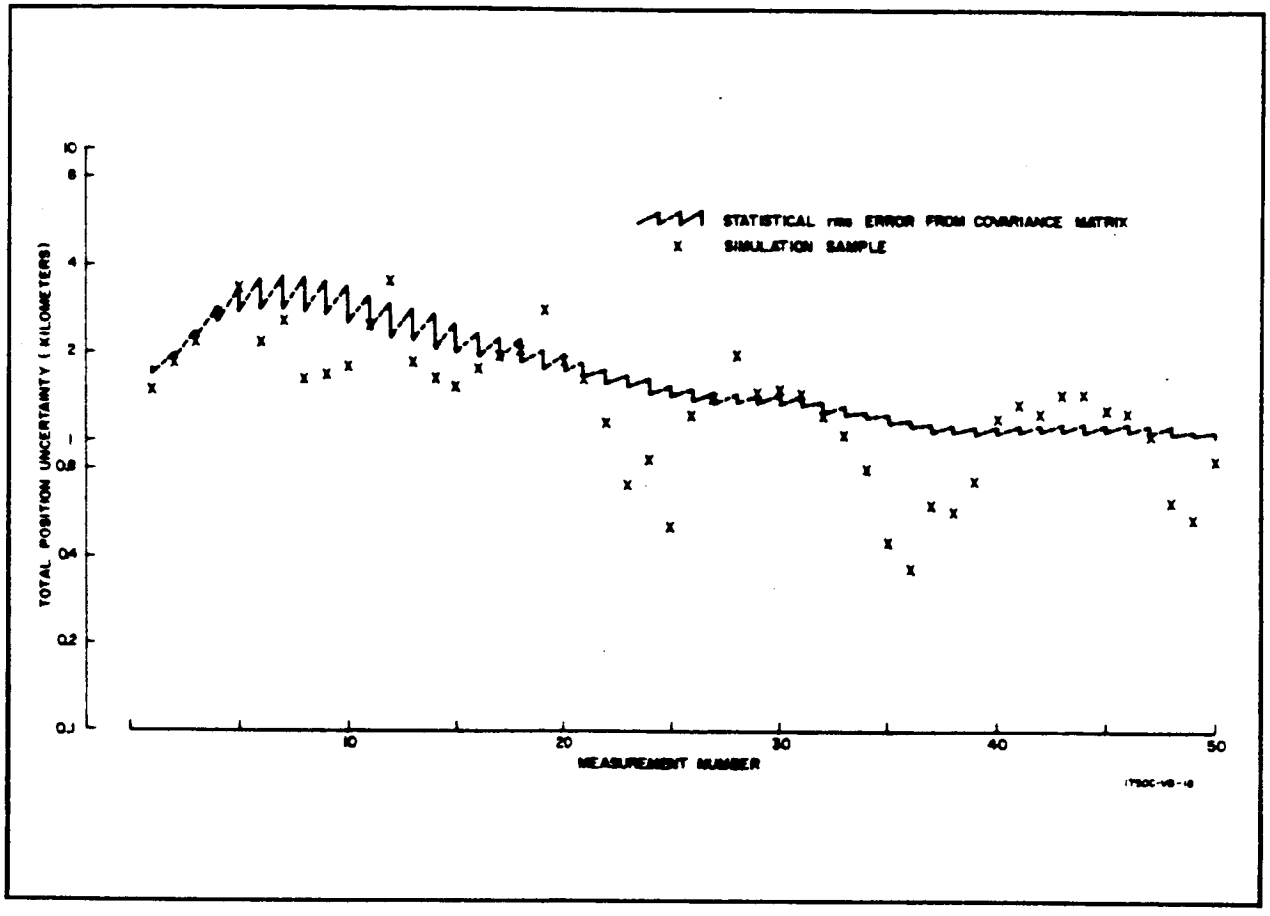

Figure 3-7. Total Position Uncertainty vs Time, Cases 5 and 6

The next computer run (Case 8) was made to determine the effects of very large displacments from the computational reference. The standard conditions with all sensitivity coefficients computed from the observed trajectory were

15/ The altitude measurements were not needed after the early portion of the trajectory. This seems to indicate that a more realistic initial uncertainty covariance matrix would have eliminated the transient rise in initial position uncertainty without the use of altitude information. Nevertheless, the utility of additional observables will remain significant in some applications.

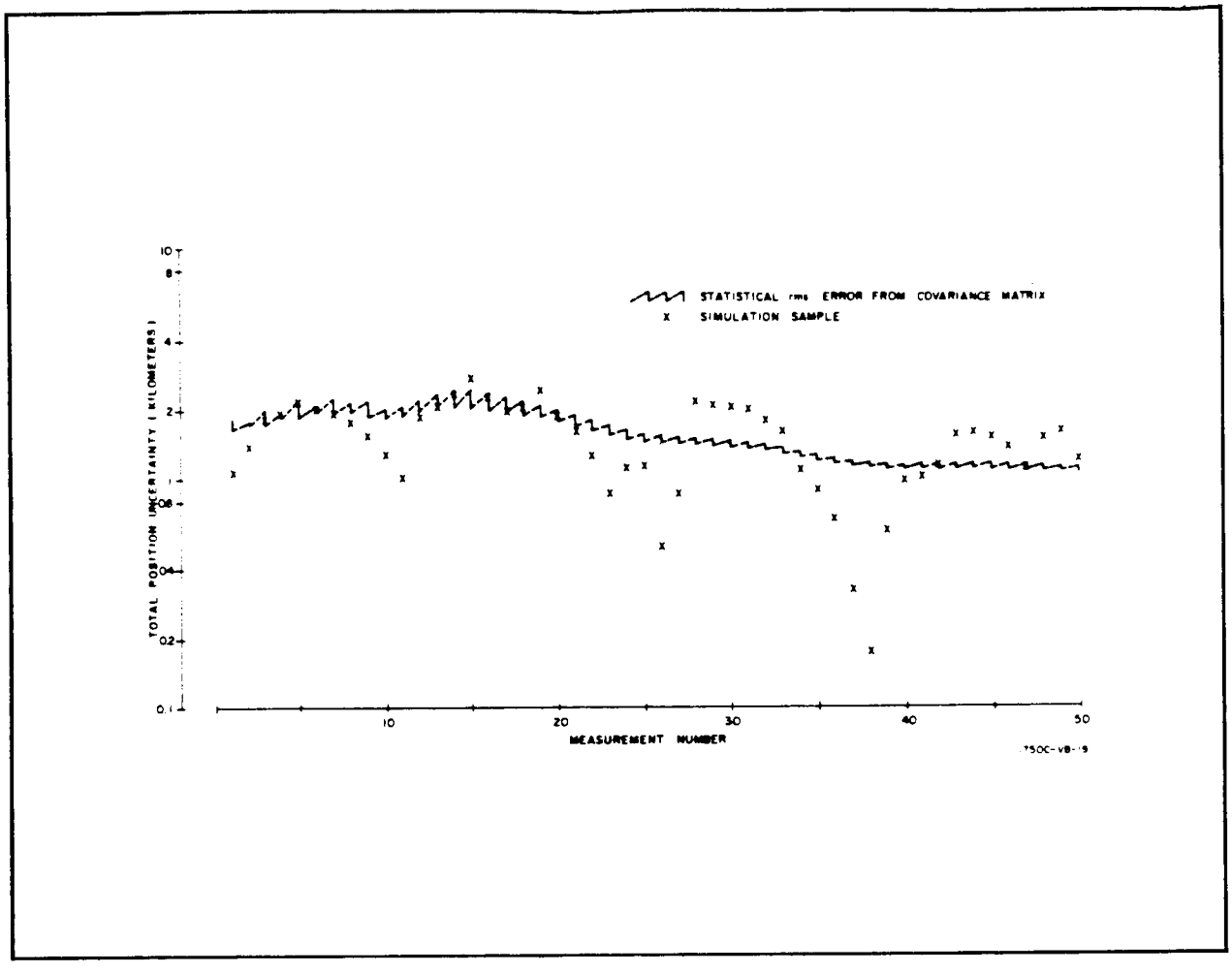

Figure 3-8. Total Position Uncertainty vs Time, Case 7

simulated with the rms initial position uncertainty changed to 100 km in each coordinate. The extent of agreement between the simulation and the linearized analysis, shown in figure 3-9,[16] is an indication of the wide range of tolerable initial error. It is the safety of the vehicle, and not some limit of mathematical convergence, which determines the allowable translunar midcourse terminal errors.

The above run was then repeated with Y_{min} set to zero (Case 9), effectively removing the pole star and permitting measurement of the inplane star as the angle approaches 180 degrees. As shown in figure 3-10,[14] the simulation results are near the 3-σ level at several points. This confirms the suggestion made earlier (in the analysis of data conditioning) that overhead stars should not be used for navigation.

16/ The ordinates for the first two measurements, for both simulation and linearized results, exceed 100 km in Case 8 and Case 9.

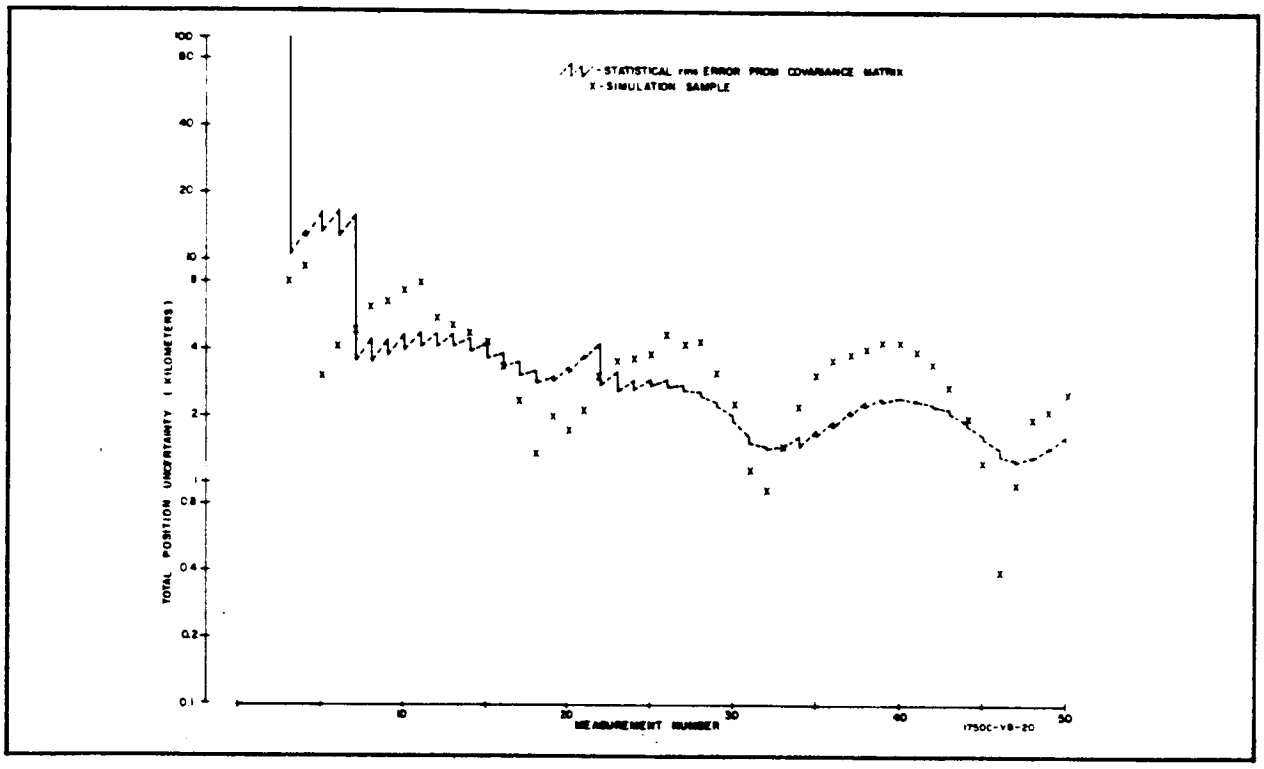

Figure 3-9. Total Position Uncertainty vs Time, Case 8

It is appropriate to mention at this point that all data shown here were obtained with the same random number starter and that subsequent simulations with other random numbers exhibited a behavior consistent with the original conclusions.

For the next series of runs (Series B) the single parking orbit revolution and descent arc of figure 3-1 were simulated to determine the required measurement accuracy. The standard conditions and inputs were used throughout, except for the time interval (τ) between measurements and the measurement accuracy. Fifteen runs were made, including all combinations of angle measurement error (σ_m) and (τ) given below.

σ_m : 0.5, 1.0. 1.5, 2.0, 3.0 milliradians
τ : 120, 180, 240 seconds

The descent thrust measurement error was assumed equal to the thrust measurement error at injection. For applied thrust at descent, however, the

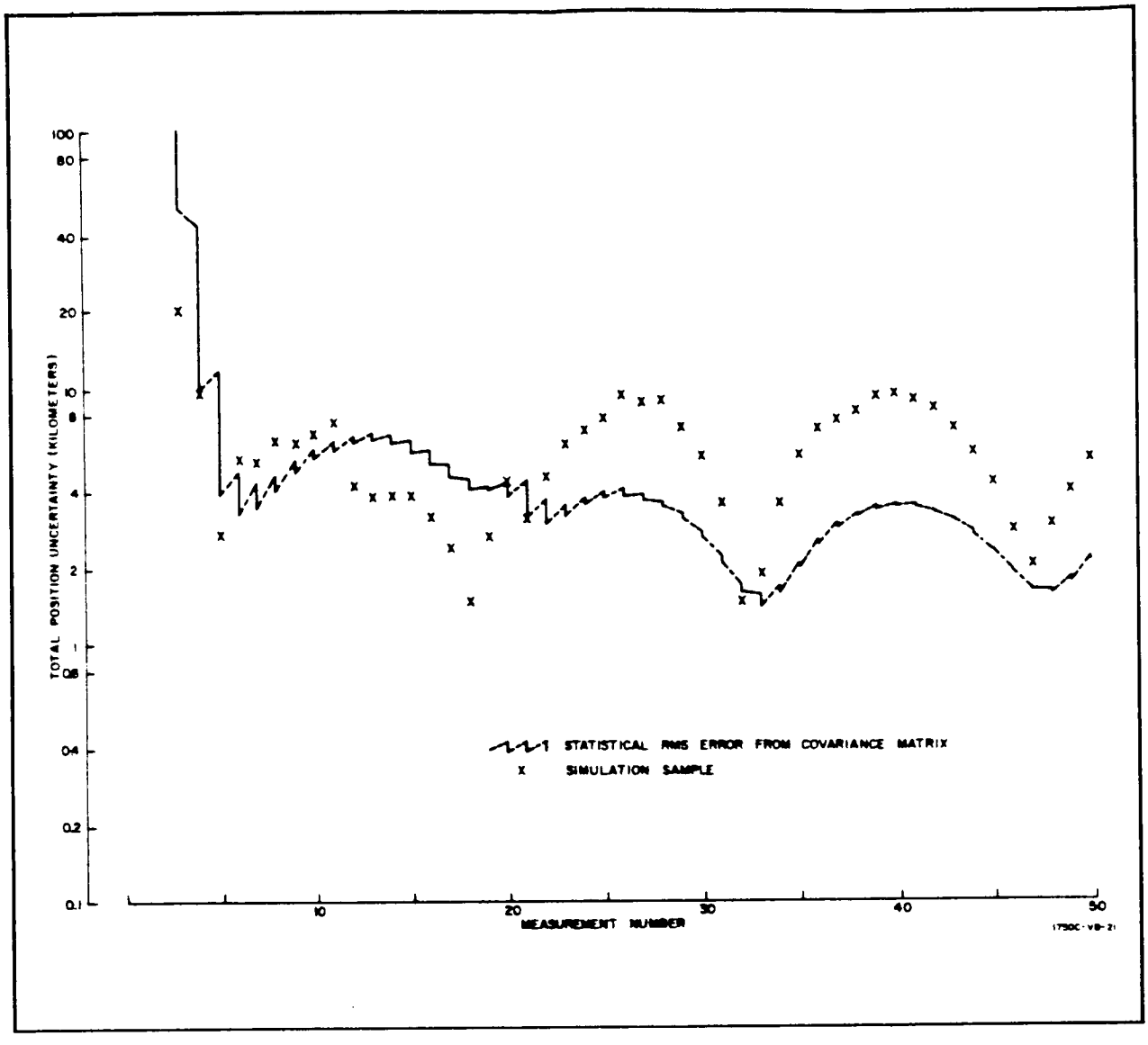

Figure 3-10. Total Position Uncertainty vs Time, Case 9

error was assumed to be 0.1 meter per second in each axis.[17] The results of this simulation series are summarized in the following paragraphs.

The extra velocity impulse needed for FTOA guidance (typically a few hundred meters per second) is excessive; a variable time guidance law will undoubtedly take preference.

17/ It should be noted that this stringent engine tolerance is not a system requirement but an assumed value, used to render the thrust error small in comparison with navigation error effects. The FTOA guidance law, an unnecessary restriction in itself, results in a high sensitivity of final miss distance to applied thrust errors.

The rms miss distance at the time of reference periselenum is very nearly a linear function of the product ($\sigma_m \sqrt{\tau}$), as shown in figure 3-11.[18] This is to be expected, since the deviation from the desired final position is (nearly) a linear function of the state uncertainty prior to the guidance command. This uncertainty in turn is proportional to the rms measurement error divided by the square root of the number of observations.

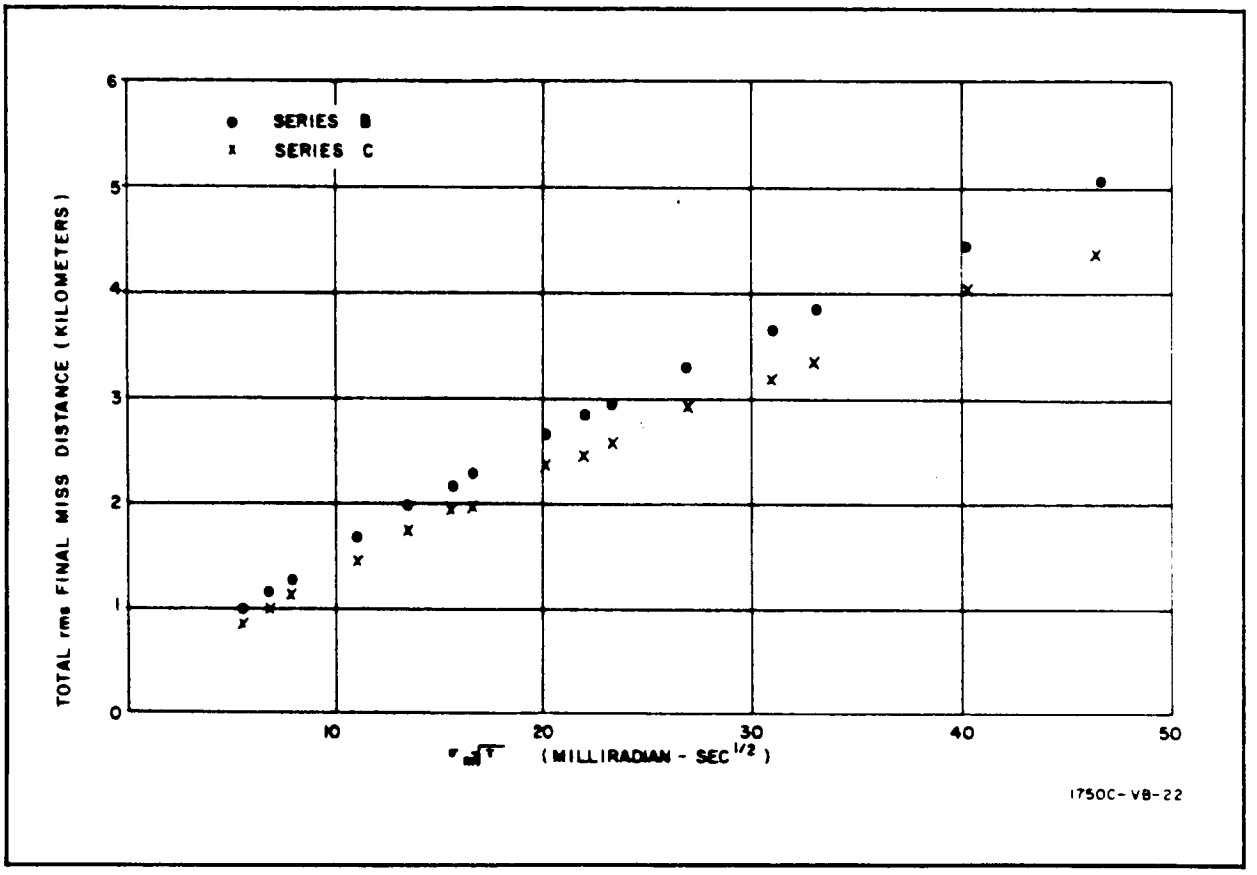

Figure 3-11. Final Miss Distance as a Function of Instrument Error and Measurement Frequency

As shown in table 3-3, the tangential, vertical, and transverse components of final miss distance are not equally sensitive to the parameter ($\sigma_m \sqrt{\tau}$). Particularly at values near the maximum allowable miss distance, the tangential error predominates.

18/ It should be noted that, due to descent thrust errors, the extrapolated curve would not pass through the origin.

TABLE 3-3

RMS MISS DISTANCE COMPONENTS AT PERISELENUM (METERS) - SERIES B

σ_m (mils) \ τ (sec) (min)	120 2	180 3	240 4
0.5	866 (T) 340 (V) 230 (Tr)	1054 (T) 378 (V) 265 (Tr)	1152 (T) 401 (V) 297 (Tr)
1.0	1527 (T) 490 (V) 381 (Tr)	1827 (T) 563 (V) 444 (Tr)	2001 (T) 614 (V) 497 (Tr)
1.5	2110 (T) 642 (V) 514 (Tr)	2486 (T) 740 (V) 592 (Tr)	2741 (T) 820 (V) 651 (Tr)
2.0	2645 (T) 789 (V) 623 (Tr)	3084 (T) 906 (V) 705 (Tr)	3431 (T) 1020 (V) 761 (Tr)
3.0	3631 (T) 1073 (V) 778 (Tr)	4187 (T) 1220 (V) 848 (Tr)	4746 (T) 1414 (V) 891 (Tr)

Legend: Tangential (T), Vertical (V), Transverse (Tr)

In view of the maximum allowable 3-σ tangential miss distance of 5 kilometers, the combination of a 2-minute interval and about 1-1/4 milliradians rms error can be cited as safe specifications for the lunar navigation phase with the 3-star configuration of observables.

In seeking a set of conditions under which this last requirement can be relaxed, the entire run sequence was repeated (Series C), using all 20 first-magnitude stars, conditioned as Case 6 of Series A. As shown in figure 3-11, however, the improvement is appreciable but not profound. Furthermore, a comparison of tables 3-3 and 3-4 shows that by selecting measurements to minimize the dominant error, the transverse errors are somewhat increased.

The case σ_m = 3 mr; τ = 120 sec from Series C was then repeated with the initial rms velocity uncertainty reduced by a factor of 10. Again, the effect was an appreciable (500-meter) but not drastic reduction in rms

TABLE 3-4

RMS MISS DISTANCE COMPONENTS AT PERISELENUM (METERS) - SERIES C

σ_m (mils) \ τ (sec) (min)	120 2	180 3	240 4
0.5	717 (T) 314 (V) 308 (Tr)	859 (T) 341 (V) 366 (Tr)	982 (T) 367 (V) 410 (Tr)
1.0	1273 (T) 433 (V) 543 (Tr)	1533 (T) 495 (V) 647 (Tr)	1695 (T) 538 (V) 716 (Tr)
1.5	1739 (T) 548 (V) 753 (Tr)	2093 (T) 643 (V) 874 (Tr)	2293 (T) 702 (V) 944 (Tr)
2.0	2174 (T) 664 (V) 918 (Tr)	2631 (T) 793 (V) 997 (Tr)	2893 (T) 874 (V) 1024 (Tr)
3.0	3054 (T) 906 (V) 1020 (Tr)	3728 (T) 1109 (V) 1041 (Tr)	4063 (T) 1218 (V) 1050 (Tr)

Legend: Tangential (T), Vertical (V), Transverse (Tr)

terminal miss distance.[19] Finally, a random number starter was found for which the displacement from nominal position at descent initiation time was relatively small, and the last simulation was repeated. The effect was a reduction of another 1100 meters from the rms miss distance, which brought the final figure (1750 meters rms) quite close to the originally specified allowable limit (5 km at 3-σ). At the same time, the rms position and velocity uncertainty at descent initiation were virtually unchanged.

With FTOA guidance for a 1/2-hour descent arc then, the sensitivity of the linearized final miss vector statistics to the parking orbit navigation errors (which is related to the slope in figure 3-11) is somewhat dependent upon the

19/ That is, the rms miss distance was reduced from about 3350 meters to 2850 meters. The smaller initial velocity uncertainty is more in line with results of the midcourse analysis referenced earlier (Ref. 3-3), but the periselenum of that trajectory is an order of magnitude beyond the orbital altitude under consideration here. At any rate, the low sensitivity of final errors to initial uncertainties indicates that reduction of midcourse navigation errors would be an inefficient means of improving the ultimate performance.

particular combination of initial errors occurring at injection. The reason for this dependence is clarified upon considering the wide range of position displacements possible at descent initiation. For some of the larger values encountered (in the vicinity of 250 kilometers), the position deviation to be compensated by guidance adjustments changes the total path length by a considerable percentage. Clearly, these variations in arc length, with fixed time at the end points, must change the average orbital velocity; the energy of the trajectory, in turn, influences the sensitivity of final errors to initial errors.

3.4.3 Discussion

Most of the results in the preceding paragraphs lend themselves to brief interpretation accompanying the data presentation and, therefore, have already been fully explained. There are, however, a few items for which a thorough explanation requires some reference to various parts of the analysis. First, in regard to navigation, it is inferred from equation 3-60 that a point of diminishing returns is reached when the quantity (Qr^2/Λ) approaches unity. For a radial distance (r) of about 2,000,000 meters and an rms measurement error $\sqrt{Q}$ of one milliradian, this indicates a position uncertainty level of 2 kilometers. The results of this analysis concur.[20]

In regard to guidance, the overall shortcomings of the FTOA scheme are clarified with the aid of an example. For the midcourse termination errors and injection thrust errors considered in this study, a change of 15 kilometers in the parking orbit semimajor axis is quite within the realm of possibility. The sensitivity of the orbital period T to variations in the semimajor axis is easily found by differentiation of Kepler's third law to be approximately 1.5 minutes per 15 kilometers in the lunar parking orbit. Over a duration of about 1-3/8 orbits (the approximate duration of the parking orbit phase), the vehicle position can "slip" to a location which it should have passed 2 full minutes ago. With a circular velocity of about 1600 meters/second then, the miss distance (i. e., the known deviation) at the time of parking orbit termination is 200 kilometers. The implications of this amount of miss distance, while not insurmountable, can only be described as undesirable.

20/ Figure 3-9 shows that the rms position uncertainty decreases slowly below 2 kilometers, whereas the large initial errors were quickly eliminated. It should be noted that an immediate reduction to 2 kilometers rms error at the beginning of figure 3-9 is inhibited by three factors:

Initial velocity uncertainties produce position uncertainties which grow with time.

Characterization of an orbit requires six parameters and, therefore, at least six scalar measurements.

Some of the earlier observations are pole star measurements.

- Since the deviation from nominal position is an appreciable percentage of the nominal orbit radius, the sensitivity coefficients computed from the nominal orbit (except those near the time of parking orbit initiation) will be inaccurate. This will affect both the measurement partial derivatives and the state transition matrix. It follows that the accuracy of a guidance law, linearized with respect to the nominal orbit, will be degraded.

- For a fixed time of arrival at the terminal point of the descent arc, the eccentric anomaly of the descent arc will deviate appreciably from the intended 90 degrees. It was mentioned in Section 5 of Volume II that the 90-degree arc provides maximum fuel efficiency for out-of-plane velocity corrections necessitated by transverse errors.

- With a fixed time of arrival (FTOA) guidance law, point (L) of figure 3-1 will not longer be the periselenum of the descent arc. An appreciable vertical velocity component will therefore exist at the time of reference periselenum. This is undesirable, since the desired velocity vector at this point is horizontal, for tangential transfer into the powered landing phase.

The above-mentioned degradation in guidance computations was circumvented by means of iterative velocity correction computations, as described in paragraph 3.3.1.3. The mere fact that this procedure is necessary, however, indicates the presence of linearization errors. Indeed, the statement in the last paragraph of paragraph 3.4.2, to the effect that linearized miss vector statistics vary with initial condition errors really means that the range of linearity has been exceeded. This point can be illustrated mathematically with the aid of equation D-22 of reference 3-3.

With FTOA guidance between the points (t_F) and (t_L), characterized by a state transition matrix

$$\Phi(t_L, t_F) = \begin{bmatrix} A_1 & A_2 \\ A_3 & A_4 \end{bmatrix} \tag{3-71}$$

the component of the miss vector statistics at (t_L) due to state vector errors at (t_F) can be written as 21/

$$\begin{bmatrix} A_1 & A_2 \end{bmatrix} \begin{bmatrix} P_F \end{bmatrix} \begin{bmatrix} A_1^T \\ A_2^T \end{bmatrix} \tag{3-72}$$

21/ In Ref. 3-3 this is presented as the final position prediction error. It can be shown, however, that this is equivalent to the position component of the time-extrapolated state vector deviation statistics, as determined by equation 3-69 with no thrust errors present.

It is important to note that the above expression is independent of the actual state vector deviation statistics N_F at descent initiation. When the actual position[22/] varies over a wide range, however, the state transition matrix itself will reflect these variations. For a given uncertainty covariance matrix P_F at descent initiation, then, the final miss vector is a function of the path subsequently followed.

The above situation hinders the specification of one particular standard for the navigation measurement accuracy and observation frequency requirements. Fortunately, however, for the variations observed here (up to about 250 kilometers) in descent initiation position, the final miss distance varies by no more than a factor of 2. A reasonable concluding assertion is that the guidance requirements can be realized by a state of the art horizon scanner (1 to 2 milliradians rms local vertical error) at an interval of 1 to 2 minutes between measurements, with the understanding that a suitable guidance law must be derived for use in conjunction with the navigation system prescribed here.

3.5 DISCUSSION OF ONBOARD COMPUTATION REQUIREMENTS

A question frequently arises in regard to the necessary complexity of an onboard computer capable of performing the minimum variance calculations. Actually the outlook is reasonably satisfying; there are several aspects of the envisioned navigation system which suggest simplicity.

The entire system is Markovian in nature; i.e., when a given state is reached, the path taken prior to that state is completely immaterial. Therefore, the use of recursive relationships permits the removal of all data accumulated prior to the most recent estimate. Storage requirements for the onboard computer will be reasonably low in this area.

Most matrix manipulations required of the system considered here are of the most elementary form (e.g., multiplication, addition). No inversion operations are required for any matrices of higher than third order.

It was found that with a sufficiently long parking orbit duration, only a few readily accessible observables are needed for navigation. It is possible to choose these observables so that lunar rotation does not affect the measurements, and no large array of stored observable data is required.

22/ Actual position deviations are emphasized in this discussion, since the position vector at descent initiation time constrains the descent flight path. In contrast, deviations from the desired velocity can be removed by the guidance law.

It has been found permissible to ignore small perturbations in the onboard navigation computations, provided that a new orbit and all necessary sensitivity coefficients be computed after each measurement. Elimination of small perturbative forces in the onboard computation is a significant saving in complexity. Repetitive computation of the trajectory and all sensitivity coefficients will not be particularly difficult; it involves only the repeated use of recursive equations and various partial derivative relations, which can be programmed as special-purpose subroutines. These routines would probably be needed even if the nominal trajectory were used as the standard because of the possibility of missing a preplanned measurement or because a complete array of precomputed coefficients would require excessive storage.

With guidance computations temporarily set aside, the only iterative calculation needed onboard is the solution of a single transcendental equation relating the incremental eccentric anomaly to time. Due to low eccentricities which will be encountered in practice, this equation will converge quite rapidly.

It is believed that a guidance technique will be established which will allow both savings in fuel and a reduction in complexity of the onboard computation. The practice of varying the descent initiation time to compensate for parking orbit terminal miss distance may provide a significant improvement.

The only factor encountered thus far which tends to complicate the calculations is the need for a word length exceeding that of the standard single precision IBM 7094. An attempt to use single precision in the covariance matrix transformations (which are definitely required in the onboard computer) failed to yield the required accuracy. The use of an equivalent double precision word length, however, will not materially complicate the logic to be used in the special purpose computing routines.

Onboard computations required for lunar orbit navigation will now be discussed. The guidance computations are not included but, as mentioned previously, it is expected that the scheme which is finally chosen will not expand the requirements to a great extent.

To begin with the onboard computer description, it will be noted that all necessary calculations can be performed with the following common routines:

- Only the simplest standard logic; e.g., the Kronecker delta, routines equivalent to the Fortran IF and DO statements

- The arithmetical operations of addition, subtraction, multiplication, division, and square root

- The trigonometric sine, cosine, and inverse cosine functions

- Any iterative technique capable of solving a single rapidly converging transcendental equation with one unknown

The storage requirements will be lenient, since the necessary stored information consists only of:

- Coordinates of selected observable stars in the celestial sphere

- Special-purpose subroutine instructions which are various combinations of the standard operations listed above

Transformation of star coordinates is accomplished by the type of computations indicated in paragraph 3.3.1.1. The fact that some of the angles are time-varying presents no problem; each variable angle is calculated for the anticipated time of measurement before the transformation matrix elements are computed.

Since the onboard navigation procedure is recursive, the operation can be defined in terms of a single trip around the loop. Any number of loop excursions can be specified without complicating the physical system requirements. The computation is assumed to begin some time between the $(m-1)^{th}$ and the mth measurements, at which time the estimated state $\underline{\hat{X}}_{m-1}$, uncertainty covariance matrix P_{m-1}, measurement sensitivity $\underline{H}_{m-1}$, weighting vector $\underline{K}_{m-1}$, and rms measurement error are stored in the onboard computer. The loop computations are performed in the following order:

- The position and velocity vector magnitudes, the dot product, and the observed semimajor axis are computed from $\underline{X}_{m-1}$, by the method exemplified in equations 3-38 to 3-41.

- Given the time $t_m - t_{m-1}$, the incremental eccentric anomaly ν_m is computed iteratively from an equation of the type 3-37.

- The predicted position vector $\underline{\bar{R}}_m$ is computed from an equation of the type 3-35. The magnitude of the vector is then determined.

- The predicted velocity vector $\underline{V}_m$ is computed from an equation of the type 3-36.

- The state transition matrix $\Phi\ (t_m, t_{m-1})$ can now be computed. The routine is fairly brief, equivalent to about one full page of printed Fortran. (See paragraph 3.3.2.2.)

- The updated uncertainty covariance matrix is determined as in equation 3-49.

- Given the next observable star, the predicted observable value is computed as illustrated by equation 3-27.

- The $\underline{H}_m$ elements can now be computed as in equation 3-34.

- The weighting vector $\underline{K}_m$ is computed from an equation of the type shown in equation 3-50.

- The difference between the measurement and its predicted value is multiplied by $\underline{K}_m$ and added to the predicted state vector.

The loop is now complete, since all quantities initially stored at time t_{m-1} have now been replaced by corresponding values at time t_m.

From the above summary it is apparent that, so long as the computations for state transition matrices, weighting elements, etc, are being performed onboard, no great sacrifice is involved in using the updated orbit as a reference. It follows that, while the theory of minimum variance orbital navigation may seem complex, the mechanization of a working system will not present any insurmountable problems.

3.6 CONCLUSIONS

The highlights of the lunar parking and descent orbit analysis are summarized in the following paragraphs.

Provided that the parking orbit has a duration of 1/2 revolution or greater, it is permissible to limit the navigation observables to 2 or 3 known stars and the local vertical. A properly chosen set of 3 stars (2 in the orbital plane and 1 near the pole of the orbit) provides navigation accuracy comparable to that obtainable with the 57 navigation stars (Ref. 3-8). Acceptable performance is also obtainable with 2 stars, both about 30 degrees out of the orbital plane.

Overhead stars (i.e., stars near the local vertical line) are not acceptable navigation aids.

The advantage of the star-vertical measurements are continuous accessibility (including the flight over the dark and unknown sides of the moon); low requirements for accompanying astrophysical data, power consumption, and field of view; insensitivity to lunar rotation; and ease to both manual and automatic implementation.

With direct radial position information (i.e., altitude measurements), the navigation errors can in some cases be reduced more quickly. Because of the prominence of tangential errors, however, no appreciable permanent improvement is achieved.

The measurement sensitivities and the state transition matrices used in the minimum variance equations must be computed from the updated trajectory estimate, rather than from a given nominal orbit.

With repeatedly updated Keplerian equations used for navigation, the observed trajectory takes the form of a time-varying conic. Because this is a valid representation of a perturbed orbit and because actual navigation measurements include the effects of orbital perturbations, it is permissible to use two-body equations for navigation, even in the presence of perturbing forces.

Complete knowledge of the initial uncertainty covariance matrix is not necessary; a pessimistic diagonal (Ref. 3-11) initial matrix leads to a conservative result. Since final navigation errors are insensitive to initial navigation errors, (Ref. 3-3) the result is only slightly pessimistic.

Measurement timing uncertainties on the order of tenths of a second have little effect upon navigation accuracy in the cases under consideration here.

Additional sources of error, not treated in this analysis, have been covered in other related studies. Lack of precise knowledge of sensor error statistics is apparently not critical, (Ref. 3-6) and the effects of unknown measurement bias and astrodynamical uncertainties can be counteracted (Ref 3-5).

The simulation conducted here is in accordance with the principle that terminal navigation errors (i.e., state vector uncertainties) are insensitive to initial errors. The guidance errors (i.e., final miss vector components) however are somwhat sensitive to initial conditions. The reason is traceable to trajectory modifications, necessitated by large displacements from reference position with fixed time guidance.

The total rms final miss distance is a linear function of the quantity ($\sigma_m \sqrt{\tau}$). The slope of this line, however, is somewhat sensitive to initial errors, as explained by the above discussion of the guidance law.

The fixed time guidance law, an unnecessary constraint, also leads to a high sensitivity of terminal miss distance to thrust errors.

The fuel consumption accompanying the FTOA guidance scheme is excessive. This remark refers to the in-plane correction at descent initiation, plus any extra fuel required because of departures from the optimum (90-degree) arc for plane corrections, and also to the unwanted vertical velocity component at the intended powered landing initiation time. Total excess (i. e., above nominal) velocity impulse figures are typically on the order of a few hundred meters per second in the system analyzed here with FTOA guidance.

In view of the above results, it is reasonable to assert that the guidance technique to be selected for actual orbital flight will be superior to the FTOA scheme and will complement the minimum variance navigation technique so that its full potential can be realized. The navigation scheme itself can be performed adequately with state of the art horizon scanner accuracy and will not be unduly degraded by nonlinearities, perturbations, imperfections in navigation computations, a limited field of observables, measurement timing uncertainties, or incomplete knowledge of parameters required for trajectory determination. In conclusion, the performance envisioned in the pioneering studies of minimum variance orbital navigation (Ref. 3-2, 3-3, and 3-4) appears to be obtainable with a practical onboard system, which lends itself readily to mechanization.

4. LUNAR LANDING PHASE

4.1 INTRODUCTION

This section deals with the descent portion of the Lunar Landing Phase. The lunar descent trajectory is initiated at periselenum of the lunar descent orbit, discussed in the preceding section, and terminates prior to final vehicle touchdown. The goal is to evaluate the effect of navigation and control sensor errors on the performance of the landing guidance and control system.

Two overall approaches to lunar landing guidance are analyzed. These two, selected as being representative of the guidance concepts presented in Volume II, are linear predictive guidance and a form of proportional navigation. Navigational information is obtained by beacon tracking in both approaches. In addition doppler navigation is considered for use with the linear predictive guidance scheme.

The two approaches will be treated as separate problems with discussion of a comparative nature confined to subsection 4.4 of this report. The analytical effort associated with each guidance technique will be reported in three parts: background analysis, error analysis, and results.

Background analysis forms a connecting link between Problem Definition and Analytical Solution. System techniques are selectedfrom among those available in the Problem Definition and a specific formulation is developed which is applicable to the Lunar Landing Phase. Among the subjects discussed in this section of the report are the state variables used and the resulting equations of motion, the observables selected and the navigation equations, the guidance technique, the reference trajectory, and the vehicle characteristics. The output of this section is a completely specified model of the lunar landing navigation, guidance, and control system.

The error analysis portion of the report contains the final formulation of the system model used for analysis and primarily qualitative discussions of the analysis techniques used to evaluate the effects of sensor errors. More quantitative descriptions of the error analyses are presented in the appendixes in Volume V.

The quantitative results of the error analysis are also presented and discussed.

Following the analytical sections outlined above is a comparative discussion of the two guidance approaches, and a concluding section.

The following is a summary of the notation used in the lunar landing analyses.

SUMMARY OF NOTATION

F	The general control quantity
f	A deviation of F from the reference value
g_o	The acceleration of gravity at the earth's surface, 9.80665 m/sec^2
h	Altitude above the lunar surface
I_{sp}	Fuel specific impulse
R	Line-of-sight range from the spacecraft to the desired landing site
r_c	The mean lunar radius, 1738 kilometers
T	The magnitude of the vehicle thrust vector
t	Time, referenced to the time of landing maneuver initiation
V	The magnitude of the spacecraft velocity vector
X	The general state variable
x	A deviation of X from the reference value
Y	The general observable quantity
y	A deviation of Y from the reference value
α	The orientation of the spacecraft thrust vector, relative to the velocity vector
γ	The spacecraft flightpath angle relative to the spacecraft local horizontal
θ	The angular displacement of the spacecraft from the desired landing site in lunar central coordinates
μ	The lunar gravitational constant; 4.89820×10^{12} m^3/sec^2
σ	Root mean squared value
ϕ	Line-of-sight angle from the spacecraft to the desired landing site, referenced to spacecraft local vertical
Ω	Line-of-sight angle from the desired landing site to the spacecraft, referenced to landing site local vertical

Superscripts

$[\ ]^T$	Matrix transpose
$[\ ]^{-1}$	Matrix inverse

Subscripts

B	Denotes quantities pertaining to a system using beacon tracker observables
D	Denotes quantities pertaining to a system using doppler navigation observables
f	Denotes final value
i, j	Matrix, or vector element indices
m	Time index
M	The maximum value of m
n	Indicates a random error quantity
o	Denotes initial value
p, q	Matrix, or vector indices
r	Denotes reference value (value on the nominal trajectory)
X	Denotes a quantity pertaining to the state variable, **X**
Y	Denotes a quantity pertaining to the observable, Y

Operators

$(\dot{\ })$	Derivative with respect to time, $\frac{d(\ )}{dt}$
$(\overset{\circ}{\ })$	Derivative with respect to τ, $\frac{d(\ )}{d\tau}$
$\langle\!\langle\ \rangle\!\rangle_{av}$	Ensemble average over all possible missions

Symbols above and below quantities

$(\hat{\ })$	Estimated value, or value computed on the basis of observed information
$(\tilde{\ })$	Estimation error, difference between the actual value and the estimated value
$\underline{(\ )}$	A vector (column matrix)

4.2 GENERAL BACKGROUND

The material presented in this subsection serves as general background for the detailed analysis of both guidance approaches considered for lunar landing. Included are the following items.

- A description of the overall mission profile and definition of the lunar descent trajectory

- Discussion of an optimum descent trajectory

- A functional description of the component subsystems of a generalized navigation, guidance, and control system for lunar landing

- Discussion of the broad analytical assumptions made for the lunar landing analyses

- Definition of the general sensor error model used

4.2.1 Mission Profile

The lunar landing phase begins at periselenum of the synchronous descent orbit defined in Section 3 of this volume. The landing maneuver to be considered is characterized by continuous, rather than impulsive thrusting. The latter, although truly optimum from the standpoint of fuel consumption, becomes impractical when engine size and acceleration levels are considered.

It is convenient to segment the total landing phase into two subphases, the descent maneuver and the final touchdown maneuver. The descent maneuver, or trajectory, commences with engine ignition at periselenum and terminates with the vehicle at some nominal offset point a short distance above the lunar surface. At this point, the final touchdown subphase begins. The work described in this section is concerned almost exclusively with the descent maneuver. For manned lunar missions, which have been given the highest priority, final touchdown is considered to be subject to manual guidance and control.

4.2.2 Trajectory Considerations

Trajectory optimization is not within the scope of this effort. However, there are some trajectory characteristics which are desirable for the descent maneuver. In particular, economical fuel usage and a near-vertical approach to the landing site are necessary, the former for obvious reasons and the latter because of visibility, attitude control, and terrain clearance considerations.

Subsection 1.2 of Appendix D (Volume V) describes the derivation of an optimum lunar descent trajectory. This trajectory is optimized from a fuel usage standpoint and ignores the desire for vertical approach. For this reason, this class of trajectories is not selected as nominal for either of the two lunar landing systems studied. However, the fuel consumption characteristics of this optimized landing maneuver can be used as a basis for evaluating the fuel economy of the nominal trajectories that are actually used.

The technique used for trajectory optimization is the method of steepest ascents (Ref. 4-1). The optimization technique applies to constant-thrust vehicles. No constraints are placed upon the terminal point of the optimized trajectory. Selection of initial altitude, initial velocity, specific impulse, and the initial thrust-to-mass ratio uniquely determines the optimum trajectory that will be obtained. The optimization criterion is minimum time, which is seen to be equivalent to minimum fuel since the thrust level is constant at a value specified prior to trajectory optimization.

4.2.3 Functional Description of the Landing Guidance System

A generalized system block diagram is shown in figure 4-1. The total block diagram comprises the overall vehicle control system used during the landing maneuver. There are four major blocks within the system: Navigation, Guidance Logic, and Control Subsystems, and the dynamic equations of motion.

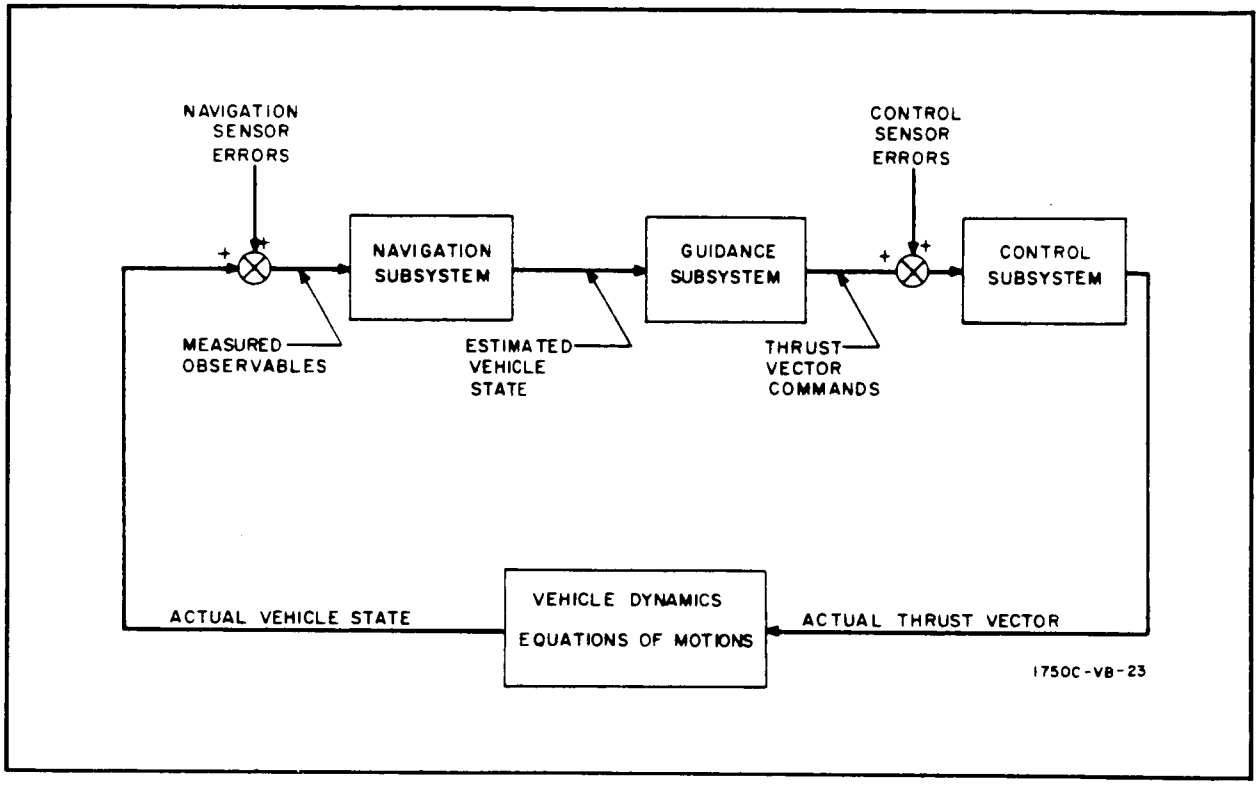

Figure 4-1. Overall Navigation, Guidance, and Control System; Block Diagram

This study is intended to be as objective an investigation of the effects of sensor errors as possible. To this end, the discussion of actual system mechanization is held to a minimum, and the system blocks tend to be defined in terms of mathematical expressions. For example, the Navigation Subsystem is defined by the navigation equations which relate the state variables to the navigation observables. In addition the analytical model of the control subsystem will be somewhat idealized in portions of the analysis. It is recognized that certain sources of system error are omitted from the idealized model; however, these error sources are not the subject of study at this time. Since the idealization reduces dependence on any particular mechanization without jeopardizing the investigation of sensor errors, it is felt to be justified by the intent of the study.

Functionally, the Navigation Subsystem is to acquire and process information which can be used to estimate the vehicle state. The data acquisition instruments are the navigation sensors, and the sensed quantities are termed observables. Since the navigation measurements are subject to error, the actual inputs to the navigation block are estimated values of the observables.

The estimated state variables obtained at the navigation block output form the inputs to the Guidance Logic Subsystem. The guidance function is to evaluate the estimated state and generate thrust vector commands which will bring the landing vehicle to the desired terminal state. Two guidance techniques are evaluated in this volume. Detailed descriptions are given in paragraphs 4.3.1.3 and 4.3.2.3 and the associated appendixes in Volume V.

In practice the control block will include the vehicle attitude control system as well as the engine control system. The function is to implement the guidance commands. As previously pointed out, idealizations will occasionally be made with respect to some aspects of the Control Subsystem. Where this is done, it will be the practice to consider control sensor errors as additional error sources and evaluate their effects.

Finally, the equations of motion are actually the same for any landing vehicle. However, since varying observables and state variables are used in the two guidance approaches, the actual formulation of these equations used in the error analysis may appear different.

4.2.4 Analytical Assumptions

Four general analytical assumptions apply throughout analysis of the lunar descent phase.

- The motion of the vehicle can be adequately described by the dynamics of a restricted two-body system. (This assumption, which is validated by the fact that space vehicle mass is negligible compared to the lunar mass, is commonly used to describe the motion of spacecraft operating in the vicinity of a massive body.)

- No dynamic perturbations such as those caused by lunar oblateness or gravitational anomalies are to be considered. (The presence of these disturbances in the analytical model will not alter the influence of sensor errors except as second order effects and therefore need not be considered.)

- The moon is considered to be stationary during the performance of the descent maneuver. (The actual rotational motion of the moon during the time occupied by landing is not negligible. However, the coordinate system used for landing navigation is referenced to a fixed point on the lunar surface. Since this coordinate system moves with the lunar rotation, the relative motion is zero. For the purposes of this investigation, it is equally valid to assume that the absolute motion is also zero.)

- The landing trajectory is assumed to be two-dimensional. That is, the plane formed by the vehicle position vector in lunar central coordinates and the vehicle velocity vector is assumed to contain the desired landing site. (In practice, deviations of the target landing site from the plane defined above are expected to be small.)

It is also appropriate to point out that the following analyses do not assume a flat moon or a uniform gravitational field. Trajectory determination uses a spherical moon and a central gravitational field.

4.2.5 Definition of Sensor Error Model

The main objective of this study is the evaluation of the effects of navigation and control sensor errors on the performance of lunar landing navigation and guidance techniques. It is clear then that the analytical model or characterization of the sensor error constitutes an important input to the analysis. The following definitions will facilitate discussion.

$Y(t)$: An observable quantity at time t
$\tilde{y}(t)$: The total error in measuring $Y(t)$ at time t

The total measurement error is considered to be the sum of four components, two bias components and two zero-mean random-noise components as illustrated in the following expression.

$$\tilde{y}(t) \equiv \tilde{y}_b + {}_Y p_b \frac{Y(t)}{100} + y_n(t) + {}_Y p_n(t) \frac{Y(t)}{100} \tag{4-1}$$

The characteristics of each component are given below.

$\tilde{y}_b$ is a bias error which is constant over the duration of flight

${}_Y p_b \frac{Y(t)}{100}$ is a time-varying bias error component which is obtained by multiplying a scale-factor bias coefficient, ${}_Y p_b/100$, by the value of the observable quantity. The coefficient ${}_Y p_b$, has the units of percent and is constant over the landing phase.

$\tilde{y}_n(t)$ is a noise error which is characterized as being a stationary Gaussian random variable with zero mean value and mean squared value denoted ${}_n\sigma_Y^2$. The units of $\tilde{y}_n(t)$ are the same as those of Y.

${}_Y p_n(t)\frac{Y(t)}{100}$ is a nonstationary random error which is the product of ${}_Y p_n(t)$ and $Y(t)/100$. The scale factor coefficient ${}_Y p_n(t)$ is defined to be a stationary Gaussian random variable with zero mean value, and mean squared value ${}_p\sigma_Y^2$. The units of ${}_Y p_n(t)$ are percent.

The bias error components, $\tilde{y}_b$ and ${}_Y p_b$, are constant over a given mission but random over the ensemble of all possible missions. The noise error components are random over a given mission as well as over the ensemble of all missions. In addition the error components of each observation error are assumed to be independent, and when more than one observable is measured, all observation errors are independent.

The general error model used throughout the investigation of lunar landing is thus defined.

4.3 ANALYSIS

4.3.1 Lunar Landing Using Linear Predictive Guidance

Of the two basic error analysis techniques, Monte Carlo simulation and linearization, the latter was selected for use in the investigation of a landing concept employing linear predictive guidance. There are two primary reasons for selecting linearization:

- Linearization is a mathematical technique and tends to deemphasize mechanization considerations which is in keeping with the intent of the study.

- Linearized analysis produces statistical information directly. Since sensor errors can only be defined statistically, their effects must also be described statistically.

In addition the linearized analysis is found to be quite flexible in that Navigation, Guidance Logic, and Control Subsystem parameters can be varied with little difficulty.

The background analysis sections include discussion of the various components of the overall Landing Guidance System. Also included are descriptions of the linearized models of each major system block which will be used to make up the overall system analytical model.

After linearization of the overall system, the resulting system model is still not amenable to ordinary analytical techniques. The reason is that many of the subsystems are characterized by time-varying gain parameters. The approach taken to this problem is quite commonly used in the investigation of time-varying control systems. Basically the scheme is to quantize time or subdivide the flight into a sequence of small time intervals. Within each interval the system is allowed to be both linear and time invariant. All time-varying parameters are sampled at the beginning of each interval and held at the sample value until the next sampling time, one quantization interval later. Then all parameters are updated and sampled again. System characteristics are updated according to stored data evaluated on the nominal trajectory, and vehicle state information is updated by using the linearized equations of motion and vehicle forces commanded at the previous sample time.

The results of the error analysis are matrices of error sensitivity coefficients which relate the mean squared terminal state errors to the mean squared values of the sensor errors which caused them.

4.3.1.1 Background Analysis

a. State Variables, Control Quantities, and the Equations of Motion. - Since a two-dimensional analysis is being performed, four state variables are required to specify vehicle position and velocity relative to the landing site. The four selected are defined below and illustrated in figure 4-2.

h is the altitude (in meters) of the spacecraft above a reference sphere. (The radius of the reference sphere is equal to the lunar radius at the nominal landing site.)

θ is the angular displacement (in radians) of the spacecraft from the desired landing site in lunar central coordinates.

γ is the flightpath angle (in radians) relative to the landing vehicle local horizontal measured in the plane of motion.

V is the magnitude of the velocity vector (in meters per second).

Quantities h and θ define position, while γ and V specify the velocity vector.

The control quantities are those parameters which define the vehicle thrust vector. Two are sufficient because of the restriction to two dimensions.

The parameters selected are defined below.

T = The magnitude of the thrust vector (in newtons)
α = The thrust vector angle measured as illustrated in figure 4-3 (in radians)

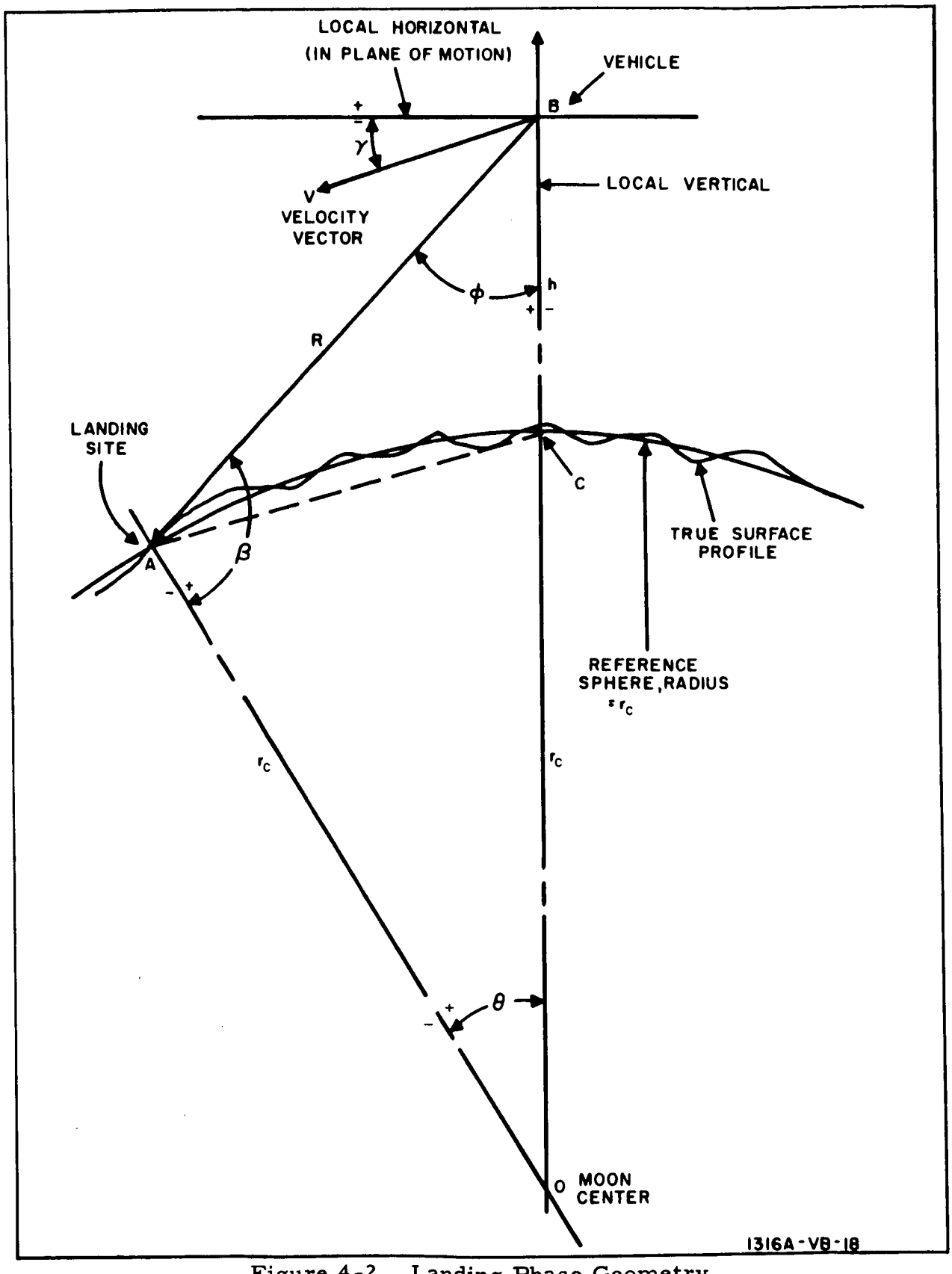

Figure 4-2. Landing Phase Geometry

Often during the course of this analysis it will be convenient to write equations in matrix form. For this purpose two column matrices or vectors are defined. $\underline{X}$ is the state vector or a column matrix of state variables, and $\underline{F}$ is the control vector or a column matrix of control quantities. In terms of the state variables and control parameters previously defined:

$$\underline{X} \equiv \begin{bmatrix} X_1 \\ X_2 \\ X_3 \\ X_4 \end{bmatrix} \equiv \begin{bmatrix} h \\ \theta \\ \gamma \\ V \end{bmatrix} \tag{4-2}$$

$$\underline{F} \equiv \begin{bmatrix} F_1 \\ F_2 \end{bmatrix} \equiv \begin{bmatrix} T \\ \alpha \end{bmatrix} \tag{4-3}$$

The equations of motion describe the motion of the vehicle. Those used in this analysis are given below and are derived with the aid of figure 4-3, which is a velocity-acceleration diagram of the lunar landing maneuver.

$$\begin{aligned} \dot{h} &= V \sin \gamma \\ \dot{\theta} &= - \frac{V}{r_c + h} \cos \gamma \\ \dot{\gamma} &= \frac{V \cos \gamma}{r_c + h} - \frac{T \sin \alpha}{mV} - \frac{\mu \cos \gamma}{V(r_c + h)^2} \\ \dot{V} &= - \frac{T \cos \alpha}{m} - \frac{\mu \sin \gamma}{(r_c + h)^2} \end{aligned} \tag{4-4}$$

The dot operator indicates a time derivative. Quantities h, μ, γ, V, T, α, and m are all implicit functions of time. Of these, all but m have been previously defined. Of course m is the mass of the vehicle and is equal to the initial mass plus the integral of the rate of mass flow.

$$m = m_o + \int_{t_o}^{t} \frac{dm}{dt} dt$$

The instantaneous rate of mass flow is defined as

$$\frac{dm}{dt} = - \frac{T}{I_{sp} g_o}$$

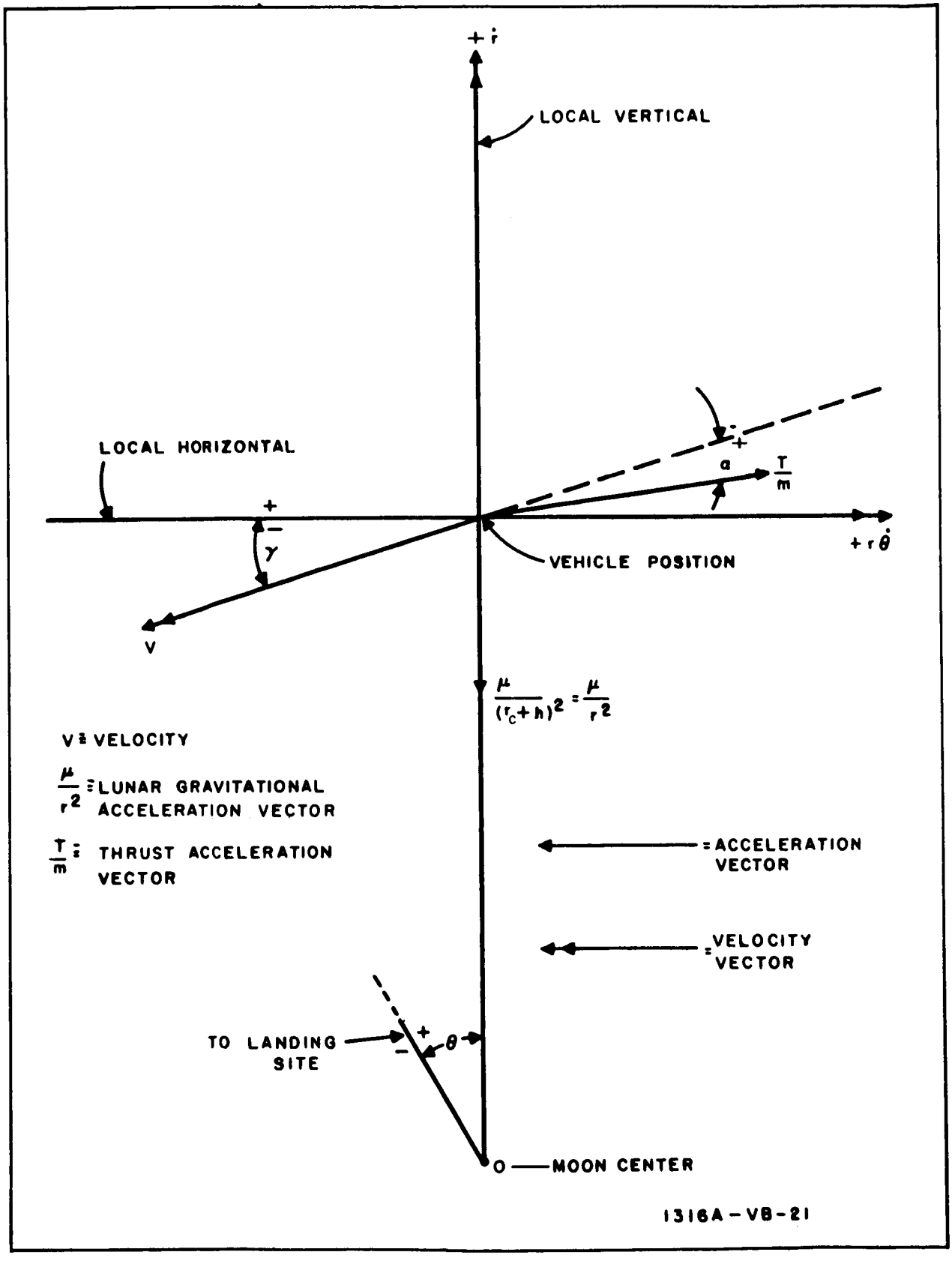

Figure 4-3. Velocity-Acceleration Diagram of Landing Maneuver

The as yet undefined quantities in this equation and in the equations of motion are constants which are defined below. The numerical values are those used for this analysis.

r_c = lunar radius at the landing site = mean lunar radius = 1.738×10^6 m

μ = lunar gravitational constant = $4.89820 \times 10^{12} m^3/sec^2$

g_o = acceleration due to gravity at the earth's surface = 9.80665 m/sec^2

I_{sp} = fuel specific impulse = 400 sec

The linearized equations of motion are obtained by expanding each equation in a multidimensional Taylor series about the reference trajectory and discarding all terms higher than first order. In terms of the generalized state variable X_i

$$\dot{X}_i \doteq (\dot{X}_i)_r + \sum_{j=1}^{4} \left\{\frac{\partial \dot{X}_i}{\partial X_j}\right\}_r \left\{X_j - X_{jr}\right\} + \sum_{j=1}^{2} \left\{\frac{\partial \dot{X}_i}{\partial F_j}\right\}_r \left\{F_j - F_{jr}\right\} \tag{4-5}$$

The subscript r indicates that the subscripted quantity is to be evaluated on the nominal or reference trajectory. If the symbols x and f are used to indicate deviations of X and F from the reference values, the above expression becomes

$$\dot{x} = \sum_{j=1}^{4} \left\{\frac{\partial \dot{X}_i}{\partial X_j}\right\}_r x_j + \sum_{j=1}^{2} \left\{\frac{\partial \dot{X}_i}{\partial F_j}\right\}_r f_j \tag{4-6}$$

When all four components of the state vector are considered, the following matrix formultaion of the linearized equations of motion results.

$$\underline{\dot{x}} = [A]\,\underline{x} + [B]\,\underline{f} \tag{4-7}$$

where $[A]$ is a 4 x 4 matrix defined by the general element a_{ij}, and $[B]$ is a 4 x 2 matrix defined by b_{ij}.

$$a_{ij} \equiv \left\{\frac{\partial \dot{X}_i}{\partial X_j}\right\}_r \quad ; \quad \left\{\begin{matrix} i = 1, 2, 3, 4 \\ j = 1, 2, 3, 4 \end{matrix}\right\} \tag{4-8}$$

$$b_{ij} \equiv \left\{\frac{\partial \dot{X}_i}{\partial F_j}\right\}_r \quad ; \quad \left\{\begin{matrix} i = 1, 2, 3, 4 \\ j = 1, 2 \end{matrix}\right\} \tag{4-9}$$

A second formulation of the equations of motion will also be useful in the error analysis. These expressions are given below.

$$\ddot{X}_1 = \dot{h} = \frac{V^2 \cos^2 \gamma}{r_c + h} - \frac{T}{m} \sin(\gamma + \alpha) - \frac{\mu}{(r_c + h)^2} \tag{4-10}$$

$$\ddot{X}_2 = \ddot{\theta} = \frac{V^2 \sin 2\gamma}{(r_c + h)^2} + \frac{T}{m} \frac{\cos(\gamma + \alpha)}{(r_c + h)}$$

$$\dot{X}_3 = \dot{\gamma} = \frac{V \cos \gamma}{r_c + h} - \frac{T \sin \alpha}{mV} - \frac{\mu \cos \gamma}{V(r_c + h)^2}$$

$$\dot{X}_4 = \dot{V} = -\frac{T \cos \alpha}{m} - \frac{\mu \sin \gamma}{(r_c + h)^2}$$

These equations are also linearized about the reference trajectory, resulting in the matrix equation

$$\dot{\underline{x}}' \equiv \begin{bmatrix} \dot{x}'_1 \\ \dot{x}'_2 \\ \dot{x}'_3 \\ \dot{x}'_4 \end{bmatrix} \equiv \begin{bmatrix} \ddot{x}_1 \\ \ddot{x}_2 \\ \dot{x}_3 \\ \dot{x}_4 \end{bmatrix} \doteq \left[A'\right] \underline{x} + \left[B'\right] \underline{f} \tag{4-11}$$

where $\left[A'\right]$ and $\left[B'\right]$ are partial derivative matrices with elements defined as follows:

$$a'_{ij} \equiv \left\{ \frac{\partial \dot{X}'_i}{\partial X_j} \right\}_r \quad ; \left\{ \begin{matrix} i = 1, 2, 3, 4 \\ j = 1, 2, 3, 4 \end{matrix} \right\} \tag{4-12}$$

$$b'_{ij} \equiv \left\{ \frac{\partial \dot{X}'_i}{\partial F_j} \right\}_r \quad ; \left\{ \begin{matrix} i = 1, 2, 3, 4 \\ j = 1, 2 \end{matrix} \right\} \tag{4-13}$$

This second formulation is used to generate the anlaytical models of the linearized equations of motion to be used in the error analysis. Figure 4-4 illustrates these equations in block diagram form.

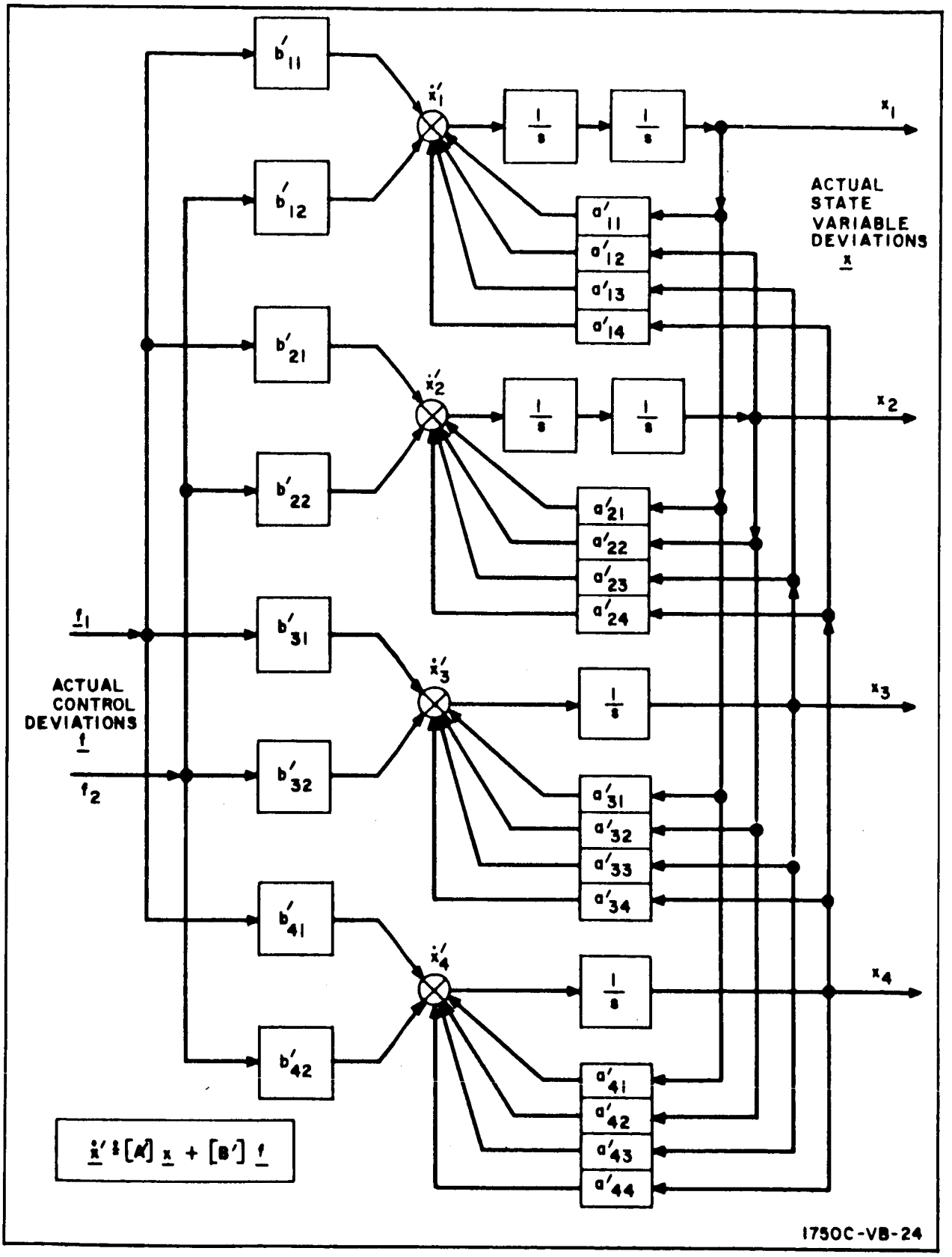

Figure 4-4. Linearized Equations of Motion Used in Error Analysis; Block Diagram

b. Navigation Subsystem - The observables that can be used for navigation during the Lunar Landing Phase are specified in Volume II - Problem Definition. From this list two combinations of observables providing sufficient information for landing navigation are selected for investigation. The criterion for sufficiency is that all state variables be calculable from a single set of navigation observations.

Prior to discussion of the selected observation schemes, it is of value to consider the landing mission to see what navigation information is required. Since there are considered to be four state variables (two-dimensional trajectory), a minimum of four different observations are required to determine vehicle state. For the landing analysis it is considered that these will be four simultaneous measurements of different observables. It is conceivable that fewer observables could be used with multiple observations required for a single determination of vehicle state. However, this technique, which is employed successfully for midcourse and orbital navigation, does not appear to be practical for the relatively brief landing phase.

It is believed that observations sufficient to allow determination of the vehicle altitude and velocity vector are essential in view of the extreme consequences likely to be caused by erroneous estimates of these quantities.

Whether or not observations must be made which will allow determination of the state variable θ is dependent on the mission requirements. Recall that θ is the angular displacement of the vehicle from the landing site (lunar central coordinates). As such, errors in θ are related to errors in the horizontal position of the vehicle relative to the landing site. If overall mission success requires that the landing be made accurately at a specific point, then determination of θ from observed data will be required because this is the only way that unknown initial deviations in θ can be compensated.

On the other hand, when accurate point landing is not required, and mission requirements are satisfied by a successful landing anywhere in the neighborhood of the nominal landing site, observations made solely to determine the value of θ will not be required. Examination of the equations of motion reveals that none contain the state variable θ. Therefore the only effect of an unknown and uncompensated initial error in θ will be a horizontal offset of the terminal state, which has been assumed not to endanger mission success in this case.

The two observation schemes selected for analysis are referred to as the beacon tracker and the doppler navigator. These are defined in paragraphs 4.3.1.1.b(1) and 4.3.1.1.b.(2) respectively. This material includes discussion of the information sensing scheme as well as presentation of the appropriate navigation equations. Direct observations to the lunar surface are characteristic of both navigation schemes. Inertial navigation was considered but quickly dropped because of large initial condition uncertainties which would be expected.

As previously mentioned, the navigation equations are to be given in succeeding paragraphs. At this time a general column matrix of observables is defined:

$$\underline{Y} \equiv \begin{bmatrix} Y_1 \\ Y_2 \\ \cdot \\ \cdot \\ \cdot \\ Y_n \end{bmatrix} \tag{4-14}$$

where N is the total number of navigation observables used and will be set equal to 4 for this analysis. The navigation equations are those expressions which yield the estimated state variables as functions of the observables. In general form they are

$$\hat{X}_i = g_i\,(\hat{Y}_i,\ \hat{Y}_2,\ \hat{Y}_3,\ \hat{Y}_4)$$

The symbol (^) over a quantity indicates an estimated value. Also important will be the linearized navigation equations which are obtained by the same process described in paragraph 4.3.1.1.a. In general matrix form these are

$$\hat{\underline{x}} = \left[G\right] \hat{\underline{y}}\ ;\quad \hat{\underline{y}} \equiv \hat{\underline{Y}} - \underline{Y}_r \tag{4-15}$$

The matrix $\left[G\right]$ is composed of partial derivatives evaluated on the reference trajectory. The general element of $\left[G\right]$ is

$$g_{ij} \equiv \left\{ \frac{\partial \hat{X}_i}{\partial \hat{Y}_j} \right\}_r \ ;\quad \left\{ \begin{matrix} i = 1,\ 2,\ 3,\ 4 \\ j = 1,\ 2,\ 3,\ 4 \end{matrix} \right\} \tag{4-16}$$

The resulting block diagram of the linearized navigation system is given in figure 4-5.

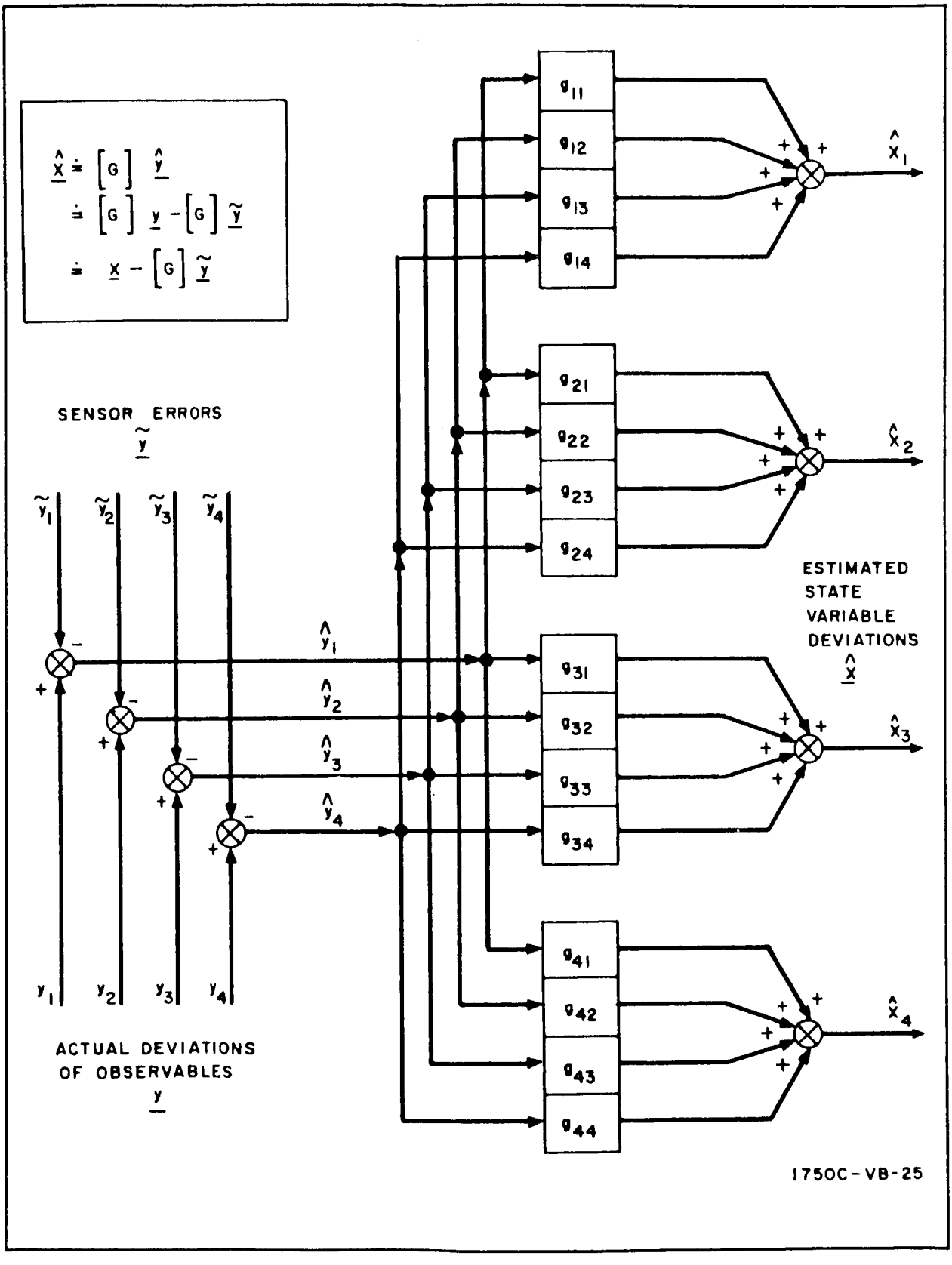

Figure 4-5. Linearized Navigation Equations: Block Diagram

(1) Beacon Tracking Navigation - As the term beacon tracking inplies, navigation information is obtained by actively tracking a beacon. For this analysis, the beacon is assumed to be located at the desired landing site. The observables are line-of-sight range, R, and angle, ϕ, as well as their time derivatives, $\dot{R}$ and $\dot{\phi}$. Observables R and ϕ are illustrated in figure 4-2. The matrix of beacon tracker observables is related to the general observable matrix as follows:

$$\begin{bmatrix} R \\ \dot{R} \\ \phi \\ \dot{\phi} \end{bmatrix} \equiv \begin{bmatrix} Y_{1B} \\ Y_{2B} \\ Y_{3B} \\ Y_{4B} \end{bmatrix} \equiv \underline{Y}_B \tag{4-17}$$

The navigation equations are derived in Subsection 2.1 of, Appendix D (Volume V) with the following results:

$$\hat{X}_1 = \hat{h} = \hat{R} \cos \hat{\phi} + \left[r_c^{\,2} - \hat{R}^2 \sin^2 \hat{\phi} \right]^{1/2} - r_c \tag{4-18}$$

$$\hat{X}_2 = \hat{\theta} = \sin^{-1} \left[\frac{\hat{R}}{r_c} \sin \hat{\phi} \right]$$

$$\hat{X}_3 = \hat{\gamma} \doteq \hat{\phi} - \frac{\pi}{2} + \tan^{-1} \left[\frac{\hat{R}\hat{\dot{\phi}}}{\hat{\dot{R}}} \right]$$

$$\hat{X}_4 = \hat{V} \doteq \left[(\hat{\dot{R}})^2 + (\hat{R}\hat{\dot{\phi}})^2 \right]^{1/2}$$

Linearization of these navigation equations yields the matrix expression:

$$\hat{\underline{x}} = \left[G_B \right] \hat{\underline{y}}_B \tag{4-19}$$

The general element of $\left[G_B \right]$ is

$$(g_{ij})_B \equiv \left\{ \frac{\partial \hat{X}_i}{\partial \hat{Y}_{jB}} \right\}_r ; \left\{ \begin{matrix} i = 1,2,3,4 \\ j = 1,2,3,4 \end{matrix} \right\} \tag{4-20}$$

Equations used for these matrix elements are given in Subsection 2.1 of Appendix D (Volume V).

The linearized navigation system model using beacon tracking observations is obtained by substitution matrix elements y_{iB} and $(g_{ij})B$ for y_i and (g_{ij}) respectively in figure 4-5.

(2) Doppler Navigation - Actually, referring to this navigation scheme as doppler navigation is only partly true. The complete system studied makes three kinds of observations, one of which is doppler in nature. The other two are altitude, h, and line-of-sight angle to the desired landing site, ϕ. Altitude and angle observations are straightforward; however, the doppler observations require some further discussion.

In general the doppler measurements will be made by a three-beam doppler device which will be termed radar for convenience. Parameters pertinent to this discussion of the doppler technique are illustrated and defined in figure 4-6. The antenna system assumed for this analysis remains fixed with respect to the coordinate system x, y, z. This is done by aligning vector $\underline{OP}$ along the local vertical which is in the negative z direction. (Errors in establishing local vertical can be lumped with the other observation errors.) The vehicle pitch axis x' and the x axis are assumed to be initially coincident. The analytical restriction to two dimensions means that these axes will remain coincident throughout the analysis. In these circumstances it can be seen that the dot product $\underline{V} \cdot \underline{OB}$ will be equal to $\underline{V} \cdot \underline{OC}$. If the range rates along the radar beam axes $\underline{OA}$, $\underline{OB}$, and $\underline{OC}$ are denoted $\dot{R}_1$, $\dot{R}_2$, and $\dot{R}_3$ respectively, the preceding statement implies that $\dot{R}_2$ and $\dot{R}_3$ are equal. Indeed,

$$\dot{R}_1 = -(\underline{V} \cdot \underline{OA})$$

and

$$\dot{R}_2 = \dot{R}_3 = -(\underline{V} \cdot \underline{OB})$$

The two range rates $\dot{R}_1$ and $\dot{R}_2$ along with observations of h and ϕ comprise the observables considered in the doppler navigation system. In matrix form,

$$Y_D \equiv \begin{bmatrix} Y_{1D} \\ Y_{2D} \\ Y_{3D} \\ Y_{4D} \end{bmatrix} \equiv \begin{bmatrix} h \\ \dot{R}_1 \\ \phi \\ \dot{R}_2 \end{bmatrix} \tag{4-21}$$

The navigation equations are:

$$\hat{X}_1 = \hat{h} = \hat{h}$$

$$\hat{X}_2 = \hat{\theta} = \frac{\pi}{2} - \hat{\phi} - \cos^{-1}\left[\frac{(r_c + \hat{h})}{r_c} \sin \hat{\phi}\right] \tag{4-22}$$

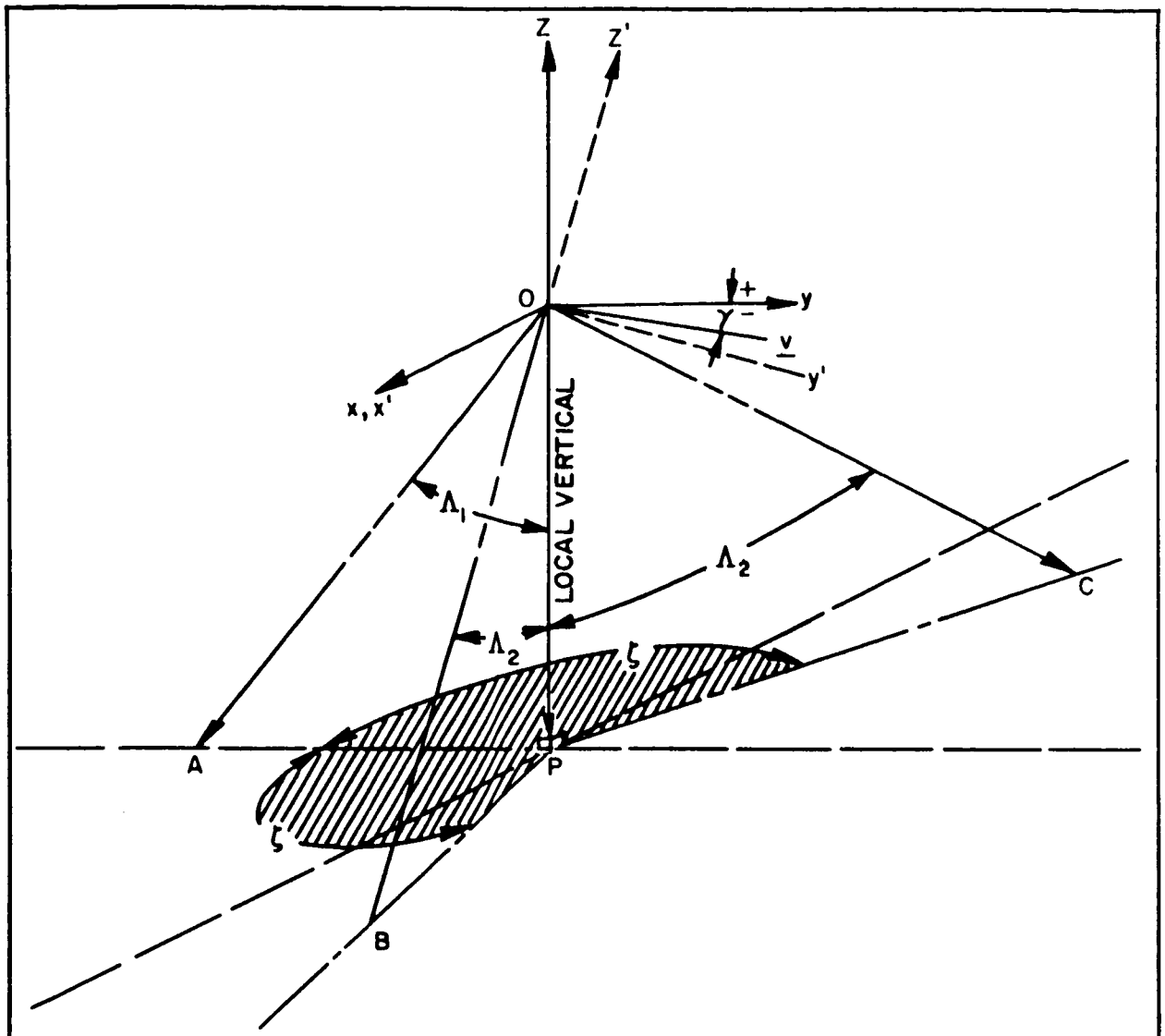

$\underline{V} \equiv$ VELOCITY VECTOR

Λ_1, Λ_2, AND ζ ARE KNOWN GEOMETRICAL PARAMETERS OF THE THREE-BEAM DOPPLER SYSTEM

x', y', Z': VEHICLE COORDINATE SYSTEM.

x, y, Z: COORDINATE SYSTEM WITH ORIGIN AT VEHICLE CENTER OF GRAVITY. x AND y FORM THE LOCAL HORIZONTAL PLANE.

VECTORS $\underline{OA}$, $\underline{OB}$, AND $\underline{OC}$ REPRESENT THE BEAM AXES.

1750C-VB-26

Figure 4-6. Doppler Navigator Geometry

$$\hat{X}_3 = \hat{\gamma} = \tan^{-1}\left[\frac{\hat{R}_2 \sin\Lambda_2 - \hat{R}_1 \cos\zeta \sin\Lambda_1}{\hat{R}_1 \cos\Lambda_1 - \hat{R}_2 \cos\Lambda_2}\right]$$

$$\hat{X}_4 = \hat{V} = \frac{\hat{R}_1\left[(\hat{R}_1 \cos\Lambda_1 - \hat{R}_2 \cos\Lambda_2)^2 + (\hat{R}_2 \sin\Lambda_2 - \hat{R}_1 \cos\zeta \sin\Lambda_1)^2\right]^{\frac{1}{2}}}{\cos\Lambda_2\left[\hat{R}_2 \sin\Lambda_2 - \hat{R}_1 \cos\zeta \sin\Lambda_1\right] + \sin\Lambda_2\left[\hat{R}_1 \cos\Lambda_1 - \hat{R}_2 \cos\Lambda_2\right]}$$

Linearization of these expressions yields:

$$\hat{\underline{x}} \doteq \left[G_D\right]\hat{\underline{y}}_D \tag{4-23}$$

where the general element of matrix $\left[G_D\right]$ is:

$$(g_{ij})_D \equiv \left\{\frac{\partial \hat{X}_i}{\partial \hat{Y}_{jD}}\right\}_r \quad ; \begin{Bmatrix} i = 1, 2, 3, 4 \\ j = 1, 2, 3, 4 \end{Bmatrix} \tag{4-24}$$

The linearized navigation system model is obtained by substitution of matrix elements y_{iD} and $(g_{ij})D$ for y_i and (g_{ij}) respectively in figure 4-5

c. Linear Predictive Guidance Technique - The discussion presented in this paragraph is primarily a qualitative description of the guidance technique. Linear predictive guidance (as described in Ref. 4-2) was selected for investigation principally on the basis of its good error-correcting capability and versatility.[1] This scheme is capable of correcting relatively large deviations from nominal initial conditions at reasonable fuel expense. In addition, the guidance technique can be adapted for use in either manned or unmanned vehicles. For detailed theoretical discussion of the guidance technique, including derivation of the guidance term matrix

$$S \equiv \begin{bmatrix} s_{11} & s_{12} & s_{13} & s_{14} \\ s_{21} & s_{22} & s_{23} & s_{24} \end{bmatrix} \tag{4-25}$$

see subsection 6.1 of Appendix A (Volume V).

Basically, the guidance concept can be described as follows.

1. Ref. 4-2 is a report dealing with the capabilities of this guidance technique prepared by Ames Research Laboratory personnel.

- Navigation information is used to estimate vehicle state at time t. (Time is referenced to the time of landing engine ignition.)

- Estimated state variables are compared with the nominal values at time t.

- Differences between estimated and nominal values are inputs to linearized equations which estimate the terminal deviations that would exist if no deviation from the nominal thrust program is commanded.

- Thrust vector deviations which will reduce certain of the estimated terminal state errors to zero are computed and are the command inputs to the control subsystem.

- The process is repeated.

It is not possible to calculate thrust vector commands which will reduce all four terminal state errors to zero. Four independent control quantities would be required to do this, and the thrust vector is completely described by two. For this reason, two of the terminal errors are selected as the basis of control. The two that are selected are considered to define the operating mode of the guidance technique. There are a total of six possible modes (Combinations of four items taken two at a time), of which two are investigated. These are designated the h-θ mode and the h-V mode. Terminal position error estimates provide the basis for control in the h-θ mode, whereas terminal altitude and velocity error estimates are used for the h-V mode.

In practice much of the computation indicated in the step-by-step outline of the guidance concept can be done prior to launch on the basis of the nominal trajectory. The result is a matrix of time varying guidance terms which are stored in the guidance computer. This matrix multiplies the column matrix of estimated state variable deviations (from nominal) to produce the control quantity deviation commands according to the equation.

$$\underline{\hat{f}} \equiv [S] \; \underline{\hat{x}} \tag{4-26}$$

Figure 4-7 is the block diagram representation of the guidance system model described by this equation which is applicable to the lunar descent analysis.

Recall that linearized equations are used to predict terminal deviations from the nominal trajectory and therefore to compute the commanded control

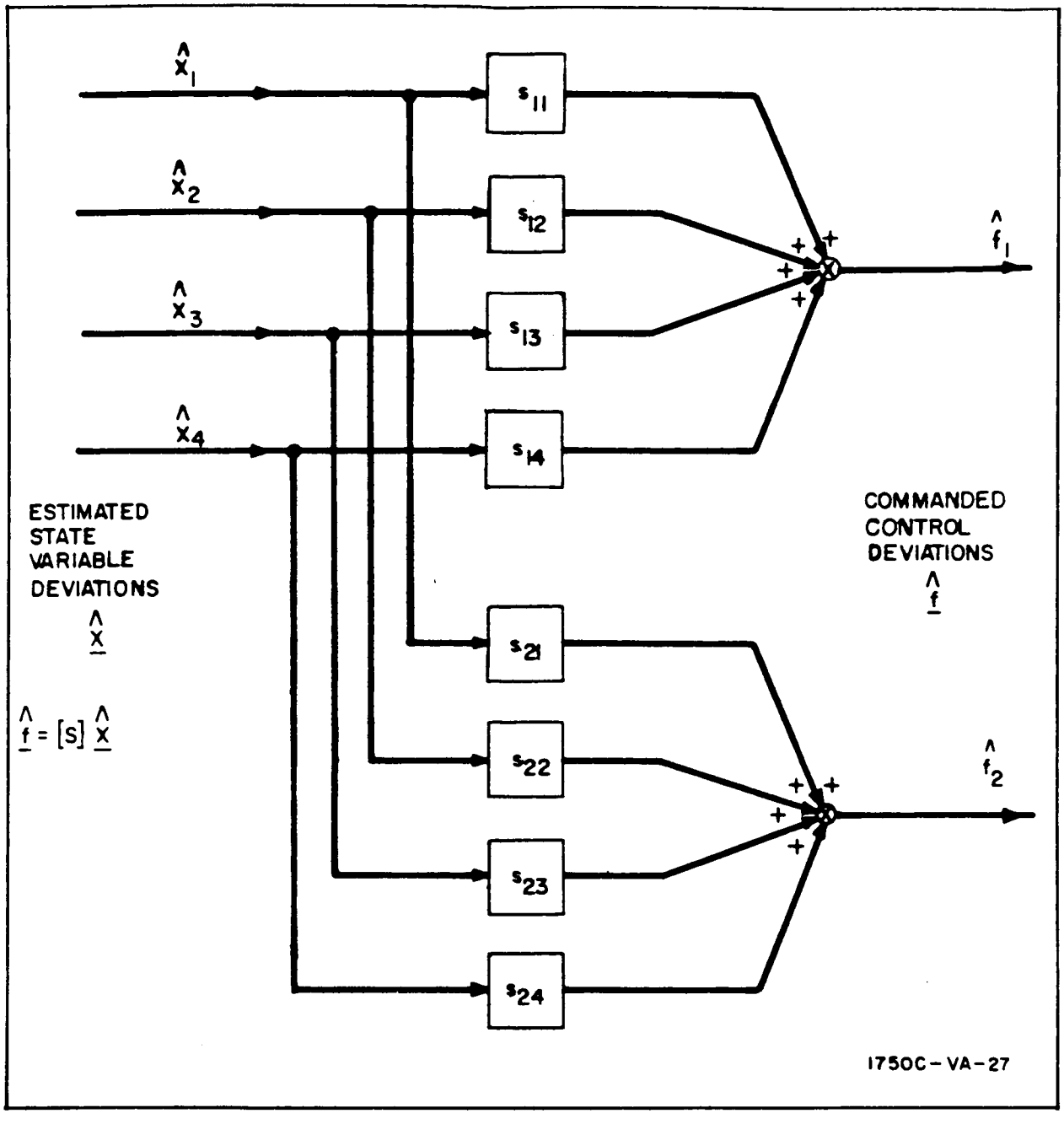

Figure 4-7. Linearized Guidance Equations; Block Diagram

deviations. Linearization error will result in erroneous thrust commands, even in the absence of sensor errors, unless the actual trajectory is coincident with the nominal trajectory initially. If the trajectory which would be flown assuming perfect sensor information is called the pseudonominal trajectory, it is true that the terminal state of the pseudonominal trajectory generally will not be identical with the nominal terminal state. Comparison is made t_f

seconds after thrust ignition, where t_f is the nominal time of flight. This terminal deviation of the pseudonominal trajectory from the nominal is caused by linearization error and is not random in nature, since a given set of initial deviations results in a determinable set of terminal deviations. If sensor information is noisy, the actual trajectory will wander from the pseudonominal, and the actual terminal state vector components will be random variables with mean values equal to the pseudonominal values.

The object of this study is to obtain information concerning the random variations in terminal state introduced by imperfect information sensing. For this reason, linearization errors will be eliminated from the analysis by assuming the vehicle is initially on the nominal trajectory. The pseudonominal and the nominal trajectories are one and the same for this case.[2]

Linear predictive guidance is basically an endpoint guidance scheme. The goal is to reduce deviations from the nominal trajectory to zero in exactly the remaining time of flight. In a sense then, the effective response time of the overall guidance and control system is equal to the nominal remaining flight time. This relationship is maintained by varying the guidance terms as time progresses. As the time-to-go approaches zero, the overall system response time will therefore also tend toward zero. The implication with regard to overall system bandwidth is that it is very small at thrust initiation, increases during flight, and becomes very large as the nominal remaining flight time approaches zero.

When this phenomenon is examined in the light of certain system characteristics, it becomes desirable to place a lower limit on the overall system response time. For example, if guidance commands are derived from sampled data, the system response time must be greater than the sampling interval. Failure to meet this requirement will result in system instability.[3] In practice, ratios of 3:1 or better are maintained between response time and sampling interval to ensure stability. The linearized system model used for error analysis is basically a sampled data system so that a lower limit on system response capability is in order. This is provided by fixing the guidance terms at time $t_f - n\Delta t$ seconds where n is an aribtrary integer and Δt is the analytical quantization or sampling interval. For this analysis n has been arbitrarily set equal to 10. Thus, over the last $10\Delta t$ seconds of flight the guidance terms are constant at the values corresponding to $t = t_f - 10\Delta t$.

2. Ref. 4-2 describes a noise-free simulation of the landing guidance technique which produced information concerning pseudonominal deviations from the nominal endpoint.
3. This statement is based on stability criteria developed in Ref. 4-3.

d. Nominal Trajectory - The guidance technique used is based on knowledge of a reference trajectory. In addition, the application of linearized analysis requires the evaluation of numerous partial derivatives using reference values of the state variables. Trajectory evaluation and optimization were not within the scope of this study, so that the nominal trajectory used, a constant-thrust gravity turn, was selected somewhat arbitrarily. This type of trajectory possesses the following characteristics which are consistent with the general guidelines discussed in paragraph 4.2.2.

- Continuous, constant thrust requires minimum engine size, reliability, and throttling.

- The gravity turn thrust program provides near minimum fuel expenditure.

- The gravity turn approach offers good terrain clearance and visibility characteristics. Final approach to the landing site is nearly vertical.

- The nominal thrust program automatically rotates the vehicle to the proper hover attitude, so that no last-second high-velocity rotations are required.

The nominal trajectory terminates at a hover point 500 meters above the desired landing site. Although variations of the initial conditions are considered, the desired terminal conditions are fixed inputs to the nominal trajectory determination program discussed in subsection 2.2 of Appendix D (Volume V).

One of the areas investigated concerns the effect of varied nominal trajectory initial conditions on the error sensitivity coefficients generated by linearized error analysis. Investigation reveals that a complete set of initial conditions cannot be arbitrarily selected. Several factors limit the selection of initial conditions.

- The terminal point is specified: zero velocity, 500 meters, directly above the nominal landing site.

- The class of nominal trajectories has been specified: a constant-thrust gravity turn. (This means that $F_1 = T$ is a constant designated T_o; and that $F_2 = \alpha$ is equal to zero nominally.)

- Engine ignition is specified to occur at periselenum of the descent orbit. Therefore $\gamma_o = 0$.

• The descent orbit is defined to be a synchronous ellipse. This implies a functional relationship between altitude and velocity at periselenum. These quantities will also be initial conditions for the descent trajectory h_o and V_o. The indicated relationship is:

$$V_o = \sqrt{\frac{\mu\left[2r_1 - (r_c + h_o)\right]}{r_1(r_c + h_o)}}$$

where r_1 is the nominal radius of the circular parking orbit.

When all these factors are considered, it turns out that there is but one independent initial condition of those that are as yet unspecified. When any one of h_o, V_o, θ_o, T_o/m_o, or t_f is specified, there is but one constant-thrust gravity turn that will satisfy all the constraints. For this study, initial altitude has been selected as the independent condition.

For details concerning the nominal trajectory determination program, as well as more complete characteristics of the five nominal trajectories generated see subsection 2.2 of Appendix D, Volume V.

e. Engine Control Subsystem - Analysis of the Lunar Landing Phase is performed assuming essentially perfect control. This is done primarily to eliminate consideration of mechanization characteristics of the vehicle attitude and engine control subsystems. To take into account the fact that these subsystems can include information sensors, control sensor errors are injected into the thrust magnitude and angle channels between the guidance subsystem output and the equations of motion. The general characteristics of these error sources are the same as those of the navigation errors described in paragraph 4.2.5. Thus,

$$\underline{f} = \hat{\underline{f}} + \tilde{\underline{f}} \qquad (4\text{-}27)$$

One limiting characteristic is applied to the engine control subsystem. This characteristic is related to bandwidth. The autocorrelation function of white noise passed through the control subsystem, denoted $\psi(\tau)$, is considered to have its first zero at $\tau = \tau_o$. Quantity τ_o is referred to as the correlation interval of the subsystem. In general the video noise bandwidth of a system is approximately equal to $1/2\tau_o$. This characteristic of the control subsystem will be recalled during discussion of the analytical sampling or quantization interval. Three values of τ_o will be considered during the error analysis: 1, 2, and 3 seconds.

On the basis of this discussion, figure 4-8 illustrates the analytical model of the engine control subsystem.

f. Sensor Errors - At any given time there are six error inputs to the overall system - four navigation and two control sensor errors. The general model of each of these errors has four components as described in paragraph 4.2.5. However, analysis of the system employing linear predictive guidance was performed with bias errors set equal to zero. Thus, each of the six sensor errors is made up to two components.

$$\tilde{\underline{y}}(t)_B = \underline{y}_n(t)_B + \frac{1}{100}\left[Y_B(t)\right]_r \; Y\underline{p}_n(t)_B \tag{4-28}$$

or

$$\tilde{\underline{y}}(t)_D = \tilde{\underline{y}}_n(t)_D + \frac{1}{100}\left[Y_D(t)\right]_r \; Y\underline{p}_n(t)_D \tag{4-29}$$

and

$$\tilde{\underline{f}}(t) = \tilde{\underline{f}}_n(t) + \frac{1}{100}\left[F(t)\right]_r F\underline{p}_n(t) \tag{4-30}$$

where

$$\left[Y_B(t)\right]_r, \left[Y_D(t)\right]_r, \text{ and } \left[F(t)\right]_r$$

are the following diagonal matrices evaluated on the reference trajectory.

$$\left[Y_B\right] \equiv \begin{bmatrix} Y_{1B} & 0 & 0 & 0 \\ 0 & Y_{2B} & 0 & 0 \\ 0 & 0 & Y_{3B} & 0 \\ 0 & 0 & 0 & Y_{4B} \end{bmatrix} \tag{4-31}$$

$$\left[Y_D\right] \equiv \begin{bmatrix} Y_{1D} & 0 & 0 & 0 \\ 0 & Y_{2D} & 0 & 0 \\ 0 & 0 & Y_{3D} & 0 \\ 0 & 0 & 0 & Y_{4D} \end{bmatrix} \tag{4-32}$$

$$\left[F\right] = \begin{bmatrix} F_1 & 0 \\ 0 & F_2 \end{bmatrix} \tag{4-33}$$

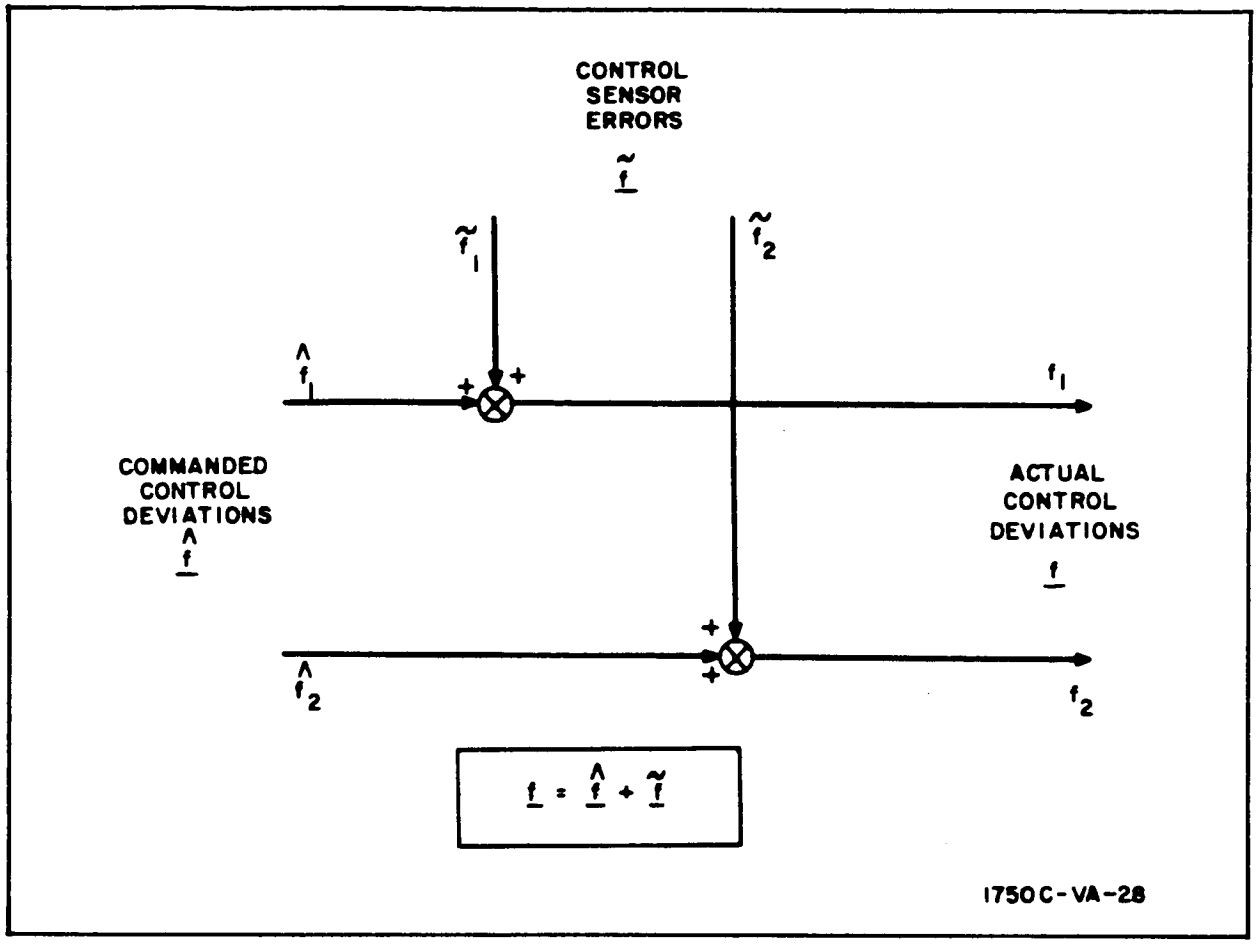

Figure 4-8. Analytical Control Subsystem Model; Block Diagram

Subscripts B and D refer to beacon tracker and doppler navigator observables respectively. Definition of the quantities included in equation 4-30 can be inferred from material presented in paragraph 4.2.5. Under the conditions specified for the nominal trajectory, the second term of equation 4-30 has exactly the same characteristics as the first term and the two can be lumped together. For this reason it will be the practice to omit the second term from the control sensor error model during the discussion of the error analysis. Then

$$\tilde{\underline{f}}(t) = \tilde{\underline{f}}_n(t) \tag{4-34}$$

4.3.1.2 Error Analysis

The preceding discussion of the analytical approach indicates that error analysis is to be performed on a linearized model of the Landing Guidance System. The linearized model of the actual system is shown in figure 4-9, and an equivalent linearized model is illustrated in figure 4-10. The latter is the model actually used for analysis. Detailed block diagrams of the linearized navigation and guidance equations and the linearized equations of motion appear in figures 4-5, 4-7, and 4-4, respectively.

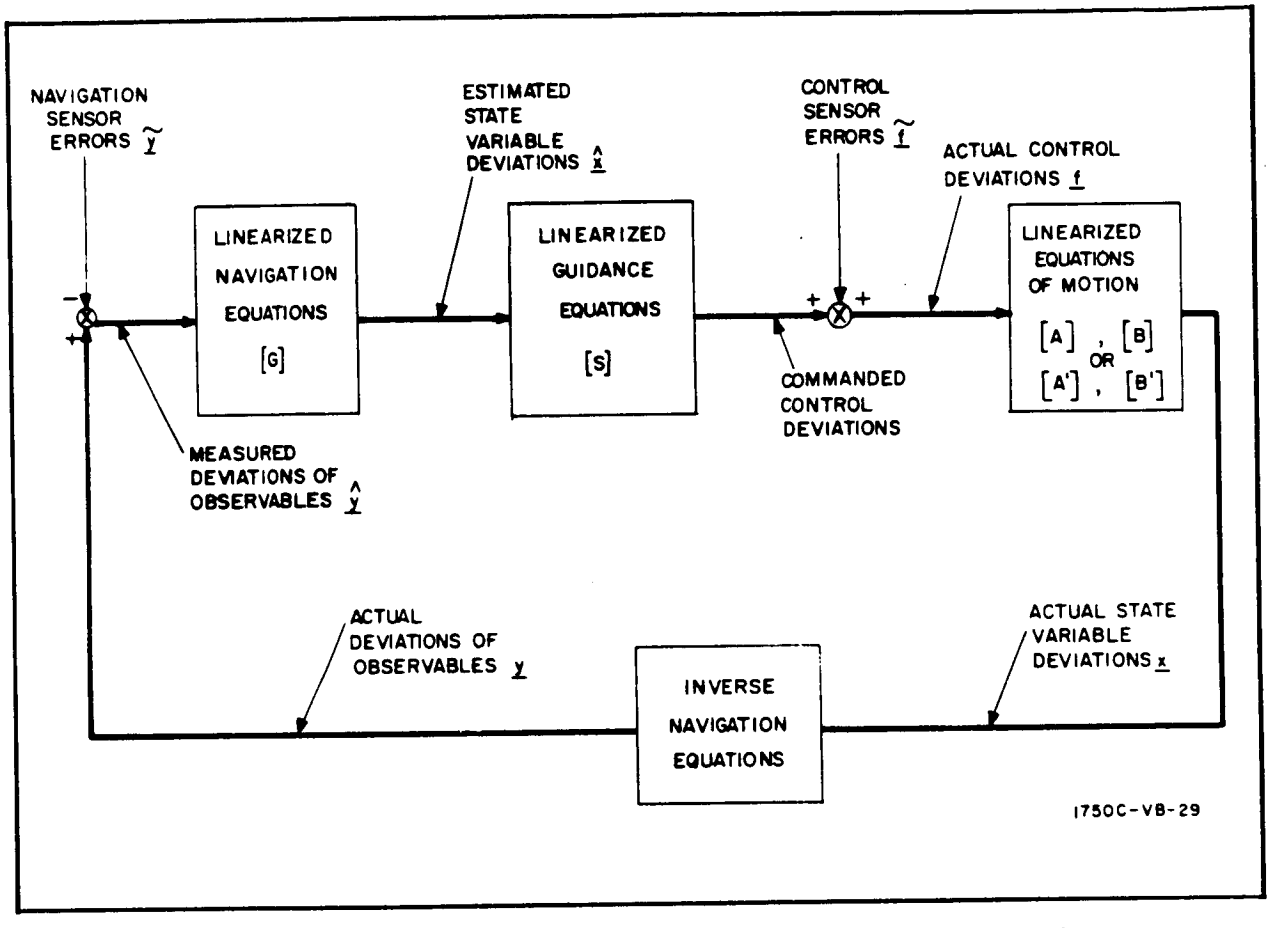

Figure 4-9. Linearized Navigation, Guidance, and Control System Model

The linearized model is still not amenable to ordinary analytical techniques. The reason is that the gain parameters of the linearized model (elements of matrices [G], [S], [A'] and [B']) are time-varying functions. This problem is met by employing a standard technique for the analysis of systems with time-varying parameters - data sampling and time quantization. The time of flight is divided into discrete intervals. At the beginning of each interval all system parameters are sampled. Control quantity deviation

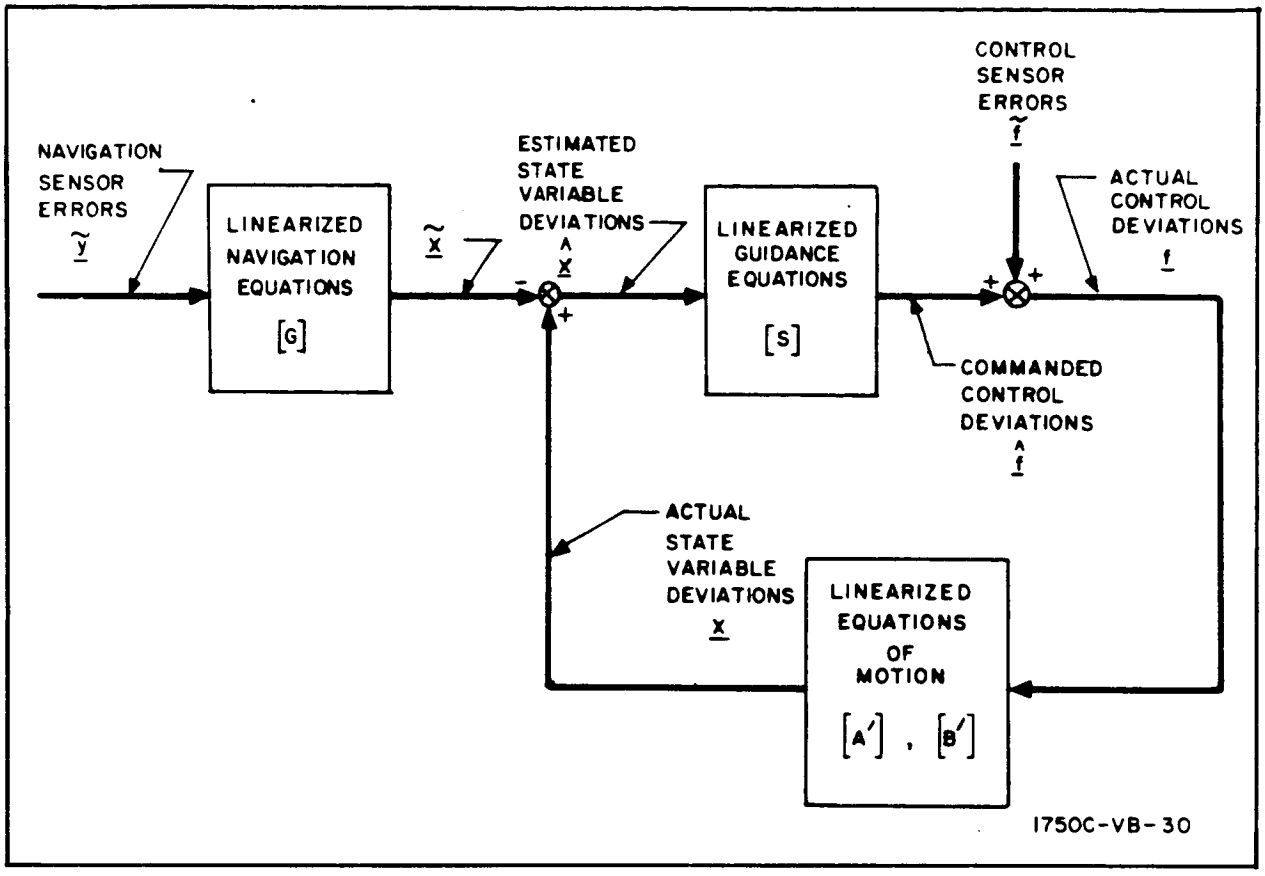

Figure 4-10. Equivalent Linearized System Model Actually Used for Error Analysis

commands are computed on the basis of the sample values. All quantities are held constant at the sampled values over the subsequent quantization interval. At the next sampling time, sensor error distributions are again sampled, system gain parameters are updated on the nominal trajectory, and the actual deviations from nominal are updated by integrating deviations in vehicle accelerations over the sampling interval and adding the results to the actual deviations at the previous sampling time. The state variable updating equations used are:

$$\delta h_{m+1} \doteq \delta h_m + \frac{(\Delta t)^2}{2} \delta \ddot{h}_m$$

$$\delta \theta_{m+1} \doteq \delta \theta_m + \frac{(\Delta t)^2}{2} \delta \ddot{\theta}_m \qquad (4\text{-}35)$$

$$\delta\gamma_{m+1} \doteq \delta\gamma_m + \Delta t\, \delta\dot{\gamma}_m$$

$$\delta V_{m+1} \doteq \delta V_m + \Delta t\, \delta\dot{V}_m$$

The subscript m is a time index indicating the value of the subscripted quantity at

$$t = t_m$$

where

$$t_m = m\Delta t; \quad m = 0,\ 1,\ 2,\ 3,\ \ldots,\ M \tag{4-36}$$

As indicated, m takes on values from zero to M where M is the highest integral number of sampling intervals contained in t_f, the nominal time of flight.

The quality Δt is the quantization or sampling interval length. In this analysis Δt must be long enough that control errors in successive intervals are essentially uncorrelated and short enough to ensure that the updating equations are good approximations. It is assumed that all navigation and control sensor bandwidths are at least equal to the bandwidth of the engine control subsystem. Then the correlation interval of the random error from each sensor will be less than or equal to τ_o which is defined to be the correlation interval of white noise passed through the engine control subsystem (paragraph 4. 3. 1. 2). In this investigation the desire for independent control errors in successive intervals requires that Δt be greater than or equal to τ_o. Since updating accuracy is inversely related to sample interval length Δt is set equal to the minimum value consistent with the previous consideration, which is τ_o. The three values of τ_o to be considered are: $\tau_o = 1,\ 2,\ 3$ seconds.

The equations used to update the actual values of the state variable deviations from one sampling time to the next are then

$$\begin{aligned}
\delta h_{m+1} &\doteq \delta h_m + \frac{\tau_o^2}{2}\, \delta\ddot{h}_m \\
\delta\theta_{m+1} &\doteq \delta\theta_m + \frac{\tau_o^2}{2}\, \delta\ddot{\theta}_m \\
\delta\gamma_{m+1} &\doteq \delta\gamma_m + \tau_o\, \delta\dot{\gamma}_m \\
\delta V_{m+1} &\doteq \delta V_m + \tau_o\, \delta\dot{V}_m
\end{aligned} \tag{4-37}$$

These equations can be written in matrix form in terms of the general state variable expressions:

$$\begin{bmatrix} x_1 \\ x_2 \\ x_3 \\ x_4 \end{bmatrix}_{m+1} = \begin{bmatrix} x_1 \\ x_2 \\ x_3 \\ x_4 \end{bmatrix}_m + \begin{bmatrix} \frac{\tau_o^2}{2} & 0 & 0 & 0 \\ 0 & \frac{\tau_o^2}{2} & 0 & 0 \\ 0 & 0 & \tau_o & 0 \\ 0 & 0 & 0 & \tau_o \end{bmatrix} \begin{bmatrix} \ddot{x}_1 \\ \ddot{x}_2 \\ \dot{x}_3 \\ \dot{x}_4 \end{bmatrix}_m \tag{4-38}$$

Written more compactly,

$$\underline{x}_{m+1} \doteq \underline{x}_m + \left[\tau_o\right] \dot{\underline{x}}'_m \tag{4-39}$$

where $\dot{\underline{x}}'_m$ is defined by equation 4-11 in paragraph 4. 3. 1. 1. a.

Equation 4-11 states that

$$\dot{\underline{x}}'_m \doteq \left[A'\right]_m \underline{x}_m + \left[B'\right]_m \underline{f}_m$$

Matrix $\underline{f}_m$ can be expanded as per equations 4-26 and 4-27:

$$\underline{f}_m = \hat{\underline{f}}_m + \tilde{\underline{f}}_m = \left[S\right]_m \hat{\underline{x}}_m + \tilde{\underline{f}}_m$$

Finally, equation 4-15 yields an expression for $\hat{\underline{x}}_m$:

$$\hat{\underline{x}}_m = \underline{x}_m - \left[G\right]_m \tilde{\underline{y}}_m$$

The general observable quantities are used in the derivation. When the final equations are to be applied, the appropriate matrices are substituted for the general matrices $\left[G\right]_m$ and $\tilde{\underline{y}}_m$. For example, $\left[G_B\right]_m$ and $(\tilde{\underline{y}}_B)_m$ would be used if the system under study used beacon tracker observables.

Substituting the above expressions into equation 4-39 yields

$$\begin{aligned} \underline{x}_{m+1} \doteq \underline{x}_m &+ \left[\tau_o\right] \left[A'\right]_m \underline{x}_m + \left[\tau_o\right] \left[B'\right]_m \left[S\right]_m \underline{x}_m \\ &+ \left[\tau_o\right] \left[B'\right]_m \tilde{\underline{f}}_m - \left[\tau_o\right] \left[B'\right]_m \left[S\right]_m \left[G\right]_m \tilde{\underline{y}}_m \end{aligned} \tag{4-40}$$

Reference to paragraph 4. 3. 1. 1. f reveals the following expressions for $\tilde{\underline{y}}_m$ and $\tilde{\underline{f}}_m$

$$\tilde{\underline{f}}_m = (\tilde{\underline{f}}_n)_m \tag{4-41}$$

$$\underline{y}_m = (\tilde{\underline{y}}_n)_m + \frac{1}{100} \left[Y\right]_{rm} (Y\underline{p}_n)_m$$

Equation 4-40 can be written more concisely:

$$\underline{x}_{m+1} \doteq \underline{x}_m + [C]_m \underline{x}_m + [D]_m (\underline{\tilde{y}}_n)_m + [E]_m (Y\underline{p}_n)_m + [H]_m (\underline{\tilde{f}}_n)_m \tag{4-42}$$

where

$$[C]_m \equiv [\tau_o] [A']_m + [\tau_o] [B']_m [S]_m$$

$$[D]_m \equiv [\tau_o] [B']_m [S]_m [G]_m$$

$$[E]_m \equiv \frac{1}{100} [\tau_o] [B']_m [S]_m [G]_m [Y]_{rm}$$

$$[H]_m \equiv [\tau_o] [B']_m$$

An equation for the deviation in the ith state variable can be obtained from equation 4-42.

$$(x_i)_{m+1} \doteq (x_i)_m + \sum_{j=1}^{4} (c_{ij})_m (x_j)_m + \sum_{j=1}^{4} (d_{ij})_m (\tilde{y}_{jn})_m + \sum_{j=1}^{4} (e_{ij})_m (Y_j p_n)_m + \sum_{j=1}^{2} (h_{ij})_m (\tilde{f}_{jn})_m \tag{4-43}$$

Quantities $(c_{ij})_m$, $(d_{ij})_m$, $(e_{ij})_m$, and $(h_{ij})_m$ the general elements of matrices $[C]_m$, $[D]_m$, $[E]_m$, and $[H]_m$ respectively.

The mean squared value of $(x_i)_{m+1}$ can be written in the following manner. The symbol $\langle () \rangle_{av}$ indicates an average over the ensemble of possible missions.

$$\left\langle (x_i)^2_{m+1} \right\rangle_{av} \doteq \left\langle \left\{ (x_i)_m + \sum_{j=1}^{4} (c_{ij})_m (x_j)_m \right\}^2 \right\rangle_{av}$$

$$\sum_{j=1}^{4} \left\langle \left\{ (d_{ij})_m (\tilde{y}_{jn})_m \right\}^2 \right\rangle_{av} + \sum_{j=1}^{4} \left\langle \left\{ (e_{ij})_m (Y_j p_n)_m \right\}^2 \right\rangle_{av} \tag{4-44}$$

$$+ \sum_{j=1}^{2} \left\langle \left\{ (h_{ij})_m (\tilde{f}_{jn})_m \right\}^2 \right\rangle_{av}$$

The right-hand side can be written in the indicated form because of the assumed independence of the sensor error sources and also the assumed independence of sensor errors and state deviations at t_m. The independence assumptions can be stated mathematically:

$$\left\langle x_{im} (\tilde{y}_{jn})_m \right\rangle_{av} = \left\langle x_{im} (Y_j p_n)_m \right\rangle_{av} = \left\langle x_{im} (\tilde{f}_{jn})_m \right\rangle_{av} = 0 \text{ for all i and j}$$

$$\left\langle (\tilde{y}_{in})_m (Y_j p_n)_m \right\rangle_{av} = \left\langle (\tilde{y}_{in})_m (\tilde{f}_{jn})_m \right\rangle_{av} = \left\langle (Y_j p_n)_m (\tilde{f}_{jn})_m \right\rangle_{av} = 0$$

for all i and j

$$\left\langle (\tilde{y}_{in})_m (\tilde{y}_{jn})_m \right\rangle_{av} = \left\langle (Y_i p_n)_m (Y_j p_n)_m \right\rangle_{av} = \left\langle (\tilde{f}_{in})_m (\tilde{f}_{jn})_m \right\rangle_{av} = 0$$

for $i \neq j$

If the guidance system were to receive perfect information at $t = t_m$, it would act to reduce the deviation from the nominal trajectory. Thus, in terms of ensemble mean squared values,

$$\left\langle (x_i)^2_{m+1} \right\rangle_{av} \doteq \left\langle \left\{ x_{im} + \sum_{j=1}^{4} (c_{ij})(x_j)_m \right\}^2 \right\rangle_{av} < \left\langle (x_i)^2_m \right\rangle_{av} \tag{4-45}$$

in the absence of sensor errors. The following inequality, which includes sensor errors can now be expressed:

$$\begin{aligned} \left\langle (x_i)^2_{m+1} \right\rangle_{av} < \left\langle (x_i)^2_m \right\rangle_{av} &+ \sum_{j=1}^{4} \left\langle \left\{ (d_{ij})_m (\tilde{y}_{jn})_m \right\}^2 \right\rangle_{av} \\ &+ \sum_{j=1}^{4} \left\langle \left\{ (e_{ij})_m (Y_j p_n)_m \right\}^2 \right\rangle_{av} \\ &+ \sum_{j=1}^{2} \left\langle \left\{ (h_{ij})_m (\tilde{f}_{jn})_m \right\}^2 \right\rangle_{av} \end{aligned} \tag{4-46}$$

Thus, the right-hand side represents an upper limit on the value of $\left\langle (x_i)^2_{m+1} \right\rangle_{av}$ which is denoted

$$\left\langle (x_i)^2_{m+1} \right\rangle_{L\,av} .$$

The term $(x_i)_{m=0}$ is the initial deviation of the pseudonominal trajectory from the nominal trajectory. As stated in paragraph 4.3.1.1.c, this quantity is set equal to zero since it is a contribution to the terminal error not caused by landing sensor errors. Therefore, $\left\langle (x_i)^2_{m=0} \right\rangle_{av}$ is considered to be equal to zero in expression 4-46.

On the basis of inequality 4-46, it is easily demonstrated that

$$\left\langle (x_i)^2_M \right\rangle_{av} < {}_L\left\langle (x_i)^2_M \right\rangle_{av} = \sum_{m=0}^{M-1} \sum_{j=1}^{4} \left\langle \left\{ (d_{ij})_m (\tilde{y}_{jn})_m \right\}^2 \right\rangle_{av}$$
$$+ \sum_{m=0}^{M-1} \sum_{j=1}^{4} \left\langle \left\{ (e_{ij})_m ({}_{Y_j}p_n)_m \right\}^2 \right\rangle_{av} \qquad (4\text{-}47)$$
$$+ \sum_{m=0}^{M-1} \sum_{j=1}^{2} \left\langle \left\{ (h_{ij})_m (\tilde{f}_{jn})_m \right\}^2 \right\rangle_{av}$$

(Sensor errors at one sampling time are independent of sensor errors at all other sampling times.)

Since $(d_{ij})_m$, $(e_{ij})_m$, and $(h_{ij})_m$ are constant over the ensemble of missions (they are evaluated on the nominal trajectory), they can be removed from the ensemble averages. Thus

$$\left\langle \left\{ (d_{ij})_m (\tilde{y}_{jn})_m \right\}^2 \right\rangle_{av} = (d_{ij})^2_m \left\langle (\tilde{y}_{jn})^2_m \right\rangle_{av}$$

$$\left\langle \left\{ (e_{ij})_m ({}_{Y_j}p_n)_m \right\}^2 \right\rangle_{av} = (e_{ij})^2_m \left\langle ({}_{Y_j}p_n)^2_m \right\rangle_{av}$$

$$\left\langle \left\{ (h_{ij})_m (\tilde{f}_{jn})_m \right\}^2 \right\rangle_{av} = (h_{ij})^2_m \left\langle (\tilde{f}_{jn})^2_m \right\rangle_{av}$$

In paragraph 4.2.5 y_{jn}, ${}_{Y_j}p_n$, and $\tilde{f}_{jn}$ are defined to be stationary, Gaussian random variables with zero mean values and mean squared values ${}_n\sigma^2_{Y_j}$, ${}_p\sigma^2_{Y_j}$ and ${}_n\sigma^2_{F_j}$ respectively. Therefore the averages indicated in the above equations can be removed from the time summations when these equations are substituted into expression 4-47.

$$
{}_L(\sigma^2_{X_{iM}}) \equiv {}_L\left\langle (x_i)^2_M \right\rangle_{av} = \sum_{j=1}^{4} \left\{ \sum_{m=0}^{M-1} (d_{ij})^2_m \right\} {}_n\sigma^2_{Y_j}
$$

$$
+ \sum_{j=1}^{4} \left\{ \sum_{m=0}^{M-1} (e_{ij})^2_m \right\} {}_p\sigma^2_{Y_j} \tag{4-48}
$$

$$
+ \sum_{j=1}^{2} \left\{ \sum_{m=0}^{M-1} (h_{ij})^2_m \right\} {}_n\sigma^2_{F_j}
$$

In matrix form:

$$
{}_L\left[\sigma^2_X\right]_M = \left[K\right] {}_n\sigma^2_Y + \left[K'\right] {}_p\sigma^2_Y + \left[K''\right] {}_n\sigma^2_F \tag{4-49}
$$

Factors $[K]$, $[K']$, and $[K'']$ are the matrices of sensitivity coefficients sought by this investigation. The general elements of these matrices, (k_{ij}), (k'_{ij}), and (k''_{ij}) are defined as:

$$
(k_{ij}) = \sum_{m=0}^{M-1} (d_{ij})^2_m \; ; \left\{ i = 1,\ 2,\ 3,\ 4;\ j = 1,\ 2,\ 3,\ 4 \right\}
$$

$$
(k'_{ij}) = \sum_{m=0}^{M-1} (e_{ij})^2_m \; ; \left\{ i = 1,\ 2,\ 3,\ 4;\ j = 1,\ 2,\ 3,\ 4 \right\} \tag{4-50}
$$

$$
(k''_{ij}) = \sum_{m=0}^{M-1} (h_{ij})^2_m \; ; \left\{ i = 1,\ 2,\ 3,\ 4;\ j = 1,\ 2 \right\}
$$

The sensitivity coefficient matrices are evaluated with the aid of a digital program written for the IBM 7094 computer.

4.3.1.3 Results

a. Presentation of Numerical Results - The sensitivity coefficients matrices are computed for each combination of the two guidance modes, two navigation sensors schemes, three values of τ_0, and five different nominal trajectories which are characterized by the nominal initial altitude. Thus, a large amount of information is generated. Graphical presentation offers the most efficient and useful means of presenting the computer results. This

is done in figures 4-11 through 4-17. Every matrix element is plotted as a function of nominal trajectory initial altitude for three values of τ_o, two guidance modes, and for both combinations of observables.

Matrix elements (k_{3j}), (k'_{3j}), and (k''_{3j}) are not computed because the nominal value of $X_3 = \gamma$ at $t = t_f$ is undefined, since the magnitude of the velocity vector at this time is nominally zero. In this situation small deviations in the velocity vector could be in practically any direction. Thus, one would expect the computed mean squared deviation in the final value of γ to be large and not very informative. In addition, matrix elements (k'_{i3}) are not included because the third observable (ϕ in both observation schemes) was thought to be best represented as not having a scale factor error component. Hence, ${}_p\sigma^2{}_{Y_3} = {}_p\sigma^2{}_\phi$ was set equal to zero. In this situation no information would be contributed by the indicated matrix elements, so they were not computed.

The sensitivity coefficient matrices are used to obtain upper boundaries on the mean squared terminal position and velocity errors by means of the equation

$$\begin{bmatrix} L(\sigma^2_{X_{i\,m}}) \\ L(\sigma^2_{X_{i\,m}}) \\ L(\sigma^2_{X_{3\,m}}) \\ L(\sigma^2_{X_{4\,m}}) \end{bmatrix} = [K] \begin{bmatrix} {}_n\sigma^2_{Y_1} \\ {}_n\sigma^2_{Y_2} \\ {}_n\sigma^2_{Y_3} \\ {}_n\sigma^2_{Y_4} \end{bmatrix} + [K'] \begin{bmatrix} {}_p\sigma^2_{Y_1} \\ {}_p\sigma^2_{Y_2} \\ {}_p\sigma^2_{Y_3} \\ {}_p\sigma^2_{Y_4} \end{bmatrix} + [K''] \begin{bmatrix} {}_n\sigma^2_{F_1} \\ {}_n\sigma^2_{F_2} \end{bmatrix} \quad (4\text{-}51)$$

When using the coefficient matrices $[K]$ and $[K']$, care must be taken to use the coefficient matrices corresponding to the particular system configuration under investigation. System configuration is determined by four pieces of information:

- Guidance mode: H-θ or H-V control
- Observations scheme: Beacon tracker or doppler navigator
- Sampling interval: Correlation interval of white noise passed through the engine control subsystem, τ_o: 1, 2, or 3 seconds.
- Initial altitude of the nominal trajectory, h_o.

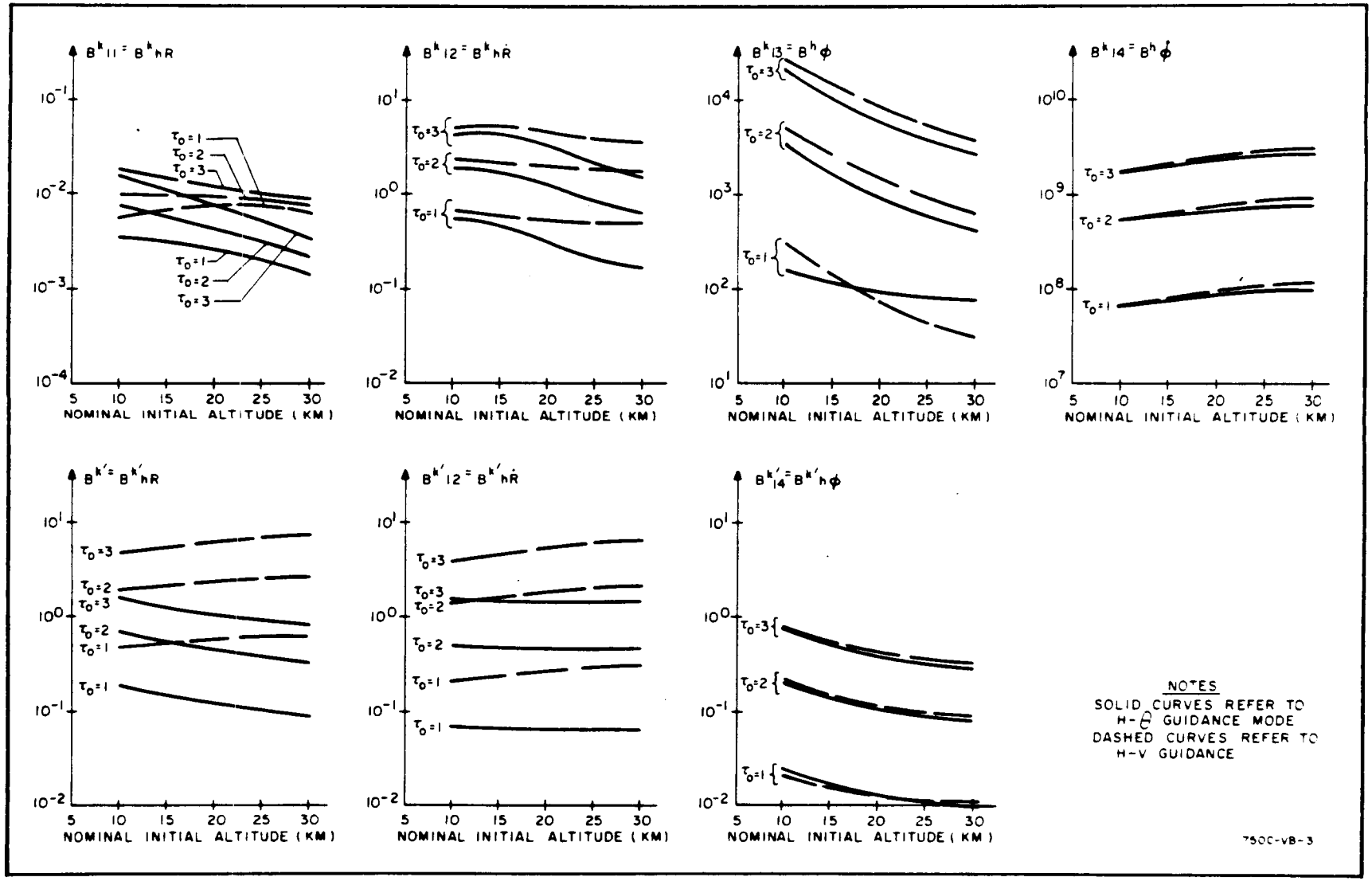

Figure 4-11. Error Sensitivity Coefficients Relating Terminal Altitude Errors to Navigation Sensor Errors (Beacon Tracker Observables)

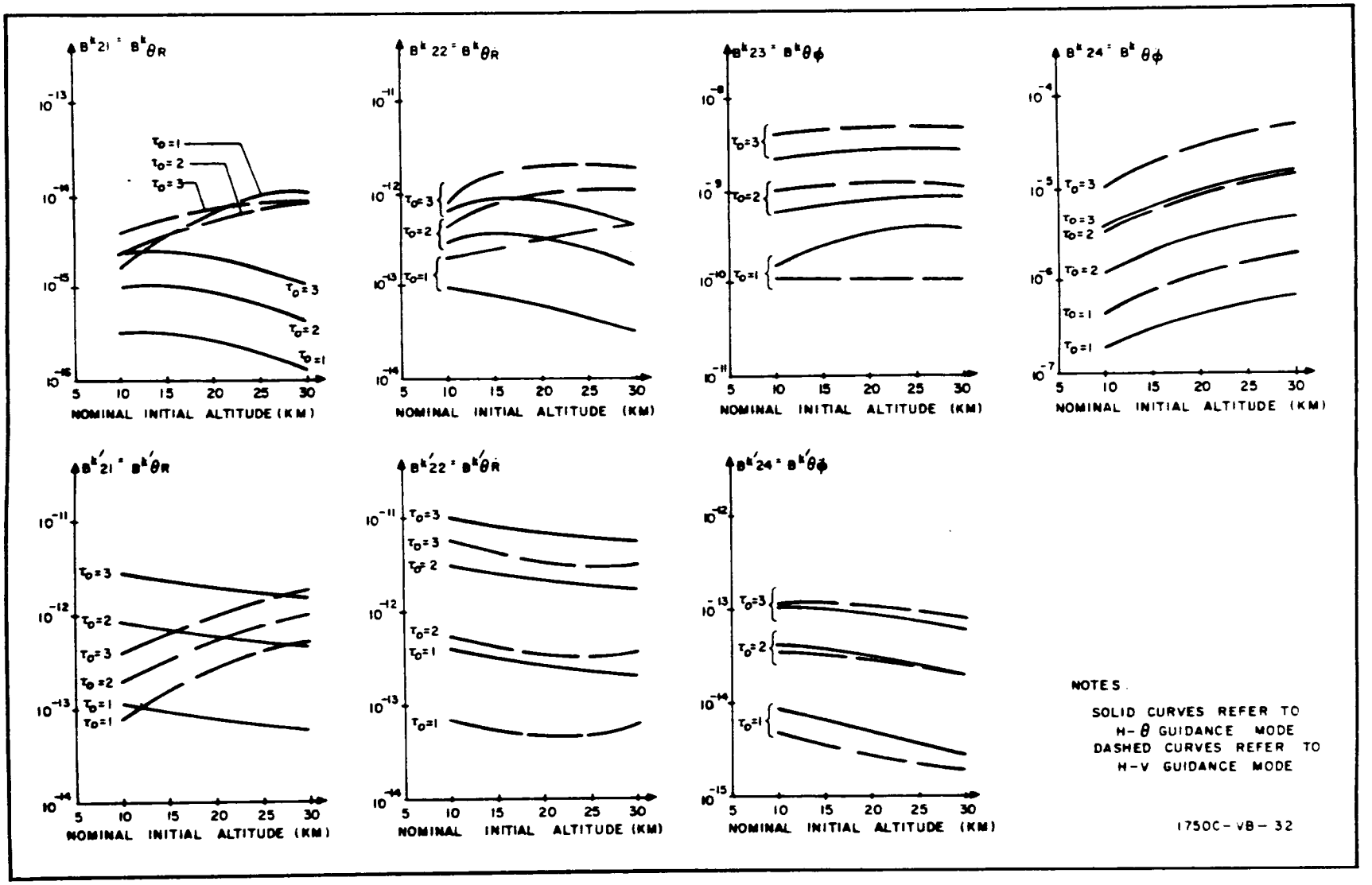

Figure 4-12. Error Sensitivity Coefficients Relating Terminal Central Angle Errors to Navigation Sensor Errors (Beacon Tracker Observables)

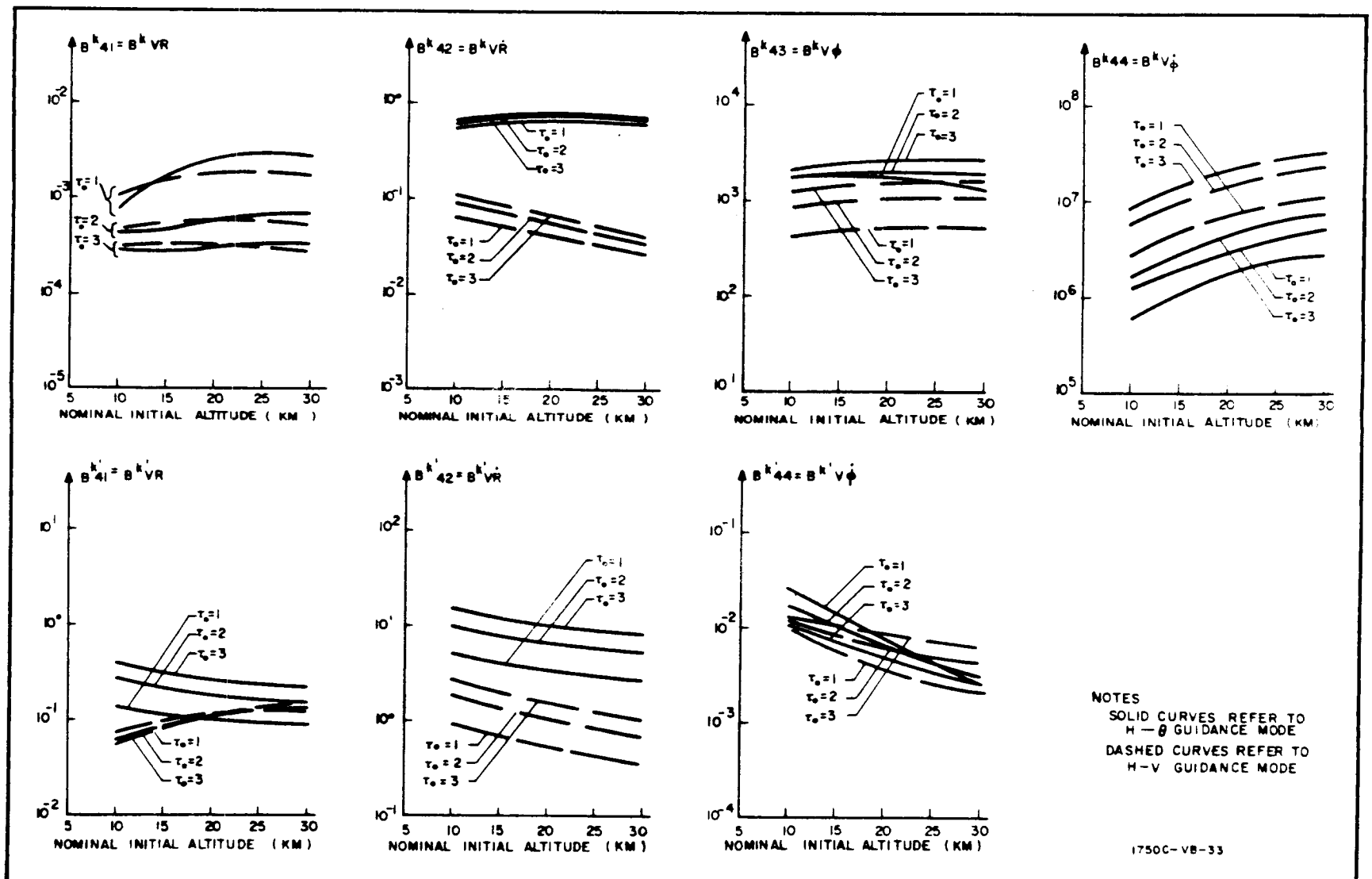

Figure 4-13. Error Sensitivity Coefficients Relating Terminal Velocity Errors to Navigation Sensor Errors (Beacon Tracker Observables)

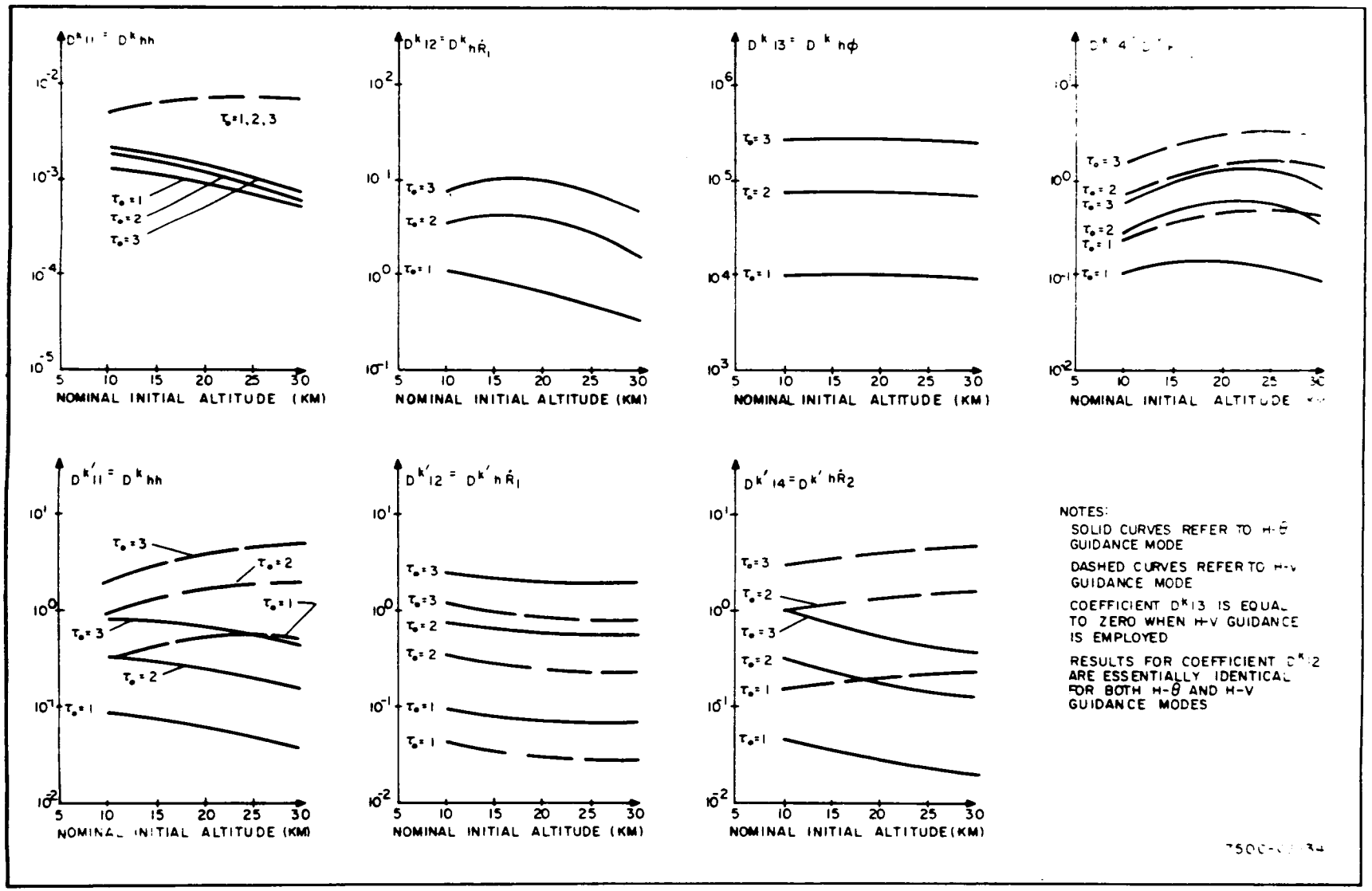

Figure 4-14. Error Sensitivity Coefficients Relating Terminal Altitude Errors to Navigation Sensor Errors (Doppler Navigation Observables)

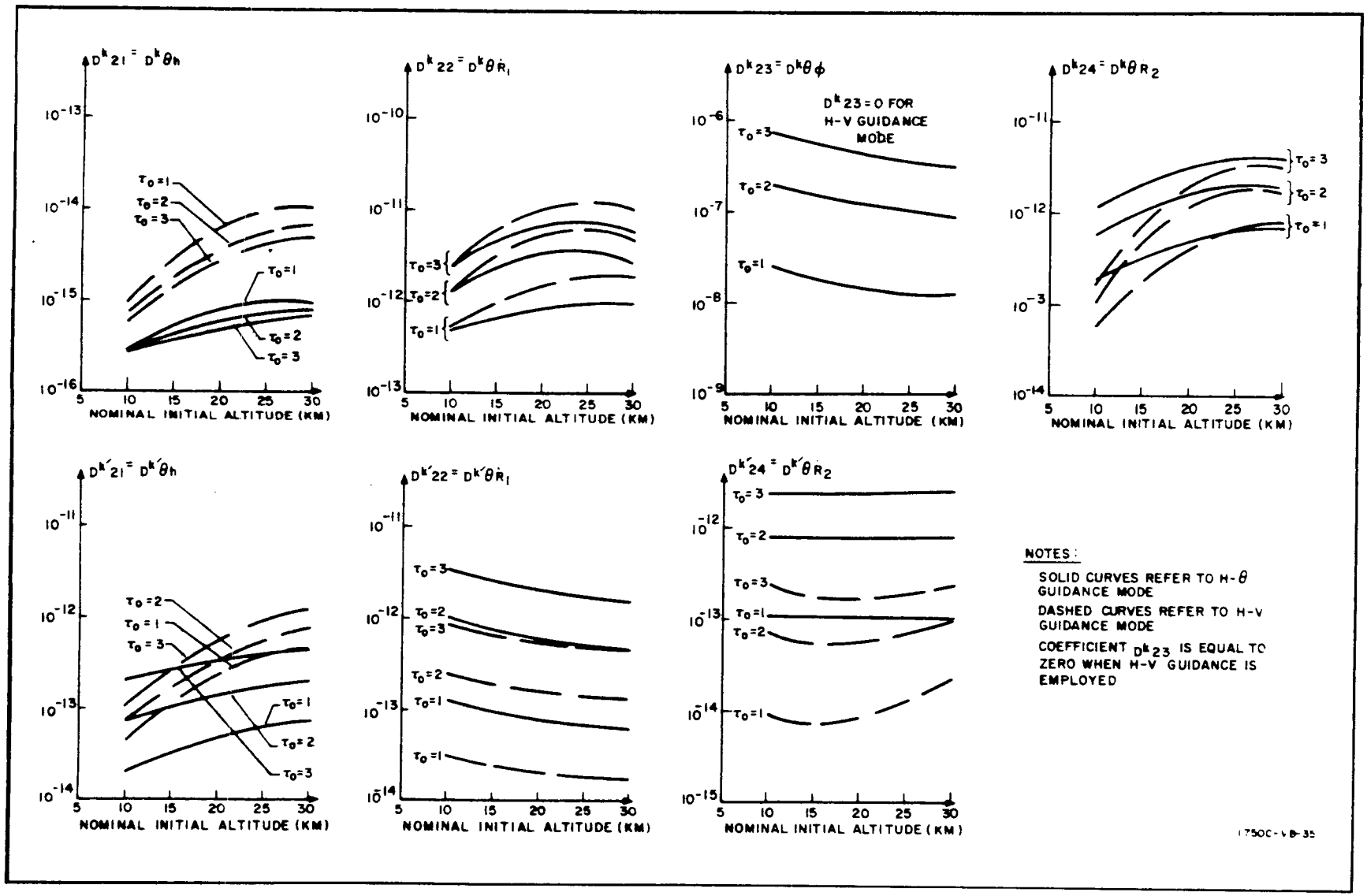

Figure 4-15. Error Sensitivity Coefficients Relating Terminal Central Angle Errors to Navigation Sensor Errors (Doppler Navigation Observables)

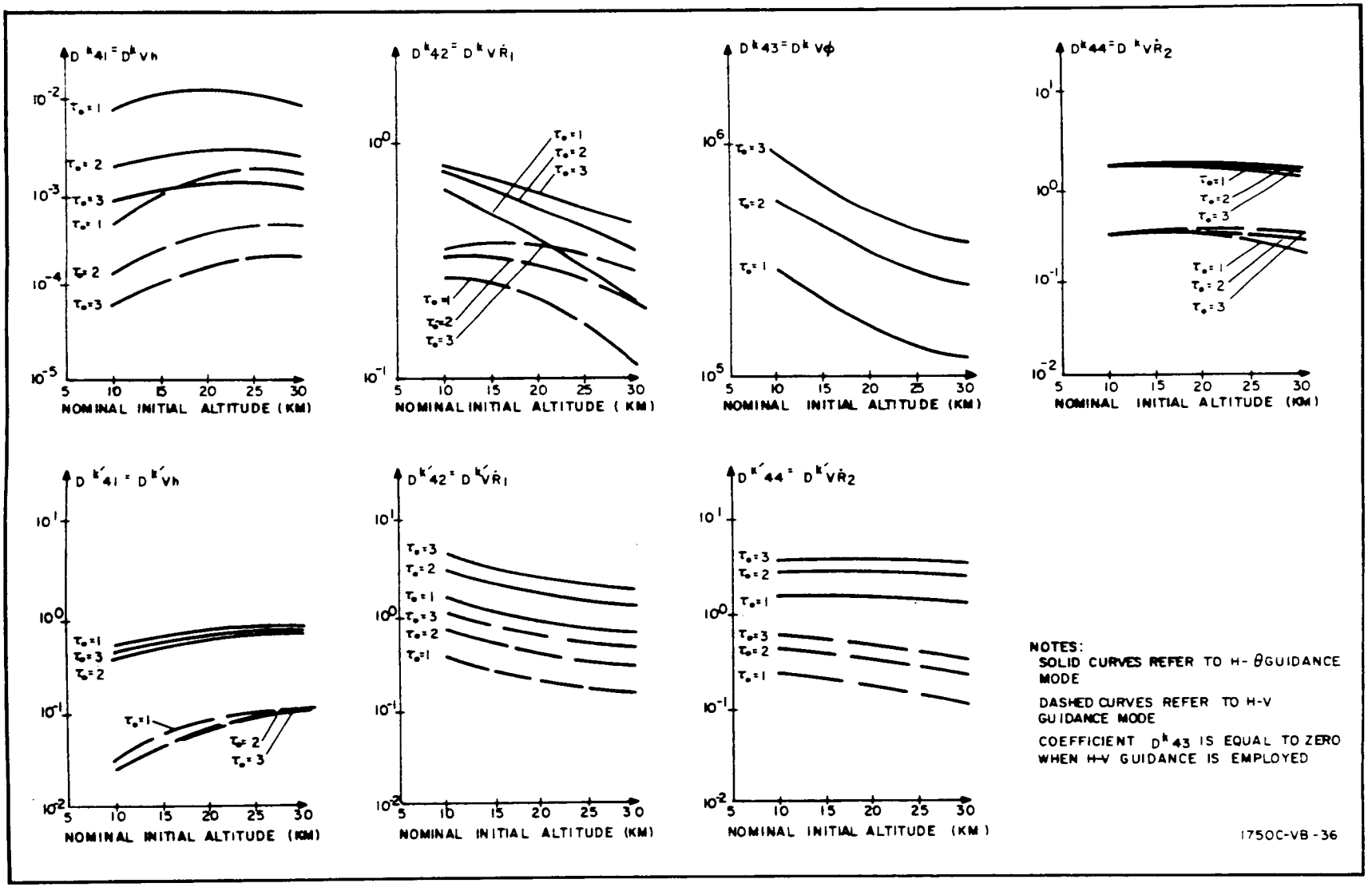

Figure 4-16. Error Sensitivity Coefficients Relating Terminal Velocity Errors to Navigation Sensor Errors (Doppler Navigation Observables)

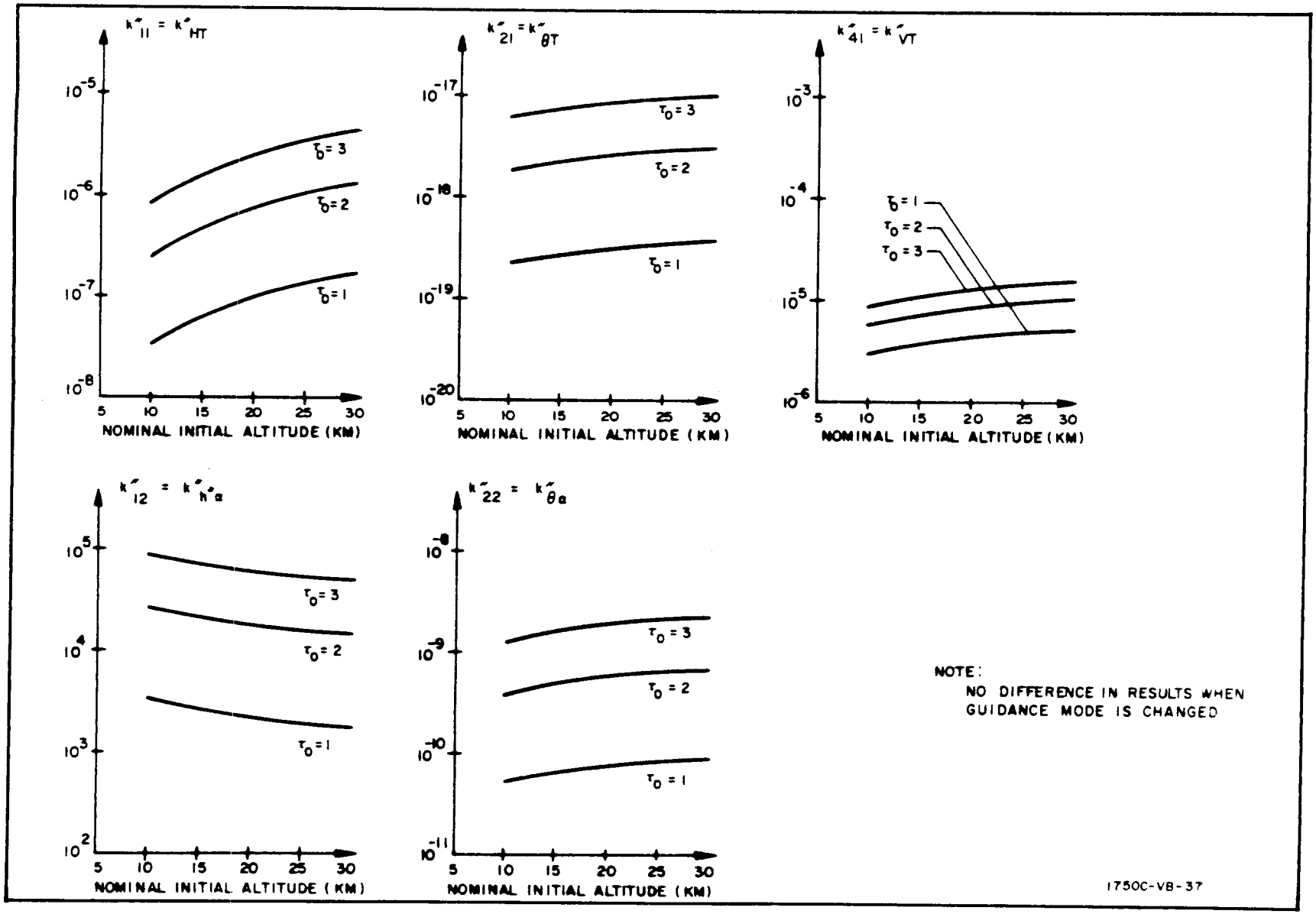

Figure 4-17. Error Sensitivity Coefficients Relating Terminal State Errors to Control Sensor Errors

b. Sample Computation. - To illustrate the use of the sensitivity coefficient matrices, a set of values for rms navigation and control sensor errors were selected and a sample calculation performed for τ_o = 1 second and h_o = 20 kilometers. The selected sensor error parameters and the resulting error components are summarized in tables 4-1, 4-2, and 4-3. Table 4-1 gives the estimated terminal position and velocity errors resulting from the assumed control sensor errors, and tables 4-2 and 4-3 contain similar data for the two sets of navigation sensors. Tables 4-2 and 4-3 also present overall error estimates.

TABLE 4-1

MEAN SQUARED TERMINAL ERRORS CAUSED BY CONTROL SENSOR ERRORS (SAMPLE COMPUTATION, h_o = 20 km, τ_o = 1 sec)

Error Source	RMS Sensor Error (Symbol and Magnitude)	Resulting Terminal Mean Squared Error Components		
		Altitude Error $L(\sigma^2_{h\,F_i})M$ (meters)	Central Angle Error $L(\sigma^2_{\theta\,F_i})M$ (radians)^2	Velocity Error $L(\sigma^2_{V\,F_i})M$
Thrust Magnitude Control Sensor	${}_n\sigma_{F_1} = {}_n\sigma_T$ = 500 new	0.0239	7.90×10^{-14}	1.23
	${}_p\sigma_{F_1} = {}_p\sigma_T$ = 0.0	0.0	0.0	0.0
Thrust Direction Control Sensor	${}_n\sigma_{F_2} = {}_n\sigma_\alpha$ = 0.035 rad.	2.73	9.25×10^{-14}	0.0
	${}_n\sigma_{F_2} = {}_p\sigma_\alpha$ = 0.0	0.0	0.0	0.0
Total Mean Squared Terminal Error Caused by Control Sensor Errors[a]		2.75	17.15×10^{-14}	1.23

a. Results presented in this table are applicable to all four possible combinations of observation (navigation) systems and guidance modes.

The sensor capabilities are typical of the state of the art, assuming 1-second smoothing time, which is compatible with the value of τ_o used in the sample.

TABLE 4-2

MEAN SQUARED TERMINAL ERRORS CAUSED BY NAVIGATION SENSOR ERRORS (SAMPLE COMPUTATION; OBSERVABLES $R\ \dot{R}\phi\ \dot{\phi}$; $h_o = 20$ km; $\tau_o = 1$ sec)

Error Source	RMS Sensor Error (Symbol and Magnitude)	Resulting Terminal Mean Squared Error Components					
		H-θ Guidance Mode			H-V Guidance Mode		
		Altitude Error $L^{(\sigma^2_{h\,Y_i})}{}_M$ (meters)^2	Central Angle Error $L^{(\sigma^2_{\theta\,Y_i})}{}_M$ (radians)^2	Velocity Error $L^{(\sigma^2_{V\,Y_i})}{}_M$ (m/sec)^2	Altitude Error $L^{(\sigma^2_{h\,Y_i})}{}_M$ (meters)^2	Central Angle Error $L^{(\sigma^2_{\theta\,Y_i})}{}_M$ (radians)^2	Velocity Error $L^{(\sigma_{V\,Y_i})}{}_M$ (m/sec)^2
Range Measurement (${}_BY_1 = R$)	${}_n\sigma_{Y_1} = {}_n\sigma_R = 5.0$ m	0.0675	0.675×10^{-14}	0.063	0.198	17.3×10^{-14}	0.0445
	${}_p\sigma_{Y_1} = {}_p\sigma_R = 0.1\%$	0.00129	0.0777×10^{-14}	0.00103	0.0059	0.276×10^{-14}	0.00115
Range rate measurement (${}_BY_2 = \dot{R}$)	${}_n\sigma_{Y_2} = {}_n\sigma_{\dot{R}} = 0.5$ m/sec.	0.0772	1.51×10^{-14}	0.165	0.131	7.72×10^{-14}	0.0102
	${}_p\sigma_{Y_2} = {}_p\sigma_{\dot{R}} = 0.5\%$	0.0165	6.90×10^{-14}	0.850	0.066	1.17×10^{-14}	0.133
Angle measurement (${}_BY_3 = \phi$)	${}_n\sigma_{Y_3} = {}_n\sigma_\phi = 0.001$ rad.	0.0001	0.034×10^{-14}	0.00174	0.00007	0.0107×10^{-14}	0.0005
	${}_p\sigma_{Y_3} = {}_p\sigma_\phi = 0.0$	0.0	0.0	0.0	0.0	0.0	0.0
Angle rate measurement (${}_BY_4 = \dot{\phi}$)	${}_n\sigma_{Y_4} = {}_n\sigma_{\dot{\phi}} = 0.001$ rad./sec	85.0	42.6×10^{-14}	1.78	94.4	115.0×10^{-14}	7.09
	${}_p\sigma_{Y_4} = {}_p\sigma_{\dot{\phi}} = 0.0$	0.0	0.0	0.0	0.0	0.0	0.0
Total Mean Squared Terminal Error Caused By Navigation Sensor Errors		85.16	51.80×10^{-14}	2.86	94.80	138.0×10^{-14}	7.28
Total Mean Squared Terminal Error Caused By Control Sensor Errors (Table 4-1)		2.75	17.15×10^{-14}	1.23	2.75	17.15×10^{-14}	1.23
Total Mean Squared Terminal Errors $L^{(\sigma^2_{X_i})}{}_M$		87.91	68.95×10^{-14}	4.09	97.55	155.1×10^{-14}	8.51
Total Root Mean Squared Terminal Errors $L^{(\sigma^2_{X_i})}{}_M$		9.38 (meters)	8.30×10^{-7} (radians)	2.02 (m/sec)	9.87 (meters)	12.5×10^{-7} (radians)	2.92 (m/sec)

TABLE 4-3

MEAN SQUARED TERMINAL ERRORS CAUSED BY NAVIGATION SENSOR ERRORS (SAMPLE COMPUTATION; OBSERVABLES $h\ \dot{R}_1\ \phi\ \dot{R}_2$; $h_o = 20$ km; $\tau_o = 1$ sec)

Error Source	RMS Sensor Error (Symbol and Magnitude)	Resulting Terminal Mean Squared Error Components					
		H-θ Guidance Mode			H-V Guidance Mode		
		Altitude Error $L^{(\sigma^2_{h\ Y_i})}{}_M$ (meters)^2	Central Angle Error $L^{(\sigma^2_{\theta\ Y_i})}{}_M$ (radians)^2	Velocity Error $L^{(\sigma^2_{V\ Y_i})}{}_M$ (m/sec)^2	Altitude Error $L^{(\sigma^2_{h\ Y_i})}{}_M$ (meters)^2	Central Angle Error $L^{(\sigma^2_{\theta\ Y_i})}{}_M$ (radians)^2	Velocity Error $L^{(\sigma^2_{V\ Y_i})}{}_M$ (m/sec)^2
Altitude measurement ($_DY_1 = h$)	$_n\sigma_{Y_1} = {}_n\sigma_h = 5.0$ m	0.0234	1.94×10^{-14}	0.298	0.177	6.58×10^{-14}	0.0362
	$_p\sigma_{Y_1} = {}_p\sigma_h = 0.1\%$	0.000595	0.048×10^{-14}	0.00709	0.00525	0.238×10^{-14}	0.000795
Range rate measurement ($_DY_2 = \dot{R}_1$)	$_n\sigma_{Y_2} = {}_n\sigma_{\dot{R}_1} = 0.2$ m/sec	0.0264	3.25×10^{-14}	0.0152	0.0264	5.91×10^{-14}	0.00895
	$_p\sigma_{Y_2} = {}_p\sigma_{\dot{R}_1} = 0.5\%$	0.0190	1.99×10^{-14}	0.222	0.00790	0.500×10^{-14}	0.0500
Angle measurement ($_DY_3 = \phi$)	$_n\sigma_{Y_3} = {}_n\sigma_\phi = 0.001$ rad.	0.0103	1.42×10^{-14}	0.159	0.0	0.0	0.0
	$_p\sigma_{Y_3} = {}_p\sigma_\phi = 0.0$	0.0	0.0	0.0	0.0	0.0	0.0
Range rate measurement ($_DY_4 = \dot{R}_2$)	$_n\sigma_{Y_4} = {}_n\sigma_{\dot{R}_2} = 0.2$ m/sec.	0.00568	2.00×10^{-14}	0.0651	0.0179	1.63×10^{-14}	0.0106
	$_p\sigma_{Y_4} = {}_p\sigma_{\dot{R}_2} = 0.5\%$	0.00675	2.65×10^{-14}	0.345	0.0500	0.210×10^{-14}	0.0398
Total Mean Squared Terminal Error Caused By Navigation Sensor Errors		0.092	13.30×10^{-14}	1.11	0.284	15.07×10^{-14}	0.146
Total Mean Squared Terminal Error Caused By Control Sensor Errors (Table 4-1)		2.75	17.15×10^{-14}	1.23	2.75	17.15×10^{-14}	1.23
Total Mean Squared Terminal Errors $L^{(\sigma^2_{X_i})}{}_M$		2.84	30.45×10^{-14}	2.34	3.03	32.22×10^{-14}	1.38
Total Root Mean Squared Terminal Errors $L^{(\sigma_{X_i})}{}_M$		1.69 (meters)	5.52×10^{-7} (radians)	1.53 (m/sec)	1.74 (meters)	5.68×10^{-7} (radians)	1.18 (m/sec)

Typical conclusions concerning results of the sample computation are:

- The dominant error source in the beacon tracking navigation scheme is the line-of-sight angle-rate measuring device.

- No error source can be regarded as dominant with the set of doppler navigation sensor errors.

- Switching from the H-θ to the H-V guidance mode increases all three terminal error components in the system using beacon tracking observables and two out of three (all but velocity) components when doppler navigation observables are used. Since velocity errors are critical, H-θ guidance is indicated with beacon tracking and H-V guidance with doppler navigation.

- In general, rms terminal errors are smaller when doppler navigation observables are used compared to beacon tracker results.

Thus the system configuration indicated by the sample computation results uses doppler navigation observables and the H-V guidance mode. This conclusion is based entirely on the magnitude of the terminal errors and does not consider mechanization, fuel consumption characteristics, or any other factors which also must be considered before final system design is attained.

c. Results of Parameter Variations - During the error analysis of linear predictive guidance, several system parameters are treated as variables:

Guidance mode: H-θ or H-V
Observables: beacon tracker or doppler navigator
Quantization interval, τ_o: 1, 2, or 3 seconds
Nominal trajectory initial attitude, h_o: 10, 15, 20, 25, and 30 kilometers.

The following paragraphs discuss the effects of these variations.

(1) Guidance Mode

H-θ guidance is the mode used in Ref. 4-1 from which the linear predictive guidance concept is taken. H-V guidance is an alternate scheme postulated as a method which would offer reduced terminal velocity errors. The computer data presented in figures 4-11 and 4-17 shows that all velocity error components are reduced by the switch to H-V guidance when doppler navigation observables are used and all but one when beacon tracking navigation is employed. The one in the latter case is the velocity error component caused by range rate measurement errors. One can conclude, therefore, that terminal velocity errors are reduced by changing from H-θ guidance to H-V

guidance when doppler navigation observables are used. A reduction is also realized when beacon tracking observables are used so long as angle rate measurement error is not the dominant contributor to the terminal state errors. The sample calculation performed indicates that this qualification is significant. The sample also indicates that the velocity error reduction obtained when doppler navigation observables are employed is not particularly signficant (1.18 m/sec rms with H-V guidance as opposed to 1.53 m/sec rms with H-θ guidance). Thus decision between the two guidance modes can be expected to be determined by other factors; e.g., fuel usage and noise-free performance.

(2) Observation Scheme

The only practical means for comparing the two observation schemes within this report lies in the sample computation using present state of the art sensor capabilities. On this basis it is seen that the doppler navigation scheme yields consistently smaller terminal error components. The pertinent results from tables 4-2 and 4-3 are summarized in table 4-4.

(3) Quantization Interval (τ_o)

The quantization interval (τ_o) used in the analytical model is set equal to the correlation interval of white noise passed through the engine control subsystem (paragraph 4.3.1.1.e). This relationship is maintained throughout the analysis so that increasing the value of τ_o is equivalent to reducing the bandwidth of the engine subsystem. In addition, the guidance term matrix [S] is frozen at some time prior to the nominal final time (paragraph 4.3.1.1.c) and this time is related to τ_o. Since τ_o is related to quantities that are significant in the design of the guidance and control system, the effects of variations are of interest. The following statements are based on the graphical presentation of computer results given in figures 4-11 through 4-17.

- Mean squared terminal error components caused by control sensor errors increase as τ_o goes from 1 to 3 seconds. The magnitude of the increase over this range is approximately a factor of 10.

- All mean squared terminal altitude error components increase as τ_o increases.

- All mean squared terminal central angle error components except that contributed by altitude measurement in the doppler navigation system increase as τ_o increases. Thus terminal angle errors increase with increasing τ_o when beacon tracking navigation is used and can be expected to increase in a similar pattern when doppler navigation is employed so long as altitude observation errors are not the dominant

TABLE 4-4

COMPARISON OF MEAN SQUARED TERMINAL ERRORS RESULTING FROM BEACON TRACKING AND DOPPLER NAVIGATION SENSOR ERRORS (BASED ON STATE OF THE ART SENSOR CAPABILITY)

τ_o = 1 second; h_o = 20 km		Mean Squared Terminal State Errors		
Guidance Mode	Observation Scheme	Altitude Error $(\text{meters})^2$	Central Angle Error $(\text{radians})^2$	Velocity Error $(\text{m/sec})^2$
H-θ guidance	Beacon tracking observables	85.16	51.8×10^{-14}	2.86
	Doppler navigation observables	0.092	13.3×10^{-14}	1.11
H-V guidance	Beacon tracking observables	94.8	13.8×10^{-14}	7.28
	Doppler navigation observables	0.284	15.07×10^{-14}	0.146

source of terminal angular error. In the sample computation performed in paragraph 4.3.1.3.b altitude sensor errors are significant but not dominant.

- All mean squared terminal velocity error components either increase or change insignificantly as τ_o increases except those caused by range measurement errors for beacon tracking navigation and altitude measurement errors for doppler navigation. Thus velocity errors increase with increasing τ_o as long so these error sources are not dominant. In the sample computation based on state of the art sensor capability, neither range nor altitude observation errors contribute dominant terminal velocity error components. Therefore velocity errors increase as τ_o increases for the sample case.

(4) Nominal Trajectory Altitude, h_o

No generalization can be made concerning the effect of changing h_o on the terminal error components. Nearly as many of the error sensitivity coefficients presented in figures 4-11 through 4-17 decrease as increase with increasing h_o. The overall effect on terminal position and velocity errors is therefore dependent on the particular characteristic of the sensitivity coefficient which yields the dominant component of the terminal state error in question. For example, angle rate measurement errors are the most significant in the sample computation performed using beacon tracking observables (see table 4-2).

Therefore the manner in which sensitivity coefficients B^k14, B^k24, and B^k44 change as h_o changes determines how the terminal position and velocity errors vary as h_o changes. Curves contained in figures 4-12, 4-13, and 4-14 indicate that all three of these coefficients increase as h_o increases so that terminal position and velocity errors can be expected to do the same.

4.3.1.4 Conclusions

The following conclusions are based on material presented in paragraphs 4.3.1.3.a, 4.3.1.3.b and 4.3.1.3.c.

- Characteristics of terminal state error distributions for any given group of sensors are highly dependent on which sensor is the dominant error source.

- Generally, increasing τ_o results in increased terminal mean squared errors.

- When state of the art sensor capabilities are assumed for both navigation sensor schemes, doppler navigation results in smaller terminal errors.

- Changing from the H-θ to the H-V guidance mode does result in reduced terminal velocity errors when doppler navigation is used; however, the reduction is not very significant. In addition, it is possible for this guidance mode switch to result in increased terminal velocity error when beacon tracking navigation is employed.

- Terminal position errors caused by navigation and control sensor errors are not serious, being on the order of a few meters (based on sample computation results). The situation with regard to velocity errors is not so clear-cut. The landing mission profile as envisioned in this study is made up of two subphases: descent-to-hover, and hover-to-touchdown. Linear predictive guidance is considered to be used down to the hover point with some undefined terminal guidance system controlling the actual touchdown. For manned flights, this touchdown maneuver is considered to be under manual control. For this case velocity errors at hover of the magnitude indicated in tables 4-2 and 4-3 are felt to be satisfactory. For the unmanned case one can expect relaxed touchdown velocity requirements so that the terminal (hover point) velocity errors resulting from state of the art sensor capability are expected to be satisfactory even if the hover-to-touchdown guidance system offers no improvement in touchdown velocity uncertainty. (This is the case if thrust is simply terminated at the hover point, allowing the vehicle to descend to the surface under gravitational acceleration).

4.3.2 Lunar Landing Using Modified Proportional Navigation

The second guidance technique investigated is modified proportional navigation. This guidance technique was evaluated by Kriegsman and Reiss (Ref. 4-4) assuming a flat moon and short initial range. This assumption is not valid for the situation presently under investigation because it is desired to use the technique over significantly longer range. (Landing engines are ignited at periselenum and burn continuously until touchdown.) Therefore the guidance equations are modified to include spherical lunar characteristics.

A digital simulation of the landing system is used to evaluate guidance system performance and also to determine the effects of navigation sensor bias errors. In addition, the adjoint method of analysis (see subsection 6.2 of Appendix A, Volume V) is used to determine error sensitivity coefficients which can be used to evaluate the effects of random navigation sensor errors.

The analytical effort can be divided into two categories, as is the analysis of linear predictive guidance. First, background analyses are discussed for the purpose of establishing a system model. Second, the actual error analysis is performed. Discussions presented herein will be primarily qualitative in nature, and as much of the actual analytical effort as possible is reported in the appendixes.

4.3.2.1 Background

a. State Variables, Control Quantities, and the Equations of Motion - The basic coordinate system used for analysis of modified proportional navigation guidance is shown in figure 4-18. It is an inertial polar coordinate system with its origin at the nominal landing site. The state variables are R, $\dot{R}$, Ω, and $\dot{\Omega}$ as defined below.

- R: Line-of-sight range from the spacecraft site to the desired landing site. (in meters)
- Ω: Line-of-sight angle to the landing site measured from landing site local vertical. (in radians)

Quantities $\dot{R}$ and $\dot{\Omega}$ are the time derivatives of R and Ω. Since the problem has been reduced to two dimensions for this analysis, only four state variables are required to specify vehicle position and velocity relative to the landing site.

In addition, an inertial rectangular coordinate system will sometimes be used. This system, also centered at the nominal landing site, is defined by the three coordinate axes X, Y, and Z:

- X: Horizontal axis in vehicle plane of motion, positive toward spacecraft
- Y: Vertical axis, positive upward
- Z: Horizontal axis forming right-hand coordinate system with X and Y

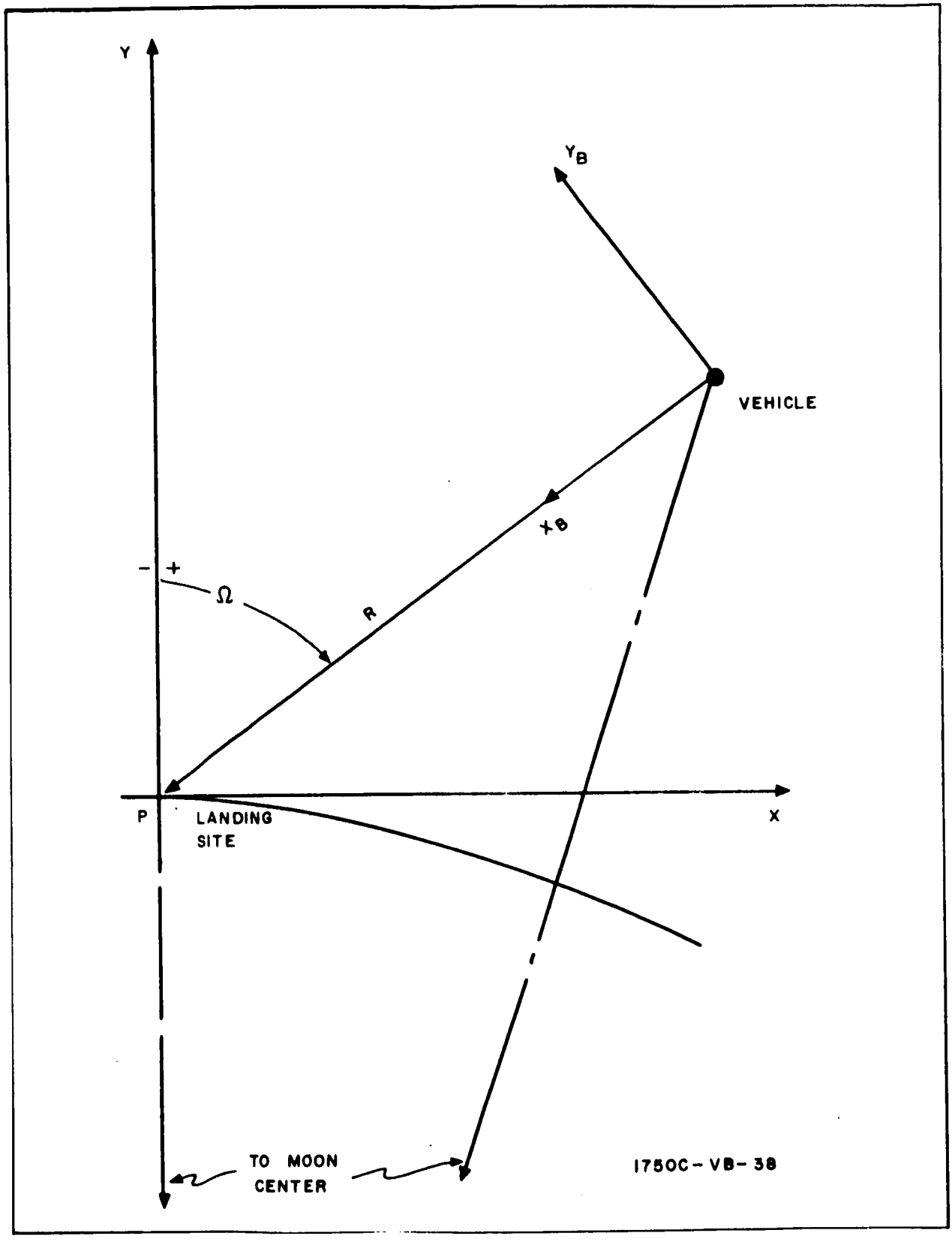

Figure 4-18. Guidance Geometry

Finally, some equations are written in terms of a rectangular coordinate system fixed to the space vehicle. The body coordinates X_B, Y_B, and Z_B are the roll, yaw, and pitch axes respectively. The attitude control system is assumed to maintain the roll axis X_B along the line-of-sight to the desired landing site. For the two-dimensional analysis performed herein, the yaw axis is assumed to be in the plane of motion.

The control quantities are accelerations along the vehicle roll and yaw axes respectively. Figure 4-19 shows the accelerations acting on the space vehicle. Note that a_R, the acceleration along the roll axis, is considered to be positive in the negative X_B direction. Similarly, the normal component of acceleration (a_Ω) is positive in the negative Y_B direction. In addition, there is the acceleration of gravity which acts along the radius vector from the lunar center of gravity.

During analysis two forms of the equations of motion are used. The first is given in terms of vehicle accelerations in the X and Y and Z directions.

$$\ddot{X} = -\frac{\mu}{r^3} X + a_X \tag{4-52}$$

$$\ddot{Y} = -\frac{\mu(r_c + Y)}{r^3} + a_Y$$

$$\ddot{Z} = \frac{\mu}{r^3} Z + a_Z$$

Quantities a_X, a_Y, and a_Z are the appropriate components of the total vehicle thrust acceleration vector. Specifically, for the two-dimensional analysis to follow,

$$\ddot{X} = -\frac{\mu}{r^3} X + a_R \sin\Omega + a_\Omega \cos\Omega \tag{4-53}$$

$$\ddot{Y} = -\frac{\mu(r_c + Y)}{r^3} + a_R \cos\Omega - a_\Omega \sin\Omega$$

$$\ddot{Z} = 0$$

This formulation of the equations of motion is used in the digital simulation analysis program to be discussed in a subsequent section.

The second formulation is proposed for use with the adjoint error analysis. In this case it is desirable to write the expressions in terms of R, Ω, a_R, and a_Ω.

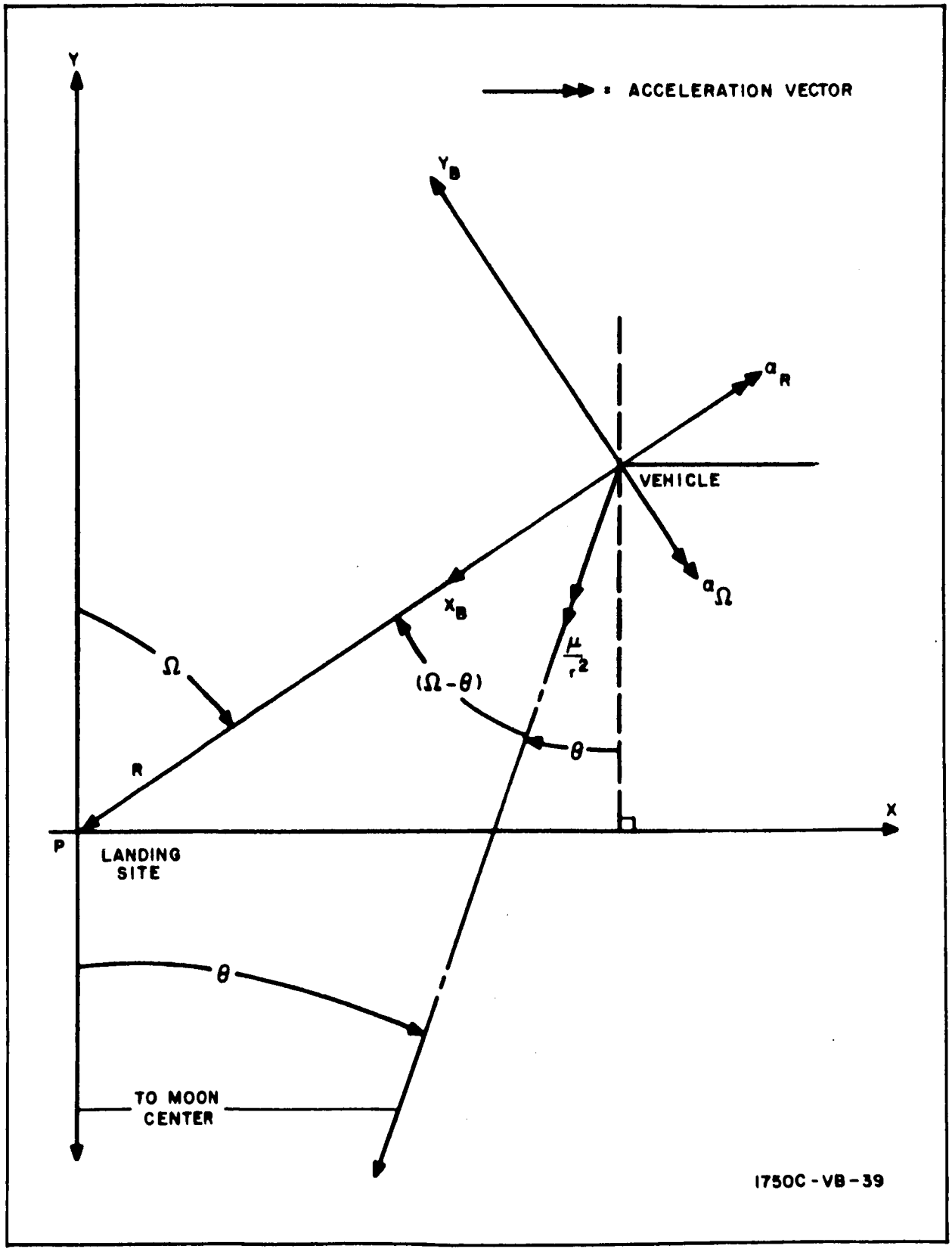

Figure 4-19. Acceleration Diagram

$$\ddot{R} = R\dot{\Omega}^2 - \frac{\mu}{r^2}\cos(\Omega - \theta) + a_R \tag{4-54}$$

$$\ddot{\Omega} = \frac{1}{R}\left[\frac{\mu}{r^2}\sin(\Omega - \theta) - 2\dot{R}\dot{\Omega} + a_\Omega\right]$$

These equations are linearized and used in the formulation of the adjoint system model. (See subsections 6.2 of Appendix A and 3.4 of Appendix D, Volume V.)

At times it will be convenient to define general state variable and control quantity matrices as in paragraph 4.3.1.1.a. These are column matrices or vectors with general elements X_i and F_i respectively.

$$\underline{X} \equiv \begin{bmatrix} X_1 \\ X_2 \\ X_3 \\ X_4 \end{bmatrix} \equiv \begin{bmatrix} R \\ \dot{R} \\ \Omega \\ \dot{\Omega} \end{bmatrix} = \text{state variable vector} \tag{4-55}$$

$$\underline{F} \equiv \begin{bmatrix} F_1 \\ F_2 \end{bmatrix} \equiv \begin{bmatrix} a_R \\ a_\Omega \end{bmatrix} = \text{control quantity vector} \tag{4-56}$$

b. Observables. - The input information is obtained by a beacon tracking sensor system. The observables are line-of-sight range R, and angle Ω to the vehicle from the landing site and their time derivatives, $\dot{R}$ and $\dot{\Omega}$. Note that the line-of-sight angle is measured in an inertial system centered at the landing site and not with respect to vehicle local vertical (figure 4-18).

The pertinent navigation equations are degenerate since the state variables and observables are identical.

c. Guidance Technique. - Basically, the guidance concept used is a form of proportional navigation. The basic guidance technique is evaluated by Kriegsman and Reiss in Ref. 4-4 assuming a flat moon and short initial range. The analysis performed in the indicated reference is herein generalized to the spherical moon case. The guidance equations are written in terms of a_R, a_Ω, and the observables assumed to be available. Finally gravity compensation terms are added to the guidance equations to counter the disturbing influence of lunar gravitation. Without the compensation terms, the vehicle is found to have a tendency to impact before reaching the designated landing site. With the indicated modifications, the equations giving the commanded values of a_R and a_Ω, denoted $\hat{a}_R$ and $\hat{a}_\Omega$ are:

$$\hat{a}_R = \frac{K-1}{K}\frac{(\hat{\dot{R}})^2}{\hat{R}} + \frac{\mu}{r_c^2}\cos\hat{\Omega} \tag{4-57}$$

$$\hat{a}_\Omega = \left(S + \frac{K-1}{K}\right)\hat{\dot{R}}\,\hat{\dot{\Omega}} - \frac{\mu}{r_c^2}\sin\hat{\Omega}$$

These equations describe what is referred to as the MPN guidance mode (Modified Proportional Navigation). The symbol ∧ indicates a measured value or a quantity computed from measured quantities. Note that the inserted gravity compensation terms are based on a constant force field approximation. The two constants, S and K, are guidance parameters.

Digital simulation shows that appropriate selection of the guidance parameters S and K will cause the vehicle to follow a trajectory very nearly identical with the optimum trajectory described in subsection 1.2 of Appendix D (Volume V). These values are S = 1.5 and K = 2.0. This is desirable from the standpoint of fuel consumption but also implies that the vehicle approaches the landing site on a rather shallow trajectory. The latter tendency is not desirable and is countered by developing a further modification to the guidance technique which results in vertical touchdown. This scheme is denoted MPN/VT guidance and is characterized by the guidance equations

$$\hat{a}_R = \frac{K_1-1}{K_1}\frac{(\hat{\dot{R}})^2}{\hat{R}} \tag{4-58}$$

$$\hat{a}_\Omega = S_1\,\hat{\dot{R}}\,\hat{\dot{\Omega}} - S_2\frac{(\hat{\dot{R}})^2}{\hat{R}}\,\hat{\Omega}$$

Note that no gravity compensation terms are included. This results from the fact that the lofting tendency of these modified guidance equations is found to provide adequate terrain clearance without additional compensation (shown by digital simulation). Quantities K_1, S_1, and S_2 are guidance parameters whose values influence system performance. In this analysis the values of these guidance parameters are: $K_1 = 3.0$, $S_1 = 3.1$, $S_2 = 0.8$.

The MPN/VT guidance equations can of course be used over the entire descent phase. However, the lofting tendency will increase fuel consumption over that noted using the MPN equations. For this reason, two combinations of MPN and MPN/VT guidance are postulated. These are denoted MPN/VT - A and MPN/VT-B.

Under MPN/VT-A guidance, the landing vehicle uses the MPN guidance scheme until the line-of-sight range is reduced to 305 meters (1000 ft) and then switches to MPN/VT for the remainder of the flight.

For MPN/VT-B guidance, a fictitious landing site is created at some arbitrary altitude, Y_H, directly above the desired landing site. (See figure 4-20.) Y_H equals 305 meters (1000 feet) in this analysis. The MPN guidance equations are used until R_1 is reduced to 305 meters, with the guidance equations evaluated as if P' is the desired landing site. Thus

$$\hat{a}_{R_1} = \frac{K-1}{K}\frac{(\hat{\dot{R}}_1)^2}{\hat{R}_1} + \frac{\mu}{r_c^2}\cos\hat{\Omega}_1 \tag{4-59}$$

$$\hat{a}_{\Omega_1} = \left(S + \frac{K-1}{K}\right)\hat{\dot{R}}_1\hat{\dot{\Omega}}_1 - \frac{\mu}{r_c^2}\sin\hat{\Omega}_1$$

$$S = 1.5;\ K = 2.0$$

As shown in figure 4-20, the vehicle attitude control system still maintains the vehicle roll axis along the sightline to the actual landing site. Thus a_R and a_Ω, the actual acceleration commands used on board the vehicle, must be written in terms of a R_1, and a Ω_1. In addition, R_1 and Ω_1 must be expressed in terms of R and Ω, since these remain the observable quantities regardless of the guidance mode employed. The appropriate equations, derived in subsection 3.1 of Appendix D (Volume V) are:

$$\hat{a}_R = \hat{a}_{R_1}\cos\hat{\beta} - \hat{a}_{\Omega_1}\sin\hat{\beta} \tag{4-60}$$

$$\hat{a}_\Omega = \hat{a}_{R_1}\sin\hat{\beta} + \hat{a}_{\Omega_1}\cos\hat{\beta}$$

where

$$\hat{\beta} \equiv \sin^{-1}\left[\frac{Y_H\sin\hat{\Omega}}{(Y_H^2 + \hat{R}^2 - 2Y_H\hat{R}\cos\hat{\Omega})^{1/2}}\right] \tag{4-61}$$

$$\hat{R}_1 = \left[Y_H^2 + \hat{R}^2 - 2Y_H\hat{R}\cos\hat{\Omega}\right]^{1/2}$$

$$\hat{\Omega}_1 = \hat{\Omega} + \sin^{-1}\left[\frac{Y_H\sin\hat{\Omega}}{(Y_H^2 + \hat{R}^2 - 2Y_H\hat{R}\cos\hat{\Omega})^{1/2}}\right] \tag{4-62}$$

When $\hat{R}_1$ is reduced to 305 meters, guidance switches to the MPN/VT mode described by equation 4-58.

Simulation of lunar landing using both hybrid guidance concepts, MPN/VT-A and MPN/VT-B, shows the latter to be more efficient from the fuel consumption aspect. Final selection of MPN/VT-B over MPN/VT-A is based primarily on this consideration.

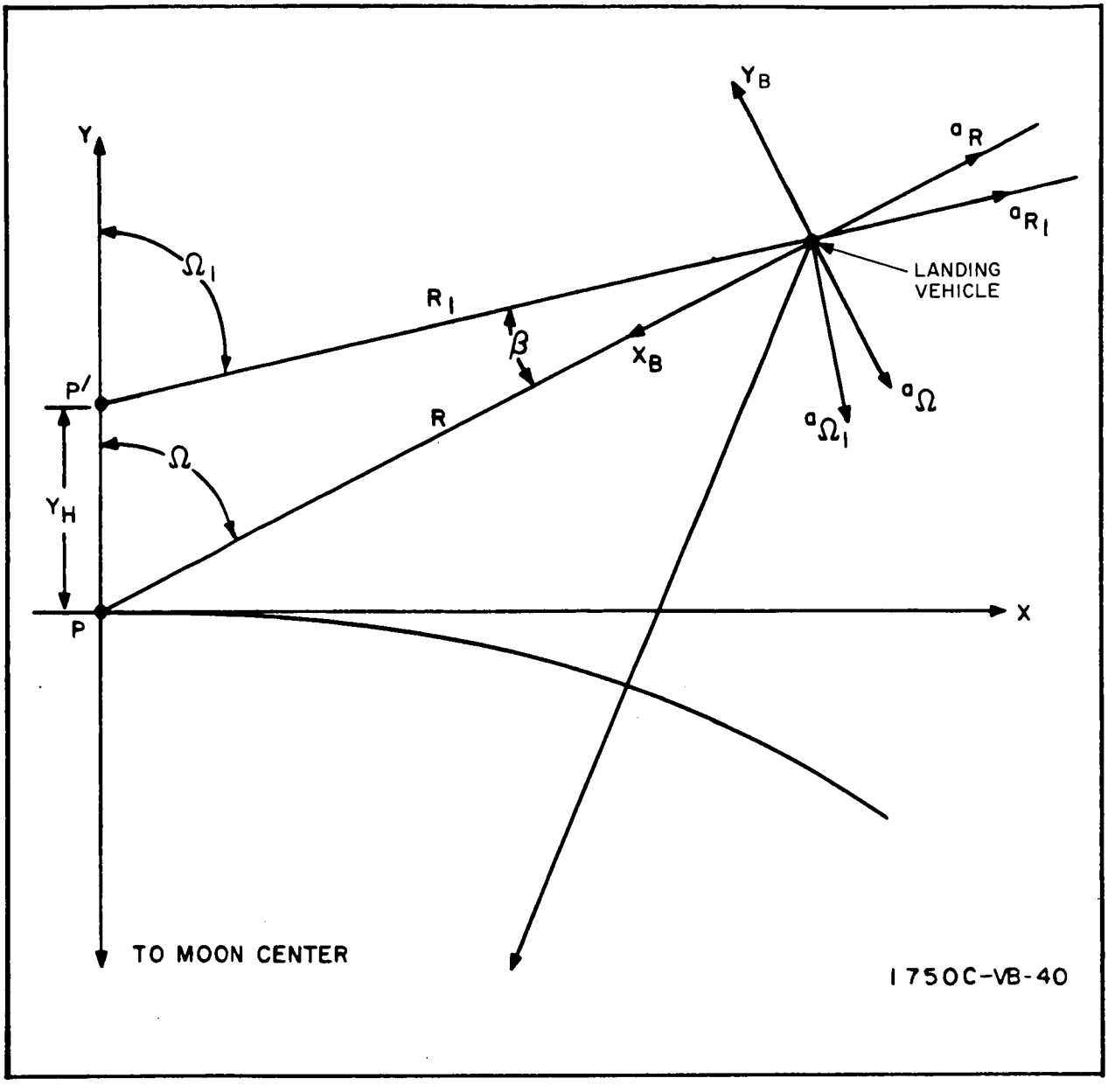

Figure 4-20. Geometry Pertinent to the MPN/VT-B Guidance Concept

By using the hybrid guidance scheme denoted MPN/VT-B, the vehicle is made to fly a trajectory very similar to that derived as being optimum in subsection 1. 2 of Appendix D (Volume V), until the line-of-sight range to the fictitious landing site has been reduced to 305 meters. At this point, the MPN/VT guidance mode is introduced by switching guidance parameters and dropping gravity compensation terms. Thereafter the vehicle flies a more lofted trajectory (compared to the MPN trajectory) which approaches the desired landing site from a nearly vertical direction in accordance with the

considerations outlined in paragraph 4. 2. 2. Note that the vehicle roll axis is always aligned toward the landing site by the attitude control system. Thus this axis is essentially along the landing site vertical at the end of the descent maneuver, and the vehicle is in the proper attitude for touchdown.

d. Vehicle Characteristics. - The following paragraph describes the mechanization considerations applicable during analysis of the MPN/VT-B guidance concept. The areas covered are: vehicle size (mass), attitude control, engine sizing and dynamics, information sensor dynamics, and fuel specific impulse (I_{sp}) selection.

The initial mass is obtained by considering a typical mission in which the total payload placed lunar orbit (assuming earth launch by a Saturn C-5 booster) is to be landed on the lunar surface. The resulting mass breakdown in kilograms is:

• Initial mass at translunar injection	40, 816
• After allocating fuel for 30. 5m/sec (100 ft/sec) correction during midcourse	40, 363
• After boil-off during midcourse	40, 068
• After allocating fuel for attitude control during midcourse	40, 045
• After lunar orbit insertion pulse	32, 109
• After transfer deorbit pulse for synchronous ellipse	31, 066
• At periselenum (landing phase initial mass)	31, 066

Thus, the initial vehicle mass used throughout the analysis of modified proportional navigation is 31, 066 kg (68, 500 pounds, earth weight).

The attitude control system assumed for the digital simulation of lunar landing is identical to that described in Appendix B of Volume IV, for use during rendezvous. Basically the attitude control system roll-rate stabilizes the vehicle while maintaining the roll axis along the line-of-sight to the landing site.

For the adjoint analysis of the linearized system using MPN/VT guidance equations (subsection 3. 4 Appendix D of Volume V), perfect attitude control is assumed. In addition, second order linear filters, characterized by the transfer functions $G_1(s)$ and $G_2(s)$ are included to represent longitudinal and lateral engine dynamics in the adjoint analysis. Thus:

$$a_R(s) = G_1(s)\,\hat{a}_R(s) \tag{4-63}$$

$$a_\Omega(s) = G_2(s)\,\hat{a}_\Omega(s)$$

where

$$G_1(s) = \frac{1}{1 + \frac{2\zeta_1}{\omega_1} s + \frac{s^2}{\omega_1^2}} \tag{4-64}$$

$$G_2(s) = \frac{1}{1 + \frac{2\zeta_2}{\omega_2} s + \frac{s^2}{\omega_2^2}}$$

$$\zeta_1 = \zeta_2 = 0.7$$

$$\omega_1 = \omega_2 = 5 \text{ radians/sec}$$

Sensor dynamics are also represented by linear second order filters in the adjoint error analysis. These filters are represented by transfer functions $G_R(s)$, $G_{\dot{R}}(s)$, $G_\Omega(s)$, and $G_{\dot{\Omega}}(s)$. The input to the sensor is the actual value of the observable plus error terms. Random error at the sensor input is assumed to be white Gaussian. (Band limiting is provided by the filter.) The measured value of the observable appears at the output of the filter assumed to characterize the sensor. All four sensor filters are allowed to be identical, and these in turn are identical in form to the filters characterizing engine response:

$$G_R(s) = G_{\dot{R}}(s) = G_\Omega(s) = G_{\dot{\Omega}}(s) = \frac{1}{1 + \frac{(2)(0.7)}{5} s + \frac{s^2}{25}} \tag{4-65}$$

The effect of fuel specific impulse, I_{sp}, on touchdown mass is shown in figure 4-21. This curve is a plot of the ratio of touchdown mass, m_f, to initial mass, m_o, versus I_{sp} based on the optimum trajectory discussed in subsection 1.2 of Appendix D (Volume V). The initial altitude and thrust are 18,288 meters (50,000 feet) and 133,500 newtons (30,000 pounds) respectively. It is seen that the ratio m_f/m_o increases as I_{sp} increases, implying that the highest I_{sp} consistent with the state of the art is the logical choice. For the analysis of modified proportional navigation, an I_{sp} equal to 420 seconds is selected. This choice appears to be commensurate with the most efficient fuels likely to be available.

For this investigation the specifications of the RL-10 engine are selected to represent the class of engines that will be available. The important parameters are:

- Maximum thrust level: 66,765 kilograms (15,000 lb)
- Mass: 136 kg (300 lb, earth weight)
- Throttling range: 10:1

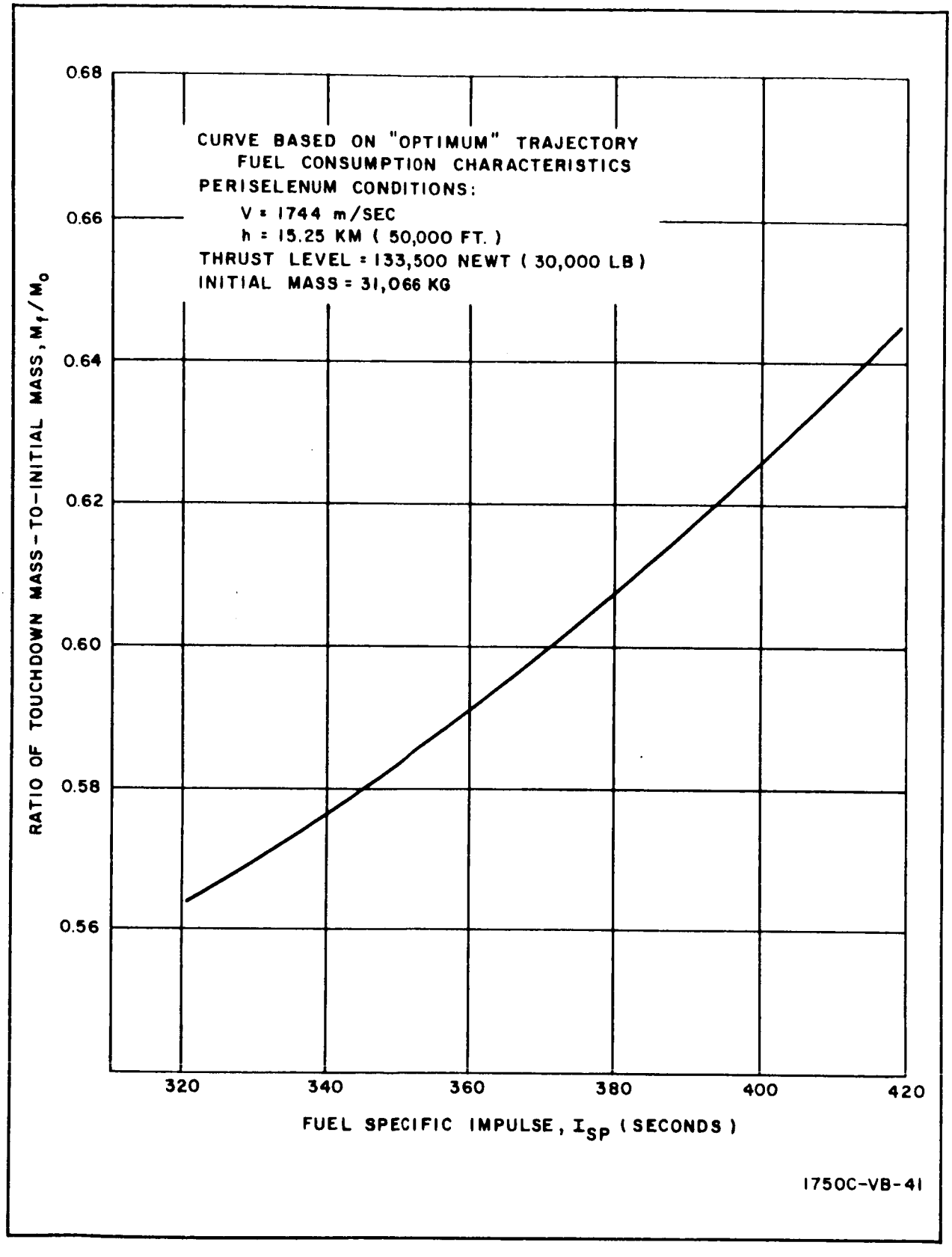

Figure 4-21. Effect of Specific Impulse on Touchdown Mass

It remains to specify the number of engines to be used. This number is selected on the basis of a tradeoff analysis involving nominal periselenum altitude, number of engines, mass remaining at touchdown, and, to some degree, abort considerations. The analysis is discussed in subsection 3.3 of Appendix D (Volume V); the resulting number of engines is two for the nominal mission. Thus the maximum thrust level is 133,500 newtons (30,000 pounds). The digital simulation program is set up with the thrust vector magnitude limited at this value. In the event that the commanded acceleration vector magnitude requires a thrust level exceeding this limit, the thrust vector is pointed in the commanded direction and maximum available thrust is applied.

e. Trajectory. - The modified proportional navigation guidance techniques as used on-board does not require knowledge of a reference trajectory. The guidance commands are obtained from nonlinear equations operating on the estimated values of the state variables. However, in reality there is some particular set of initial conditions that is more desirable than others. Typical reasons for preference are thrust magnitude requirements, landing site visibility, and fuel consumption. These factors are considered in a tradeoff investigation described in subsection 3.3 of Appendix D (Volume V). The values selected as nominal initial (periselenum) conditions are:

R_o = 312.7 km (1.026×10^6 feet)

V_o = 1,723 m/sec. (5654 ft/sec)

h_o = 38.1 km (1.25×10^5 feet)

where V_o and h_o are the initial velocity and altitude respectively.

During descent the guidance mode is switched from MPN to MPN/VT when the range to the fictitious landing site is reduced to 305 meters (1000 feet). Based on digital simulation, the values of R, and $\dot{R}$ at the interface between the two guidance modes are:

R = 496 meters (1,629 feet)

$\dot{R}$ = 43.6 m/sec (-143 ft/sec.)

Knowledge of a reference trajectory is required to implement the linearized adjoint analysis of the terminal portion of the landing maneuver (that portion using MPN/VT guidance). Approximate closed form solutions to the nonlinear differential equations are developed in Appendixes D of both Volumes IV and V for this purpose. These closed form solutions are used to evaluate the time varying coefficients of the linearized equations describing the adjoint of the Landing Guidance, System.

f. Sensor Error Model. - Basically the error model is the same as the general model described in paragraph 4.2.5. The general statements describe the error characteristics at the output of the filter describing sensor dynamics.

Random fluctuation errors are evaluated by means of a linearized error analysis technique, whereas the effects of bias error components are evaluated by using a forward digital simulation of the nonlinear system. The filter transfer functions describing sensor dynamics are not the same in these two approaches. For the linearized analysis, sensor dynamic characteristics are approximated by a second order filter with transfer function $G_{X_i}(s)$ given by

$$G_{X_i}(s) = \frac{1}{1 + \frac{2\zeta_{X_i}}{\omega_{X_i}} s + \frac{s^2}{\omega_{X_i}^2}} \quad \text{(for random error components)} \tag{4-66}$$

X_i = the general state variable

$\zeta_{X_i} = 0.7$

$\omega_{X_i} = 5.0$ rad/sec

On the other hand, bias errors are evaluated assuming a first-order time lag characterization of sensor dynamics:

$$G_{X_i}(s) = \frac{1}{1 + \tau_{X_i}(s)} \quad \text{(for bias error components)} \tag{4-67}$$

(The values of τ_{X_i} used for error analysis are unknown.) In addition, first-order time lags are assumed to be present in the engine responses (lags of 1 and 2 seconds are considered).

The measured values of R, Ω, and their time derivatives occur at the outputs of the sensor filters and are denoted by the symbol (^); e.g., the measured value of R is $\hat{R}$.

No control sensor errors per se are considered in the analysis of modified proportional navigation.

4.3.2.2 Error Analysis

The complete error analysis of lunar landing using the hybrid guidance concept MPN/VT-B is performed in two parts. Bias errors are treated using the digital simulation of the nonlinear Landing Guidance system, and the effects of random fluctuation errors are evaluated using the adjoint error analysis technique.

a. Bias Errors - The degradation of the MPN/VT-B guidance concept by the two types of bias errors (constant magnitude and constant percent) is

determined by means of the same digital simulation program used for determining the error-free performance of the guidance scheme. To do this, the values of R, $\dot{R}$, Ω, and $\dot{\Omega}$ used in the guidance equations are replaced by the measured values of these quantities denoted $\hat{R}$, $\hat{\dot{R}}$, $\hat{\Omega}$, and $\hat{\dot{\Omega}}$.

For this part of the analysis, sensor dynamics are characterized by a simple time lag. In general the measured value of the ith observable can be obtained from the expression

$$\hat{Y}_i(s) = \left[\frac{1}{1 + \tau_{Y_i} s}\right]\left[Y_i(s) + \tilde{y}_{ib} + {}_{Y_i}p_b \frac{Y_i(s)}{100}\right]$$

where $\tilde{y}_{ib}$ and ${}_{Y_i}p_b$ are defined in paragraph 4.2.5. Then

$$\left[1 + \tau_{Y_i} s\right]\left[\hat{Y}_i(s)\right] = Y_i(s) + \tilde{y}_{ib} + {}_{Y_i}p_b \frac{Y_i(s)}{100}$$

and

$$\hat{Y}_i(s) = \frac{Y_i(s) - \hat{Y}_i(s) + \tilde{y}_{ib} + {}_{Y_i}p_b \frac{Y_i(s)}{100}}{\tau_{Y_i} s}$$

The factor s in the denominator indicates an integration. Therefore

$$\hat{Y}_i(t) = \int_0^t \left[\frac{Y_i(t) - \hat{Y}_i(t) + \tilde{y}_{ib} + {}_{Y_i}p_b \frac{Y_i(t)}{100}}{\tau_{Y_i}}\right] dt \qquad (4\text{-}68)$$

Thus the measured values of the state variables are:

$$\hat{Y}_1 \equiv \hat{R} = \int_0^t \frac{R - \hat{R} + R_b + {}_Rp_b \frac{R}{100}}{\tau_R} dt \qquad (4\text{-}69)$$

$$\hat{Y}_2 \equiv \hat{\dot{R}} = \int_0^t \frac{\dot{R} - \hat{\dot{R}} + \dot{R}_b + {}_{\dot{R}}p_b \frac{\dot{R}}{100}}{\tau_{\dot{R}}} dt$$

$$\hat{Y}_3 \equiv \hat{\Omega} = \int_0^t \frac{\Omega - \hat{\Omega} + \Omega_b + {}_\Omega p_b \frac{\Omega}{100}}{\tau_\Omega} dt$$

$$\hat{Y}_4 \equiv \hat{\dot{\Omega}} = \int_0^t \frac{\dot{\Omega} - \hat{\dot{\Omega}} + \dot{\Omega}_b + {}_{\dot{\Omega}}p_b \frac{\dot{\Omega}}{100}}{\tau_{\dot{\Omega}}} dt$$

The digital simulation program integrates the equations of motion forward (starting with the nominal initial values of the state variables) until $Y = 0$. At this time the values of $\dot{Y}$, X, and $\dot{X}$ are printed out, and the effects of the bias errors are ascertained by comparison with error-free performance. (X and Y here refer to the artesion coordinate system centered at the landing site, see figure 4-18.) The digital simulation uses MPN guidance with a fictitious landing site 305 meters (1000 feet) above the nominal landing site over most of the descent. (See paragraph 4.3.2.1.c for the guidance equations.) When $\hat{R}_1$ (observed range to the fictitious landing site) is reduced to 305 meters (1000 feet), the guidance equations are switched to those defining the MPN/VT guidance mode.

The analysis technique is to assign a value to the error components of one of the measurement errors; i.e., R_b and RP_b, the range measurement errors. All other bias error components are set equal to zero. Then the simulation program is run, making use of equations 4-69. The terminal values of $\dot{Y}$, X, and $\dot{X}$ that result are the terminal errors produced by bias errors in the range information sensor. Information concerning the effects of range-rate, angle, and angle-rate measurement bias errors is obtained in a similar manner.

b. Random Fluctuation Errors. - Random fluctuation errors are evaluated by computing error sensitivity coefficients using the adjoint error analysis technique described in subsections 6.2 of Appendix A and 3.4 of Appendix D (Volume V). The important steps in the adjoint error analysis are:

- Construct a linearized model of nonlinear guidance and control system (block diagram form).
- Derive the block diagram of the adjoint linear system.
- Develop a digital simulation of the adjoint system and use it to compute sensitivity coefficients relating statistical parameters of the random sensor error components ($\tilde{y}_n$ and $Y_i p_n \frac{Y_i}{100}$) to the statistics of the resulting terminal state errors.

The adjoint analytical technique is applied only to that portion of the landing maneuver employing MPN/VT guidance equations ($\hat{R}_1$ less than 305 meters, or $\hat{R}$ less than 497 meters). Terminal position and velocity errors are caused primarily by random sensor errors occurring in the final portion of the landing maneuver because of the self-correcting character of the closed loop guidance and control system. (Past experience supports this statement.) This is the reason that only the MPN/VT guided portion of the landing maneuver is analyzed using the adjoint technique.

In the adjoint analysis, sensor dynamics are represented by second-order filters as stated in paragraph 4.3.2.1.d. When error analysis results are discussed, input random fluctuation errors will be characterized by their rms

values: ${}_n\sigma_{Y_i}$ and ${}_p\sigma_{Y_i}$. These quantities refer to sensor noise characteristics at the output of the filter representing the ith sensor. (For the adjoint analysis, white noise is assumed at the sensor inputs.)

4.3.2.3 Results

This paragraph demonstrates the methodology developed to estimate sensor error effects and indicates dynamic range requirements for the nominal lunar landing mission considered herein.

The results and discussions of error analysis presented in this paragraph are pertinent only to the guidance scheme and the nominal mission profile selected in paragraph 4.3.2.1. Since the effect of random errors will be governed by the performance of the guidance system during the final phase of the landing trajectory, random error propagation coefficients will be generated for the MPN/VT portion of the trajectory. Bias errors and dynamic lags will be evaluated by simulating specific bias error levels in the forward trajectory program which considers the entire trajectory. Consequently, the effect of bias errors on fuel consumption is available.

The term "bias error" refers to an error which is random over an ensemble of trajectories but which is fixed for any given trajectory. Hence one can refer to the standard deviation associated with such an error.

The term "random error" or "random disturbance" refers to an error which is random during any single trajectory. This also appears as a "fluctuation error" since the error level fluctuates with time. It is possible to reduce the level of a random error during any given trajectory by means of smoothing, whereas bias errors, although random over an ensemble of trajectories, cannot be reduced by smoothing during the course of any given trajectory.

a. Sensor Error Effects for the MPN/VT-B Guidance Concept. - The accuracies with which range, range rate, line-of-sight angle, line-of-sight angular rate (defined in paragraph 4.3.2.1.a) must be measured depend upon attendant fuel penalties and allowable touchdown condition deviations. Sensor accuracy requirements generated herein will be appropriate only for the reference mission profile selected in paragraph 4.3.2.1; namely the MPN/VT-B guidance concept with thrust limited to 133,500 newtons (30,000 pounds) maximum.

The first results to be presented are the sensitivity coefficients generated by the adjoint error analysis. These coefficients relate the mean squared terminal deviations in Y, $\dot{Y}$, X, and $\dot{X}$ to the mean squared values of the random sensor errors which cause them according to the matrix equation given below:

$$\begin{bmatrix} \sigma_Y^2 \\ \sigma_{\dot{Y}}^2 \\ \sigma_X^2 \\ \sigma_{\dot{X}}^2 \end{bmatrix} = \begin{bmatrix} k_{11} & k_{12} & k_{13} & k_{14} \\ k_{21} & k_{22} & k_{23} & k_{24} \\ k_{31} & k_{32} & k_{33} & k_{34} \\ k_{41} & k_{42} & k_{43} & k_{44} \end{bmatrix} \begin{bmatrix} {}_n\sigma_R^2 \\ {}_n\sigma_{\dot{R}}^2 \\ {}_n\sigma_\Omega^2 \\ {}_n\sigma_{\dot{\Omega}}^2 \end{bmatrix} + \begin{bmatrix} k'_{11} & k'_{12} & k'_{13} & k'_{14} \\ k'_{21} & k'_{22} & k'_{23} & k'_{24} \\ k'_{31} & k'_{32} & k'_{33} & k'_{34} \\ k'_{41} & k'_{42} & k'_{43} & k'_{44} \end{bmatrix} \begin{bmatrix} {}_p\sigma_R^2 \\ {}_p\sigma_{\dot{R}}^2 \\ {}_p\sigma_\Omega^2 \\ {}_p\sigma_{\dot{\Omega}}^2 \end{bmatrix}$$

Here, X and Y refer to the cartesian coordinate system centered at the landing site (see figure 4-18). Since the quantities ${}_p\sigma^2$ and ${}_p\sigma^2$ are set equal to zero for this analysis, the third and fourth columns of matrix of primed coefficients are not computed. With this fact into account, the numerical values of the two sensitivity coefficients are as follows:

$$\begin{bmatrix} k_{11} & k_{12} & k_{13} & k_{14} \\ k_{21} & k_{22} & k_{23} & k_{24} \\ k_{31} & k_{32} & k_{33} & k_{34} \\ k_{41} & k_{42} & k_{43} & k_{44} \end{bmatrix} = \begin{bmatrix} 1.59 \times 10^{-1} & 1.98 \times 10^{-1} & 3.49 \times 10^{-2} & 5.40 \times 10^{1} \\ 1.08 \times 10^{0} & 1.25 \times 10^{0} & 8.64 \times 10^{-2} & 1.32 \times 10^{2} \\ 9.54 \times 10^{-15} & 1.10 \times 10^{-13} & 5.63 \times 10^{-9} & 3.39 \times 10^{-7} \\ 1.69 \times 10^{-14} & 5.29 \times 10^{-14} & 5.29 \times 10^{-10} & 5.11 \times 10^{-8} \end{bmatrix}$$

$$\begin{bmatrix} k'_{11} & k'_{12} \\ k'_{21} & k'_{22} \\ k'_{31} & k'_{32} \\ k'_{41} & k'_{42} \end{bmatrix} = \begin{bmatrix} 7.78 \times 10^{-6} & 1.23 \times 10^{-5} \\ 3.78 \times 10^{-3} & 3.54 \times 10^{-5} \\ 1.62 \times 10^{-17} & 6.48 \times 10^{-17} \\ 4.45 \times 10^{-18} & 9.49 \times 10^{-18} \end{bmatrix}$$

These coefficients are used to evaluate sensor capability expected to exist in the 1970 time period. These typical sensor error levels are presented in table 4-5. Three degrees of sensor error are postulated: low, medium, and high.

Table 4-6 gives the individual contributions of each random error source to the total terminal mean squared position and velocity deviations for each of the three levels of sensor capability. In general it can be seen that the horizontal error components, σ_X^2 and $\sigma_{\dot{X}}^2$ are small enough to be considered negligible. However, the vertical error components, especially $\sigma_{\dot{Y}}^2$ (vertical velocity) are not negligible. Table 4-6 shows that the rms terminal velocity error increases sharply as the sensor error level increases, as expected.

TABLE 4-5

TYPICAL SENSOR ERROR LEVELS (USED FOR SAMPLE COMPUTATION)

Error Source	Symbolic Designation And Units	Random Errors (1σ)			Bias Errors (1σ)		
		Error Level			Error Level		
		Low	Medium	High	Low	Medium	High
Range observation	${}_n\sigma_R$ (m)	0.61	1.52	3.05	-	-	-
	${}_p\sigma_R$ (%)	0.2	0.5	1.0	-	-	-
	R_b (m)	-	-	-	0.305	0.61	3.05
	${}_bp_R$ (%)	-	-	-	0.2	0.5	2.0
Range rate observation	${}_n\sigma_{\dot{R}}$ (m/sec)	0.0305	0.152	0.61	-	-	-
	${}_p\sigma_{\dot{R}}$ (%)	0.05	0.20	0.50	-	-	-
	$\dot{R}_b$ (m/sec)	-	-	-	0.0305	0.152	0.61
	${}_{\dot{R}_d}q$ (%)	-	-	-	0.05	0.20	0.50

TABLE 4-5 (Continued)

Error Source	Symbolic Designation And Units	Random Errors (1σ)			Bias Errors (1σ)		
		Error Level			Error Level		
		Low	Medium	High	Low	Medium	High
Line-of-sight angle observation	${}_n\sigma_\Omega$ (rad)	0.0001	0.0002	0.001	-	-	-
	${}_p\sigma_\Omega$ (%)	0.0	0.0	0.0	-	-	-
	Ω_b (rad)	-	-	-	0.001	0.005	0.010
	${}_bP_\Omega$ (%)	-	-	-	0.0	0.0	0.0
Line-of-sight angle rate observation	${}_n\sigma_{\dot\Omega}$ (rad/sec)	0.00003	0.0001	0.0002	-	-	-
	${}_p\sigma_{\dot\Omega}$ (%)	0.0	0.0	0.0	-	-	-
	$\dot\Omega_b$ (rad/sec)	-	-	-	0.00003	0.0001	0.0002
	${}_bP_{\dot\Omega}$ (%)	-	-	-	0.0	0.0	0.0

TABLE 4-6

RESULTS OF SAMPLE COMPUTATION SHOWING TERMINAL EFFECTS OF RANDOM SENSOR ERRORS

Error Source		Terminal Mean Squared Error Components											
		Low Sensor Error Level				Medium Sensor Error Level				High Sensor Error Level			
		$\sigma^2_{Y_i}$	$\sigma^2_{Y_i}$	$\sigma^2_{X_i}$	$\sigma^2_{\dot{X}_i}$	$\sigma^2_{Y_i}$	$\sigma^2_{\dot{Y}_i}$	$\sigma^2_{X_i}$	$\sigma^2_{\dot{X}_i}$	$\sigma^2_{Y_i}$	$\sigma^2_{\dot{Y}_i}$	$\sigma^2_{X_i}$	$\sigma^2_{\dot{X}_i}$
Range measurement	$n\sigma^2_R$	0.059	0.400	3.54×10^{-15}	6.26×10^{-15}	0.366	2.48	2.20×10^{-14}	3.88×10^{-14}	1.48	10.0	8.90×10^{-14}	1.57×10^{-13}
	$p\sigma^2_R$	3.11×10^{-5}	1.51×10^{-4}	6.48×10^{-19}	1.78×10^{-19}	1.94×10^{-4}	9.42×10^{-4}	4.05×10^{-18}	1.11×10^{-18}	7.75×10^{-4}	3.77×10^{-3}	1.62×10^{-17}	4.44×10^{-18}
Range rate measurement	$n\sigma^2_{\dot{R}}$	1.84×10^{-4}	1.16×10^{-3}	1.02×10^{-16}	4.92×10^{-17}	4.60×10^{-3}	2.90×10^{-2}	2.55×10^{-15}	1.23×10^{-15}	7.35×10^{-2}	4.65×10^{-1}	4.08×10^{-14}	1.97×10^{-14}
	$p\sigma^2_{\dot{R}}$	3.08×10^{-8}	8.85×10^{-8}	1.62×10^{-19}	2.37×10^{-20}	4.93×10^{-7}	1.42×10^{-6}	2.59×10^{-18}	3.85×10^{-19}	3.08×10^{-6}	8.86×10^{-6}	1.62×10^{-17}	2.41×10^{-18}
Angle measurement	$n\sigma^2_{\Omega}$	3.49×10^{-4}	8.64×10^{-4}	5.63×10^{-11}	5.29×10^{-12}	1.40×10^{-3}	3.45×10^{-3}	2.25×10^{-10}	2.11×10^{-11}	3.50×10^{-2}	8.62×10^{-2}	5.62×10^{-9}	5.27×10^{-10}
Angle rate measurement	$n\sigma^2_{\dot{\Omega}}$	4.86×10^{-2}	1.19×10^{-1}	3.05×10^{-10}	4.60×10^{-11}	5.40×10^{-1}	1.32×10^{0}	3.38×10^{-9}	5.10×10^{-10}	2.16×10^{0}	5.28×10^{0}	1.35×10^{-8}	2.04×10^{-9}
Total mean squared error (rss)		0.108 $(\text{meters})^2$	0.521 $(\text{m/sec})^2$	3.61×10^{-10} $(\text{meters})^2$	0.513×10^{-10} $(\text{m/sec})^2$	0.912 $(\text{meters})^2$	3.83 $(\text{m/sec})^2$	36.0×10^{-10} $(\text{meters})^2$	5.31×10^{-10} $(\text{m/sec})^2$	3.76 $(\text{meters})^2$	15.8 $(\text{m/sec})^2$	1.91×10^{-8} $(\text{meters})^2$	25.7×10^{-10} $(\text{m/sec})^2$
Total rms Error		0.329 meters	0.722 m/sec	1.90×10^{-5} meters	7.16×10^{-6} m/sec	0.955 meters	1.96 m/sec	6.00×10^{-5} meters	2.31×10^{-5} m/sec	1.94 meters	3.98 m/sec	1.38×10^{-4} meters	5.07×10^{-5} m/sec

In addition, the most significant contributors to the terminal velocity errors are range measurements and line-of-sight angular rate measurements. This is true for all three sample levels of sensor capability.

Next the effect of the bias components of sensor error are considered. Estimates of bias error effects can be obtained through the use of the adjoint analysis technique, but they are not in this study. Rather the forward digital simulation program is used with the bias errors introduced by means of the equations discussed in paragraph 4.3.2.2.a. Thus the bias error analysis is not subject to the assumptions attendant to linearization and provides the effect of sensor bias error components on X, $\dot{X}$, and $\dot{Y}$ at the true touchdown point, Y = 0. This analysis technique also allows one to determine the effects of bias error components on fuel consumption.

As described in subsection 3.1 of Appendix D (Volume V) the digital simulation program accepts both types of bias error components (constant magnitude and constant percent, scale factor) in all observed quantities. As in the analysis of random errors, three degrees of sensor capability are selected. (These are given in table 4-5.) The bias error components indicated in table 4-5 are applied to the landing vehicle during the entire landing trajectory (periselenum to touchdown), and the values of X, $\dot{X}$, $\dot{Y}$, and the total fuel consumed are determined at the point Y = 0. The results are given in tables 4-7, 4-8, and 4-9, which show dynamic errors (X, $\dot{X}$, and $\dot{Y}$) and the total fuel consumption respectively. The results contained in these tables are discussed in the following paragraphs. Recall that the bias error components are assumed to be independent (see paragraph 4.3.2.2.a) so that the total error figures quoted in table 4-7 are the root sum square of the individual contributors. (Statistical quantities refer to averages taken over the ensemble of possible missions.)

It is pertinent to point out that the range and range-rate bias error components are introduced into the computer simulation in such a manner as to cause the control law to command less acceleration (a_R) than that required if sensor errors were not present. If the sign of $\dot{R}_b$ is reversed, then the spacecraft tends to approach the landing site more slowly, and a softer landing results. Likewise reversing the sign of range bias causes the spacecraft to arrive at a hover point a distance R_b meters above the landing site. Proper termination of engine thrust would likewise result in a softer landing. (If R_b equals 0.61 meters [2 feet], and a_R equals 1.31 meters/second^2 from the hover point to touchdown, the terminal value of $\dot{Y}$ is -0.61 meters/second. This is a softer touchdown than that shown in table 4-7 for the case R_b = 0.61 meters).

Using the numerical results given in tables 4-6 and 4-7, the touchdown velocity standard deviations are computed for each sensor error level in the

manner indicated by the following example performed with results corresponding to the low sensor error level.

$$\begin{pmatrix}\text{Touchdown velocity}\\ \text{Standard deviation}\end{pmatrix} = \left[(1\sigma \text{ bias deviation})^2 + (1\sigma \text{ random deviation})^2\right]^{1/2}$$
$$= \left[(1.01)^2 + (0.723)^2\right]^{1/2}$$
$$= 1.24 \text{ meters/ second}$$

This represents the 1σ velocity deviation. The 99 percent confidence level is 2.5 times the 1σ deviation, which is 3.08 meters per second for the sample case. The total touchdown velocity error is 3.46 meters per second when the 0.381 meter-per-second error contributed by dynamic lag is included. (Dynamic lag errors are not statistical in nature and thus are added directly to the 99 percent confidence level.) Maximum touchdown velocities with a 99 percent confidence level for all three sensor error levels are summarized in table 4-10. These results indicate that rather stringent accuracy requirements will be imposed upon the sensors if the MPN/VT-B guidance concept is used all the way to the touchdown point.

A possible way to overcome this difficulty is to use the MPN/VT guidance concept to arrive at a hover point above the desired landing site and to devise a separate guidance concept (likely to be manual for manned missions) for the hover-to-touchdown maneuver. The penalties to be paid for this capability are a slightly increased fuel requirement and possibly a more complex guidance and control system.

Table 4-10 shows the effect of sensor bias error components and engine dynamic lag upon total fuel consumption. In all cases the fuel usage figure has been adjusted, in the event that a hard landing is indicated, by the magnitude of $\dot{Y}$; that is, if ΔV is 1800 meters/per second to the point $Y = 0$ with Y at the corresponding time equal to -15 meters/per second, then the ΔV recorded in table 4-9 is 1815 meters/per second. The digital simulation program is run once for each bias error level listed in table 4-9.

b. Sensor Dynamic Range Requirements. - If it is necessary to obtain relative measurements from the spacecraft to the landing site prior to the time of landing-engine ignition to avoid gross errors in the initial conditions for descent, the navigation sensor system must be able to acquire the landing site beacon prior to reaching periselenum of the synchronous descent orbit. Since the nominal range from periselenum to the landing site depends on the initial thrust-to-mass ratio, the acquisition range requirement is also a function of this quantity. For the nominal case investigated herein (periselenum altitude equals 38.1 kilometers or 125,000 feet, line-of-sight range at periselenum is approximately 300 kilometers (10^6 feet). Consequently the sensor is to be capable of 99 percent probability of acquisition at approximately a 300-kilometer range.

TABLE 4-7

BREAKDOWN OF TOUCHDOWN ERRORS CAUSED BY SENSOR BIAS ERRORS

Error Level	Error Source	Symbolic Designation, Value, and Unit	Touchdown Errors		
			$\dot{Y}$ (m/sec)	X(m)	$\dot{X}$ (m/sec)
	Range Observation	$R_b + {}_R p_b \left(\frac{R}{100}\right) = 0.305 + 0.002\ R$ (meters)	-0.915	0.0	0.0915
Low	Range Rate Observation	$\dot{R}_b + {}_{\dot{R}} p_b \left(\frac{\dot{R}}{100}\right) = 0.0305 + 0.005\ \dot{R}$ (meters/sec)	-0.336	0.0	0.0153
	Angle Observation	$\Omega_b + {}_{\Omega} p_b \left(\frac{\Omega}{100}\right) = 0.00003 + 0$ (radians)	0.0	0.0	0.0
	Angle Rate Observation	$\dot{\Omega}_b + {}_{\dot{\Omega}} p_b \left(\frac{\Omega}{100}\right) = 0.00003 + 0$ (rad/sec)	0.0	0.0	0.0
	Root Sum Square Errors		-0.975	0.0	0.0915
Medium	Range Observation	$R_b + {}_R p_b \left(\frac{R}{100}\right) = 0.61 + 0.005\ R$ (meters)	-1.68	0.0	0.0915
	Range Rate Observation	$\dot{R}_b + {}_{\dot{R}} p_b \left(\frac{\dot{R}}{100}\right) = 0.1525 + 0.002\ \dot{R}$ (meters/sec)	-0.746	0.0	0.0153
	Angle Observation	$\Omega_b + {}_{\dot{\Omega}} p_b \left(\frac{\Omega}{100}\right) = 0.0001 + 0$ (radians)	0.0	0.0	0.0
	Angle Rate Observation	$\dot{\Omega}_b + {}_{\dot{\Omega}} p_b \left(\frac{\dot{\Omega}}{100}\right) = 0.0001 + 0$ (rad/sec)	-0.061	0.0	0.0
	Root Sum Square Errors		-1.83	0.0	0.0915

TABLE 4-7 (Continued)

Error Level	Error Source	Symbolic Designation, Value, and Unit	Touchdown Errors		
			$\dot{Y}$ (m/sec)	X (m)	$\dot{X}$ (m/sec)
High	Range Observation	$R_b + {}_R p_b \left(\frac{R}{100}\right) = 3.05 + 0.02\,R$ (meters)	-5.19	0.0	0.244
	Range Rate Observation	$\dot{R}_b + {}_{\dot{R}} p_b \left(\frac{\dot{R}}{100}\right) = 0.61 + 0.005\,\dot{R}$ (meters/sec)	-2.08	0.0	0.0762
	Angle Observation	$\Omega_b + {}_\Omega p_b \left(\frac{\Omega}{100}\right) = 0.1 + 0$ (radians)	-0.061	0.0	0.0
	Angle Rate Observation	$\dot{\Omega}_b + {}_{\dot{\Omega}} p_b \left(\frac{\dot{\Omega}}{100}\right) = 0.0002 + 0$ (rad/sec)	-0.122	0.0	0.0
	Root Sum Square Errors		-5.55	0.0	0.256

TABLE 4-8

TOUCHDOWN ERRORS CAUSED BY ENGINE LAG

Engine Dynamic Lag τ	Touchdown Errors		
	$\dot{Y}$ (m/sec)	X (m)	$\dot{X}$ (m/sec)
0 (no lag)	0	0	0
1 second	0.762	0	0
2 second	0.381	0	0

TABLE 4-9

EFFECT OF SENSOR BIAS ERRORS AND ENGINE LAGS ON FUEL CONSUMPTION. (AS MEASURED BY THE PARAMETER ΔV.)

Sensor Bias Errors (1σ) or Engine Lay	Total ΔV Required, (mps) Periselenum to Touchdown
Nominal: no error, no lag	1871
Dynamic Lag: $\tau = 2$ sec	1874
Range bias: $R_b + {}_R p_b \left(\frac{R}{100}\right) = 0.305 + 0.002\ R$ (m)	1873
Range bias: $R_b + {}_R p_b \left(\frac{R}{100}\right) = 0.61 + 0.005\ R$ (m)	1874
Range bias: $R_b + {}_R p_b \left(\frac{R}{100}\right) = 3.05 + 0.02\ R$ (m)	1872
Range Rate bias: $\dot{R}_b + {}_{\dot{R}} p_b \left(\frac{\dot{R}}{100}\right) = 0.0305 + 0.0005\ \dot{R}$ (m/sec)	1874
Range Rate bias: $\dot{R}_b + {}_{\dot{R}} p_b \left(\frac{\dot{R}}{100}\right) = 0.152 + 0.002\ \dot{R}$ (m/sec)	1875
Range Rate bias: $\dot{R}_b + {}_{\dot{R}} p_b \left(\frac{\dot{R}}{100}\right) = 0.61 + 0.005\ \dot{R}$ (m/sec)	1874
Angle bias: $\Omega_b + {}_{\Omega} p_b \left(\frac{\Omega}{100}\right) = 0.00003 + 0$ (rad)	1875
Angle bias: $\Omega_b + {}_{\Omega} p_b \left(\frac{\Omega}{100}\right) = 0.1 + 0$ (rad)	1872
Angle Rate bias: $\dot{\Omega}_b + {}_{\dot{\Omega}} p_b \left(\frac{\dot{\Omega}}{100}\right) = 0.00003 + 0$ (rad/sec)	1875
Angle Rate bias: $\dot{\Omega}_b + {}_{\dot{\Omega}} p_b \left(\frac{\dot{\Omega}}{100}\right) = 0.0001 + 0$ (rad/sec)	1878

TABLE 4-10

MAXIMUM TOUCHDOWN VELOCITY (99 PERCENT CONFIDENCE LEVEL)

Sensor Error Level	1 σ Velocity Errors Caused By Bias Error (meters/sec)	1 σ Velocity Errors Caused By Random Error (meters/sec)	Combined Velocity Error, (1σ) (meters/sec)	99 Percent Maximum Touchdown Error Confidence Level (2.5 σ)* (meters/sec)	Velocity Error Caused By Engine Lag (2 sec) (meters/sec)	Overall 99 Percent Touchdown Velocity Confidence Level (meters/sec)
Low	0.975	0.721	1.21	3.03	0.381	3.41
Medium	1.83	1.97	2.69	6.73	0.381	7.13
High	5.55	3.98	6.82	17.1	0.381	17.5

* Because the bias errors represent "worst case" 1σ values, the 99 percent confidence level is assumed to correspond to the 2.5σ error level. Actually, 99 percent of all events are included between ±2.65σ for the normal distribution.

Table 4-11 indicates the sensor dynamic range requirements for navigation and guidance from periselenum to touchdown for the nominal trajectory.

TABLE 4-11

SENSOR DYNAMIC RANGE REQUIREMENTS

Observable	Dynamic Range	
	High	Low
Range	300 km	0 km
Range rate	2000 m/sec	0 m/sec
LOS Angle*	120 deg	0 deg
LOS Angle rate	50 mr/sec	0 mr/sec
* This depends upon the method of LOS angle determination over the horizon.		

4.3.2.4 Conclusions

Results and conclusions drawn from the preceding effort are summarized in the following statements.

- A combination of two proportional navigation guidance laws provides a guidance concept which approaches an optimum fuel trajectory over most of the flight and then makes a vertical approach to touchdown.

- Terminal vertical velocity errors are significant for all three assumed levels of sensor capability. Terminal vertical position and horizontal position and velocity errors are not critical even at the high sensor error level assumed.

- The most significant random error contributions to the terminal velocity error are range observation and line-of-sight angle rate observation. This suggests the use of low error level sensors for these observations and higher error level sensors for the remaining observables.

- Sensor bias errors contribute significantly to the terminal velocity error at all three assumed levels and must be kept as low as possible. Bias errors in the observation of range and range rate are the most critical.

- The increase in fuel consumption caused by engine lag and sensor bias errors is not particularly significant. If the largest increases for each error source in table 4-9 are added directly (this is pessimistic), the total increase in ΔV is 21 meters/per second or approximately 1 percent of the nominal ΔV requirement.

4.4 COMPARATIVE DISCUSSION OF GUIDANCE CONCEPTS

This final subsection is a comparative discussion of the two lunar landing guidance concepts analysed: linear predictive guidance, and modified proportional navigation with vertical touchdown capability.

Direct comparison of the two system models is not possible in many areas, because of differences in system parameters and analytical constraints; e.g., initial mass and engine size constraints. As a result, the material presented in this subsection is restricted to a comparison of nominal fuel consumption (as indicated by the quantity ΔV) and a comparison of mean squared terminal errors resulting when identical navigation sensors and sensor accuracies are assumed. In addition, brief consideration is given to the relative computational requirements and sensor dynamic range requirements of the two approaches.

4.4.1 Nominal Fuel Consumption.

The basis for comparison of fuel consumption is the curves of nominal ΔV required to complete the nominal descent maneuver as a function of nominal initial altitude presented in figure 4-22. Curves are illustrated for the linear predictive guidance gravity-turn trajectory (LPG), a modified proportional navigation trajectory with no vertical touchdown provision (MPN), a modified proportional navigation trajectory with vertical touchdown (MPN/VT-B), and the optimum trajectory derived in subsection 1.2 of Appendix D (Volume V). The MPN/VT-B curve is estimated on the basis of one point and comparison with the MPN curve and so is probably somewhat in error. However, the general form is believed to be correct. The LPG curve is based on a specific impulse of 400 seconds and terminal point 500 meters above the lunar surface. All other curves use a specific impulse of 420 seconds and 0 terminal altitude.

To provide a better basis for comparison, an estimated LPG curve is developed for 420 seconds specific impulse and zero terminal altitude. This estimated curve along with the MPN curves and the optimum characteristic are shown in figure 4-23. The LPG curve is corrected to zero terminal altitude by subtracting 500 meters (nominal hover altitude) from the initial altitude axis in figure 4-22. Thus the ΔV figure at 20.0 kilometers originally corresponds to 19.5 kilometers in figure 4-23. This is the curve labeled "LPG, zero terminal altitude, I_{sp} = 400 sec." From this curve the zero altitude 420-second-I_{sp} curve is estimated by determining the sensitivity of ΔV to a change in I_{sp} for the constant-thrust gravity-turn LPG trajectory and using this parameter to estimate the ΔV versus h_o curve for I_{sp} = 420 seconds. Quantity

$$S_{\Delta V}^{I_{sp}} \quad .$$

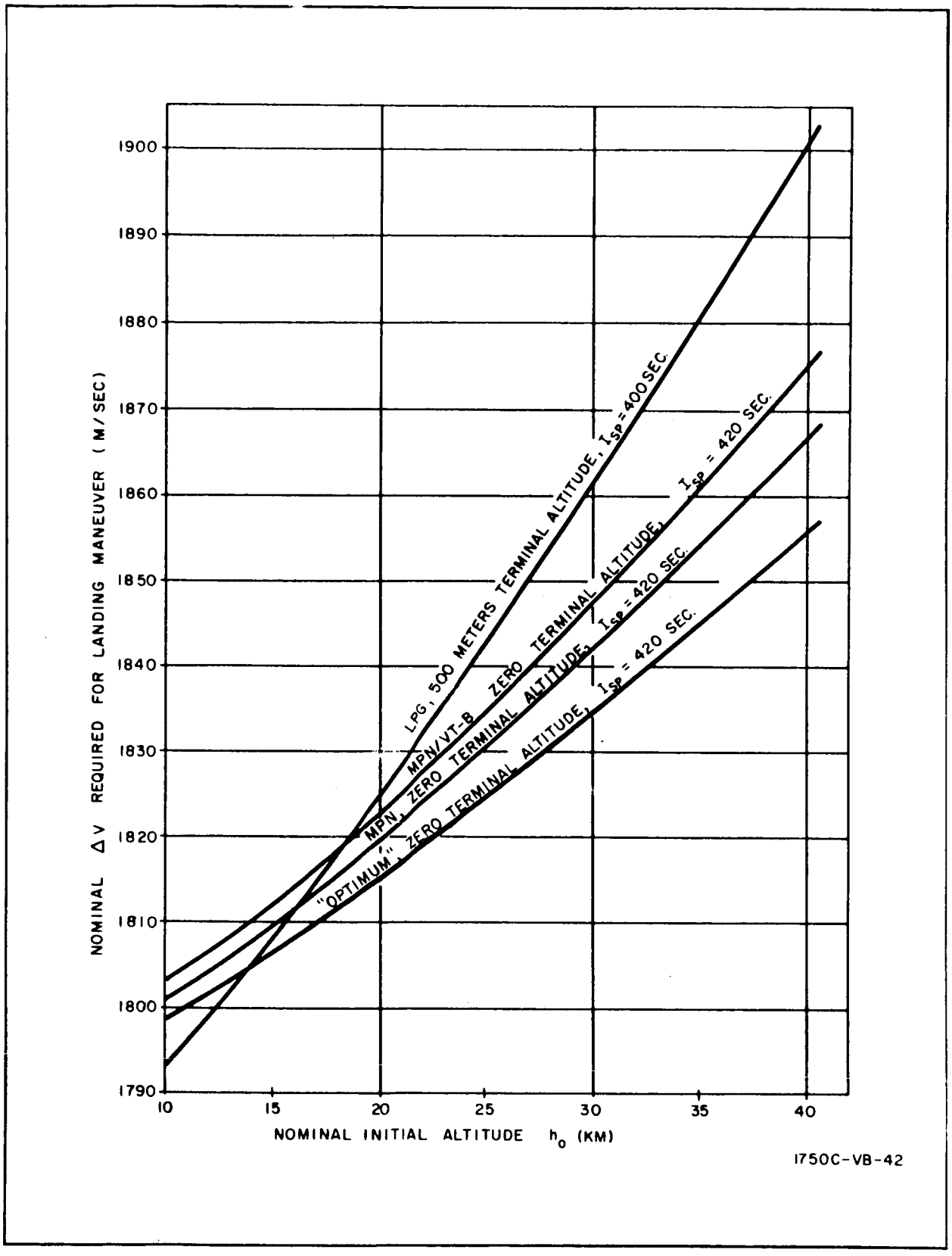

Figure 4-22. Comparative ΔV Requirements

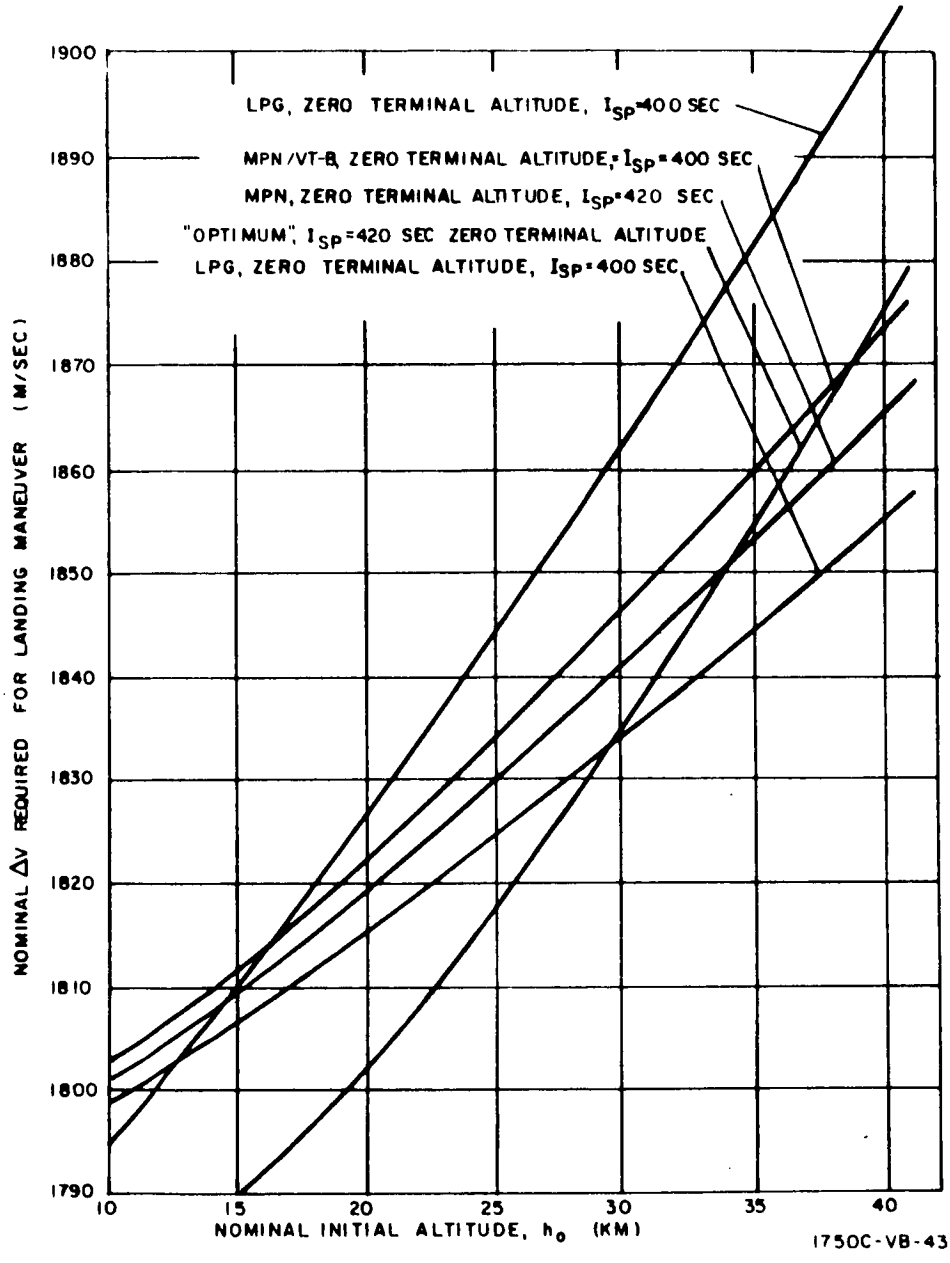

Figure 4-23. Comparative ΔV Requirements (After Normalization)

is defined to be the sensitivity of ΔV to a change in I_{sp} as determined from the expression

$$S_{\Delta V}^{I_{sp}} = \frac{\partial(\Delta V)}{\partial(I_{sp})} \left(\frac{I_{sp}}{\Delta V} \right) \tag{4-71}$$

where ΔV is given by the following expression for a constant thrust trajectory

$$\Delta V = I_{sp}\, g_o \ln \left[\frac{m_o}{m_o - \dfrac{T_o\, t_f}{I_{sp}\, g_o}} \right] \tag{4-72}$$

Increasing specific impulse generally decreases the total amount of fuel required to perform a given maneuver. With regard to a constant-thrust landing trajectory this implies that the product $T_o\, t_f$ must decrease as I_{sp} increases. (T_o is the constant-thrust level, t_f is the total time of flight, and the product is directly proportional to actual fuel consumption.) The determination of

$$S_{\Delta V}^{I_{sp}}$$

which follows is based on the assumption that the product $(T_o\, t_f)$ is constant. The value of

$$S_{\Delta V}^{I_{sp}}$$

resulting is too high, but this is seen to be a pessimistic approximation in the following sense. The gravity turn fuel consumption curve (LPG) shown in figure 4-23 for I_{sp} = 420 seconds is actually pessimistic. If the variations of T_o and t_f with increasing I_{sp} are considered, the actual value of ΔV corresponding to a given initial altitude is lower than that shown. The equation for

$$S_{\Delta V}^{I_{sp}}$$

subject to the indicated approximation is

$$S_{\Delta V}^{I_{sp}} = 1 - \frac{T_o\, t_f}{g_o\, I_{sp}} \left[\frac{1}{\left(m_o - \dfrac{T_o\, t_f}{I_{sp}\, g_o} \right) \ln \left(\dfrac{m_o}{m_o - \dfrac{T_o\, t_f}{I_{sp}\, g_o}} \right)} \right] \tag{4-73}$$

The change in ΔV resulting from a given change in specific impulse, $\delta(I_{sp})$ is

$$\delta(\Delta V) = S_{\Delta V}^{I_{sp}} \quad \frac{\Delta V}{I_{sp}} \quad \delta(I_{sp}) \tag{4-74}$$

where all quantities are evaluated on the known curve. To illustrate, the change in ΔV at h_o = 19.5 kilometers is calculated. Parameters corresponding to 19.5 kilometers on the I_{sp}-equals-400-seconds curve in figure 4-23 are given below.

T_o = 48,212.5 newtons

t_f = 344.3 seconds

I_{sp} = 400 seconds

ΔV = 1827.5 meters per second

m_o = 11,340 kilograms

g_o = 9,807 meters per second^2

The calculated value of

$$S_{\Delta V}^{I_{sp}}$$

is -0.275. Thus

$$\delta(\Delta V) = (-0.275)\,\frac{(1827.5)}{400}\,\delta I_{sp}$$

when $\delta(I_{sp})$ = 20 seconds, $\delta(\Delta V)$ is seen to be -25.2 meters per second, and the value of ΔV corresponding to h_o equals 19.5 km is estimated to be 1802 meters per second for a specific impulse of 420 seconds. Repeating this process at other values of h_o yields the curve shown in figure 4-23.

It can be seen that the estimated gravity turn ΔV requirement curve is below the optimum curve for h_o less than 29 kilometers. Thus there seems to be a contradiction. Actually no contradiction exists. The optimum curve is only optimum for the set of constraints under which it is generated (minimum time trajectory from a given initial altitude using a given constant-thrust level). The gravity-turn trajectory is derived using a different set of constraints, so that it is quite reasonable that differing and perhaps less stringent ΔV requirements result. Note that the slopes of these two curves differ significantly also.

This subsection compares the two types of nominal trajectories on the basis of information generated during the course of study. Information presented shows that the gravity turn offers a somewhat more economical landing at low altitudes, whereas this advantage decreases and eventually reverses sign as the nominal initial altitude increases. Perhaps the most important conclusion to be drawn, though, is that caution must be used when

the word optimum is applied to a landing maneuver. One must always include the assumptions and restrictions under which optimization is performed.

4.4.2 Comparison of Terminal Errors

In this paragraph the terminal error characteristics of the two navigation and guidance concepts are compared when identical random error characteristic are present at the input. Only random error effects are compared because no bias error information is available for the linear predictive guidance system. Table 4-12 contains this comparative information. The assumed rms navigation sensor errors are in the second column. The individual components of the mean squared terminal errors are generated by using the sensitivity coefficients presented in paragraphs 4.3.1.3 and 4.3.2.3 respectively. The H-θ guidance mode is selected so that the same observables are used in each system. It is not possible to use the same initial altitude for the two systems. However, rough extrapolation of results obtained for linear predictive guidance to the 38.1-kilometer initial altitude used by the MPN/VT guidance concept shows that the total mean squared errors would differ from those presented in table 4-12 for h_o = 30 kilometers by only a slight amount.

It is important to recall that the linear predictive guidance error estimates are upper limits and are therefore pessimistic. Results corresponding to modified proportional navigation guidance are obtained from linearized analysis of the actual closed loop system and cannot be called either optimistic or pessimistic. Comparatively the rms terminal altitude and velocity errors corresponding to linear predictive guidance are smaller (particularly velocity). This is particularly interesting since error estimates using linear predictive guidance are known to be pessimistic.

Horizontal position errors are apparently much smaller with MPN/VT-B guidance, although this cannot be stated positively because of the pessimistic nature of LPG error estimates. In any event neither estimate of horizontal deviations is significantly large. Horizontal position error estimates for linear predictive guidance are obtained by multiplying mean squared central angle errors by the square of mean lunar radius.

4.4.3 Onboard Computation

Consideration of the relative onboard computational requirements of the two guidance concepts is not really within the scope of this study. However, a few general remarks can be made on the basis of basic characteristics of the guidance systems.

Perhaps the most obvious computational difference between linear predictive guidance and modified proportional navigation is the reference trajectory

TABLE 4-12

COMPARISON OF TERMINAL ERRORS

		Linear Predictive Guidance Beacon Tracker Observables H-θ Guidance Mode h_o = 30 km; τ_o = 1 sec			MPN/VT-B Beacon Tracking Observables h_o = 38.1 km		
Navigation Errors Source	RMS Sensor Errors (low sensor errors table 4-7)	Altitude Errors (m^2)	Horizontal Errors (m^2)	Velocity Errors $(m/sec)^2$	Altitude Errors (m^2)	Horizontal Errors (m^2)	Velocity Errors $(m/sec)^2$
Range measurement	${}_n\sigma_R$ = 0.61 m	0.00053	0.00014	0.00100	0.059	0.00004×10^{-10}	0.400
	${}_p\sigma_R$ = 0.2 %	0.00374	0.00680	0.00348	0.00003	0.00000×10^{-10}	0.00015
Range rate measurement	${}_n\sigma_{\dot{R}}$ = 0.0305 m/s	0.00016	0.00009	0.00002	0.00018	0.00000×10^{-10}	0.00116
	${}_p\sigma_{\dot{R}}$ = 0.05 %	0.00016	0.00155	0.00660	0.00000	0.00000×10^{-10}	0.00000
Line-of sight angle measurement	${}_n\sigma_\phi = {}_n\sigma_\Omega = 10^{-4}$ rad	0.00000	0.00001	0.00001	0.00035	0.563×10^{-10}	0.00086
	${}_p\sigma_\phi = {}_p\sigma_\Omega$ = 0.0	0.0	0.0	0.0	0.0	0.0	0.0
Line-of-sight angle rate measurement	${}_n\sigma_{\dot{\phi}} = {}_n\sigma_{\dot{\Omega}} = 3 \times 10^{-5}$ rad/sec	0.086	0.00189	0.00254	0.0486	3.05×10^{-10}	0.119
	${}_p\sigma_{\dot{\phi}} = {}_p\sigma_{\dot{\Omega}}$ = 0.0	0.0	0.0	0.0	0.0	0.0	0.0
Total mean squared errors		0.0906	0.0105	0.0136	0.108	3.61×10^{-10}	0.521
Total root mean squared errors		0.301 meters	0.125 meters	0.170 m/sec	0.329 meters	1.90×10^{-5} meters	0.722 m/sec

information required by the former. There are several ways of making this reference data available:

- Precomputation of reference trajectory and storage of trajectory data in tabular or analog form

- Storage of reference initial conditions and the equations of motion reference trajectory computed on board by integration (storage requirements reduced compared to previous method)

- Precomputation of reference trajectory and approximation of state variable time functions by low order polynominals (This approach offers reduced storage requirements without necessitating integration. Some inaccuracy is introduced, but this can be kept to a minimum by careful selection of the approximating functions).

The modified proportional navigation guidance concept does not require reference trajectory knowledge on board the landing vehicle.

If both concepts use the same observables and the same state variables, the navigational computations required are identical. It is obvious from paragraph 4.3.2.1.b that navigation computations can be minimized by making the state variables and observables identical.

In general each of the guidance concepts can use time-varying gain parameters in the guidance equations. When this is the case, the time functions must be stored in the onboard computer. Of the two specific concepts considered herein, linear predictive guidance requires considerably more storage capacity for gain parameters. No special effort has been made to reduce this requirement with respect to linear predictive guidance. It is very likely that investigation into the nature of the linear predictive guidance gain parameters will reveal that good system performance characteristics can be maintained when these parameters are approximated by simple time functions (perhaps constants in some cases), thereby reducing onboard computation requirements.

Overall, the linear predictive guidance concept is expected to require greater onboard computer capacity, primarily because of the need to store reference trajectory data.

4.4.4 Sensor Dynamic Range

If the two systems use the same combination of sensors, the sensor dynamic range requirements are identical for all practical purposes. This is determined primarily by the overall similarity of the mission profiles assumed for analysis of linear predictive guidance and modified proportional navigation. Typical dynamic range requirements are given in table 4-11.

5. LUNAR ASCENT PHASE

5.1 INTRODUCTION

This section deals with the ascent phase of the lunar mission. Specifically this study is concerned with determining the feasibility of a given guidance system and specifying the requirements for sensors used during the boost phase of the lunar ascent to rendezvous. Only conventional guidance schemes are considered and these are evaluated only to the extent necessary to establish sensor requirements.

The sensor requirements are determined on the basis of errors associated with position and velocity prediction. This requires the selection of a navigation method and a specific system configuration. Actual hardware in terms of types and numbers must be named.

For a mission of this type, it is desirable to specify the minimum accuracies required of the sensors. The choice of a guidance system can be made somewhat arbitrarily by selecting very accurate sensors and a computer with comparable accuracy; however, very accurate sensors and the attendant supporting equipment plus a computer which has computational capabilities that are greater than needed entails a severe system weight penalty. Any weight put into orbit from the moon must initially start from earth, be put into an earth orbit, than a lunar orbit, and then landed on the lunar surface. By specifying minimum sensor requirements, the initial cost and weight penalty are kept to a minimum. The accuracy of the sensors and the weight of the system together with the type of ascent trajectory selected are principal factors which determine fuel requirements.

The scope of this portion of the lunar mission study is to determine the sensors required for two different types of ascents - a parking and a direct ascent. Each type has its advantages. This study does not rule out either ascent in favor of the other since such a choice must take into consideration factors other than sensor accuracies.

The following is a glossary of notations used in this section.

σ	standard deviation
x, y, z	navigational coordinates
α	angle of inclination between two orbital planes
H	specific angular momentum
$\mu = GM$	gravitational constant of moon
G	universal gravitational constant
M	mass of moon
T	rocket thrust
m	mass of vehicle
R	radial distance from lunar center to vehicle
A_x, A_z	thrust acceleration components
$\psi(t)$	thrust inclination with respect to z-x plane in navigational reference
Δh	position error of vehicle
Δv	velocity error of vehicle
ϕ_f	central angle traversed during boost
ΔS	vehicle position error along trajectory
Δy	vehicle position error normal to orbit plane
Δr	vehicle position error radial to orbit plane
ΔV_r	radial velocity error of vehicle
ΔV_T	tangential velocity error of vehicle
ΔV_N	normal velocity error of vehicle
$d_{11}, d_{12}, \ldots d_{66}$	elements of transfer matrix
$\Delta a_{x, y, z}$	acceleration error components
a_{ni}	accelerometer error coefficients where
n	0, 1, 2, ... 7
i	x, y, z
$\phi_{x,y,z}$	gyro angular velocity error
b_{ni}	gyro error coefficients where
n	0, 1, 2, 3
i	x, y, z
ϕ_{xy}	platform misalignment error
$\phi_{xy}(0)$, $\phi_{xz}(0)$, $\phi_{yz}(0)$	initial platform misalignment
e_x, e_y, e_z	platform servo error
p_{ij}, q_{ij}	platform deformation where i and j take on cyclical values of x, y, z

5.2 BACKGROUND

This portion of the lunar mission makes use of the Apollo vehicle parameters when required even though the present study is for post-Apollo missions. This allows the use of an existing vehicle design rather than attempting to predict the design of a post-Apollo vehicle. The physical configuration of the vehicle has no direct bearing on the choice of the guidance schemes or sensors.

However, the lunar ascent employs an optimized boost trajectory which requires the use of certain performance parameters. The choice of the Apollo vehicle is also in keeping with the rest of the lunar mission.

No attempt is made to consider all possible guidance schemes since such a task would involve more time and effort than the present study allows. Certain simplified guidance schemes depend heavily upon the human operator performing in an alien environment under relatively unknown circumstances. Consequently, the choice of a guidance scheme is conservative and is based upon "true and tried" techniques.

5.2.1 Description of Problem

A description of the lunar ascent includes the launch site, the trajectory kinematics, and the terminal target conditions. The launch site description consists primarily of approximating the error expectation which will be encountered. The ascent trajectory kinematics are influenced by the type of boost trajectory and the type of ascent chosen. The types of ascents are categorized as minimum time, minimum energy, parking, and direct.

The orbit of the target vehicle is assumed to be circular at an altitude of 200 kilometers. The ascent-to-rendezvous maneuver consists of launching at a predetermined time to attain a prescribed kinematic juxtaposition of space, time, and velocity.

The overall sensor selection is influenced by the type of guidance scheme chosen, the trajectory kinematics, the error expectation at the launch site, the vehicle performance parameters, and the terminal target kinematic conditions. The actual sensor specifications are based on the errors associated with position and velocity prediction. The ascents are optimized with respect to fuel to achieve rendezvous for a set of prescribed conditions and mission constraints. For example, a minimum time ascent requires maximum fuel expenditure; however, fuel requirements are held to a minimum for this particular type of ascent by employing an optimized boost trajectory.

5.2.2 Definition and Comparison of Parking and Direct Ascents

Two methods of ascent are considered from the lunar surface to terminal rendezvous, a direct ascent and a parking ascent. Both types of ascents employ an optimum boost trajectory consistent with the minimum fuel constraint. The target vehicle is assumed to be in a circular orbit at an altitude of 200 kilometers above the mean lunar surface.

The following definitions are adopted:

a. Direct ascent: Two types of direct ascents are considered. (1) A minimum energy ascent characterized by a powered boost phase from launch to an intermediate 30-kilometer orbit followed by a Hohmann orbit coast phase which terminates at target acquisition. (2) A minimum time ascent characterized by a powered boost trajectory from launch to final target acquisition. (See figure 5-1.)

b. Parking ascent: A powered boost phase yielding an intermediate circular orbit which after an arbitrary time delay may be followed by injection into a transfer orbit which terminates in target acquisition. (See figure 5-2.)

The minimum energy ascent should be qualified. Theoretically, such a mission would be accomplished by thrusting tangentially at the launch site to attain the required velocity to achieve a Hohmann transfer to terminal rendezvous. Such an ascent is not possible nor practical to try to approximate. The thrust cutoff at 30 kilometers facilitates terrain avoidance and the safety of the mission. The minimum time ascent should also be qualified since such an ascent is minimum time only within the mission constraints. The ascent time can be reduced further by the expenditure of additional fuel.

The intermediate orbits are assumed to be concentric and coplanar with the target orbit for both types of ascents. A nominal 30-kilometer orbit is chosen for both ascents to tie in with the analysis of the rendezvous portion of the lunar mission.

The minimum energy (short boost) and minimum time (long boost) ascents are chosen in order to give an upper and lower bound on the class of direct ascent trajectories. The sensor accuracies are determined for both ascent trajectories.

Two different intermediate orbits at nominal heights of 30 and 150 kilometers are chosen for the parking ascent to rendezvous. Both intermediate orbits have higher angular rates than the target at 200 kilometers with the consequence that the interceptor can adjust its angular position relative to the target vehicle prior to injection into an elliptic transfer orbit. The parking orbit thus allows extra time between boost and the final transfer maneuver.

The boost phase of the direct ascent requires minimal timing errors prior to launch and during the thrust period. Any timing deviations at the cutoff point must be made up by fuel expenditure some time during the transfer orbit.

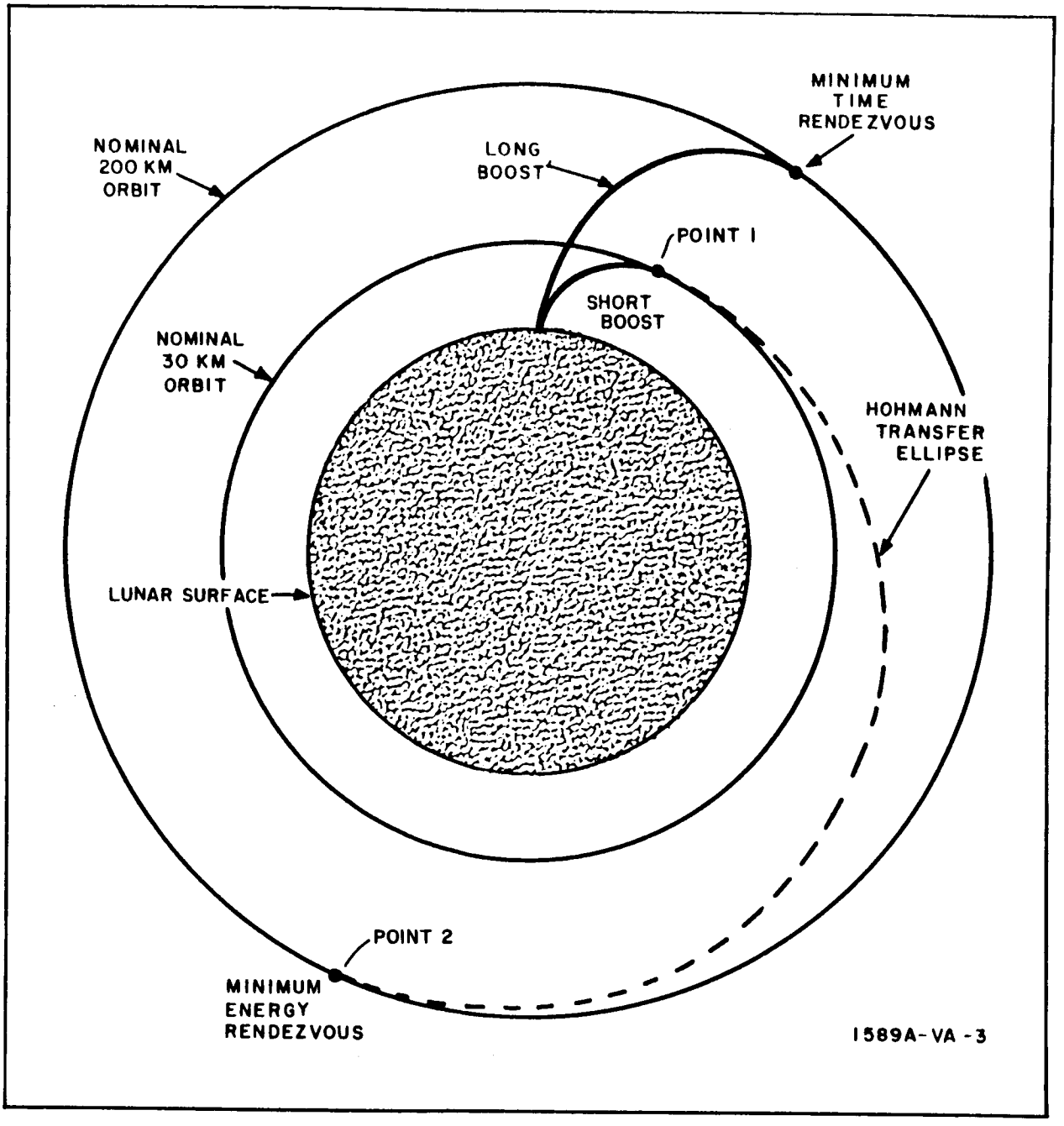

Figure 5-1. Direct Ascent to Rendezvous

For a typical lunar rendezvous with a low altitude target orbit, the orbital velocity is approximately 1.6 km/sec. Hence, a countdown delay of a few tenths of a second can result in a miss distance of a several tenths of a kilometer if uncorrected. Should there be insufficient fuel to compensate for this delay, the only choice with a passive target is to delay the launch until the target has completed another orbit.

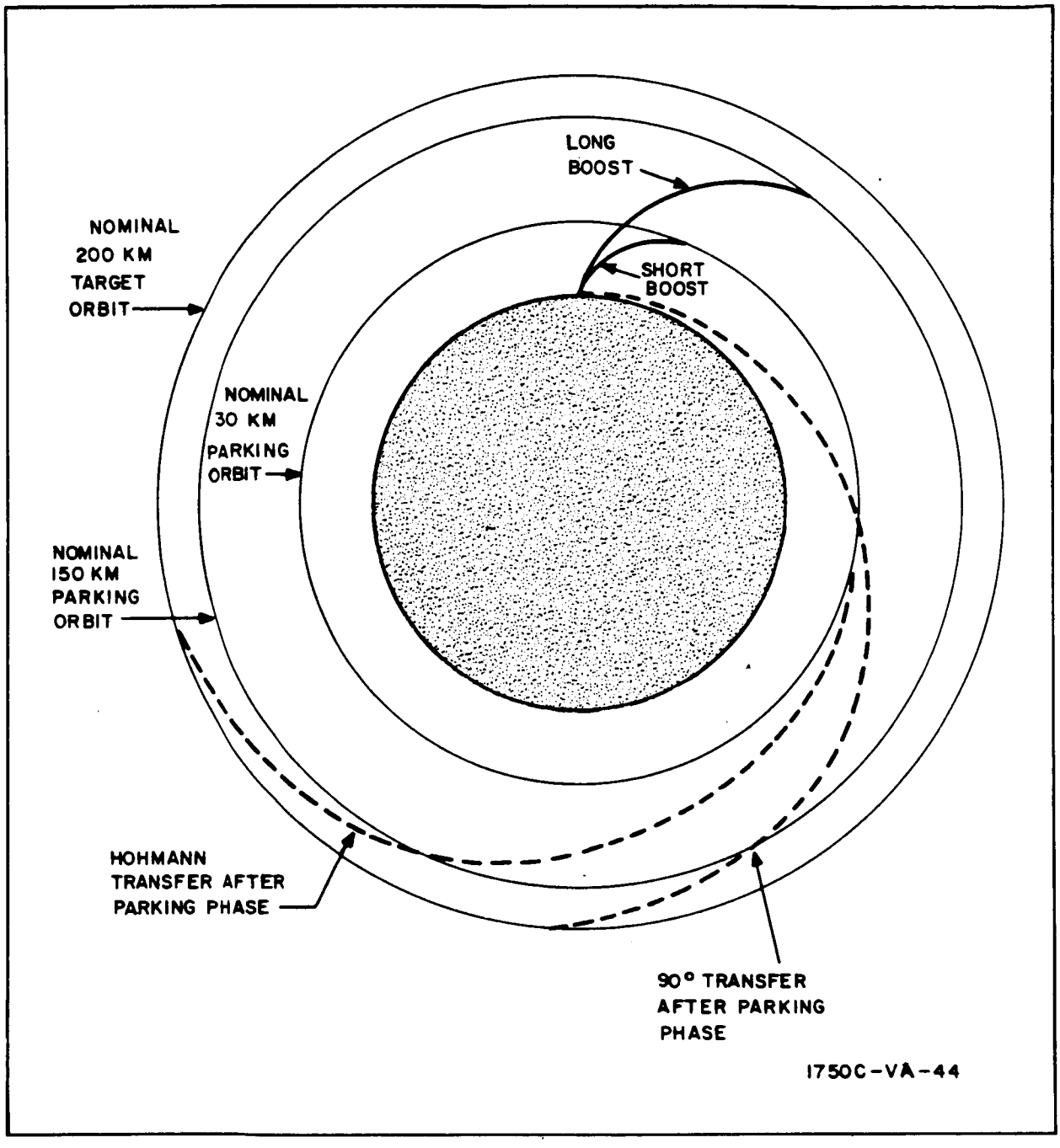

Figure 5-2. Parking Ascent to Rendezvous

A comparison of both ascents indicates that, neglecting launch delays and the flight times, the nominal fuel consumption is very nearly the same if the thrust cutoff altitudes are the same. Regardless of the method selected many techniques and equations are common to both especially when an optimized boost trajectory is employed. If the additional fuel requirement is less important than that needed for a quick rendezvous time, then the direct ascent

is indicated. On the other hand, the parking orbit facilitates launch at all times during the exploration period. Operationally, this is a distinct advantage if an abort situation should arise. It should be noted that the time in the parking orbit can be made any length desired as long as the period of the target orbit and the relative positions of the two vehicles are compatible.

It is not to be assumed that the sensor requirements of one ascent are necessarily more stringent than the other. It is difficult to recommend either ascent on the basis of the required sensor accuracies. The mission constraints and the conditions which develop during the mission could be the decisive factors.

The relative advantages and disadvantages of the two types of ascents are listed below:

a. Launch delays are more critical for direct ascent.
b. Errors committed prior to injection into the coast phase could cause a direct ascent to be converted into a parking ascent.
c. Direct ascent does not handle out-of-plane launches as easily as the parking ascent.
d. Direct ascent requires less restarting of rocket engines.
e. Direct ascent can require more fuel.
f. Parking ascent requires more time.
g. Parking ascent allows extra time between boost and injection phase to compensate for launch delays.
h. Long periods in parking orbit will require more life support equipment.
i. Parking ascent requires more accurate sensors if position is not updated.

5.2.3 Assumptions

The following assumptions were used:

a. The vehicle is assumed to be capable of constant thrust during the boast phase.
b. Thrust can be terminated when required during the boost phase and restarted when required.
c. The vehicle has a self-contained inertial guidance system.
d. The target vehicle is assumed passive during the ascent; however, both vehicles can communicate with each other.
e. The observables at launch are direction and magnitude of the gravity vector and time.
f. The observables during flight are linear acceleration, angular displacement, and time.
g. The target vehicle has the capability of determining its orbital parameters.

h. The lunar parameters are

r_m = 1738 km = mean radius of the moon,

μ = 4.9×10^3 km^3/sec^2 ≐ GM where G is the gravitational constant and M is the mass of the moon.

i. The target orbit is assumed circular with a 200-km altitude.

5.3 ANALYSIS

5.3.1 Background Analysis

5.3.1.1 Selection of Navigation System

The direct ascent consists of a powered boost and a ballistic trajectory which terminates at the target vehicle. The parking ascent is similar with the difference being the parking orbit phase of the mission. Both trajectories suggest the use of ballistic missile guidance techniques. The ballistic trajectory of a missile is established when the required position, velocity, and direction of the velocity vector are established at thrust termination. The errors at the target, ignoring gravitational anomalies and atmospheric effects at the target (which do not exist in a lunar atmosphere), are a function of the errors in position, velocity, and attitude at thrust termination.

The choice of a means of navigating from the launch site to terminal rendezvous becomes apparent. The experience with inertial systems in ballistic missiles is quite extensive. Very accurate systems in varying stages of complexity are available as off-the-shelf-items. Such a system offers a method capable of furnishing all the elements required for guidance in a self-contained unit requiring only inertial quantities and time.

An inertial system is chosen for this study. The sensor accuracies are based on the boost phase of the ascent and the permissible errors at thrust termination.

5.3.1.2 Error Criterion

To conduct an error analysis, some standard must be set up as a reference upon which to base the final results. This standard is the allowable error in position and velocity that can be tolerated at the initiation of the Hohmann transfer coast phase from a nominal 30-kilometer parking orbit. The assumption is arbitrarily made that a 3-σ error in any one injection parameter will not result in more than a 20 percent increase in fuel consumption over the nominal case (zero error) utilizing the Hohmann orbit transfer. The fuel consumption for the nominal case denotes the total fuel required for injection into the Hohmann transfer ellipse and synchronization at the target orbit. The 3-σ errors in position and velocity are:

Δh = 1.4 kilometers (3 σ value)
ΔV = 1.5 meters/sec (3 σ value)

The errors are extracted from table 1 of Appendix F (Volume V).

The error analysis for the sensors is based on the short boost trajectory for both direct and parking ascents since the error criterion is specified for that altitude. The same error coefficients are used in conjunction with the long boost acceleration profiles for the sensor specifications associated with the long boost.

5.3.1.3 Trajectory Determination

a. Ascent Trajectory Selection and Subphases - The ascent trajectory is initiated at launch and ends with terminal rendezvous at the target vehicle. The ascent is considered in two separate classes for purposes of this study, a direct and a parking ascent.

For the direct ascent, two trajectories have been chosen. A powered ascent from launch terminating at target acquisition using an optimized boost trajectory accomplishes rendezvous in a minimum time and, consequently, with a maximum fuel expenditure. An alternate ascent course is a minimum energy trajectory which becomes a maximum time for the direct ascent. The minimum energy ascent is accomplished by a powered boost from launch to a 30-kilometer nominal orbit from which a Hohmann transfer is initiated directly to attain terminal rendezvous. The range angle for this ascent after thrust cutoff is 180 degrees. See figure 5-1. These two ascents represent a maximum and minimum energy bound for the direct ascent trajectories.

The parking ascent is very similar to the minimum energy direct ascent. The parking ascent is initiated using a powered boost from launch to some intermediate orbit from which, after a prescribed coast time, the launch vehicle is injected into an elliptic transfer orbit which terminates at the target vehicle. Two parking ascents have been considered, a short boost from launch to a nominal 30-kilometer altitude and a long boost to a 150-kilometer altitude. These two altitudes bracket a family of parking ascent trajectories. The 30-kilometer orbit gives a close comparison with the direct ascent to the same altitude. Ascent above the nominal 150-kilometer altitude might as well be accomplished by the direct ascent route.

All ascents use an optimized boost phase. A vertical boost height of 1.5 kilometers is used for all launches for terrain avoidance. For purposes of this study, the range angle will be defined as the angle measured from the point of injection at the initiation of the coast phase to the point of terminal rendezvous. The maximum range considered is 180 degrees for a Hohmann transfer. For determining the sensor specifications, range angles less than 180 degrees are not considered although for the actual ascent mission different

range angles could be included in the guidance computer to give flexibility to the ascent trajectory. If the range angle is less than 57 degrees a failure of the rocket at terminal rendezvous would result in an intersection of the orbit and the lunar surface with obvious disastrous results.

b. Launch Site Definition - For determination of sensor requirements, the boost trajectory is considered as a two-dimensional problem. This assumption affords an analytical simplification and does not detract from the basic problem. Consequently, the launch site, the boost trajectory, and the target lie in the same plane.

Under actual conditions, errors in establishing the target orbit and uncertainties of the spin axis of the moon will result in a launch site that is not located in the orbit plane with the result that an out-of-plane ascent must be made. For such considerations, when thrust is applied normal to the orbiting plane, the resulting motion will be a combination of precession of the nodes and a change in the orbit inclination. When a velocity increment is applied normal to the orbit at some point remote from the nodes of the existing and desired orbit, the maneuver will be inefficient since part of the fuel expended will cause a precession of the nodes rather than a change of the orbit plane. The change in inclination between the existing orbit and the desired orbit is given by (Ref. 5-1, Chapter 2):

$$\Delta\alpha = \frac{r\Delta v}{H}$$

where

Δv = the velocity increment normal to the orbit plane
H = the specific angular momentum of the orbiting vehicle
r = radius of the orbit
$\Delta\alpha$ = angle of inclination between the existing and the desired orbit.

The above equation is for the case where the thrust is at the line of nodes. It can be seen that $\Delta\alpha$ varies inversely as the specific angular momentum. This would imply that for the direct ascent any changes in the launch plane be made from as low an altitude as possible to conserve fuel.

c. Boost Trajectory - For launch from a planetary body into an orbit, the usual technique consists of a short vertical takeoff followed by a gravity turn phase. For boost trajectories from the lunar surface where no atmosphere exists, the heating and bending from aerodynamic loads are not present with the consequence that an optimized boost may be employed starting at takeoff.

The equations of motion for an airless ascent are:

$$\ddot{x} + \frac{\mu x}{R^3} = \frac{T}{M} \cos \psi = A_x \tag{5-1}$$

$$\ddot{z} + \frac{\mu z}{R^3} = \frac{T}{M} \sin \psi = A_z \tag{5-2}$$

where

μ	$= GM = 4.900 \times 10^3 \ km^3/sec^2$
G	= universal gravitational constant
M	= mass of the moon
T/m	= thrust to mass ratio
m	= mass of the vehicle
A_x, A_z	= thrust acceleration along x and z axes.

The quantities T/m and ψ are functions of time and the trajectory depends on how they vary. If T/m is assumed a known function of time, the problem becomes one of selecting $\psi(t)$ for a maximum tangential velocity at a specified altitude. These equations assume no gravity anomalies and are based on a two dimensional analytical model. The geometry of the problem is shown in figures 5-3 and 5-4.

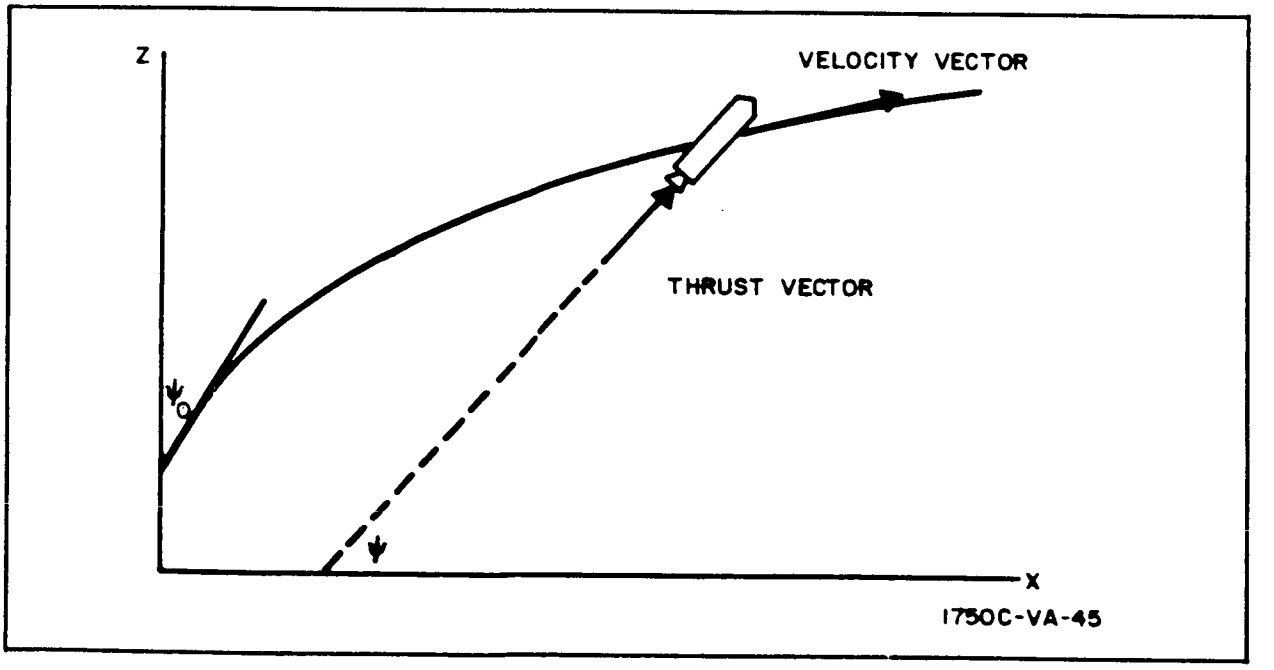

Figure 5-3. Optimum Boost Geometry

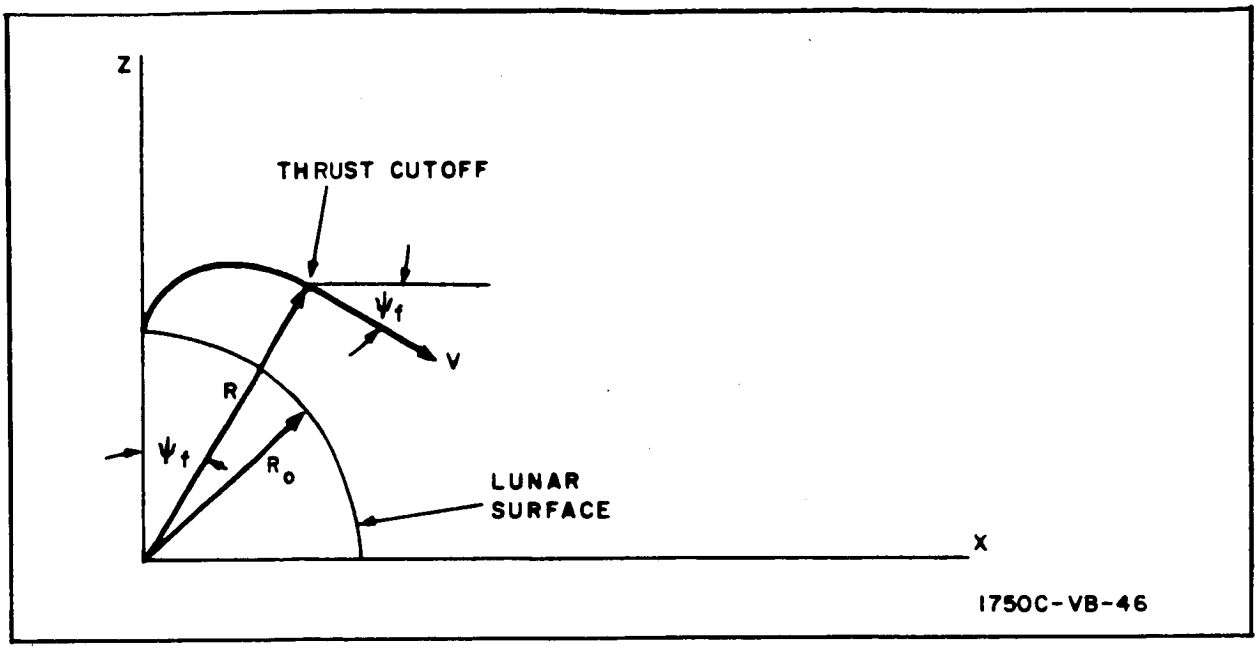

Figure 5-4. Geometry of Boost Trajectory

It should be noted that an analytical solution of the nonlinear simultaneous equations 5-1 and 5-2 is not known. The constraint requiring a maximum tangential velocity at a specific altitude results in a linear tangent relation,

$$\tan \psi = \tan \psi_o - bt. \tag{5-3}$$

Equation 5-3 defines ψ as a function of time, t, and maximizes the mass in orbit. An approximate solution using the linear tangent relationship is given by MacKay (Ref. 5-2). The assumptions are:

a. R is constant during boost
b. T is constant
c. m is a known function of time, defined by equation 5-4.

$$m = m_o + \dot{m}t = \text{mass of vehicle at time t} \tag{5-4}$$

where

m_o = initial mass of the vehicle

$\dot{m}$ = time derivative of mass

Burley and Weber (Ref. 5-3), using a calculus of variations computer program, have obtained optimized lunar boost trajectories. Curves for optimum T/W_o (W_o is lunar surface weight: mg_m), and characteristic velocity versus altitude are shown in figure 5-5. The optimized boost parameters are listed in table 5-1. The thrust accelerations A_x and A_z versus time are plotted in figures 5-6 and 5-7 for the direct and parking ascents respectively.

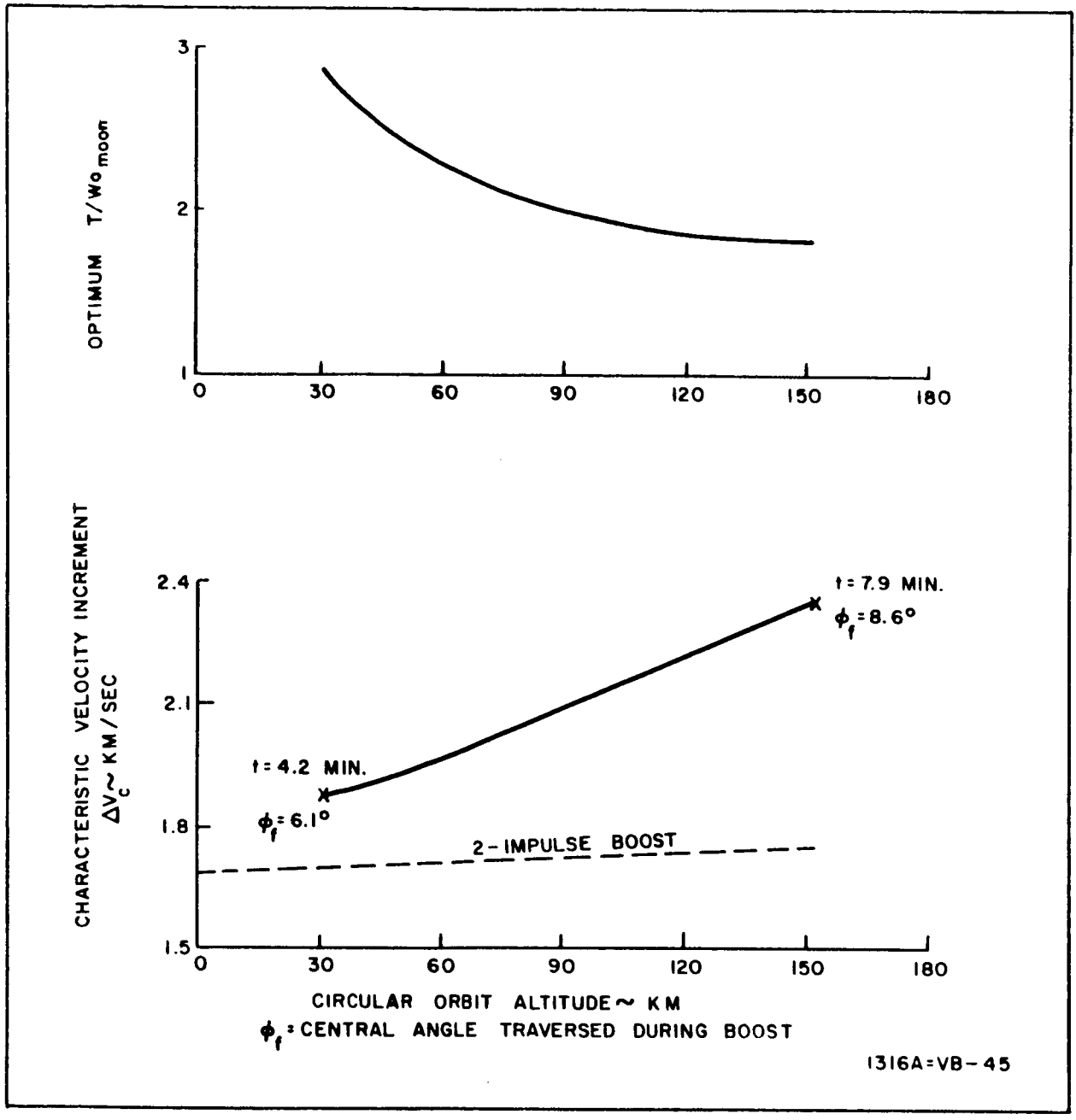

Figure 5-5. Constant Thrust Optimized Lunar Ascent

It should be noted that the linear tangent relationship is derived from the conditions imposed on the boost equations requiring an optimum ascent and does not influence the choice of a guidance system. The linear tangent relation does influence the shape of the thrust acceleration profiles which in turn are used to determine the miss velocity and miss distance coefficients in the error analysis section.

TABLE 5-1

OPTIMIZED BOOST TRAJECTORY PARAMETERS

	Direct Ascent		Parking Ascent	
	Short Boost	Long Boost	Short Boost	Long Boost
1. Thrust cutoff altitude	31.5 km	200 km	30.5 km	152.4 km
2. Cutoff radius	1769.5 km	1938 km	1768 km	1886 km
3. Cutoff velocity	1.702 km/sec	1.590 km/sec	1.665 km/sec	1.613 km/sec
4. Initial T/W_o	3	2	3	2
5. Vertical boost time	30 sec	30 sec	30 sec	42 sec
6. Total boost time	260 sec	460 sec	255 sec	462 sec
7. Central angle traversed	6.38°	8.71°	6.10°	8.62°
8. ψ_o	30°	70°	30.46°	70.16°
9. I_s	300 sec	300 sec	300 sec	300 sec
10. b	3.08×10^{-3} sec^{-1}	7.34×10^{-3} sec^{-1}	3.5×10^{-3} sec^{-1}	8.76×10^{-3} sec^{-1}
	Mean lunar radius assumed for sensor calculations = 1738 km			

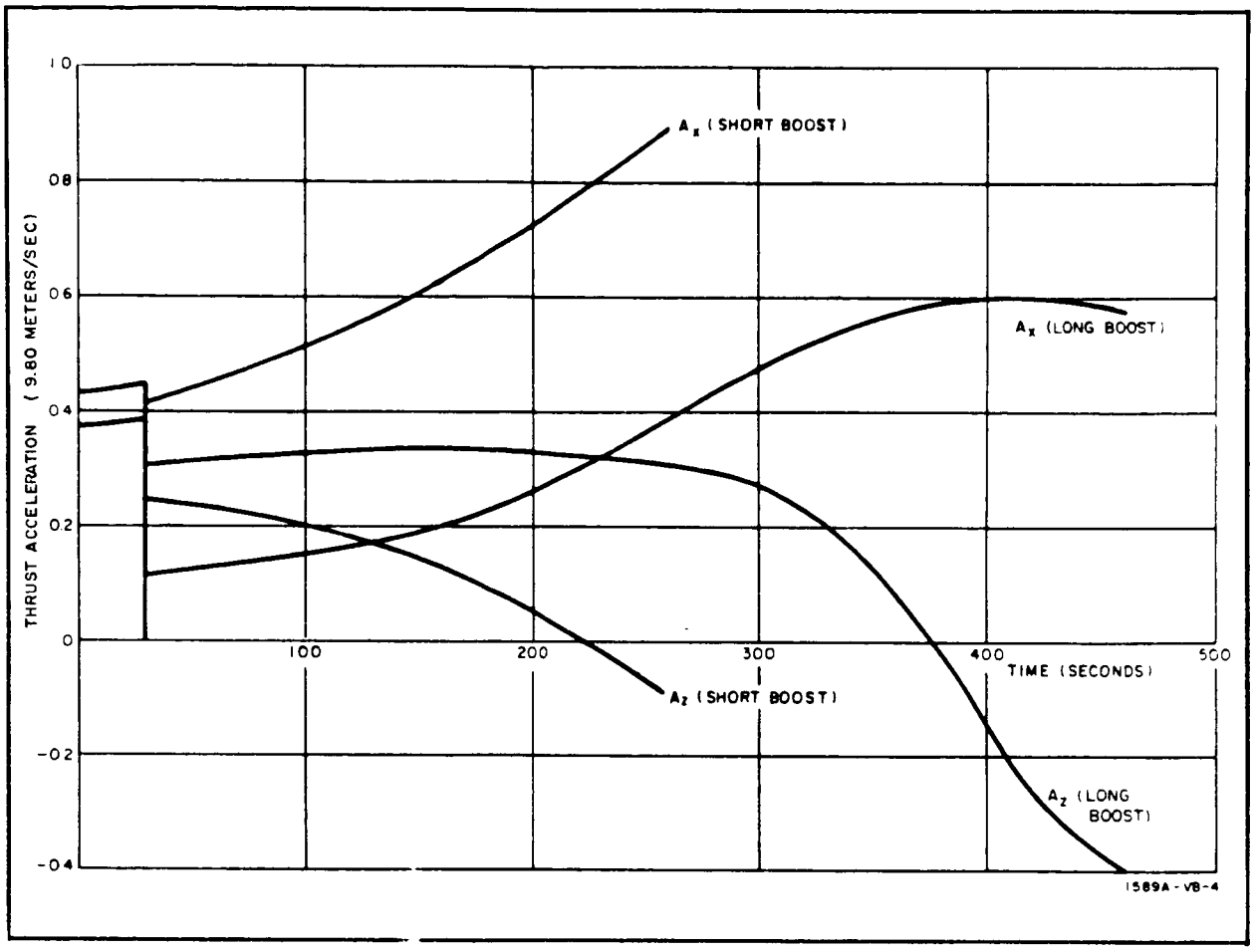

Figure 5-6. Direc Ascent Nominal Boost Acceleration Profiles

d. Target Definition - The target vehicle is assumed to be in a circular orbit at a height of 200 kilometers above the mean lunar surface. Consequently, only two parameters, the constant μ and the circular radius r, are needed to define the target trajectory. Since the value of μ is known prior to the lunar mission, only r need be determined from the orbiting vehicle under the assumptions used for this study.

For the problem of defining minimum sensor requirements, little is gained by varying the other orbital parameters. Under actual conditions, the target vehicle is expected to be in a nearly circular, equatorial orbit.

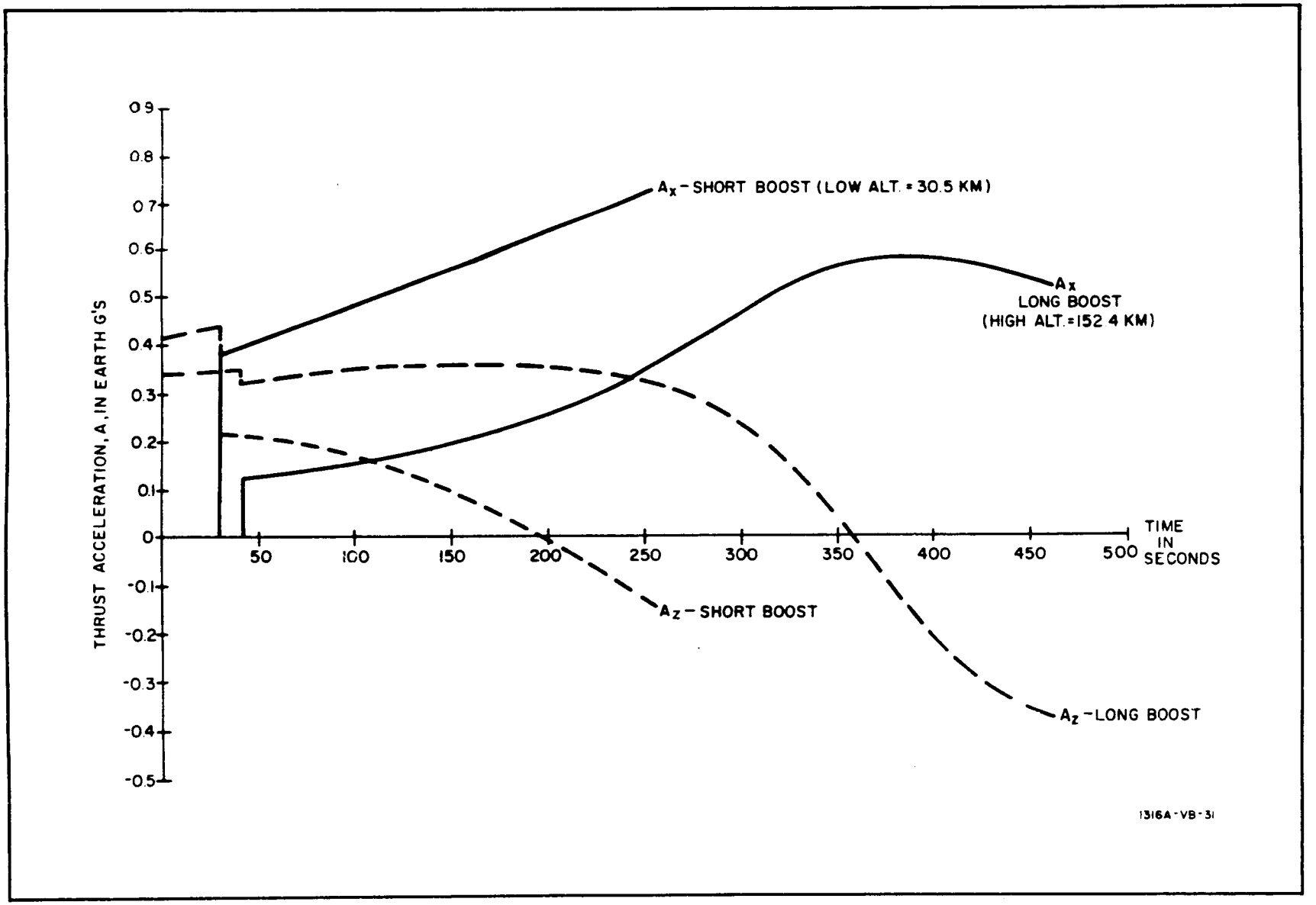

Figure 5-7. Parking Ascent Nominal Boost Acceleration Profiles

5.3.1.4 Guidance Scheme

a. Boost Sensors and Observables - The specification of sensors must be preceded by the selection of the guidance to be used during the boost portion of the lunar ascent. A generalized analysis of the errors associated with the ascent trajectory without specifying the guidance system and sensors is not enough. As previously mentioned, the choice of inertial guidance is indicated by the salient features of the ascent trajectory plus the advantages that such a system has.

Functionally, the inertial system consists of a set of gyros, accelerometers and integrators, a gravity computer, a clock, and a navigation computer. The integrators, gravity computer, clock and navigational computer are all considered as part of the computer.

The observables at launch are the magnitude and direction of the gravity vector and time which may be used to determine the launch position coordinates. During flight, the observables are inertial acceleration, angular displacement, and time.

b. Guidance Mechanization - Guidance navigation for the lunar ascent is performed in a nonrotating reference frame located at the moon's center. The assumption that such a reference frame is equivalent to an inertial reference is reasonable since the orbital motion of the moon relative to the sun and earth does not induce any measurable errors into the guidance system during ascent. Position and velocity within the navigational reference frame are obtained from three orthogonally oriented accelerometers mounted on a gyro-stabilized platform. Orientation of the platform is provided by three single-degree-of-freedom gyros; however, two two-degree-of-freedom gyros can perform equally well. The present state of the art is to use rate-integrating gyros rather than the straight rate sensing instruments. The error analysis technique employed does not differentiate between the two types. The mechanization chosen is referred to as a three-axis space-stabilized inertial system.

Either an analog or digital computer can be used with an inertial guidance system. Errors associated with analog computation in inertial systems are larger than for digital computation. Digital computers have a much greater accuracy potential which reduces many computational errors to negligible quantities. Quite often, the more the computations, the more complex the computer, and generally the bigger the computer. Consequently, the reduction in errors must be paid for in computer cost and weight.

The guidance system could conceivably be implemented along several different lines. The system could be all inertial, a celestial system, a hybrid inertial-celestial, or primarily a radar command or homing system. For the error analysis, a definite system and a definite type of mechanization must be chosen. The choice of inertial guidance was made on the basis that such a system is

self-contained, that a large amount of experience has been gained with similar systems used on ballistic missiles, and that stabilization of the vehicle would be required regardless of the choice of the guidance system.

An alternate choice of inertial guidance, the gimballess system or strapped down system, was ruled out. In such a system the accelerometers are not fixed in the navigational coordinate system. Instead, they have a fixed orientation along the axes of the vehicle with the consequence that their outputs must be transformed along the navigational coordinate axes before relative acceleration and position can be obtained. The transformation matrix which replaces the isolation gimbals of the stable platform must be derived in a computer from knowledge of the angular velocity of the vehicle relative to the navigational coordinate system.

The gimballess system eliminates the weight and errors associated with a stable platform; however, the major errors which predominate are in the gyros. Gyro drift and gyro torqueing errors cause the reference trajectory to change, thus causing the vehicle to follow the error trajectory rather than the true trajectory. In the gimbaled system the gyros operate in a very narrow linear range, whereas in a gimballess system the linear operating range for the gyros is considerably greater. The size of the computer and the required amount of computation is much greater for a gimballess system than for a gimbaled platform system. As a consequence, the error sources and the error analysis are different for the two systems.

c. Guidance Equations - The function of a guidance system is to generate a sequence of command signals which guide the vehicle and terminate thrust in such a way that the guidance constraints are satisfied and the intended mission accomplished. The intended mission may be accomplished without satisfying all the guidance constraints and conversely. One does not imply the other.

The sequence of command signals which steer the vehicle and terminate its thrust for a given mission is based upon a comparison of inertially derived position and velocity and desired position and velocity derived from a reference trajectory. The generation of these command or error signals is accomplished through the use of guidance equations. A guidance technique based on the required velocity concept is now generally used. The required velocity concept is based on the fact that at any space-time point in the powered region the required velocity of the missile is a function of the present missile position and the target parameters.

Two of the more common types of guidance equations are explicit guidance equations and delta guidance equations. Both are based on the required velocity concept. Explicit equations are rather complicated from a mechanization viewpoint but require a minimum of precomputations. For delta equations the

reverse is essentially true. Delta equations are essentially perturbation equations. Both approaches are methods of approximation. For the explicit equations, the guidance model is simplified first and then exact equations are written. For the perturbation or delta equations, a realistic guidance model is first employed then approximate equations are obtained, usually by simulation. Explicit equations require less precomputation but their complexity generally requires a larger computer. Delta equations are simple to mechanize and are inherently more flexible, since all guidance constraints can be changed simply by changing the constraints. Either can be made to perform the same task.

For the lunar ascent, the smaller size computer required and the greater flexibility of the equations would indicate the choice of delta guidance equations.

The designations "delta guidance" or "explicit guidance" do not mean precise mathematical formulations but rather approaches. A variety of both types of equations can be written.

It should be noted that the error analysis of this study is based on the choice of a guidance system (inertial guidance) and a specific type of mechanization (space stabilized platform). The choice of the guidance equations is independent of the error analysis. The commentary on guidance equations is included here to indicate the boundaries of the error analysis in determining the sensor errors.

5.3.2 Error Analysis

5.3.2.1 Method of Approach

The method that is used in this discussion is to define an overall error allowance for position and velocity. This error allowance is based on the position and velocity errors which can be tolerated at the initiation of the Hohmann transfer coast phase from the nominal 30-kilometer parking orbit. This error allowance is extracted from table 1 of Appendix F (Volume V). This allowance is defined on the basis that 3-σ error in any one injection parameter shall not result in more than a 20 percent increase in fuel expended for a nominal ascent (zero error ascent trajectory) to rendezvous. This error allowance is

Δh = 1.4 kilometers (3 σ value),
Δv = 1.5 meters/sec (3 σ value).

This overall error allowance may be composed of contributions from several sources; however, for this study it is assumed to be comprised only of guidance system errors and errors due to selenophysical uncertainties at the launch site.

The guidance system is arbitrarily allotted an overall error allowance. These errors plus the selenophysical errors must be less than the total error allowances set up as the standard. The overall errors in the guidance system can be controlled by varying the sensor tolerances. All the error contributions which exist in the guidance system are combined in an error budget. Each error producing source must operate within a specified tolerance. If the error in a given component contributes excessively to the overall error, the overall guidance system error must be relaxed or a general tightening of the error source must take place. The errors allotted in the budget must be within the state of the art accuracy for each component.

Figure 5-8 shows the minimum energy direct ascent trajectory. The error relationships are similar for the other ascents with the exception of the minimum time direct ascent which effects rendezvous at thrust termination.

5.3.2.2 Error Sources

The position and velocity errors of the launch vehicle that occur during the lunar ascent originate from several sources. This discussion is primarily concerned with the sensor errors; however, other error sources influence the specifications of the sensors and must be considered.

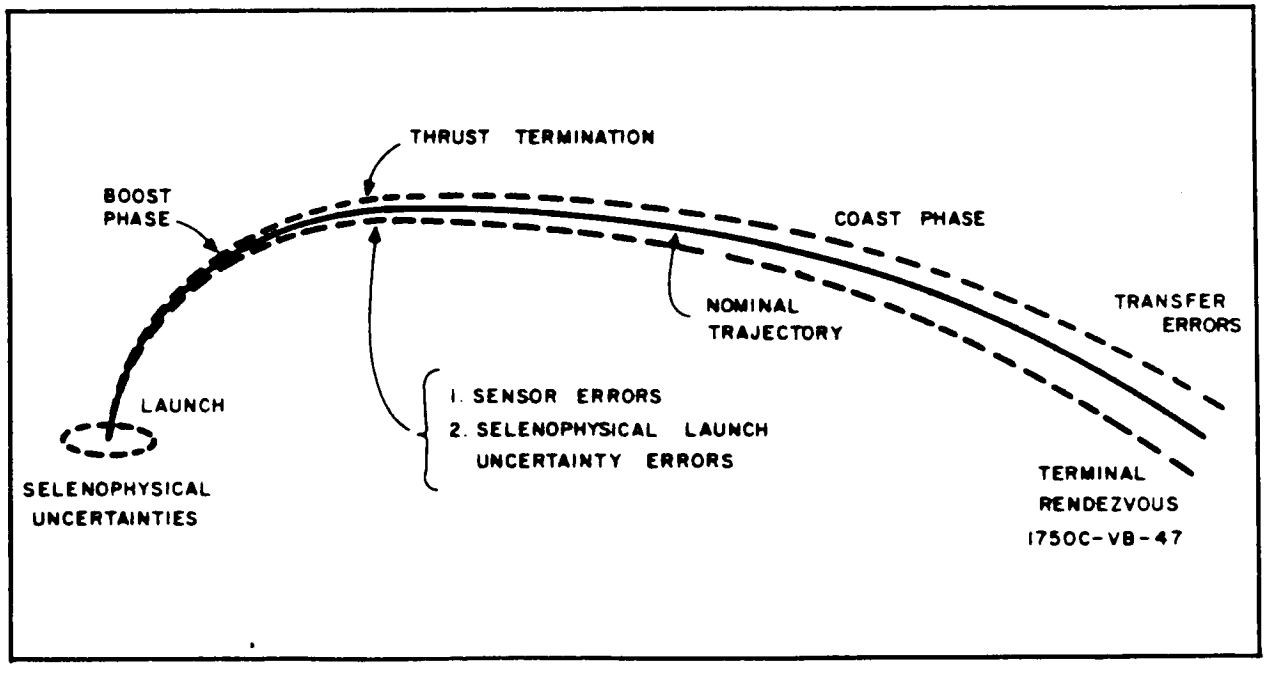

Figure 5-8. Ascent Trajectory

The error sources within the guidance system are:

a. Accelerometer errors
b. Gyro errors

c. Alignment errors
d. Computer errors

Errors within the inertial guidance systems are only part of the total mission errors since factors outside the guidance package also contribute to the total error. The following are error sources not chargeable to the inertial system.

a. Thrust termination errors
b. Transfer errors
c. Selenophysical uncertainties
d. Target location errors and uncertainties

Accelerometer, gyro, and alignment errors cause more than 90 percent of the total guidance system errors in most applications. When digital computers are used in conjunction with a gimbaled platform, the accelerometer, gyro, and alignment errors predominate to the extent that all errors associated with the computer are neglected. Consequently, a discussion of computer errors will not be included since the percentage of the error can be arbitrarily controlled by the complexity of the computer. With the velocity control concept of guidance, the ballistic trajectory of a vehicle can be determined if the position, magnitude, and direction of the velocity vector are known at thrust termination. Although the precise time of thrust cutoff can be generated by the computer, the sequence of events in the cutoff process produces errors. This generation is not chargeable to the inertial system. Within the present state of the art of rocket propulsion systems, this error with respect to the inertial system errors becomes of second order importance and will be neglected for this discussion. The other error sources will be discussed in subsequent sections.

5.3.2.3 Boost Sensor Errors

The analytical formulation of the error analysis for the boost sensors is given in Appendix E (Volume V). The following discussion summarizes the method and provides the motivation for the particular choice of analysis. In an inertial system the errors in position and velocity are initially manifested as imperfections within the sensors plus orientation errors. The significant error sources within the guidance package are listed below.

Sensor	Error Sources
a. Accelerometers	Bias
	Linear scale factor
	Cross axis effects
	Nonlinear effects
b. Gyros	Fixed drift rate
	Mass unbalance
	Anisoelasticity

c. Platform

Misalignment
Servo error
Table deformation

Analytical models for the accelerometers, gyros, and platform errors are formulated. These models furnish a mathematical definition of error coefficients in terms of boost accelerations. The subsequent procedure involves evaluating each term in the error model to determine its effect on vehicle position and velocity at thrust termination. These error models for each component indicate the mechanism by which each error source propagates its respective errors.

An error budget is drawn up for the boost sensors which shows the contribution of each error source to the final position and velocity error of the vehicle at the end of the boost trajectory. The error coefficients are initially assigned on a somewhat arbitrary basis. The governing criterion is that these coefficients should be within the present-day state of the art.

The error analysis must be done in terms of a specific mechanization. The particular mechanization for which the error coefficients are determined in this study is a stable platform configuration containing three single-degree-of-freedom gyros orthogonally oriented and three accelerometers with their input axes oriented along the reference axes determined by the gyros. If a different mechanization is considered, such as a gimballess system, different error models must be formulated. The orientation of the navigation reference frame which is determined by the gyro orientation is shown in figure 5-9. The reference axes are moon-centered, nonrotating and constitute for the accuracies of this study an inertial reference frame. The boost trajectory is in the x-z plane.

There are three generalized error analysis procedures commonly used for relating guidance component errors to the position and velocity errors at thrust termination (Ref. 5-4).

The first procedure consists of using normalized integrals of the thrust acceleration components in conjunction with error coefficients to formulate error models for the various sensors. A slight modification of this method is used for the error analysis in this study. Some of the various methods of evaluating the error coefficient integrals are digital computer computation, analytical hand integration, graphical integration, and a combination of graphical and hand integration in conjunction with polynominals. For a few nominal trajectories this method is extremely useful and yields quick results.

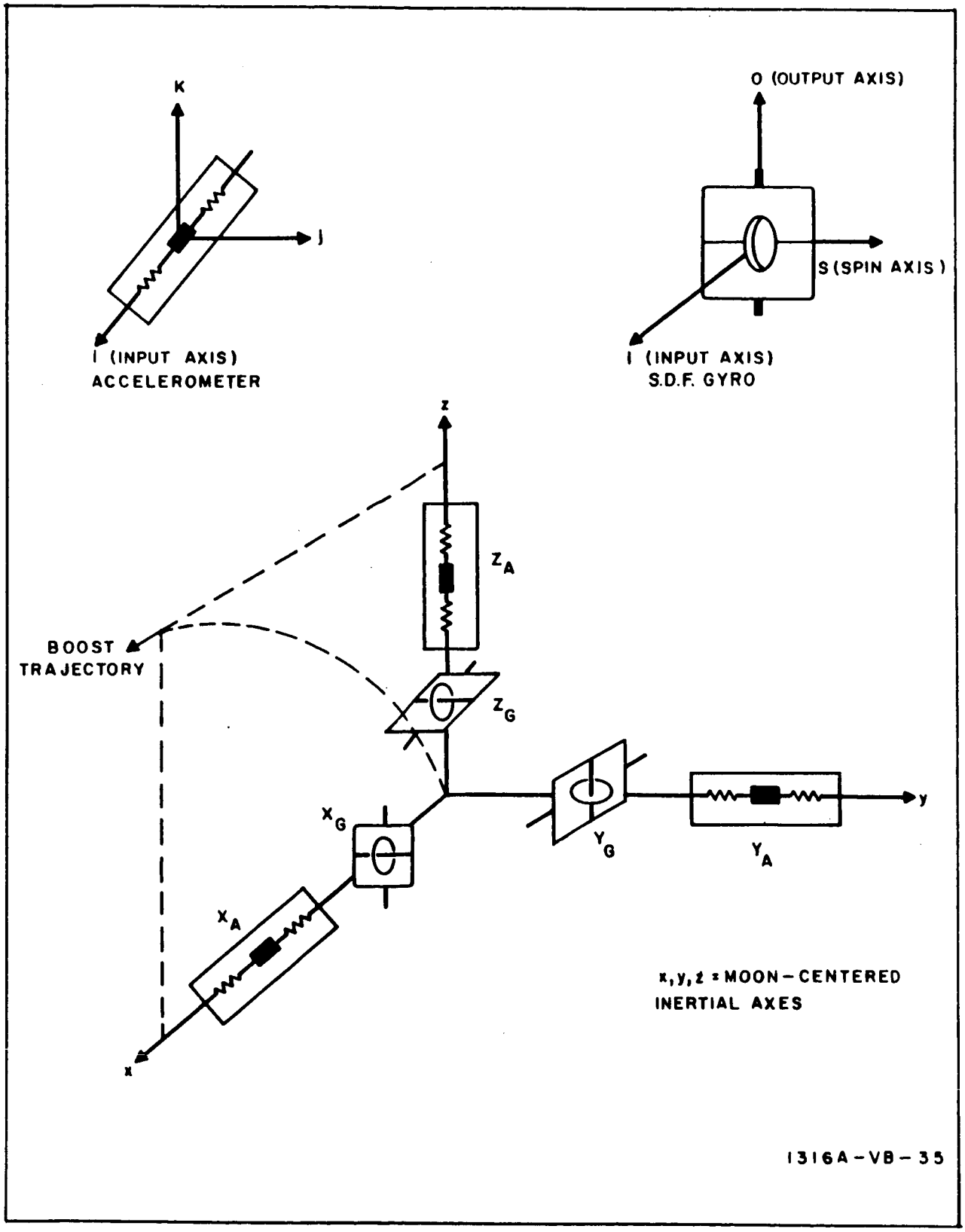

Figure 5-9. Orientation of Inertial Sensors and Navigation Reference Frame

A second procedure consists of a special digital computer program for exact integration of the error equations over the nominal boost trajectory using the sensor error sources as forcing functions. Such a program can be used to obtain results for a wide range and magnitude of error sources and is very useful for extensive and detailed work. The procedure can be used to evaluate any inertial measurement unit and is especially useful for optimization work. For this particular study such a method involves too much computer work for the information that is required.

The third procedure is a flight simulation program. This type of program provides an accurate method for evaluating error coefficients; however, since a complete flight is required to evaluate each error source, the method is wasteful of computer time except for special cases.

The determination of many optimized trajectories is beyond the scope of this study and not essential for determining the sensor specifications for the lunar launch. For these reasons the first procedure previously described is used in conjunction with two ascents each for the direct and parking ascents for ascertaining the sensor requirements.

5.3.2.4 Transfer Errors

As previously discussed, two methods are available for achieving the final phase of the lunar ascent after the powered phase. The vehicle may be either injected directly into a Hohmann transfer ellipse after the powered phase or enter a parking orbit and then be injected into a transfer ellipse. At thrust termination there will be an accumulation of errors in position and velocity caused by errors in the sensors within the guidance system and by selenophysical uncertainties at the launch site. Each initial error is propagated along the coast portion of the trajectory and is ultimately manifested as the final error at terminal rendezvous. These errors have secular and periodic propagation characteristics. The cumulative errors which occur during the coast phase are referred to collectively in this study as transfer errors and are independent of the guidance system.

The errors at thrust termination are expressed in the rectangular coordinates of the navigational reference frame. The position errors are transformed to cylindrical coordinates by the following expression.

$$\begin{bmatrix} \Delta S_o \\ \Delta y_o \\ \Delta r_o \end{bmatrix} = \begin{bmatrix} \cos\phi_f & 0 & -\sin\phi_f \\ 0 & 1 & 0 \\ \sin\phi_f & 0 & \cos\phi_f \end{bmatrix} \begin{bmatrix} \Delta x \\ \Delta y \\ \Delta z \end{bmatrix}$$

where:

φ_f = the central angle traversed during boost
ΔS = the error tangentially along the trajectory
Δy = the error normal to the orbital plane
Δr = the radial or cross-track error.

The velocity errors may be transformed by substituting the velocity components. It should be noted that all y-values are unchanged since rotation is about the y-axis. The resulting errors are in the correct coordinates to be transformed for the coast phase.

The transfer error matrix will be given in the most general form which may be used for any central angle traversed. The matrix for the transfer errors is

$$\begin{bmatrix} \frac{\Delta r}{r} \\ \frac{\Delta S}{S} \\ \frac{\Delta y}{y} \\ \frac{\Delta V_r}{V_r} \\ \frac{\Delta V_T}{V_T} \\ \frac{\Delta V_N}{V_N} \end{bmatrix} = \begin{bmatrix} d_{11} & d_{12} & d_{13} & d_{16} \\ d_{21} & & & \\ d_{31} & & & \\ d_{41} & & & \\ d_{51} & & & \\ d_{61} & & & d_{66} \end{bmatrix} \begin{bmatrix} \frac{\Delta r_o}{r_o} \\ \frac{\Delta S_o}{S_o} \\ \frac{\Delta y_o}{y_o} \\ \frac{\Delta V_{or}}{V_{or}} \\ \frac{\Delta V_{oT}}{V_{oT}} \\ \frac{\Delta V_{oN}}{V_{oN}} \end{bmatrix}$$

The elements of the matrix d_{11}, d_{12}, - - - and the definition of the terms are given in Appendix E (Volume V). It should be noted that this matrix may be used on multipulse coast trajectories. The inputs to the matrix are still the burnout errors at the end of each stage or firing and the output errors are at the injection point or the end of each coast phase. The overall error on a multipulse mission is the respective products of each coast phase. This subject is treated in more detail in Ref. 5-5.

5.3.2.5 Selenophysical Launch Site Uncertainties

The purpose of this paragraph of the lunar ascent study is to ascertain a maximum error expectation in the navigation coordinates at the launch site. These selenophysical uncertainties are three-dimensional position errors which originate from the following sources.

a. Errors in the lunar surface launch site location
b. Errors in determining the lunar radius
c. Local vertical uncertainties.

These error sources will be discussed in detail later.

One method of determining the error expectation is to make a comparison of similar conditions on earth with what can be encountered on the moon. This is not an easy task since the exact nature of the lunar surface is not known. Most of the information on the physical characteristics of the moon is derived through various types of observations of the lunar surface. Various parameters such as the mass, the mean density, the principal radii of the observable portion, and the gravitational constant are known. The density gradient within the moon is not well known. The characteristics of the central core and the mean density and nature of the lunar surface are open to conjecture. In general the number of lunar theories is approximately equal to the number of theorists.

The task of navigating on the moon is in many respects easier than on earth. Three factors enter into this consideration; the absence of an atmosphere, the slower rotation, and the greater sphericity of the moon. The absence of an atmosphere eliminates the usual problems associated with celestial sightings on earth. There are no refraction corrections or delays from cloud coverage.

The synchronized rotation of the moon with its orbital rotation due to the torque effect of the gravity gradient causes the effects of centripetal acceleration on lunar gravity measurements to be insignificant.

The observed triaxial radii of the moon are:

$R_1 = 1738.57 \pm 0.07$ km (equatorial)

$R_2 = 1738.21 \pm 0.07$ km (equatorial)

$R_P = 1737.49 \pm 0.07$ km (polar)

The average equatorial radius is $\overline{R} = 1738.39 \pm 0.07$ km. The oblateness of the moon is

$$\frac{\overline{R} - R_P}{\overline{R}} = 5.177 \times 10^{-4}.$$

The oblateness of the earth is

$$\frac{1}{297} = 3.367 \times 10^{-3}$$

or almost seven times greater than the lunar oblateness.

The lunar oblateness discussion is only about the observed portion. The same side of the moon always points in the earth's direction - apparently the result of tidal effects between the two bodies earlier in history when the lunar body was in a plastic state. The gravitational attraction probably caused the moon to be distorted in the shape of an egg. The mechanism of obtaining this distortion as purely conjecture; however, the synchronism of the lunar rotation with the earth requires that the moon have a mass preponderance in the earth's direction. 1/ The amount of distortion is probably not more than a few hundred meters at the most - which is small compared to the moon's diameter. Consequently, the oblateness of the moon about any axis of its suspected triaxial ellipsoidal shape will not differ appreciably from the oblateness determined from the view presented to earth.

The main source of navigation errors of the lunar launch site is suspected to originate from gravity anomalies. An estimation of gravity anomalies will begin on earth. It has been known for many years that the observed values for the deflection of the plumb line at certain locations on earth are considerably less than the estimated values. This disparity has long been suspected to originate from unequal densities of material immediately beneath the surface or specifically, by regions of deficient density lying beneath the mountain ranges and by regions of excessive density beneath low areas and under the ocean bottom. It is supposed that at some depth the excess above the surface is compensated by a deficiency below the surface and conversely.

If the earth were composed of homogeneous matter, its normal shape under equilibrium conditions without strain would be a true spheriod of revolution; however, if the earth's composition were heterogeneous, its shape would no longer be spheriodal. Accumulations of lighter density material would tend to bulge above the mean surface while heavier matter would tend to be depressed or sink below the mean surface. This condition of equilibrium of the earth's crust is called isostasy. There are several different isostatic theories 2/ which represent variations on a similar theme. The main interest here is contrasting a maximum error in vertical measurement on earth with a similar measurement on the lunar surface.

The determination of position is tied in closely with the local vertical especially if local reference points are not used. The maximum deflection of the vertical on earth is 1 minute of arc. This vertical deflection causes an error in surface measurement of one nautical mile or 1.85 kilometers. This same angular deviation on the moon would result in an error in surface position of 0.5 kilometer. However, the vertical deflection on earth is altered by the isostatic nature of its crust. It is highly probable that the lunar surface is not in isostatic equilbrium. This conclusion is predicated on the estimated surface and interior temperatures, the density, and the interior pressures of the moon.

1/ Ref. 5-6, p. 66 and 160.

2/ Ref. 5-7, Chap. 5

The lunar mountains have heights that easily equal or exceed those on earth. A direct comparison is not valid. The heights on earth are related to sea level. Since the moon possesses no water and no sea level, the measured height of a lunar mountain corresponds to its height above the surrounding surface. The tallest earth mountains tend to be on plateaus or in a mountainous area, whereas the lunar mountains may stand isolated. Based on the formation of the lunar mountains and the fact that the moon does not have an isostatic crust, the maximum deflection of the vertical could approach twice that on earth. For these reasons the maximum vertical deflection on the moon is taken as 2 minutes of arc and the maximum position error as 1 kilometer.

The accelerometer accuracy of 2×10^{-5} g's allows the determination of the lunar radius to within 100 meters. This accuracy is based upon the ideal conditions of a spherical moon and a well-defined reference datum. The lunar oblateness plus gravity anomalies compounded by the accelerometer accuracies would increase the error in determining the lunar radius several times. For these reasons the maximum lunar radius error is taken as 1 kilometer.

It is expected that prior to the lunar landing, the landing site including reference land marks will have been chartered using high definition photographic techniques from orbiting vehicles. On earth a 1:50,000 scale aerial photograph allows the location of a point to within a few meters. It is not unreasonable to expect similar accuracies on the moon. However, such considerations have not been used in determining the sensor requirements in this study.

5.3.2.6 Error Contributions From Lunar Radius and Launch Position Uncertainties

The error contributions at thrust termination from selenophysical uncertainties at the launch site are obtained by using a differential error analysis of the boost equations. This is equivalent to neglecting any effects or higher order than first. Figure 5-10 shows the position error contribution at the nominal 30 kilometer orbit from launch site errors in surface position and the lunar radius. Figure 5-11 shows a similar error relationship, the velocity error contribution at thrust termination at the 30-kilometer orbit from launch site errors in surface position and the lunar radius. The errors are kept separate in order to show the contribution from each source. The curves in figures 5-10 and 5-11 show no overwhelming contribution from any one source; however, lunar radius uncertainties produce a greater error contribution at thrust termination.

5.3.2.7 Launch Times

For direct ascent the time of launch must be very precise if a given ascent trajectory is adhered to. The range of the trajectories considered in this study vary from the direct ascent under thrust with its minimum time of 460 seconds to the minimum energy ascent of 260 seconds powered boost plus half the period

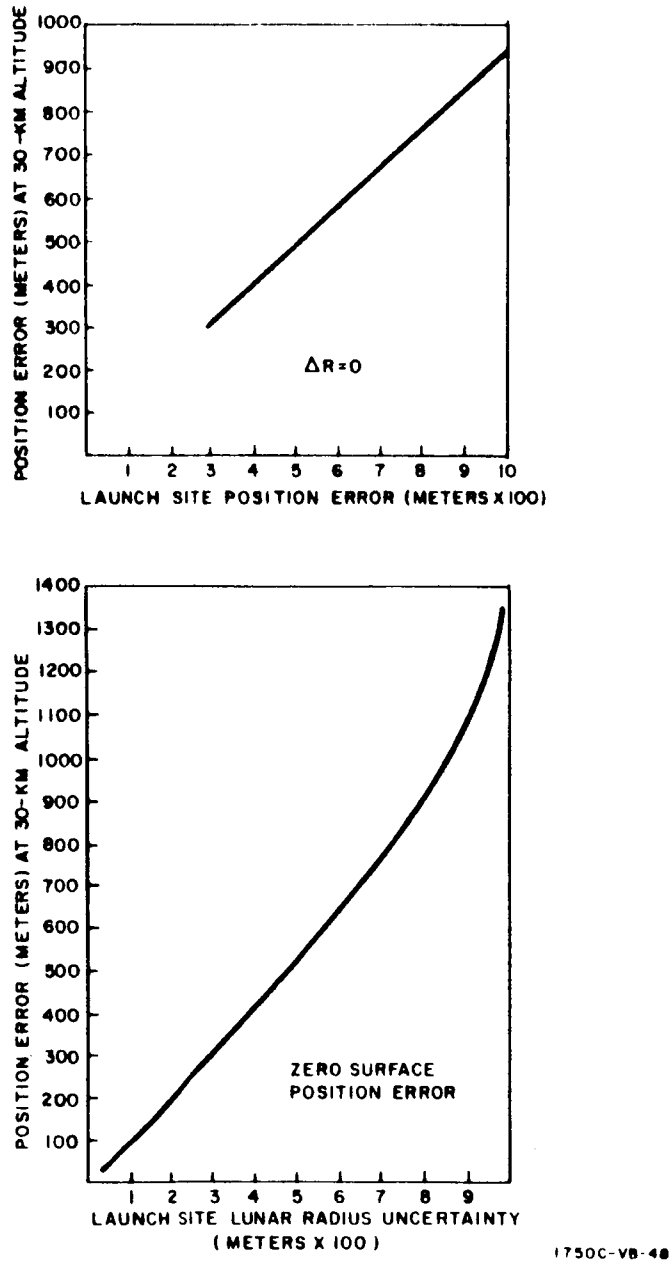

Figure 5-10. Position Errors at a 30-Kilometer Altitude Caused by Launch Site Location Uncertainties

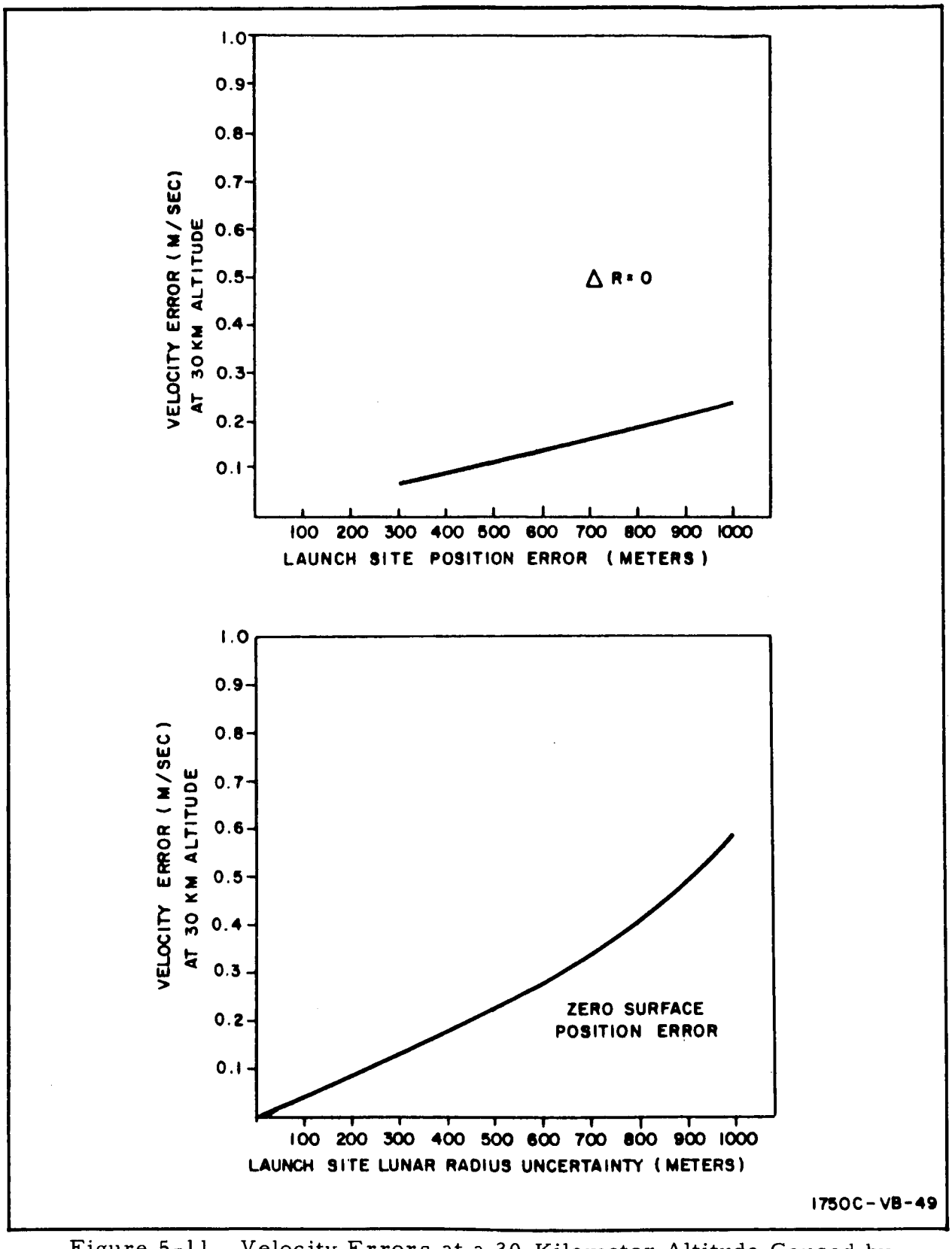

Figure 5-11. Velocity Errors at a 30-Kilometer Altitude Caused by Launch Site Location Uncertainties

of the Hohmann transfer ellipse. These time extremes pertain to only one period of the target vehicle. Delays in launching can be handled by changing from a direct ascent to a parking ascent or by utilizing some intermediate direct ascent trajectory lying between the minimum energy and minimum time ascent considered in this study. A consideration of the tolerances on initial launch times must also take into account out-of-plane launches and a consideration of launch windows. As a consequence, a detailed discussion of launch times and launch errors will not be considered in this study.

5.4 RESULTS

5.4.1 Sensor Requirements for Lunar Ascent

The sensor errors determined in this study are based on an overall error allowance in position and velocity at thrust termination prior to initiation of the Hohmann transfer coast phase from the nominal 30-kilometer parking orbit. This overall error allowance includes the guidance system errors and the errors caused by selenophysical anomalies at the launch site. This error allowance is based on a 3σ error which can be permitted in any one injection parameter and not result in more than a 20-percent increase in fuel expenditure over a nominal ascent (zero error). This total error allowance is

Δh = 1.4 kilometers (3σ value)
Δv = 1.5 meters/sec (3σ value).

The position and velocity errors at thrust termination for the accelerometers, gyros, and platform are tabulated in tables 5-2 through 5-6 and include the direct and parking ascents. It should be noted that sensor accuracies are normally specified by their standard deviations (1σ values); however, to eliminate confusion between the sensor specifications and the position and velocity errors, all quantities are given in 3σ values.

The boost sensor errors are budgeted in such a manner that the root sum square values of the total guidance system errors and the selenophysical errors are less than the error allowance set up as a standard. The results for the direct ascent are given in table 5-7.

The sensor specifications are listed for the direct and parking ascents in table 5-8.

5.4.2 Error Comparison at Terminal Rendezvous

Errors in determining the position coordinates at the launch site are introduced into the guidance system as errors in the nominal trajectory and nominal velocity profile with the consequence of producing position and velocity errors at thrust termination. Since the long boost for the direct ascent ends

TABLE 5-2

ACCELEROMETER POSITION AND VELOCITY ERRORS FOR DIRECT ASCENT

Accelerometers			Miss Velocity Coefficients			Miss Distance Coefficients			Short Boost Velocity Errors (m/sec)			Long Boost Velocity Errors (m/sec)			Short Boost Position Errors (m)			Long Boost Position Errors (m)		
Component Error Source	Error Symbol	Uncompensated 3σ Value	ΔV_x	ΔV_y	ΔV_t	ΔX	ΔY	ΔZ	ΔV_x	ΔV_y	ΔV_z	ΔV_x	ΔV_y	ΔV_z	ΔX	ΔY	ΔZ	ΔX	ΔV	Δt
Bias	a_{0x}	6×10^{-5} g	t			$\frac{1}{2}t^2$			0.153			0.270			19.89			62.25		
	a_{0y}	6×10^{-5} g		t			$\frac{1}{2}t^2$			0.153			0.270			19.89			62.25	
	a_{0z}	6×10^{-5} g			t			$\frac{1}{2}t^2$			0.153			0.270			19.89			62.25
Scale factor	a_{1x}	6×10^{-5} g/g	I_1			$_1I_1$			0.087			0.093			9.72			15.54		
	a_{1y}	6×10^{-5} g/g		0			0			0			0			0			0	
	a_{1z}	6×10^{-5} g/g			I_4			$_4I_4$			0.015			0.108			0.510			18.63
Nonlinearity effects	a_{2x}	3×10^{-5} g/g^2	I_2			$_2I_2$			0.030			0.009			2.73			2.57		
	a_{2y}	3×10^{-5} g/g^2		0			0			0			0			0			0	
	a_{2z}	3×10^{-5} g/g^2			I_5			$_5I_5$			0.003			0.009			1.59			3.24
Nonlinearity effects	a_{3x}	3×10^{-5} g/g^3	I_3			$_3I_3$			0.003			0.001			0.15			0.09		
	a_{3y}	3×10^{-5} g/g^3		0			0			0			0			0			0	
	a_{3z}	3×10^{-5} g/g^3			I_6			$_6I_6$			-			-			0.030			0.06
Cross axis sensitivity	a_{4x}	$3 \times 10^{-5} \frac{g}{\text{cross-g}}$	0			0			0			0			0			0		
	a_{4y}	$3 \times 10^{-5} \frac{g}{\text{cross-g}}$		I_4			$_4I_4$			0.006			0.054			1.41			9.30	
	a_{4z}	$3 \times 10^{-5} \frac{g}{\text{cross-g}}$			I_1			$_1I_1$			0.042			0.045			4.86			7.77
Cross axis sensitivity	a_{5x}	$3 \times 10^{-5} \frac{g}{g \text{ cross-g}}$	0			0			0			0			0			0		
	a_{5y}	$3 \times 10^{-5} \frac{g}{g \text{ cross-g}}$		0			0			0			0			0			0	
	a_{5z}	$3 \times 10^{-5} \frac{g}{g \text{ cross-g}}$			I_7			$_7I_7$			0.006			0.006			0.42			1.95
Cross axis sensitivity	a_{6x}		0			0			0			0			0			0		
	a_{6y}			0			0			0			0			0			0	
	a_{6z}				0			0			0			0			0			0
Cross axis sensitivity	a_{7x}	$3 \times 10^{-5} \frac{g}{g \text{ cross-g}}$	I_7			$_7I_7$			0.006			0.006			0.42			1.95		
	a_{7y}	$3 \times 10^{-5} \frac{g}{g \text{ cross-g}}$		0			0			0			0			0			0	
	a_{7z}	$3 \times 10^{-5} \frac{g}{g \text{ cross-g}}$			0			0			0			0			0			0
RSS-values									0.180	0.153	0.159	0.285	0.276	0.294	22.32	19.95	20.55	64.2	63.0	65.4

TABLE 5-3

GYRO POSITION AND VELOCITY ERRORS FOR DIRECT ASCENT

Gyros			Miss Velocity Coefficients			Miss Distance Coefficients			Short Boost Velocity Errors (m/sec)			Long Boost Velocity Errors (m)			Short Boost Position Errors (m)			Long Boost Position Errors (m)		
Component Error Source	Error Symbol	Uncompensated 3σ Value	ΔV_x	ΔV_y	ΔV_t	ΔX	ΔY	ΔZ	ΔV_x	ΔV_y	ΔV_z	ΔV_x	ΔV_y	ΔV_z	ΔX	ΔY	ΔZ	ΔX	ΔY	ΔZ
Average drift rate	b_{0x}	$= 1.5 \times 10^{-6} \frac{rad}{sec}$		I_9			$_9I_9$			0.023			0.150			3.54			52.2	
	b_{0x}	= 0.3 deg/hr			0			0			0			0			0			0
	b_{0y}	= 0.3 deg/hr			I_8			$_8I_8$			0.284			0.060			18.96			7.11
	b_{0y}	= 0.3 deg/hr	$-I_9$			$_9-I_9$			-0.023			-0.150			-3.54			-52.2		
	b_{0z}	= 0.3 deg/hr	0			0			0			0			0			0		
	b_{0z}	= 0.3 deg/hr		$-I_8$			$_8-I_8$			-0.284			-0.60			-18.96			-7.11	
Mass unbalance along input axis	b_{1x}	$= 6 \times 10^{-6} \frac{rad}{sec\text{-}g}$		I_{11}			$_{11}I_{11}$			0.051			0.090			12.96			37.65	
	b_{1x}	= 1.2 deg/sec-g			0			0			0			0			0			0
	b_{1y}	= 1.2 deg/sec-g			0			0			0			0			0			0
	b_{1y}	= 1.2 deg/sec-g	0			0			0			0			0			0		
	b_{1z}	= 1.2 deg/sec-g	0			0			0			0			0			0		
	b_{1z}	= 1.2 deg/sec-g		$-I_{12}$			$_{12}-I_{12}$			-0.190			-0.691			-21.06			-102.9	
Mass unbalance along spin axis	b_{2x}	= 1.2 deg/sec-g		0			0			0			0			0			0	
	b_{2x}	= 1.2 deg/sec-g			0			0			0			0			0			0
	b_{2y}	= 1.2 deg/sec-g			I_{12}			$_{12}I_{12}$			0.190			0.691			21.06			102.9
	b_{2y}	=1.2 deg/sec-g	$-I_{13}$			$_{13}-I_{13}$			-0.020			-0.237			-9.12			-77.1		
	b_{2z}	=1.2 deg/sec-g	0			0			0			0			0			0		
	b_{2z}	=1.2 deg/sec-g		0			0			0			0			0			0	
Anisoelasticity	b_{3x}	$= 6 \times 10^{-6} \frac{rad}{sec\text{-}g^2}$		0			0			0			0			0			0	
	b_{3x}	= 1.2 deg/sec-g^2			0			0			0			0			0			0
	b_{3y}	= 1.2 deg/sec-g^2			0			0			0			0			0			0
	b_{3y}	= 1.2 deg/sec-g	0			0			0			0			0			0		
	b_{3z}	= 1.2 deg/sec-g	0			0			0			0			0			0		
	b_{3z}	= 1.2 deg/sec-g		0			0			0			0			0			0	
RSS-values									0.0031	0.348	0.342	0.0301	0.714	0.696	14.40	33.09	28.35	93.30	121.35	103.20

TABLE 5-4

PLATFORM POSITION AND VELOCITY ERRORS FOR DIRECT ASCENT

Platform			Miss Velocity Coefficients			Miss Distance Coefficients			Short Boost Velocity Errors (m/sec)			Long Boost Velocity Errors (m/sec)			Short Boost Position Errors (m)			Long Boost Position Errors (m)		
Component Error Source	Error Symbol	Uncompensated 3σ Value	ΔV_x	ΔV_y	ΔV_z	ΔX	ΔY	ΔZ	ΔV_x	ΔV_y	ΔV_z	ΔV_x	ΔV_y	ΔV_z	ΔX	ΔY	ΔZ	ΔX	ΔY	ΔZ
Initial misalignment	$\phi_{xy}(0)$	$= 3 \times 10^{-4}$ rad	I_2			$_2I_2$			0.294			0.192			27.36			25.68		
	$\phi_{xy}(0)$	= 60 arc-sec		$-I_1$			$_1-I_1$			-0.432			-0.462			-44.15			-77.4	
	$\phi_{yz}(0)$	= 60 arc-sec		I_3			$_3I_3$			0.210			0.090			16.02			9.60	
	$\phi_{yz}(0)$	= 60 arc-sec			$-I_2$			$_2-I_2$			-0.294			-0.192			-27.36			-25.68
	$\phi_{xz}(0)$	= 60 arc-sec			I_1			$_1I_1$			0.432			0.462			44.10			77.4
	$\phi_{xz}(0)$	= 60 arc-sec	$-I_3$			$_3-I_3$			-0.210			-0.090			-16.02			-9.60		
Servo bias	e_x	= 60 arc-sec		I_3			$_3I_3$			0.210			0.090			16.02			9.60	
	e_x	= 60 arc-sec			$-I_2$			$_2-I_2$			-0.294			-0.192			-27.36			-25.68
	e_y	= 60 arc-sec			I_1			$_1I_1$			0.432			0.462			44.10			77.4
	e_y	= 60 arc-sec	$-I_3$			$_3-I_3$			-0.210			-0.090			-16.02			-9.60		
	e_z	= 60 arc-sec	I_2			$_2I_2$			0.294			0.191			27.36			25.68		
	e_z	= 60 arc-sec		$-I_1$			$_1-I_1$			-0.432			-0.462			-44.15			-77.4	
Deformation	p_{xy}	$= 3 \times 10^{-4} \frac{\text{rad}}{g}$	0			0			0			0			0			0		
	p_{xy}	= 60 arc-sec/g		$-I_2$			$_2-I_2$			-0.294			-0.192			-27.36			-25.68	
	p_{yz}	= 60 arc-sec/g		0			0			0			0			0			0	
	p_{yz}	= 60 arc-sec/g			0			0			0			0			0			0
	p_{xz}	= 60 arc-sec/g			I_7			$_7I_7$			0.048			0.072			4.18			19.38
	p_{xz}	= 60 arc-sec/g	$-I_5$			$_5-I_5$			-0.018			-0.096			-15.72			-32.28		
	q_{xy}	= 60 arc-sec/g	0			0			0			0			0			0		
	q_{xy}	= 60 arc-sec/g		0			0			0			0			0			0	
	q_{yz}	= 60 arc-sec/g		I_5			$_5I_5$			0.018			0.096			15.72			32.28	
	q_{yz}	= 60 arc-sec/g			0			0			0			0			0			0
	q_{xz}	= 60 arc-sec/g			I_2			$_2I_2$			0.294			0.192			27.36			25.68
	q_{xz}	= 60 arc-sec/g	$-I_7$			$_7-I_7$			-0.048			-0.072			-4.18			-19.38		
RSS-values									0.510	0.736	0.690	0.324	0.696	0.738	46.92	73.32	78.48	54.12	117.84	119.16

TABLE 5-5

ACCELEROMETER POSITION AND VELOCITY ERRORS FOR PARKING ASCENT

Accelerometers			Miss Velocity Coefficients			Miss Distance Coefficients			Short Boost Velocity Errors (m/sec)			Long Boost Velocity Errors (m/sec)			Short Boost Position Error (m)			Long Boost Position Errors (m)		
Component Error Source	Error Symbol	Uncompensated 3σ value	ΔV_x	ΔV_y	ΔV_z	ΔX	ΔY	ΔZ	ΔV_x	ΔV_y	ΔV_z	ΔV_x	ΔV_y	ΔV_z	ΔX	ΔY	ΔZ	ΔX	ΔY	ΔZ
Bias	a_{0x}	6×10^{-5} g	t			$\frac{1}{2}t^2$			0.150			0.272			19.14			62.79		
	a_{0y}	6×10^{-5} g		t			$\frac{1}{2}t^2$			0.150			0.272			19.14			62.79	
	a_{0z}	6×10^{-5} g			t			$\frac{1}{2}t^2$			0.150			0.272			19.14			62.79
Scale factor	a_{1x}	6×10^{-5} g/g	I_1			${}_1I_1$			0.073			0.090			7.37			13.86		
	a_{1y}	6×10^{-5} g/g		0			0			0			0			0			0	
	a_{1z}	6×10^{-5} g/g			I_3			${}_3I_3$			0.023			0.036			2.59			15.63
Cross axis sensitivity	a_{4x}	$3 \times 10^{-5} \frac{g}{\text{cross-g}}$	0			0			0			0			0			0		
	a_{4y}	$3 \times 10^{-5} \frac{g}{\text{cross-g}}$		I_3			${}_3I_3$			0.011			0.018			1.30			7.83	
	a_{4z}	$3 \times 10^{-5} \frac{g}{\text{cross-g}}$			I_1			${}_1I_1$			0.037			0.045			3.68			6.93
Cross axis sensitivity	a_{5x}	$3 \times 10^{-5} \frac{g}{g\ \text{cross-g}}$	0			0			0			0			0			0		
	a_{5y}	$3 \times 10^{-5} \frac{g}{g\ \text{cross-g}}$		0			0			0			0			0			0	
	a_{5z}	$3 \times 10^{-5} \frac{g}{g\ \text{cross-g}}$			I_{11}			${}_{11}I_{11}$			0.007			0.001			0.59			1.38
Cross axis sensitivity	a_{6x}	$3 \times 10^{-5} \frac{g}{\text{cross-g}}$	I_3			${}_3I_3$			0.011			0.018			1.30			7.83		
	a_{6y}	$3 \times 10^{-5} \frac{g}{\text{cross-g}}$		I_1			${}_1I_1$			0.037			0.045			3.68			6.93	
	a_{6z}	$3 \times 10^{-5} \frac{g}{\text{cross-g}}$			0			0			0			0			0			0
Cross axis sensitivity	a_{7x}	$3 \times 10^{-5} \frac{g}{g\ \text{cross-g}}$	I_{11}			${}_{11}I_{11}$			0.007			0.001			0.59			1.38		
	a_{7y}	$3 \times 10^{-5} \frac{g}{g\ \text{cross-g}}$		0			0			0			0			0			0	
	a_{7z}	$3 \times 10^{-5} \frac{g}{g\ \text{cross-g}}$			0			0			0			0			0			0
RSS-values									0.167	0.154	0.156	0.287	0.276	0.278	20.55	19.53	19.68	64.78	63.65	65.11

5-35

TABLE 5-6

GYRO AND PLATFORM POSITION AND VELOCITY ERRORS FOR PARKING ASCENT

Gyros			Miss Velocity Coefficients			Miss Distance Coefficients			Short Boost Velocity Errors (m/sec)			Long Boost Velocity Errors (m/sec)			Short Boost Position Errors (m)			Long Boost Position Errors (m)		
Component Error Source	Error Symbol	Uncompensated 3σ Value	ΔV_x	ΔV_y	Δ_z	ΔX	ΔY	ΔZ	ΔV_x	ΔV_y	ΔV_z	ΔV_x	ΔV_y	ΔV_z	ΔX	ΔY	ΔZ	ΔX	ΔY	ΔZ
Average drift rate	b_{0x}	$3 \times 10^{-7} \frac{rad}{sec}$		I_6			$_6I_6$			0.007			0.006			1.049			9.63	
	b_{0y}	= 0.06 deg/hr	$-I_6$		I_4	$_6-I_6$		$_4I_4$	-0.007		0.065	-0.006		0.139	-1.049		4.179	-9.63		15.99
	b_{0z}	= 0.06 deg/hr		$-I_4$			$_4-I_4$			-0.065			-0.139			-4.179			-15.99	
Mass unbalance along input axis	b_{1x}	$3 \times 10^{-7} \frac{rad}{sec\text{-}g}$		I_7			$_7I_7$			0.008			0.002			1.04			1.05	
	b_{1y}	= 0.06 deg/hr-g	0			0			0			0			0			0		
	b_{1z}	= 0.06 deg/hr-g		$-I_8$			$_8-I_8$			-0.012			-0.058			-0.99			-4.35	
Mass unbalance along spin axis	b_{2x}	= 0.06 deg/hr-g		0			0			0			0			0			0	
	b_{2y}	= 0.06 deg/hr-g	I_9		I_8	$_9I_9$		$_8I_8$	0.038		0.012	0.134		0.058	2.52		0.99	2.82		4.35
	b_{2z}	= 0.06 deg/hr-g		0			0			0			0			0			0	
Anisoelasticity	b_{3x}	$= 3 \times 10^{-7} \frac{rad}{sec\text{-}g^2}$		0			0			0			0			0			0	
	b_{3y}	= 0.06 deg/hr-g^2			0			0			0			0			0			0
	b_{3z}	= 0.06 deg/hr-g	0			0			0			0			0			0		
RSS-values									0.038	0.066	0.066	0.134	0.150	0.150	2.73	4.54	4.30	10.03	19.20	16.57
Platform																				
Initial misalignment	$\phi_{xy}(0)$	$= 3 \times 10^{-4}$ rad	0			0			0			0			0			0		
	$\phi_{xz}(0)$	= 60 arc-sec	$-I_3$			$_3-I_3$			-0.113			-0.182			-36.84			-78.18		
	$\phi_{yx}(0)$	= 60 arc-sec		$-I_1$			$_1-I_1$			-0.365			-0.449			-12.93			-69.18	
	$\phi_{yz}(0)$	= 60 arc-sec		I_3			$_3I_3$			0.113			0.182			36.84			78.18	
	$\phi_{zx}(0)$	= 60 arc-sec			I_1			$_1I_1$			0.365			0.449			12.93			69.18
	$\phi_{zy}(0)$	= 60 arc-sec			0			0			0			0			0			0
Servo bias	e_x	= 60 arc-sec		$-I_1$			$_1-I_1$			-0.365			-0.449			-12.93			-69.18	
	e_y	= 60 arc-sec		I_3			$_3I_3$			0.113			0.182			36.84			78.18	
	e_z	= 60 arc-sec	$-I_3$		I_1	$_3-I_3$		$_1I_1$	-0.113		0.365	-0.182		0.449	-36.84		12.93	-78.18		69.18
RSS-values									0.160	0.540	0.517	0.258	0.685	0.635	52.10	55.20	18.30	110.50	147.63	97.83

TABLE 5-7

3σ ERRORS AT THRUST TERMINATION (30 KILOMETERS)

	Δh (kilometers)	Δv (meters/sec)
Guidance system errors	0.131	1.264
Selenophysical errors	1.380	0.598
Guidance plus selenophysical errors (rss)	1.383	1.398
Total allowable error	1.400	1.500

TABLE 5-8

SENSORS SPECIFICATIONS FOR LUNAR ASCENT TYPE-ALL INERTIAL, SPACE STABILIZED PLATFORM-ALL SENSORS ORTHOGONALLY ORIENTED

Sensor	Direct Ascent	Parking Ascent	Units
Accelerometer	3-σ Values	3-σ Values	
Number	3	3	
Range	±1.5	±1.5	g
Bias	6×10^{-5}	6×10^{-5}	g
Scale factor	6×10^{-5}	6×10^{-5}	g/g
Nonlinear effect	3×10^{-5}	3×10^{-5}	g/g^2
Nonlinear effect	3×10^{-5}	3×10^{-5}	g/g^3
Cross axis bias sensitivity	3×10^{-5}	3×10^{-5}	g/cross-g
Cross axis scale factor	3×10^{-5}	3×10^{-5}	g/g cross-g
Gyro			
Single-degree-of-freedom-integrating			
Number	3	3	
Drift rate	0.3	0.06	deg/hr
Mass unbalance	1.2	0.06	deg/hr/g
Anisoelasticity	1.2	0.06	$deg/hr/g^2$
Platform			
Initial misalignment	60	60	arc-sec
Servo bias	60	60	arc-sec
Deformation	60	60	arc-sec
$g = 9.8 \times 10^{-3}$ km/sec^2			

at terminal rendezvous, a comparison of the terminal errors at thrust cutoff for the two ascents is not valid. It is of interest to compare the final position and velocity errors at terminal rendezvous. This is accomplished by multiplying the short boost thrust termination errors by the transfer matrix. The same guidance sensors are used for booth ascents. The results are shown in table 5-9.

It should be emphasized that the terminal errors listed in table 5-9 represent the worst possible conditions and do not represent the final terminal rendezvous conditions. On the surface it would appear that the terminal error conditions for the direct long boost ascent are much better; however, this ascent requires on the basis of nominal conditions, 77 percent more fuel. The errors are never realized in an actual rendezvous situation since midcourse and terminal maneuvers are used to effect the final rendezvous closure.

5.4.3 Mission Constraints and Tradeoff Considerations

The following is a list of constraints used in this study.

a. The boost sensors are based on a maximum allowable error in position and velocity at the nominal 30-kilometer orbit just prior to injection into a Hohmann transfer ellipse.

This error allowance is

Δh = 1.4 kilometers (3-σ value),
Δv = 1.5 meters/sec (3-σ value).

b. The sensors are based on an optimized boost trajectory.

c. The target orbit is assumed circular at an altitude of 200 kilometers.

d. The short and long boost use a thrust to weight ratio of 3 and 2 respectively.

e. A specific impulse of 300 seconds is assumed.

The error allowance is based on an expected maximum 20 percent fuel expenditure over the fuel requirements for a nominal Hohmann ascent from a 30-kilometer parking orbit. This error allowance is comprised of contributions from the guidance system and position errors in the navigation coordinates at the launch site. A reduction in the overall error allowance would require more accurate sensors and a reduction in the maximum error expectation at the launch site. The results show that the selenophysical launch site uncertainties contribute primarily to position errors whereas the guidance system contributes principally to the velocity errors. Thus, it is better to reduce proportionally the errors from both the guidance system and the selenophysical uncertainties.

TABLE 5-9

TERMINAL RENDEZVOUS ERRORS

Error	Short Boost			Long Boost		
	Guidance System Error	Selenophysical Launch Site Errors	Total Error	Guidance System Error	Selenophysical Launch Site Errors	Total Error
Δr (kilometers)	2.475	1.403	2.840	0.189	1.050	1.064
ΔS (kilometers)	13.20	24.03	27.42	0.0992	0.120	0.156
ΔV_r (meter/sec)	0.803	2.05	2.20	1.12	0.879	1.42
ΔV_T (meter/sec)	1.01	0.1145	1.018	0.273	1.59	1.613
Position (rss-km)	13.42	24.04	27.50	0.280	1.055	1.090
Velocity (rss-m/sec)	1.53	2.055	2.56	1.55	1.81	2.38

Selenophysical launch site errors contain a 1-km lunar surface error and a 1-km lunar radius uncertainty. All errors are 3-σ values

Any weight in the form of payload put into a lunar orbit entails a severe fuel penalty since the fuel requirements for the various stages of the lunar mission represent payloads for the previous stage. This weight becomes an important factor for any tradeoff considerations. As the sensor accuracy increases, the complexity and weight of the associated electronics increases. The computer capacity and weight also tend to increase. Therefore, increased sensor accuracy which implies increased system weight must be weighed against the saving in fuel. Conversely, less accurate sensors imply a slightly lighter weight guidance system which requires more fuel. Consequently, the final optimization of the guidance system must be based on the tradeoff considerations of the sensor accuracies, the fuel penalties, and the overall cost.

Midcourse corrections were not considered in this study since such considerations are more properly within the province of the rendezvous study section. However, midcourse corrections could be used to compensate for errors at thrust termination and to alleviate the terminate rendezvous maneuver requirements. Midcourse corrections would allow less accurate sensors and a smaller computer at the expense of additional fuel expenditure; however, the reduction in terminal maneuvers might offset the midcourse fuel expenditure.

5.5 CONCLUSIONS

The sensor specifications in this study are based on the allowable injection errors at the initiation of the Hohmann transfer ellipse from the nomial 30-kilometer parking orbit. The same error criterion was applied to both direct and parking ascents. However, the initial errors at thrust termination for the parking ascent do not remain constant. These errors are a function of the time spent in the parking orbit and have both secular and periodic propagation characteristics. Consequently, the sensors for the parking ascent are required to be more accurate. It is possible that if the position of the launch vehicle is updated that sensors requirements can be made less accurate. The accuracy of the updated position requires an assumption on the accuracy of the sensors of the orbiting vehicle.

The major contribution to the velocity errors at thrust termination is from the guidance system whereas the errors in the position coordinates at the launch site represent the major contribution to the position errors at thrust termination. The launch site uncertainties which represent the maximum error expectation in position coordinates do not present a major obstacle in the guidance techniques for a lunar ascent. It is highly probable that other methods such as high definition photographic techniques will reduce this error appreciably.

As previously stated, this study does not recommend one type of ascent in preference to another. The difference between the sensor requirements for the two types of ascents is not sufficiently great to make this choice. It is felt that mission requirements will dictate the choice of ascent. As a safety precaution, it is possible to program both direct and parking ascents; thus, if there is a malfunction during the direct ascent, a changeover is made to a parking ascent.

The sensors obtained in this study are well within the state of the art. Considering the accuracy requirements, the entire inertial guidance package could well fall within the category of off-the-shelf items; however, weight and space considerations may dictate redesigns of existing equipment.

6. LUNAR RENDEZVOUS

6.1 INTRODUCTION

Lunar rendezvous is the procedure of bringing two vehicles into close spatial proximity while in orbit about the moon. To determine sensor requirements which will make rendezvous possible, a rendezvous model is selected which is not only practicable but representative of a number of systems being proposed for lunar missions. The area examined begins at the termination of the lunar ascent into parking orbit phase of the chaser vehicle, and ends when the chaser vehicle is brought to within a preset standoff range of the target vehicle with essentially zero relative velocity.

The following summary of notation is applicable to the lunar rendezvous analysis.

SUMMARY OF NOTATION

a_x	longitudinal acceleration of chaser due to thrusting
a_z	vertical acceleration of chaser due to thrusting
C, C_1, C_2	control parameters
e	orientation of LOS with respect to an inertial reference
$\dot{e}$	LOS angular rate with respect to inertial space
g	$9.81\ m/sec^2$
h	altitude of chaser
i	orbital plane inclination
I_{sp}	fuel specific impulse
K_1, K_2	control parameters
K_m	gravitational constant of moon = $4.90 \times 10^3\ km^3/sec^2$
M_o	initial mass of chaser
M_p	mass of propellant consumed by chaser due to rocket firing
R	chaser-to-target range
$\dot{R}$	chaser-to-target range rate
R_o	chaser-to-target range at initiation of active rendezvous
r_m	radius of moon = 1738 km
R_s	smoothed value of measured chaser-to-target range
R_1	range at which longitudinal control of chaser switches from coarse to vernier
R_2	standoff range at termination of active rendezvous
t	time

t_F	amount of time for which chaser rocket is to be fired
t_s	storage time for data smoothing process
Δt_i	interval between subsequent data points
Δt_{fx}	amount of time, during measurement interval, that the longitudinal engine is thrusting
Δt_{f2}	amount of time, during measurement interval, that the vertical engine is thrusting
ΔV	velocity increment
ΔV_H	total velocity increment required to perform a Hohmann transfer
ΔV_1	velocity impulse required for injection of Hohmann transfer
ΔV_2	velocity impulse required during Hohmann transfer to synchonize the chaser with the target
ψ	yaw (out-of-plane) altitude angle of chaser
γ	pitch (in-plane) attitude angle of chaser
ϕ	central angle between the radius vectors of chaser and target during rendezvous

6.2 BACKGROUND

During rendezvous, the vehicle with which rendezvous is to be established maintains a 200-km circular orbit about the moon. This vehicle is designated the target vehicle. The second vehicle, designated the chaser, is initially in a 30-km parking orbit essentially coplanar with the target orbit.

6.2.1 Mission Profile

The overall rendezvous procedure comprises four phases:

- Injection
- Midcourse
- Active Rendezvous
- Docking

6.2.1.1 Injection

When the chaser, on the basis of prior or present lunar and target measurements, determines that it is correctly phased with the target, it imparts a computed incremental velocity vector by means of rocket propulsion. This velocity maneuver establishes an ascending transfer orbit which is nominally cotangential to the target orbit at the anticipated rendezvous point.

6.2.1.2 Midcourse

This phase constitutes the major portion of the time that the chaser is traveling the transfer orbit. No active maneuvering is performed by the chaser during this time.

6.2.1.3 Active Rendezvous

The active phase commences when the chaser-to-target range has decreased to 25 km. On the basis of sensor measurements to the target, the chaser performs a series of propulsion maneuvers to close on the target in a prescribed manner. The active phase terminates when the chaser achieves a preset standoff range at essentially zero velocity with respect to the target.

6.2.1.4 Docking

Docking covers the process of bringing the chaser into physical contact with the target. Since docking is envisioned as being manually controlled using visual observations by a pilot, this phase is not investigated. Consequently, the study area of interest covers injection through to termination of the active rendezvous phase.

6.2.2 Guidance and Control

The guidance method assumes that the chaser vehicle applies a rocket impulse while in the parking orbit to establish the transfer orbit which subsequently intercepts the target orbit cotangentially. It is assumed that injection is sufficiently accurate so that no midcourse correction is required. The active phase of rendezvous commences at a range of 25 km.

6.2.2.1 Attitude Control

During most of the Midcourse Phase, chaser vehicle attitude stabilization requirements are not determined by thrust control considerations, but they may be dictated by sensor limitations. For the active phase, however, the chaser vehicle attitude must be controlled so that the longitudinal rockets are in the general direction of the chaser-to-target line of sight, and the normal rockets are in the plane of line-of-sight rotation.

6.2.2.2 Longitudinal Control

Longitudinal control is exercised to cause relative chaser-to-target range rate to decrease as the range decreases. The desired relationship of range versus range rate is shown by the dashed line in the phase plane plot of figure 6-1. If a constant level thrust control is assumed, however, this trajectory cannot be followed. Instead, an upper and a lower boundary are defined. Longitudinal thrust is initiated when the phase plane trajectory crosses the upper boundary and is shut down when it crosses the lower boundary. A typical trajectory resulting from this procedure is shown by the dotted line.

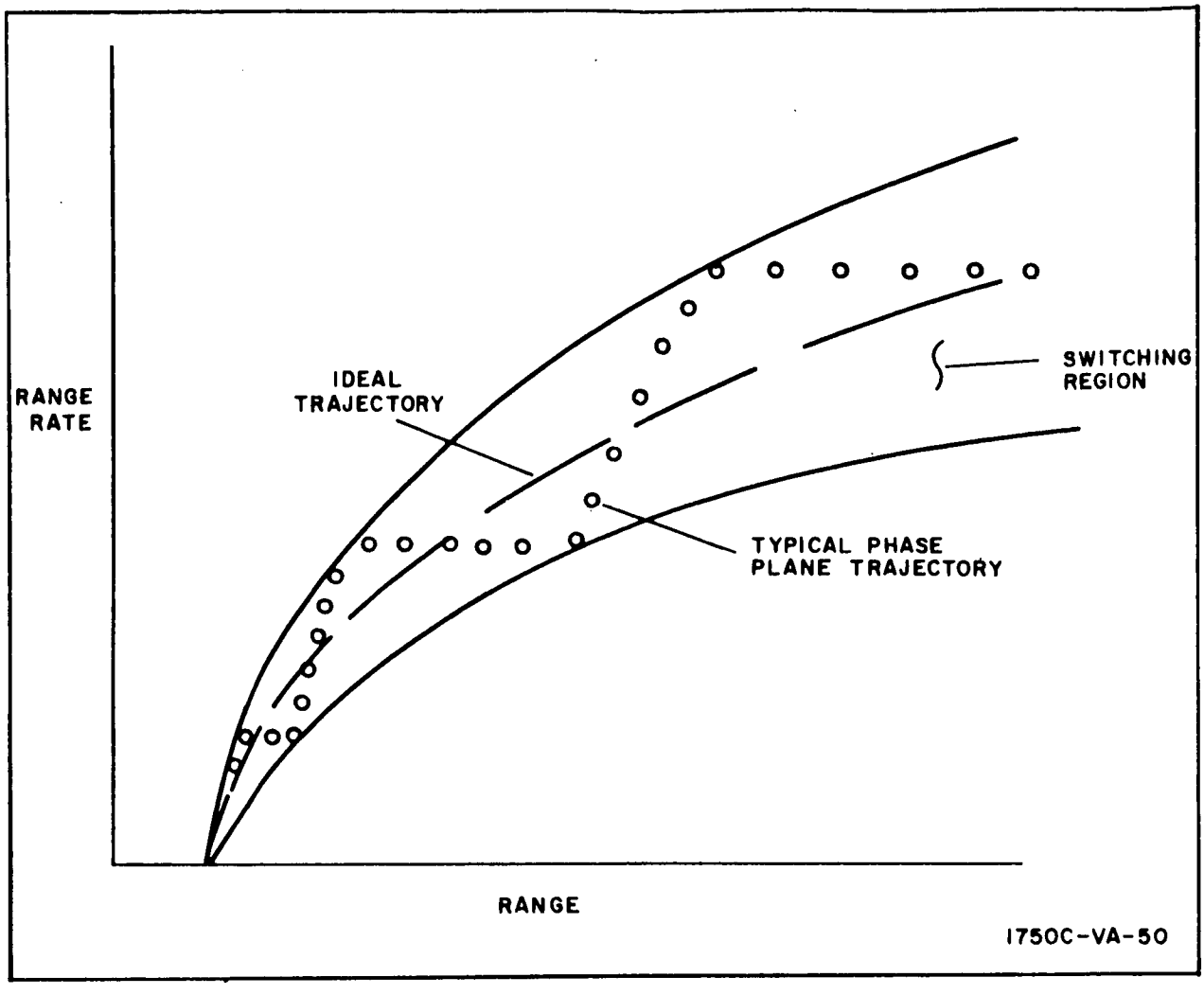

Figure 6-1. Phase Plane Representation of Longitudinal Control

6.2.2.3 Normal Control

The angular rate of the LOS is maintained at a value near zero by exercising normal control. Thrust is applied normal to the LOS and in the plane of LOS rotation when the magnitude of the LOS rate exceeds a specified upper threshold. The direction of thrusting is such that the magnitude of the LOS rate is reduced. When the rate falls below a specified lower threshold, thrust is shut down.

Normal control is mechanized in two channels which are defined by two orthogonal axes normal to the LOS. Control of each channel is identical. For purposes of this study, one channel is assumed to lie in the orbital plane (also the plane of LOS rotation) and control is simulated in the computer program that is utilized. The out-of-plane channel is handled analytically.

6.2.3 Observables

The rendezvous problem is essentially one of controlling the relative geometry and dynamics of the two vehicles involved. Consequently, it is desired to measure, with the onboard sensor system, observables which yield information concerning these relationships.

Observables selected for the lunar rendezvous are:

a. Chaser-to-target range
b. Chaser-to-target range rate
c. Azimuth LOS angular rate
d. Elevation LOS angular rate

6.2.4 Error Characterization

6.2.4.1 System Errors

Errors occurring during the injection maneuver can be introduced in position, velocity vector, and timing. Position errors are assumed to comprise three components: radial, down-range, and lateral (out of plane). Velocity vector errors may develop in the magnitude of the imparted velocity increment or in the direction of its application. A directional error is equivalent to an error in attitude of the chaser.

Timing errors are the result of performing the injection at the improper time. This type of error is essentially the same as a down-range position error.

Various levels of error in the following parameters were investigated to determine their effect on the rendezvous procedure:

a. Altitude (radial position error)
b. Magnitude of the incremental velocity vector
c. Direction of the incremental velocity vector
d. Central angle - corresponding to a timing error

Injection errors are a combination of measurement errors and control errors. Because of the assumed impulsive nature of the injection maneuver, no attempt was made to separate the sources.

6.2.4.2 Active Rendezvous

Errors inherent in the measurement of the observables by the onboard system are assumed to have the following form:

• Range errors. - It is assumed that the range measurement inaccuracies are random in nature and follow a Gaussian distribution about the actual range. The noise level is further assumed to be either a percentage of total range or the same percentage of 1 kilometer, whichever is greater.

• Range rate errors. - It is assumed that the range rate inaccuracies follow a normal distribution, are random in nature, and are uncorrelated to range errors. Range rate errors are considered to be fixed levels independent of range.

• LOS angular rate errors. - It is assumed that angular rate inaccuracies are random in nature and follow a normal distribution about the actual rates. The angular rate noise is considered to be uncorrelated to either the range or range rate noise.

6.2.5 Error Criterion

Sensor errors result in erroneous control of the rendezvous procedure, thereby demanding increased thrusting over an ideal transfer to achieve the correct end conditions. These increased thrust demands result in increased propellant consumption. The amount of propellant expended in executing an orbital transfer and rendezvous is of great importance to a space mission because of the equivalent vehicle mass penalty. All analyses in this phase of the study consider an equivalent incremental velocity, ΔV, applied during the rendezvous phase, as the nondimensional measure of propellant consumption, independent of I_{sp} and vehicle masses. The equivalent mass of propellant consumed can be determined by the relation:

$$M_p = M_o \left[1 - \exp\left(-\Delta V/gI_{sp}\right)\right] \text{ (kg) (assuming constant thrust)}$$

where

M_o = initial vehicle mass (kg)
g = 9.81 m/sec^2
I_{sp} = specific impulse (sec)

Next to the requirements for mission safety, the cost in incremental velocity is the primary consideration in evaluating the effects of injection errors and rendezvous sensor errors.

All analyses in this portion of the study refer the required incremental velocity to that of the ideal Hohmann transfer, thereby providing for each run a nondimensional measure of effectiveness in consumed propellant.

It is specified that any given 3σ injection error shall not result in more than a 20-percent incremental velocity increase over the ideal Hohmann transfer for the entire rendezvous when no errors are included on the measurements during the active rendezvous phase. Individual 3σ sensor errors during active rendezvous shall not result in more than a 50-percent increase in incremental velocity over the ideal Hohmann transfer.

6.3 ANALYSIS

A general objective approach to the determination of sensor requirements was used in this study. It is important to note that specific types of equipment are not assembled into a given configuration to determine whether or not its operation is satisfactory. Instead, the analytical solution concerns a somewhat ideal, nominal solution as well as parametric studies of variations about nominal values.

6.3.1 Model

The moon is presumed to develop an ideal central force field with a gravitational parameter of:

$$K_m = 4.90 \times 10^3 \text{ km}^3/\text{sec}^2$$

The mean lunar surface radius is assumed to be:

$$r_m = 1738 \text{ km}$$

6.3.1.1 Geometry

As previously mentioned, the rendezvous model selected for the lunar case involves a target vehicle considered to be in a 200-km circular orbit about the moon as indicated in figure 6-2. The manned chaser vehicle is presumed to be in a 30-km circular parking orbit coplanar with the target orbit. It is not essential for this sensor study that either orbit be circular or even coplanar, but for convenience, the computer program used for simulation is so arranged. When the chaser obtains information indicating that is is correctly phased to the target by central angle ϕ, or by measured range, R, it imparts a computed incremental velocity vector at point 1. The application of this velocity maneuver places the chaser in an ascending transfer ellipse which is designed to intercept the target orbit cotangentially at point 2, at which time a tangential velocity increase of the correct magnitude would theoretically bring the two vehicles together with zero final relative velocity. Practically, as further described, a series of active rendezvous maneuvers commences at short range and continues until the two vehicles are in the same orbit but displaced

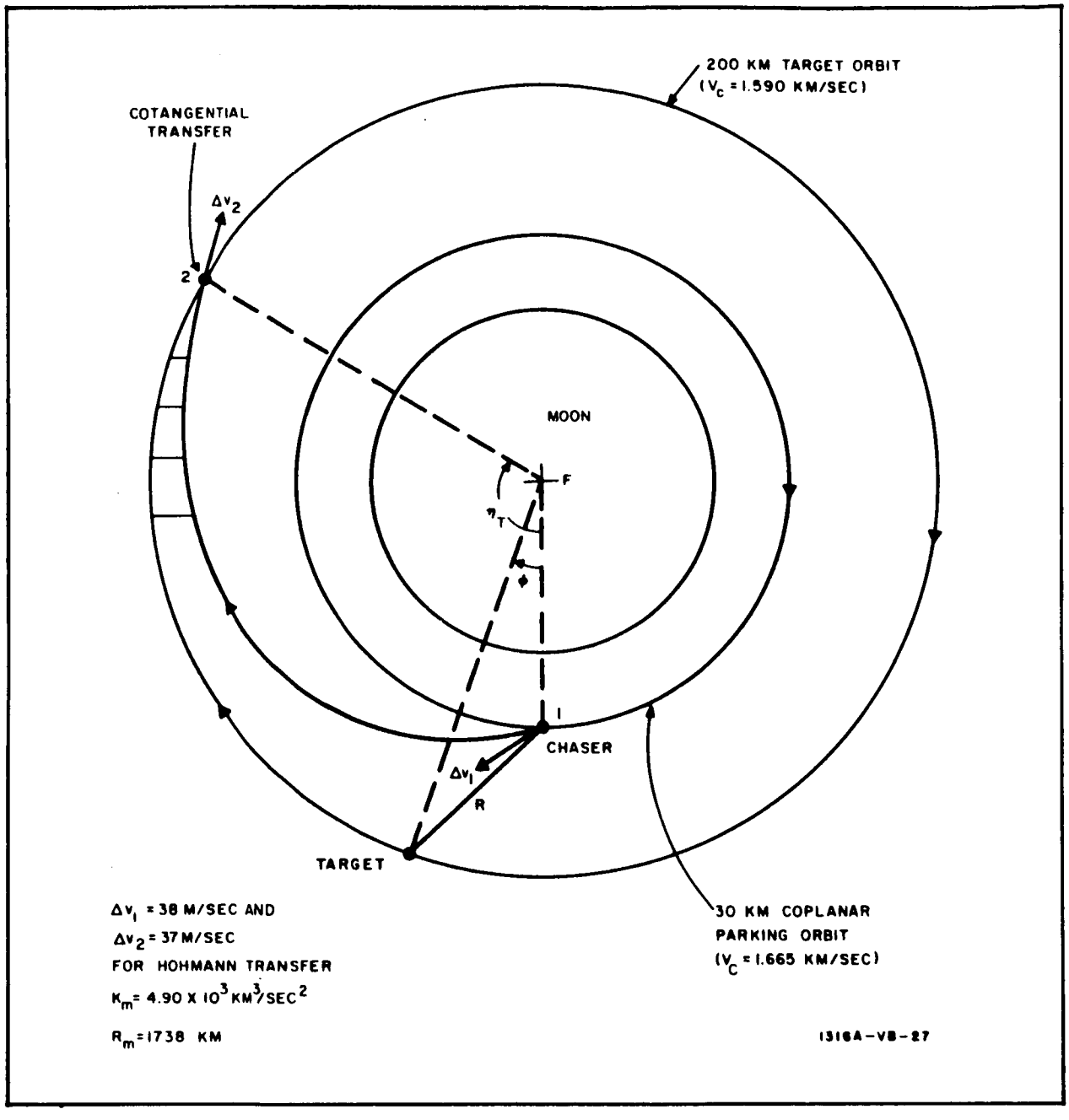

Figure 6-2. Lunar Orbital Rendezvous

by a preset standoff range. The computer program is designed to accommodate any desired transfer angle, η_T, and to modify the velocity maneuvers and ascent ellipse accordingly. In this study, however, all runs are taken with the full 180 degrees - nominally the Hohmann transfer - in the interests of propellant conservation.

For the nominal 180-degree case, the chaser vehicle fires a posigrade tangential velocity increment of 37.75 m/sec at point 1, where the range is 414.2 km and the range is -203.6 m/sec.

6.3.1.2 Guidance and Control

a. Guidance Description - The guidance method assumes that the chaser vehicle applies a rocket impulse while in the parking orbit to establish a transfer orbit which subsequently intercepts the target orbit cotangentially. Proper phasing is required to assure a successful rendezvous. It is assumed that the injection is sufficiently accurate so that no midcourse correction is required. At a relatively short range (less than 25 km) the active phase of rendezvous commences.

The guidance method used for the lunar rendezvous is illustrated by figure 6-3. As the chaser rises toward the target it approaches ahead of the target but its velocity decreases and the target tends to overtake the chaser vehicle. At a range of 25 km the inertial reference of the chaser is aligned, as indicated, to the range vector and to the selenocentric vertical; thereafter, it is space stabilized to that particular space reference. The chaser vehicle is then attitude stabilized to this space reference for the duration of the approach. Dual thrust level maneuvering rockets with a multiple restart capability are aligned to the body axes, so that an incremental velocity can be established along any body axis without altering the attitude of the chaser, thereby permitting rapid velocity maneuvering without the necessity for changing vehicle attitude. With this type of transfer, there is little improvement in propellant conservation with the alternative use of thrust vector control.

b. Control Description - In control of vehicle attitude and rendezvous maneuvering, it is assumed that rendezvous is completed when the chaser vehicle is ahead of the target at a standoff range of 50 ±10 meters while the magnitude of the range rate is less than 0.5 m/sec. The variation of range with transit time is illustrated by figure 6-4 for the nominal 30/200-km ascent trajectory. Because of the semilog plot, the slope of this curve is not indicative of $\dot{R}$. The variation of elevation angle with transit time for the same ascent is presented by the curve of figure 6-5.

(1) Attitude Control - During most of the trip in the parking orbit and in the ascent trajectory the chaser vehicle may be considered to be approximately stabilized to the selenocentric vertical and to the orbital plane, although it makes little difference to this study. Departures from this attitude may be undertaken to accommodate angular limitations on any sensors.

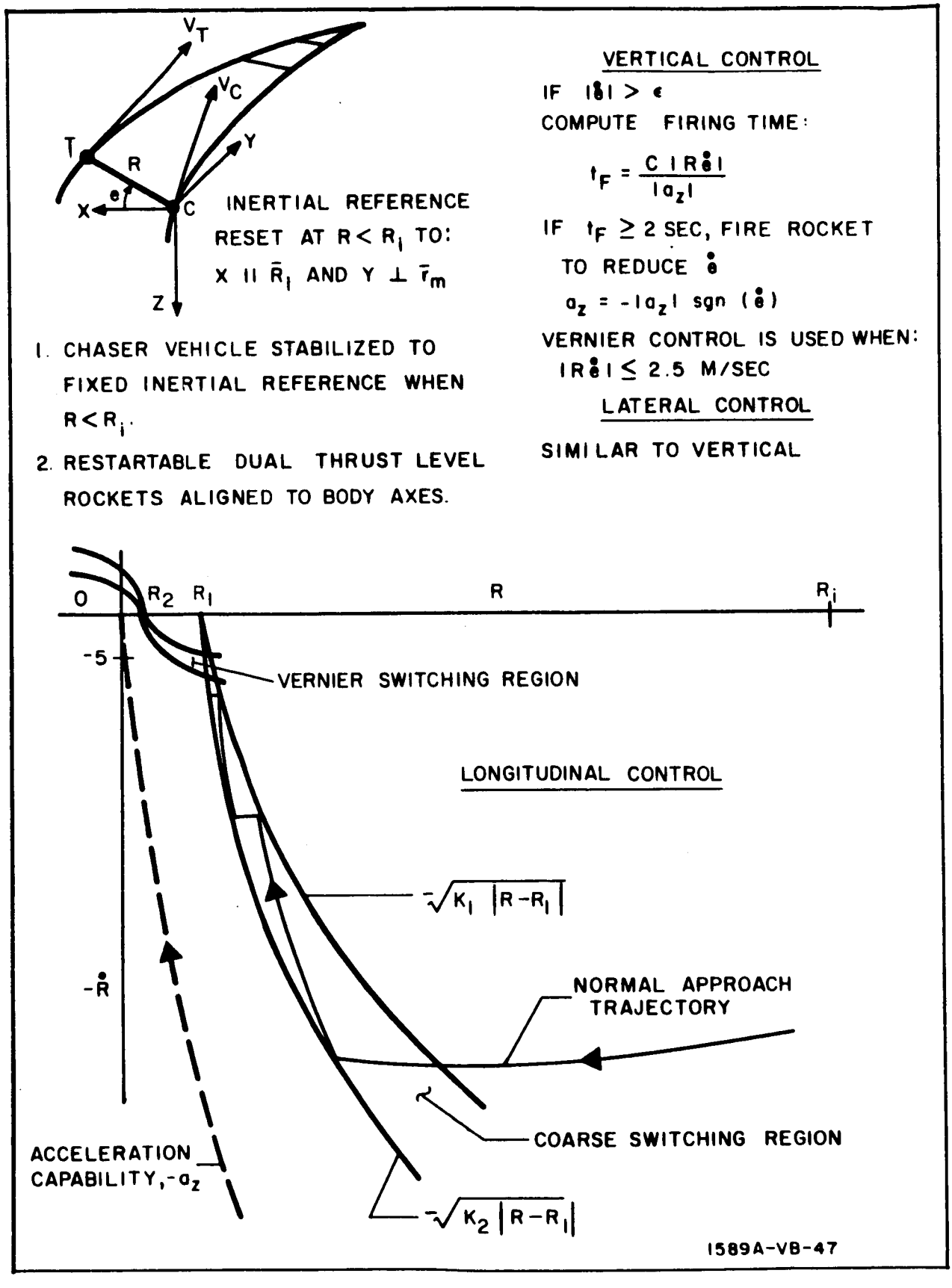

Figure 6-3. Rendezvous Guidance (Lunar Orbital Rendezvous)

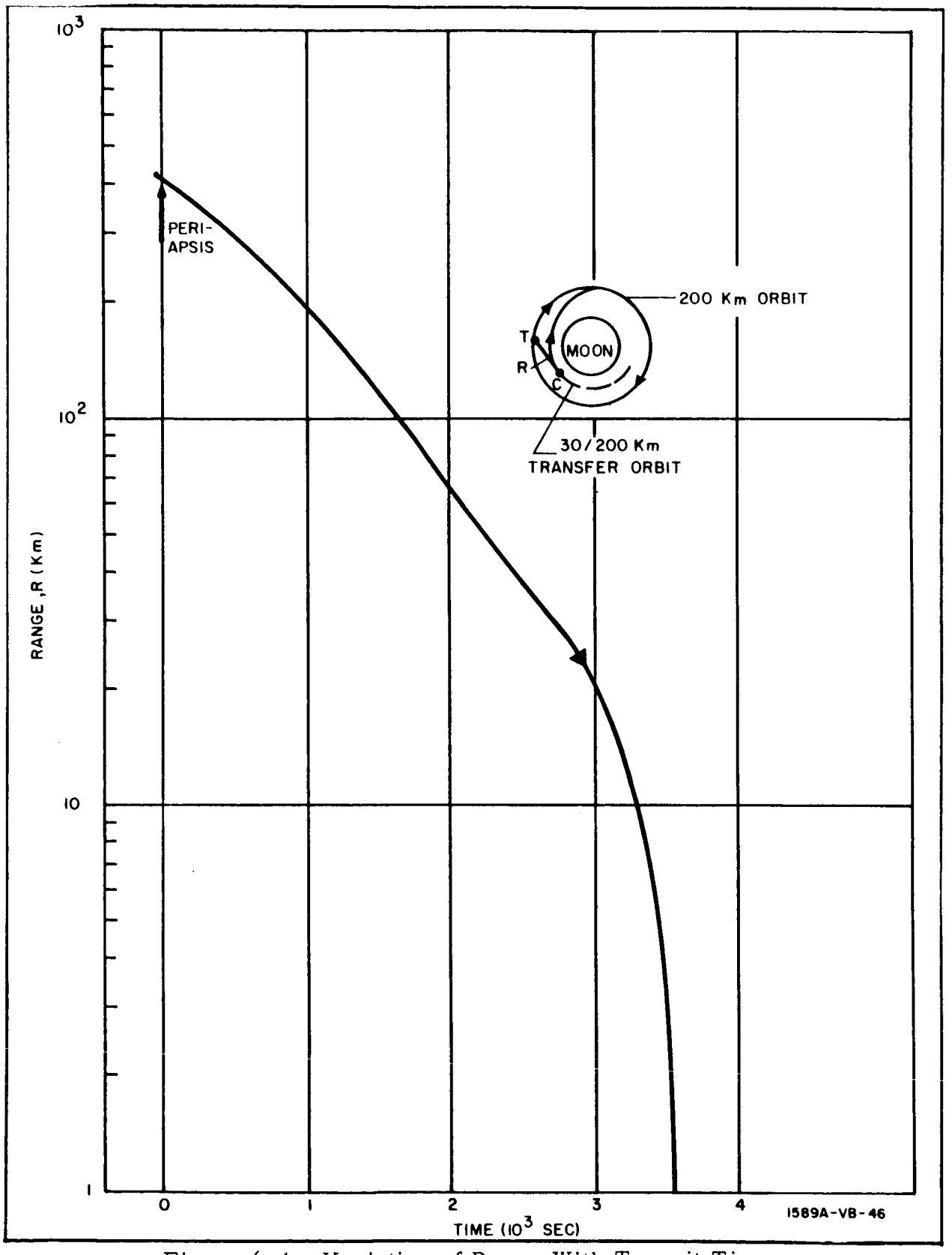

Figure 6-4. Variation of Range With Transit Time

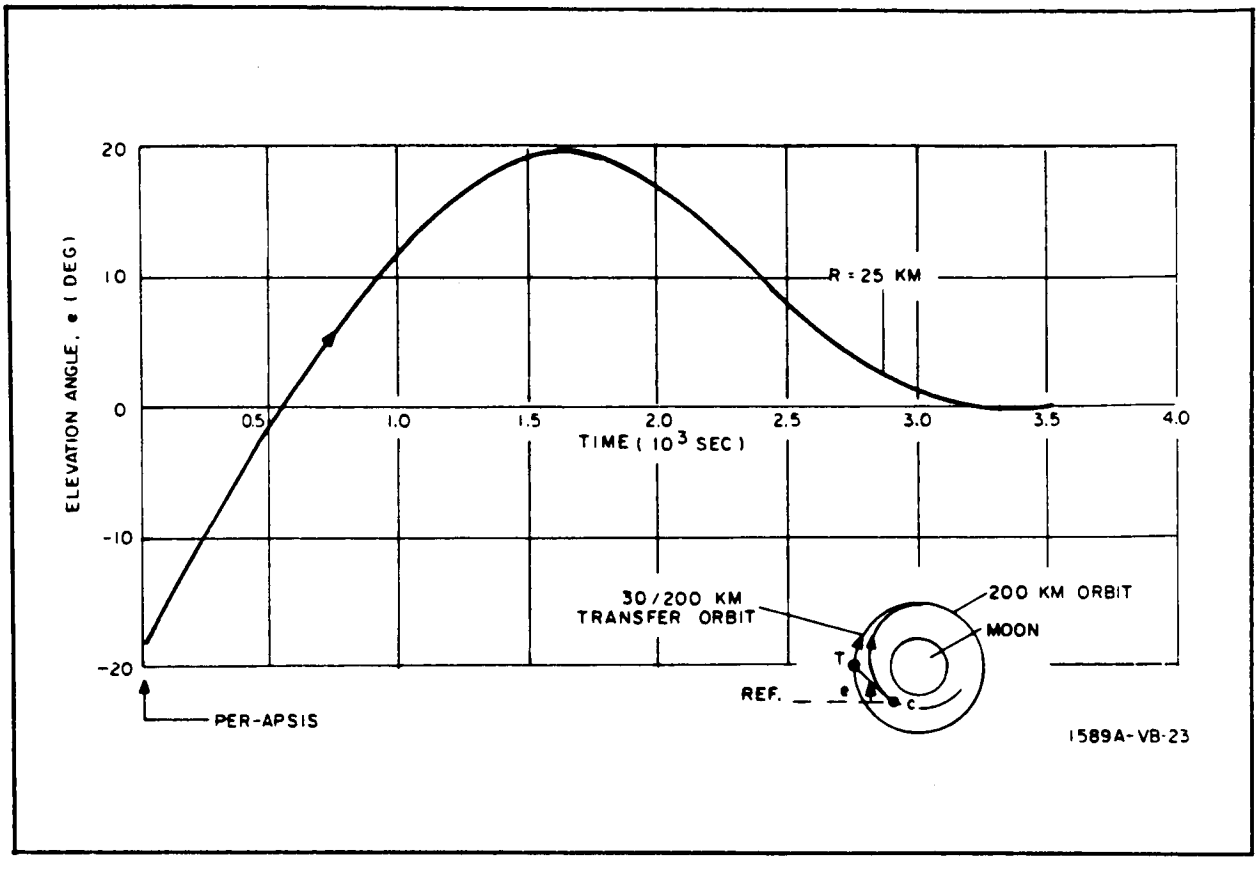

Figure 6-5. Variation of Elevation Angle With Transit Time

At the enabling range, however, the inertial reference of the chaser vehicle is inertially stabilized by aligning the longitudinal axis to that range vector and the lateral axis normal to that local selenocentric vertical. This space stabilized reference is used to control vehicle attitude during the active phase of rendezvous.

(2) Normal Control - Normal control is enabled when:

$R = R_i = 25$ km

The elevation angular rate, $\dot{e}$, is monitored continuously. The following conditions are applied to reduce the likelihood of responding to a large random error. If either:

$\dot{e} > 0.3$ mr/sec for two consecutive seconds

or

$\dot{e} < -0.3$ mr/sec for two consecutive seconds

determine whether coarse or vernier control is indicated:

a. If $|R\dot{e}| > 2.5$ m/sec use coarse control.
b. If $|R\dot{e}| < 2.5$ m/sec use vernier control.

The rocket firing time is then calculated:

$$t_F = \frac{C\,|R\dot{e}|}{|a_z|} \qquad \text{(sec)}$$

where:

$C = 0.9$ (providing for deliberate undershoot)
$|a_z| = 0.5$ m/sec^2 (coarse)
(large enough to accommodate any reasonable orbital acceleration)

or:

$|a_z| = 0.1$ m/sec^2 (vernier)
(satisfactory for terminal rendezvous)

The proper rocket is fired for the computed time and in a direction to reduce the LOS rate, $\dot{e}$:

$$a_z = -\,|a_z|\ \mathrm{sgn}\,(\dot{e})$$

A mandatory coast period of at least 3 seconds is required between all vertical rocket firings.

In a further effort to reduce wasteful nuisance firings due to noise, firing is inhibited whenever the firing time is less than 2 seconds. In coarse control this is equivalent to a velocity error of 1.1 m/sec, while in vernier control it represents a velocity deadzone of 0.22 m/sec.

(3) Longitudinal Control - Longitudinal control commences at close range and matches target velocity and establishes a standoff position relative to the target.

Longitudinal control is enabled when:

$$R < R_i = 25 \text{ km}$$

and is initiated on the initiating boundary of the desired switching region - defined by parabolic curves as illustrated by figure 6-6 when:

$$|\dot{R}| \gtrsim \sqrt{K_2\ |R - R_1|}$$

where:

R_1, the coarse standoff range = 200 meters

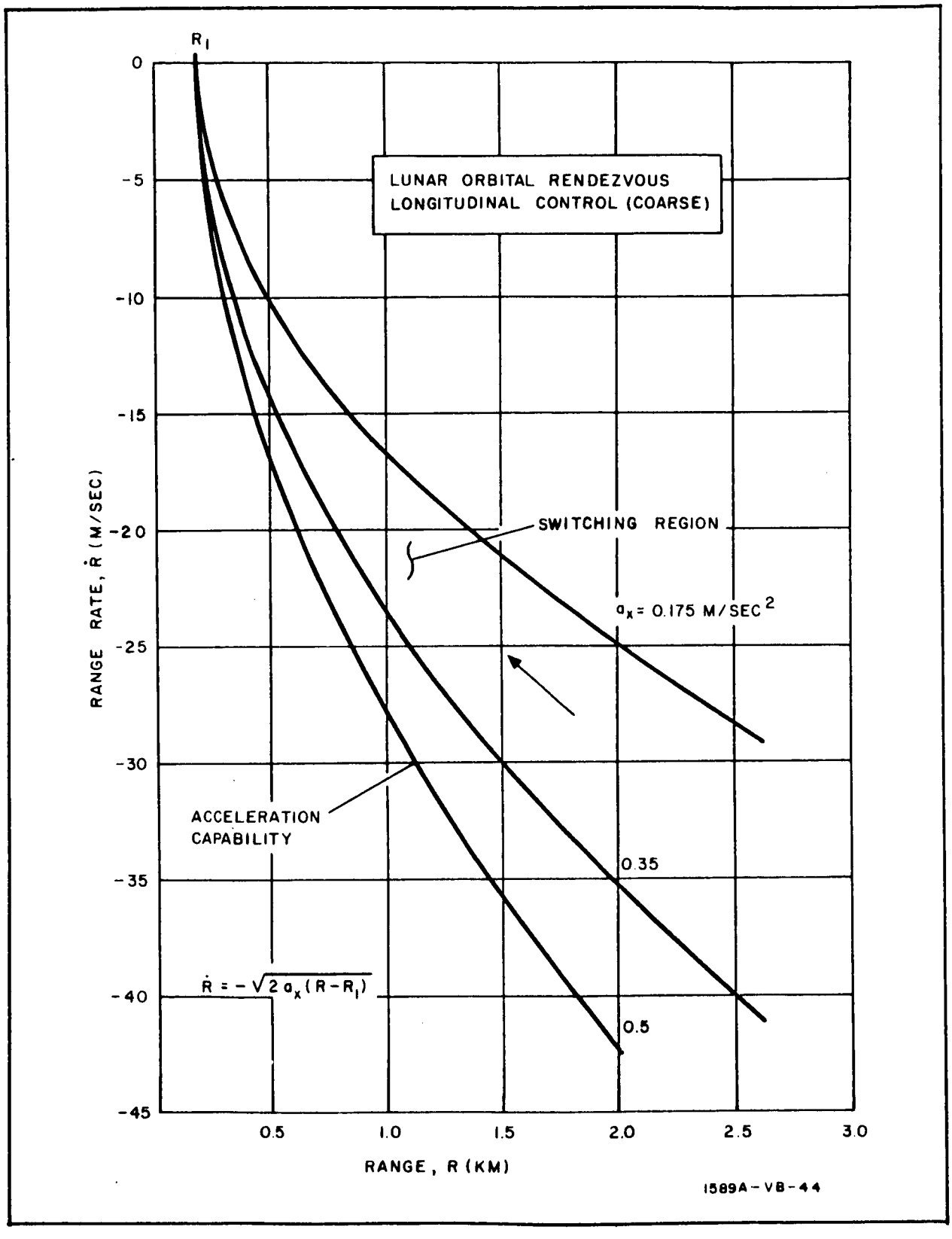

Figure 6-6. Longitudinal Control - Coarse

The control endeavors to contain the phase plane trajectory within this switching region. When the trajectory intercepts the switching boundary, a rocket firing time is computed:

$$t_F = \frac{C\left(-\sqrt{K_1 \left|R - R_1\right|} + \left|\dot{R}\right|\right)}{a_x} \qquad \text{(sec)}$$

where:

$C = 1.7$ (affording margin of undercontrol)
$K_1 = 0.35\ \text{m/sec}^2$
$\left|a_x\right| = 0.5\ \text{m/sec}^2$

The chaser vehicle is then accelerated for the above time as defined by the relation:

$$a_x = -\left|a_x\right| \operatorname{sgn}(R - R_1) \qquad (\text{m/sec}^2)$$

As soon as $\left|\dot{R}\right| < 5$ m/sec, the system is switched to vernier control.

Vernier control is a complete four-quadrant control of the phase plane trajectory, of which the fourth (normal approach) quadrant is shown in figure 6-7. As before, the trajectory is maintained within the desired switching region. With reasonable rendezvous sensor accuracy levels, the trajectory will be transferred from coarse to vernier control and will then be contained within the switching region until the desired vernier standoff range of 50 meters is achieved with substantially zero relative velocity. The rendezvous is considered to be complete when:

$R = 50 \pm 10$ meters
and $\left|\dot{R}\right| \leq 0.5$ m/sec

The phase plane quadrant is first established:

Quadrant	$(R - R_2)$	$\dot{R}$
I	+	+
II	-	+
III	-	-
IV (normal approach)	+	-

In quadrant I or III (range opening from rendezvous point:

$$t_F = \frac{C_1\left(\sqrt{K_1 \left|R - R_2\right|} + \left|\dot{R}\right|\right)}{\left|a_x\right|} \qquad \text{(sec)}$$

where:

$$C_1 = 0.9$$
$$K_1 = 0.07 \text{ m/sec}^2$$
$$R_2 = 50 \text{ m}$$
$$|a_x| = 0.1 \text{ m/sec}^2$$

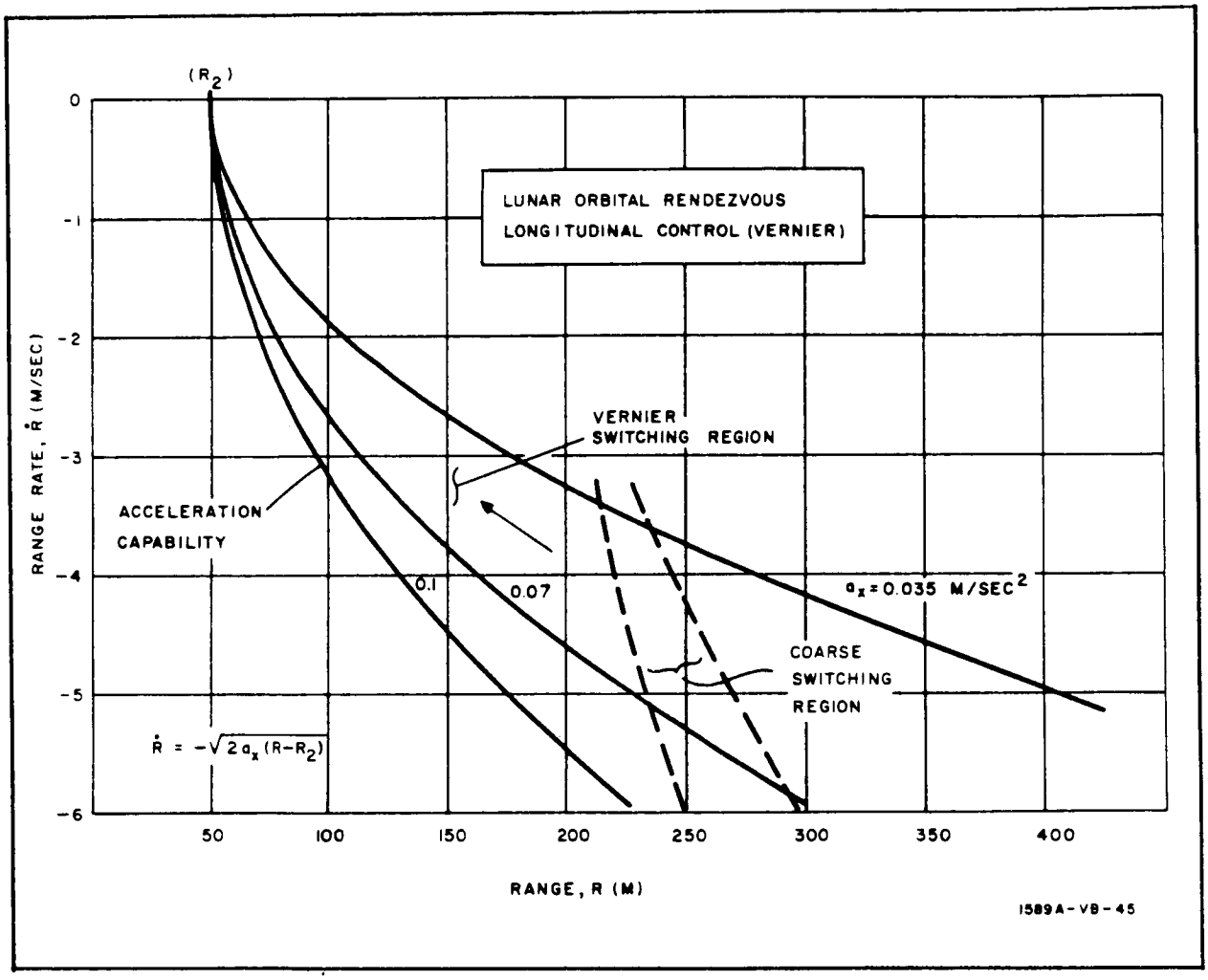

Figure 6-7. Longitudinal Control - Vernier

Accelerate for the above time:

$$a_x = |a_x| \text{ sgn } (R - R_2) \qquad (\text{m/sec}^2)$$

In quadrant II or IV, if $|\dot{R}| > \sqrt{K_2 |R - R_2|}$ where $K_2 = 0.14$ m/sec^2 (too rapid a closure):

$$t_F = \frac{C_2 \left(- \sqrt{-K_1 |R - R_2|} + |\dot{R}| \right)}{|a_x|} \quad \text{(sec)}$$

where:

$C_2 = 1.75$ (providing a reasonable margin of undercontrol)

Accelerate for the above time:

$$a_x = - |a_x| \operatorname{sgn} (R - R_2)$$

If $|\dot{R}| < \sqrt{K_1 |R - R_2|}$ (too slow a closure)

$$t_F = \frac{C_1 \left(\sqrt{K_1 |R - R_2|} - |\dot{R}| \right)}{|a_x|} \quad \text{(sec)}$$

Accelerate for the above time:

$$a_x = |a_x| \operatorname{sgn} (R - R_2) \quad \text{(m/sec}^2\text{)}$$

As in normal control, a coasting period of at least 3 seconds is mandatory between longitudinal rocket firings, and no attempt is made to fire if the computed firing time is less than 2 seconds. This latter restriction introduces a longitudinal velocity deadzone of 1.0 m/sec in coarse control and 0.2 m/sec in vernier.

(4) Lateral Control - Although the chaser transfer orbit is nominally coplanar with the target orbit, nominal lateral (out of plane) corrections will be required. The lateral control scheme is essentially identical with vertical control.

6.3.1.3 Data Processing

A digital data smoother is required for smoothing range, range rate, and angular rate data prior to using them for control purposes.

Each smoother, as seen in figure 6-8 provides not only smoothing of the raw data during the coasting phase, but also affords velocity compensation during rocket firing periods in any axis. Smooth tracking can thereby be attained even when firing maneuvering rockets.

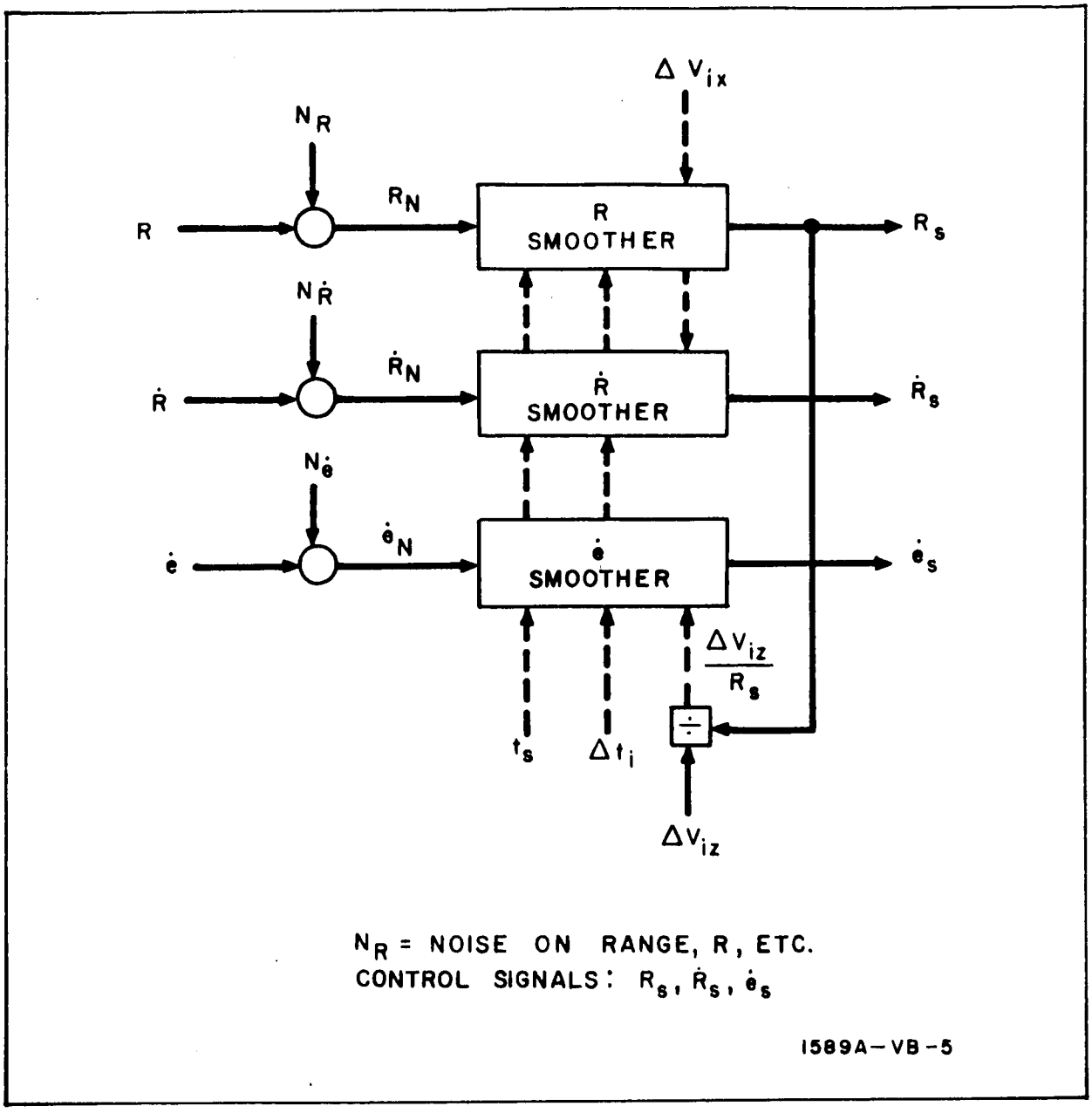

Figure 6-8. Digital Data Smoother

The following relations apply:

Δt_i = data storage interval (the 1-second interval used in the program appears to be adequate for rendezvous control)

t_s = smoothnig time (sec)

n = number of data samples used in the smoothing process

$$= \frac{t_s}{\Delta t_i} + 1$$

The incremental velocity provided during the last computing interval is.

$$\Delta V_{ix} = a_x \Delta t_{Fx} \quad \text{for the x-axis}$$
$$\Delta V_{iz} = a_z \Delta t_{Fz} \quad \text{for the z-axis}$$

At each Δt_i enter present raw value of data, a_o, and reject from storage the oldest smoothed value, $a_n|_{t-1}$. Determine present smoothed value of data, a_1, as follows.

a. <u>During Coasting Periods (no rocket firing)</u> - Collect present raw value, a_o, and n-1 most recent smoothed values; i.e., a_2, a_3, - - , a_n. Using method of least squares, determine best first or second order of fit (first order was used for this program) to these n data samples. Using this fit, project (extrapolate) for the present smoothed value, a_1. This present smoothed value is the value to be used for control. This value is stored and becomes the most recent smoothed value for the next computation, at which time it will become a_2.

b. <u>During Firing Periods in any Axis</u> - Apply, as applicable, a weighted correction each second to each smoothed data sample as indicated below:

Range, R

$a_o|_t$ = present raw data value

$a_2|_t = a_1|_{t-1} - 0.5\,\Delta V_{ix}$

$a_3|_t = a_2|_{t-1} - 1.5\,\Delta V_{ix}$

$a_4|_t = a_3|_{t-1} - 2.5\,\Delta V_{ix}$

etc.

Range rate, $\dot{R}$

$a_o|_t$ = present raw datum

$a_2|_t = a_1|_{t-1} - \Delta V_{ix}$

$a_3|_t = a_2|_{t-1} - \Delta V_{ix}$

etc.

Elevation rate, $\dot{e}$

$a_o|_t$ = present raw value of data

$a_2|_t = a_1|_{t-1} - \Delta V_{iz}/R_s$

$a_3|_t = a_2|_{t-1} - \Delta V_{iz}/R_s$

etc.

where: R_s = present smoothed value of range.

6.3.1.4 Description of Sensors

The sensing elements required for orbital injection and for the active rendezvous are discussed separately.

a. Injection Sensors - Prior to executing the injection maneuver it is necessary that the chaser vehicle in effect know the orbital elements of both the target and the chaser vehicles. It is assumed that target orbit data has been previously transmitted to the chaser. Chaser altitude must be measured as must the relative phase angle between the two vehicles.

On the basis of orbital information, the chaser computes the incremental velocity vector that must be applied and determines when to apply it in order to establish the properly phased transfer orbit.

The execution of the injection maneuver is affected not only by errors in determination of chaser altitude and phase angle, but also by the incremental velocity vector actually imparted to the chaser vehicle. A directional error is introduced by vehicle pitch and yaw attitude errors as well as by thrust misalignment within the vehicle itself, although for this study it is considered solely a consequence of vehicle attitude error. A velocity magnitude error is considered to be a velocity cutoff error regardless of the cause.

b. Rendezvous Sensors - For this portion of the study it is assumed that the rendezvous sensors afford a direct measure of range, range rate, and two angular rates - corresponding to space rates of the antenna gimbals.

6.3.2 Error Analysis - Digital Program

A digital computer program to simulate lunar rendezvous was prepared for the IBM 7094. The program simulates the measurements, data conditioning, computations, and maneuvering of a chaser in achieving a rendezvous with a nonmaneuvering target.

Inputs to the program have been designed so that the effects of a number of different parameters can easily be studied. Among the inputs to the program are four quantities which represent errors in the injection of the chaser into its parking orbit and ascent ellipse. Other inputs include the specification of standard deviations of noise quantities, the order of smoothing to be used on the simulated observables, and the number of points to be smoothed.

6.3.2.1 Analysis of Injection Errors

Four types of injection errors are considered:

a. Altitude
b. Incremental velocity magnitude

c. Incremental velocity direction (tangential for the 180-degree transfer)
d. Phasing (timing)

To obtain insight of the relative effect of these injection errors, the miss distance sensitivity coefficients were determined as follows:

The computer program was run without the active rendezvous guidance engaged. Each error was inserted independently and the horizontal and vertical components of chaser-to-target range were noted when the chaser had completed the full 180 degrees of the transfer ellipse. The sensitivity coefficients are presented in table 6-1.

TABLE 6-1

MISS DISTANCE SENSITIVITY COEFFICIENTS
(30/200-km) LUNAR ORBIT TRANSFER

Error	Horizontal Coefficients		Vertical Coefficients		Units
altitude	$\partial M_x/\partial h_1$	4.94	$\partial M_y/\partial h_1$	1.14	$\frac{km}{km}$
velocity	$\partial M_x/\partial V_1$	11.0	$\partial M_y/\partial V_1$	4.77	$\frac{km}{m/sec}$
attitude	$\partial M_x/\partial \gamma_1$	-2.94	$\partial M_y/\partial \gamma_1$	0	$\frac{km}{deg}$
target lead (timing)	$\partial M_x/\partial t_1$	0.274	$\partial M_y/\partial t_1$	0	$\frac{km}{sec}$

Allowable injection errors were obtained by making a series of computer runs with the active rendezvous guidance engaged and a particular injection error inserted in each run. Rendezvous was considered to be complete when:

$$R = 50 \pm 10 \text{ meters}$$

and

$$|\dot{R}| \leq 0.5 \text{ m/sec}$$

The propellant consumption (in terms of ΔV) for each run was compared with the incremental velocity (ΔV_H) required for the ideal Hohmann transfer to provide a meaningful comparison among runs, A $\frac{\Delta V}{\Delta V_H}$ of 1.0 (100 percent) would thus constitute a perfect run.

In establishing tolerable levels of injection errors it was arbitrarily assumed that a 20-percent increase in propellant consumption ($a\Delta V/\Delta V_H$ of 1.2) would correspond to a 3σ level of tolerable injection error. It was further decided that if the error was unbalanced around zero, the lower error level obtained from this criterion would be selected in the interest of conservation.

Because of the two-dimensional nature of the digital program. The allowable yaw attitude error is obtained analytically.

A yaw error results in a lateral (out-of-plane) velocity increment of:

$$\Delta V_{LAT} = \Delta V_1 \sin \Delta\psi$$

An equal increment at rendezvous is required to compensate for this lateral component. The maximum allowable velocity increment which can be used for compensation is $0.2\ \Delta V_H$.

Therefore:

$$\Delta V_1 \sin \Delta\psi = 0.2\ \Delta V_H$$

or

$$\Delta\psi = \sin^{-1}\left(\frac{0.2\ \Delta V_H}{\Delta V_1}\right)$$

where

$$\Delta V_H = 75 \text{ m/sec}$$

$$\Delta V_1 = 38 \text{ m/sec}$$

6.3.2.2 Analysis of Rendezvous Sensor Errors

A series of IBM 7094 computer runs is made for the nominal injection case (zero injection error) with various levels of random uncorrelated error or noise inserted into the simulated range, range rate, and angular rate inputs. A fixed ratio of the three corresponding errors in range, range rate, and angular rate is roughly established by determining that each type of error results in a corresponding propellant consumption for a particular injection condition. This error ratio, determined to be 2 percent of R, 1 m/sec of R, and 0.1 mr/sec of $\dot{e}$, is maintained throughout the analysis.

At each noise level a series of 25 computer runs is made with automatic rendezvous engaged and with random noise inputs; i.e., each run has a different random number routine superimposed on each of the observables. Rendezvous is considered accomplished for each run when:

$$R = 50 \pm 10 \text{ meters}$$

and

$$|\dot{R}| \leq 0.5 \text{ m/sec}$$

The incremental velocity ratio, $\Delta V/\Delta V_H$, required to perform a satisfactory rendezvous is determined for each run.

The results of these runs are plotted in figure 6-9 which presents for each noise level the arithmetic mean, the maximum of 25 noise samples, and the mean-plus-3σ value. This latter value is then used in establishing the level of acceptability. A least-squares second-order fit is then applied to the plotted points to present smooth curves. Although the type of distribution of the deviations from the mean is not readily determinable from the limited number of samples (25) considered at each level of noise ratio, the 3σ value lies somewhere between the theoretical minimum of 89 percent up to the maximum (at normal distribution) of 99+ percent.

6.4 RESULTS

6.4.1 Results of Injection Analysis

The effects of initial injection errors on propellant consumption are separately displayed by the curves of figures 6-10, 6-11, 6-12, and 6-13, which show respectively the consequences of errors in altitude, incremental velocity magnitude and direction, and phase angle. By combining these results with the yaw attitude error computed analytically, tolerable levels of injection errors are portrayed in table 6-2.

Attitude and range measurements can be made using radar to the state of the art accuracy indicated. Integrating accelerometers form a ready means of measuring incremental velocity. Pitch (and roll) attitude references can be measured with infrared horizon scanners, while the yaw reference angle can be determined by gyro-compassing techniques. Inclination can be determined by lunar navigation methods.

It should be observed that in every case the state of the art accuracies for the injection sensors are significantly better than required for the rendezvous mission. The system, however, appears to be sensitive to positive velocity errors.

The effects of injection errors on the phase plane trajectory for an active rendezvous are illustrated by figure 6-14, which indicates the dispersion from the nominal error-free case. Variations in elevation angle with range during the active rendezvous are presented by figure 6-15, which shows the dispersion from the nominal case as introduced by injection errors.

6.4.2 Results of Active Rendezvous Analysis

The point where the smoothed curve of the mean plus 3σ value results in a $\frac{\Delta V}{\Delta V_H}$ of 150 percent is postulated as providing a conservative level of acceptability. These "tolerable" rendezvous sensor errors are presented in table 6-3.

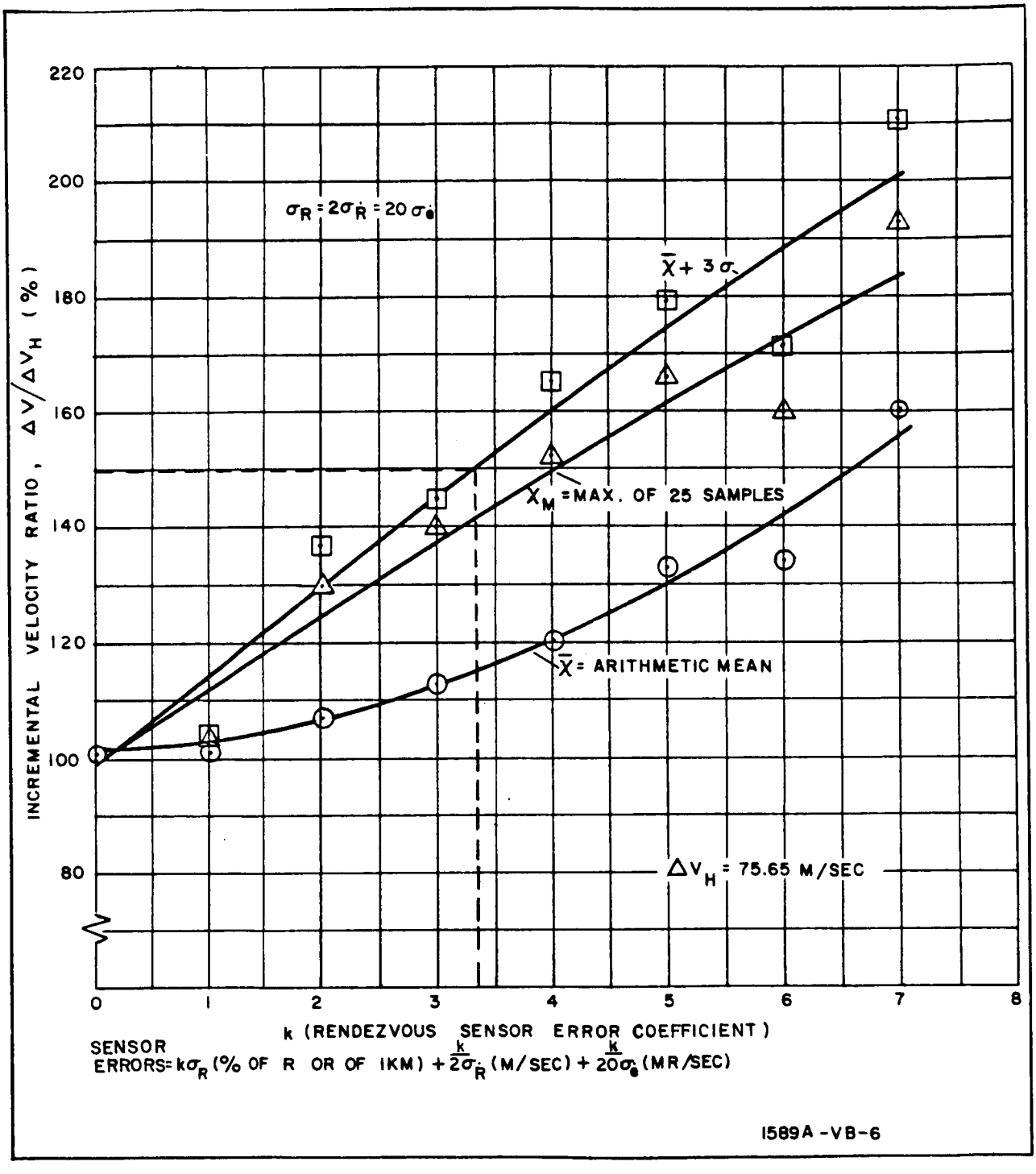

Figure 6-9. Effect of Rendezvous Sensor Errors on Propellant Consumption

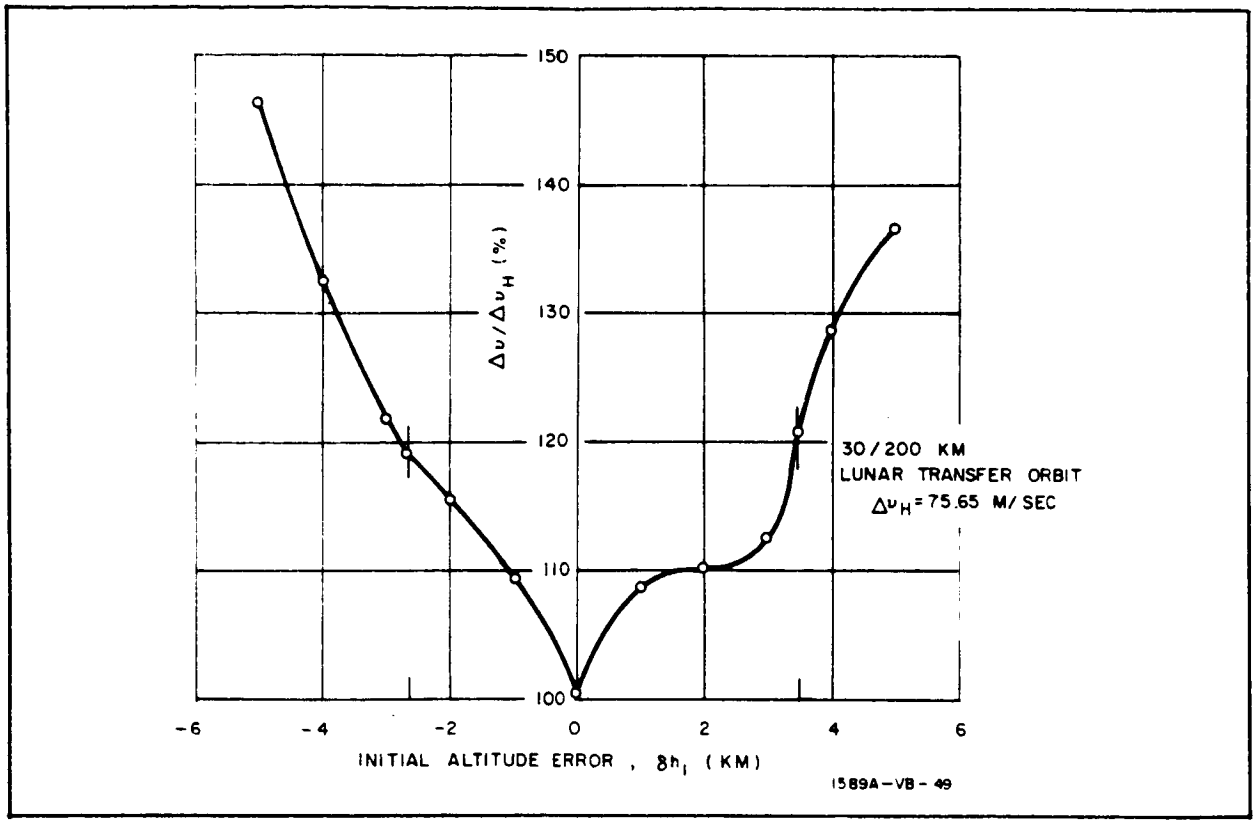

Figure 6-10. Effect of Initial Altitude Error on Propellant Consumption

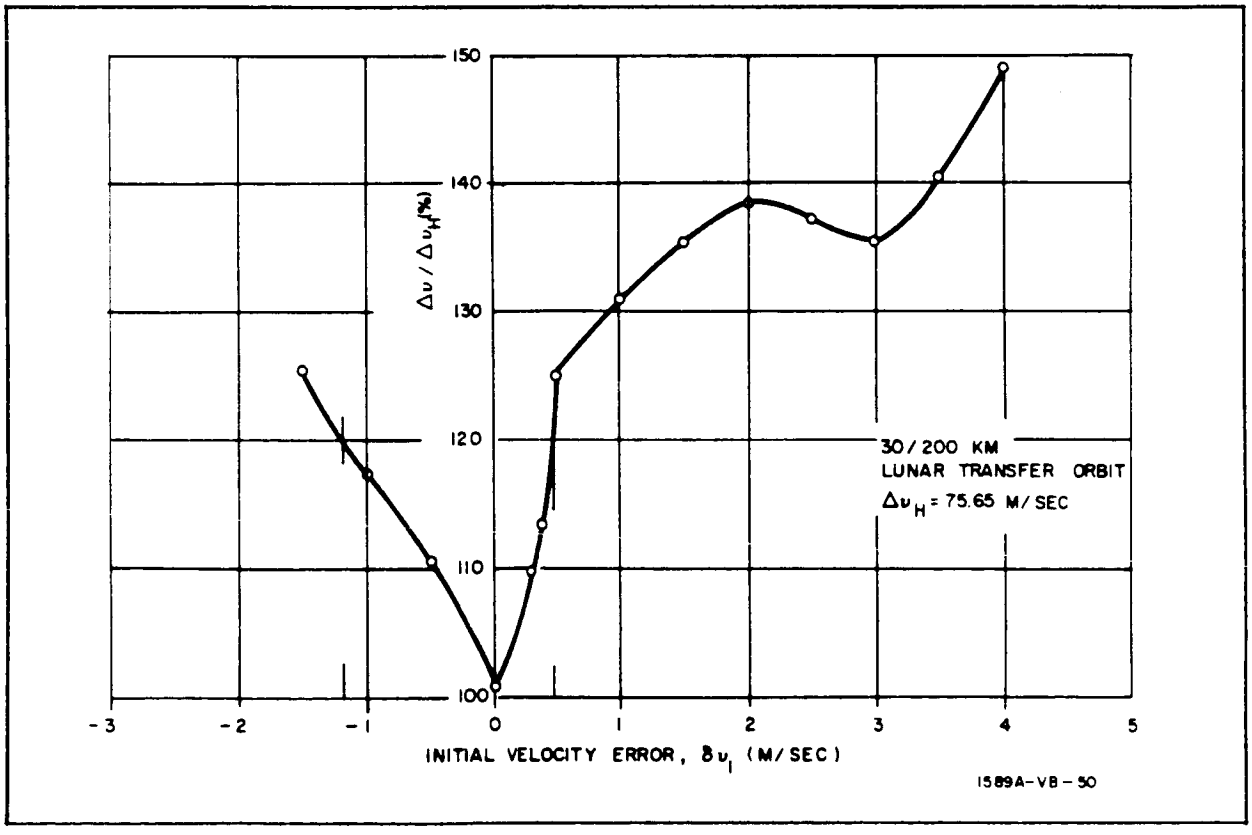

Figure 6-11. Effect of Initial Velocity Error on Propellant

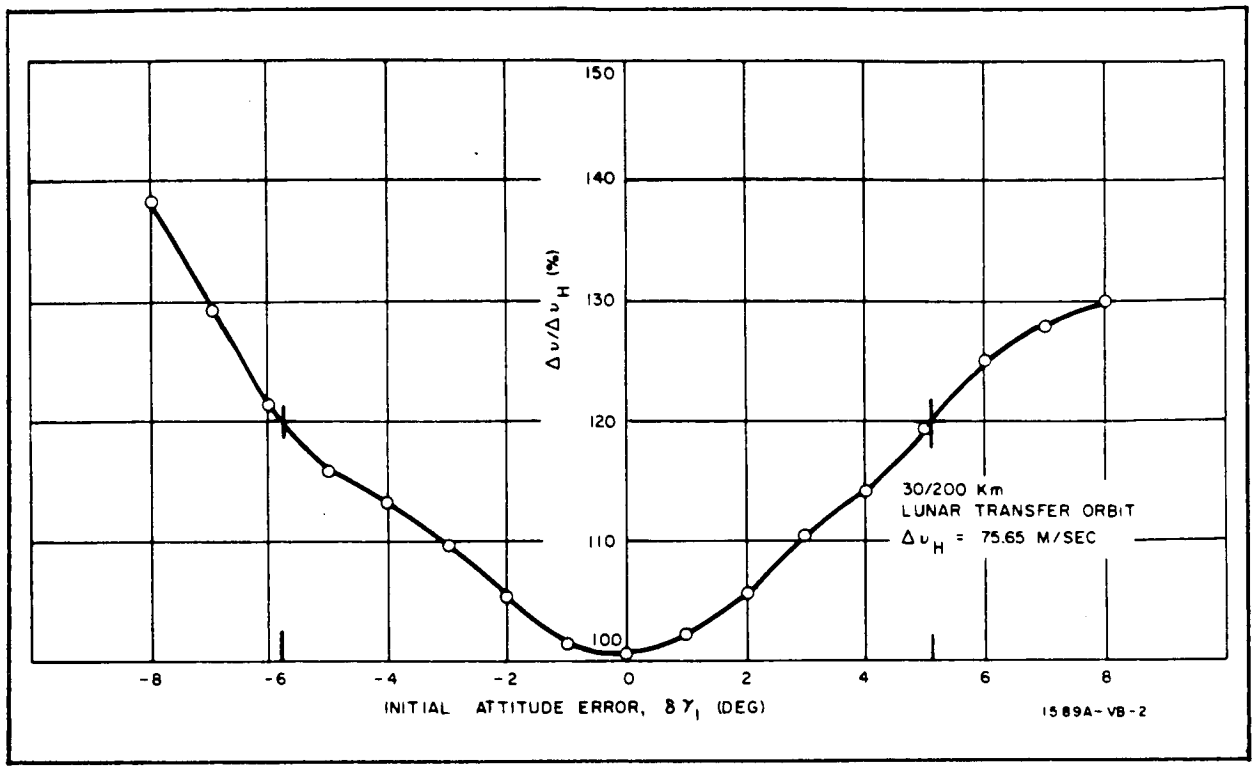

Figure 6-12. Effect of Initial Attitude Error on Propellant Consumption

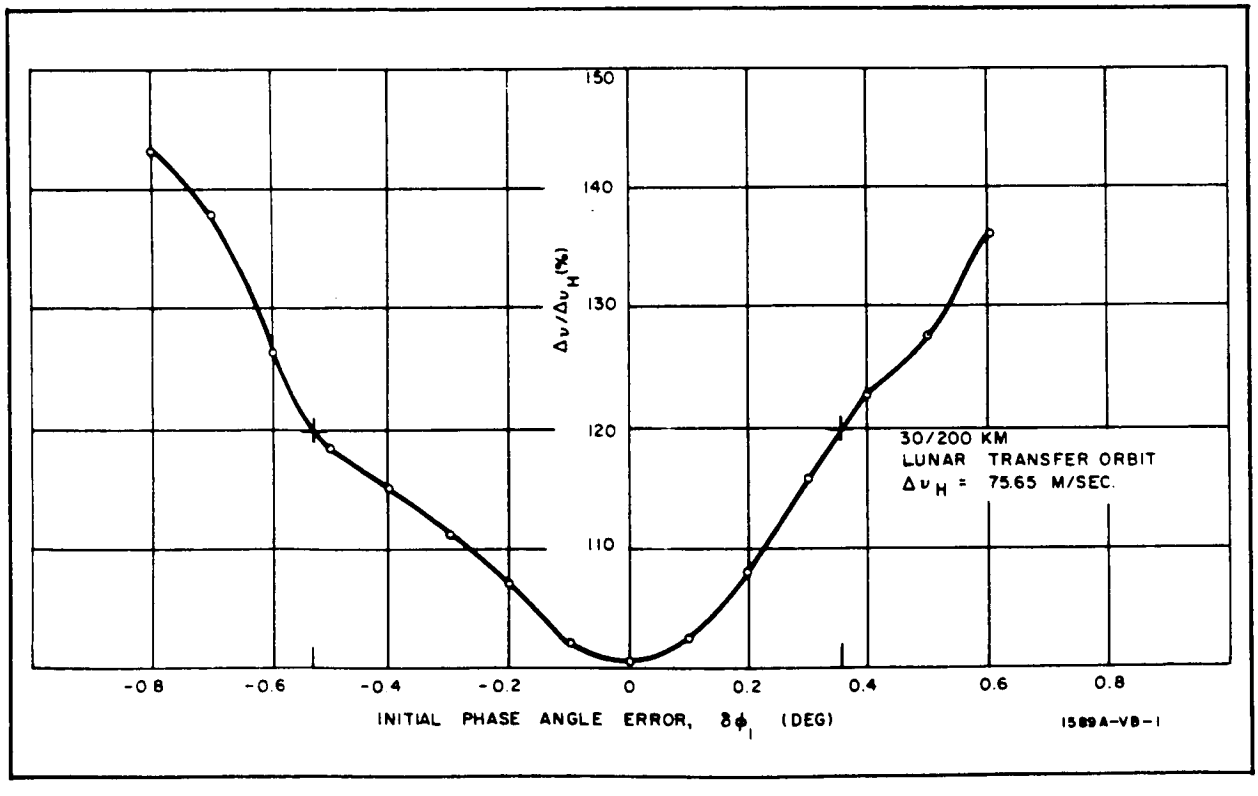

Figure 6-13. Effect of Initial Phasing Error on Propellant Consumption

TABLE 6-2

INJECTION SENSOR ERRORS

Symbol	Quantity	Sensor Accuracy (3 σ)	State of the Art Accuracy (3 σ)
Δh	Altitude	2.8 km	30 m (0.1% of h)*
$\Delta \gamma$	Pitch attitude	5.1 deg	0.3 deg
ΔV	Velocity	0.5 m/sec	0.3 m/sec
$\Delta \psi$	Yaw attitude	22.2 deg	0.3 deg
$\Delta \phi$	Central angle	0.36 deg	--
ΔR	Range	2.57% of R	0.1% of R
Δt	Timing	52.2 sec	3 sec
Δi	Inclination	0.8 deg	0.1 deg

* While a radar altimeter can measure terrain altitude this accurately, the absolute altitude from a lunar reference datum could not be determined to this degree of precision.

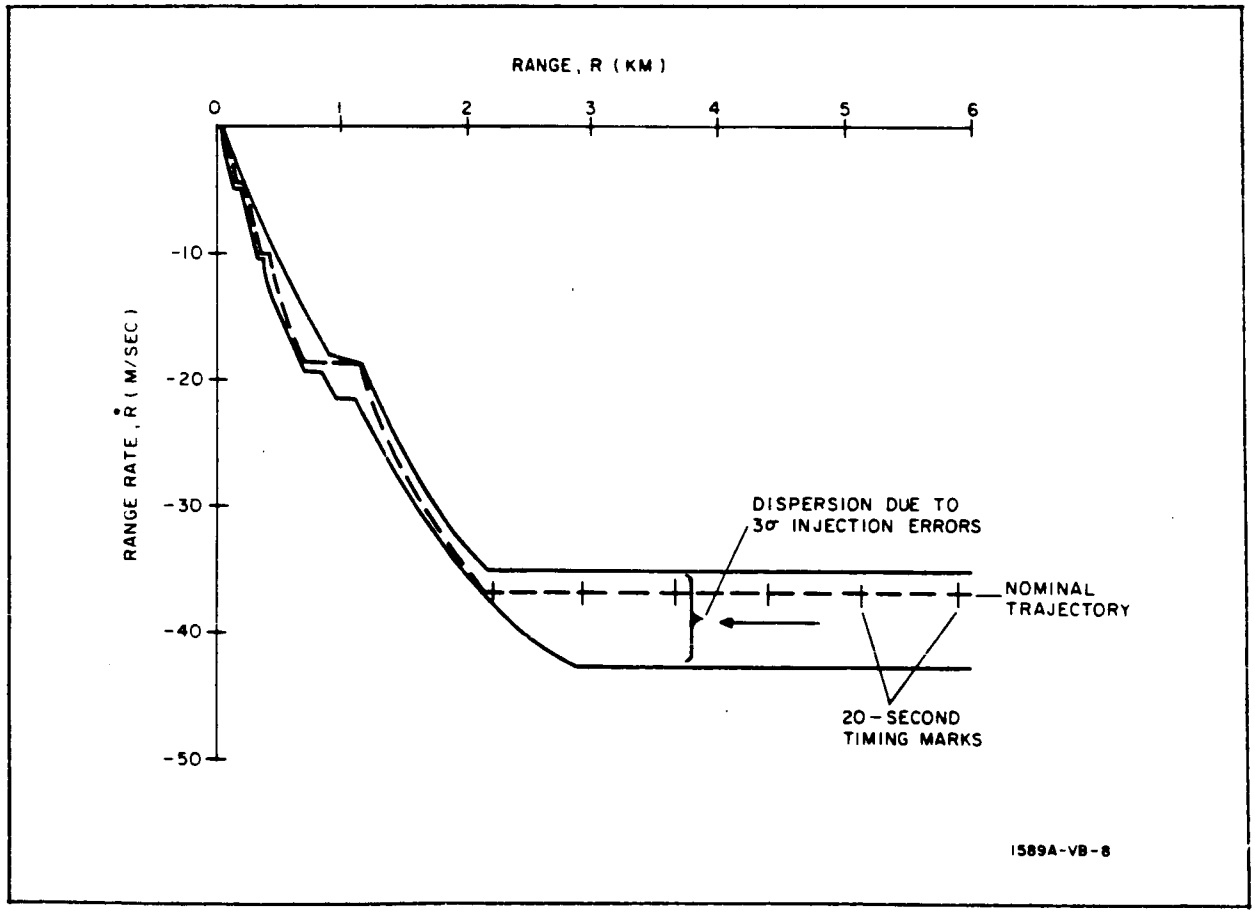

Figure 6-14. Rendezvous Phase Plane Illustrating Effect of Injection Errors

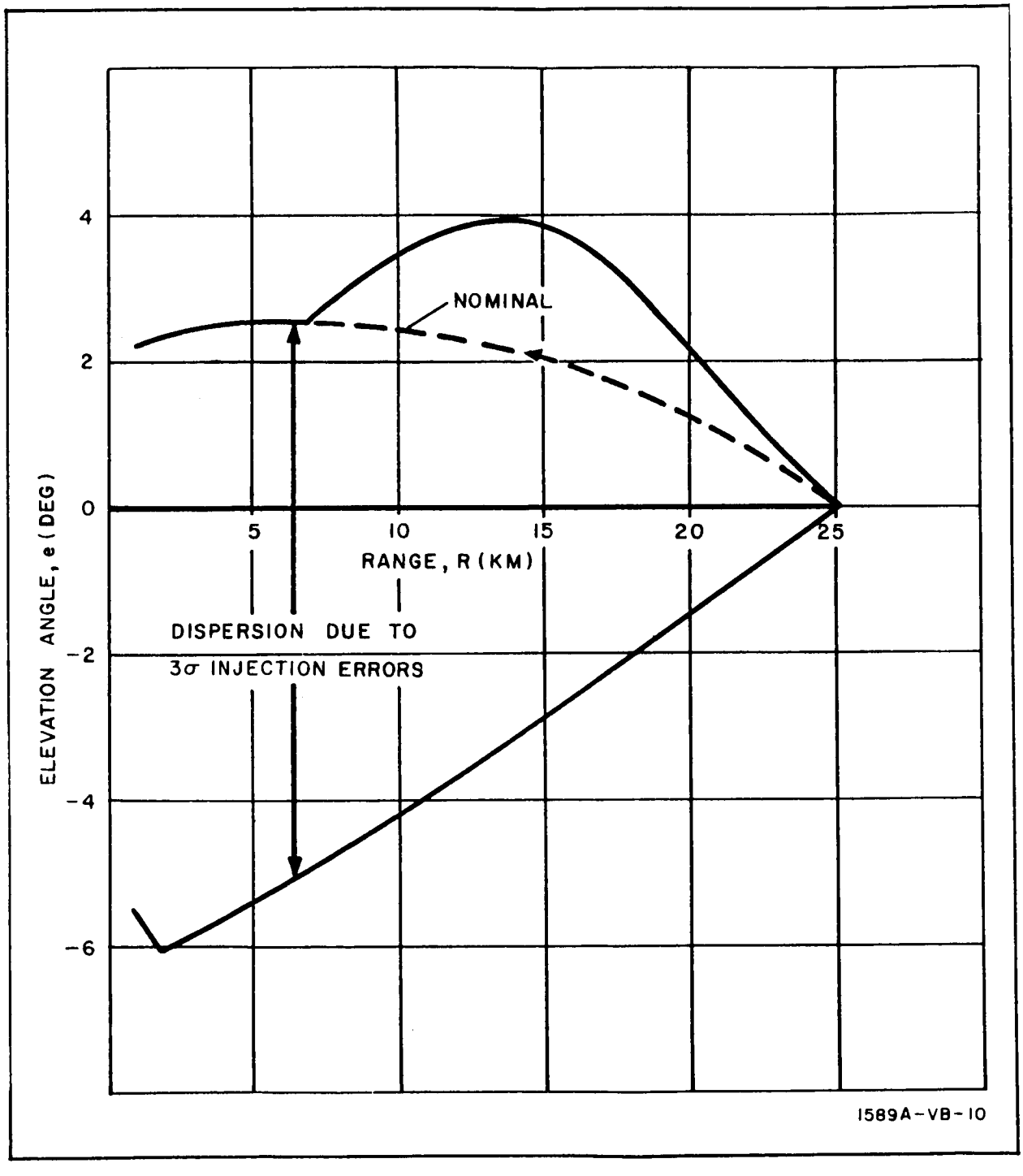

Figure 6-15. Variation in Elevation Angle With Range

TABLE 6-3

RENDEZVOUS SENSOR ERRORS

Quantity	Sensor Accuracy (3σ)	State of the Art Accuracy (3σ)
Range	3.3% or 33 m	0.5 % or 1 m
Range rate	1.65 m/sec	0.03 m/sec
Angular rate	0.165 mr/sec	0.05 mr/sec

From the curves of figure 6-9 it is seen that for any but the smallest sensor errors the deviation from the mean is appreciable, indicating primarily the sensitivity of the active rendezvous control system to LOS rate errors.

Large random angular rate errors early in the approach trigger premature normal corrections (and corresponding overshoots) which must be subsequently countered. It is apparent that the normal system should be made less susceptible to angular rate errors particularly at long range. It should be made more selective in initiating a long-range correction and probably should deliberately try for a larger under-shoot when making a correction.

The accuracy requirement for the angular rate observations appears to be unnecessarily severe. Tightening the range and range rate accuracy requirements will in some measure alleviate the severity of the angular rate accuracy requirement. Operation was attempted only at the one accuracy ratio indicated, but it appears most desirable to try other ratios favoring lower LOS rate accuracies, particularly since the range requirement offers considerable latitude.

For purposes of direct comparison, additional runs definitely should be made using the identical rendezvous control model, but with LOS rates derived from LOS angles rather than observed directly.

Terminal accuracy suffers with larger error levels. The standoff range of 50 meters is probably too close for the larger error levels. In any event, the use of higher accuracy sensors will definitely result in lower propellant consumption.

6.5 CONCLUSIONS

For the lunar orbital rendezvous phase of the mission, several types of sensing devices are necessary. As determined from the preceding subsections, certain minimum levels of accuracy are required of each sensor for successful completion of the mission while also considering the important factor of propellant conservation.

6.5.1 Injection Sensor Requirements

The dynamic ranges and accuracy requirements are presented in table 6-4.

TABLE 6-4

INJECTION SENSOR REQUIREMENTS

Quantity Measured	Dynamic Range		Max Allowable rms (1 σ) Sensor Error
	Max	Min	
Altitude	+40 km	0	0.93 km
Incremental velocity*	+50 m/sec	0	0.17 m/sec
Pitch angle*	+90 deg	-90 deg	1.7 deg
Yaw angle*	+180 deg	-180 deg	7.4 deg
Range	+500 km	0	0.86% of R
Inclination angle	+5 deg	-5 deg	0.27 deg

* With the quantities so indicated, the listed error is the total error permitted in that particular quantity, including both measurement and control system inaccuracies.

While sensors with the above accuracy levels will produce a satisfactory rendezvous ascent, it should be emphasized that the use of more accurate sensors will normally conserve propellant - a precious commodity at the moon.

6.5.2 Rendezvous Sensor Requirements

The dynamic range and accuracy requirements of rendezvous sensors necessary to complete a satisfactory rendezvous mission without serious propellant expenditure are presented in table 6-5. These requirements are based on a 15-second smoothing time and a 1-second sampling interval.

In this study, where LOS rates are observed directly, the LOS rate requirement is severe. This apparently severe angular rate requirement should be resolved by tightening up range and range rate requirements and by directly comparing observed versus derived angular rate information.

Although the above sensor requirements will afford a satisfactory rendezvous it should be stressed that greater accuracy will generally reduce the energy expended during the rendezvous phase.

6.6 ADDITIONAL ANALYSIS

A second analysis of lunar rendezvous was performed. However, the guidance system used for this analysis is not typical of a rendezvous system

TABLE 6-5

RENDEZVOUS SENSOR REQUIREMENTS

Quantity Measured	Dynamic Range		Max Allowable rms (1 σ) Sensor Error
	Max	Min	
Range	30 km*	0	1.1% of 11 m
Range rate	+10 m/sec (opening)	-50 m/sec (closing)	0.55 mr/sec
LOS angular rates (az & el)	2 mr/sec	-2 mr/sec	0.055 mr/sec
Vehicle attitude (pitch, roll, yaw)	+180 deg (yaw) +90 deg (pitch and roll)	-180 deg (yaw) -90 deg (pitch and roll)	0.2 deg firing period (to reduce cross-coupling) 5 deg during tracking (vehicle may change attitude to accommodate LOS angle limits)

* The maximum range of the ranging device is that required for the active phase of rendezvous. Actually this device should probably be the same sensor that measures target range prior to injection and which may also occasionally monitor the target during the coasting period of the rendezvous ascent.

and is quite expensive from the standpoint of fuel consumption. For this reason, the sensor requirements obtained are not considered to be realistic and the analysis is not included in this report.

7. REFERENCES

2-1 Smith, G. L., and Harper, E. V.; Midcourse Guidance Using Radar Tracking and Onboard Observation Data; NASA Ames Research Center; NASA TN D-2238, April 1964.

2-2 Battin, R. H.; A Statistical Optimizing Navigation Procedure for Space Flight; ARS Journal; Vol. 32, No. 11; November 1962; pp. 1681-1696.

2-3 Moulton, F. R.; An Introduction to Celestial Mechanics; The MacMillan Co., 1959.

2-4 Gapcynski, J. H., and Tolson, R. H.; Analysis of the Lunar Return Mission; NASA Langley Research Center; NASA TN D-1939, August 1963.

2-5 Bellman, R. E.; Introduction to Matrix Analysis; McGraw-Hill Book Company, Inc.; New York, 1960.

2-6 Kalman, R. E.; A New Approach to Linear Filtering and Prediction Problems; Trans. ASME; Series D; Journal of Basic Engineering; Vol. 8, No. 1; March 1960, pp. 35-45.

2-7 Smith, G. L.; Secondary Errors and Off-Design Conditions in Optimal Estimation of Space Vehicle Trajectories; NASA Ames Research Center; NASA TN D-2129; January 1964.

2-8 Denham, W. A.; and Speyer, J. L.; Optimal Measurement and Velocity Correction Programs for Midcourse Guidance; AIAA Journal; Vol. 2, No. 5; May 1964.

2-9 McLean, J. D., Schmidt, S. F., and McGee, L. A.; Optimal Fittering and Linear Prediction Applied to Midcourse Navigation for the Circumlunar Mission; NASA Ames Research Center; NASA TN D-1208; March 1962.

2-10 Private correspondence with G. L. Smith, Ames Research Center, 1963.

2-11 Marshall Document.

2-12 Baker Jr., R. M. L.; Westrom, G. W.; Analysis and Standardization of Astrodynamic Constants; AAS Preprint 61-27; 1961.

3-1 Kalman, R. E., A New Approach to Linear Filtering and Prediction Problems, Trans. ASME, Series D, Jour. Basic Engr., Vol. 82, No. 1, March 1960, pp. 35-45.

3-2 Smith, G. L., Schmidt, S. F., and McGee, L. A.; Application of Statistical Filter Theory to the Optimal Estimation of Position and Velocity on Board a Circumlunar Vehicle, NASA TR R-135, 1962.

3-3 McLean, J. D., Schmidt, S. F., and McGee, L. A.; Optimal Filtering and Linear Prediction Applied to a Midcourse Navigation System for the Circumlunar Mission, NASA TN D-1208, 1961.

3-4 Battin, R. H.; A Statistical Optimizing Navigation Procedure for Space Flight, ARSJ Vol. 32, No. 11, November 1962, pp. 1681-1696.

3-5 Smith, G. L., and McGee, L. A.; Midcourse Navigation Scheme, NASA Intercenter Technical Conference on Control, Guidance, and Navigation Research for Manned Lunar Missions, July 24-25, 1962.

3-6 Gunckel, T. L.; Orbit Determination Using Kalman's Method, Journal of the Institute of Navigation, Vol. 10, No. 3, Autumn, 1963.

3-7 Tunnell, P. J. and Lessing, H. C.; Guidance Techniques for Lunar Approach and Letdown of the Apollo Spacecraft; Intercenter Technical Conference on Control, Guidance and Navigation Research for Manned Lunar Missions; Ames Research Center, July 24 and 25, 1962, pp. 320-331.

3-8 Bowditch, N.; American Practical Navigator, U.S. Hydrographic Office, Washington, 1962, p 1149.

3-9 Pines, S., Wolf, H.; Woolston, D., and Squires, R.; Goddard Minimum Variance Orbit Determination Program, Goddard Space Flight Center Report No. X-640-62-191.

3-10 Levine, G. M.; Application of Midcourse Guidance Technique to Orbit Determination, IAS Paper No. 63-16; IAS 31st Annual Meeting, January 21-23, 1963, New York.

3-11 Schlegel, L. B.; Covariance Matrix Approximation, AIAA Journal, Vol. 1, No. 11, November 1963, p 2672.

4-1 Bryson, A. E., and Denham, W. F; A Steepest Ascent Method for Solving Optimum Programming Problems, Journal of Applied Mechanics, June, 1962, pp. 247-257.

4-2 Tunnell, P. J., and Lessing, H. C.; Guidance Techniques for Lunar Approach and Letdown of the Apollo Spacecraft, Intercenter Technical Conference on Control, Guidance, and Navigation Research for Manned Lunar Missions, Ames Research Center, July 24 and 25, 1962, pp. 32-331.

4-3 Gille, J. C., Pelegrin, M. J., and Decaulne, P.; Feedback Control Systems, McGraw-Hill Book Company, Inc., New York, 1959.

4-4 Kriegsman, B. A., and Reiss, M. H.; Terminal Guidance and Control Techinques for Soft Lunar Landing, ARS Journal, Vol. 32, March 1962, pp. 401-413.

5-1 Sterns, E. V. B.; Navigation and Guidance in Space, Prentice-Hall, Inc., 1963, Chap. 2.

5-2 MacKay, J. S.; Approximate Solution for Rocket Flight With Linear-Tangent Thrust Attitude Control, ARS Journal, Vol. 30, No. 16, November 1960, pp. 1091-1093.

5-3 Burley, R. R., and Weber, R. J., Lunar Takeoff, ARS Journal, Vol. 32, No. 8, August 1962, 1296.

5-4 Pitman, G. R. (Editor), Inertial Guidance, John Wiley and Sons, Inc. 1962.

5-5 Gretz, R. W., Error Sensitivities in Satellite Ascent and Orbital Transfer, ARS Journal, Vol. 32, No. 12, December 1962, pp. 1860-1866.

5-6 Nelson, W. C., and E. E. Loft, Space Mechanics, Prentice-Hall, Inc., 1962, pp. 66 and 160.

5-7 Heiskanen, W. A., and Vening Meinesz, F. A.; The Earth and Its Gravity Field, McGraw-Hill Book Co., Inc., 1958, Chap. 5.